PRODUCTION AND CHARACTERIZATION OF 94NBT-6BT PIEZOELECTRIC SINGLE CRYSTAL MATERIALS

Mevlüt GÜRBÜZ

PhD Dissertation

Ceramic Engineering

May-2013

ANADOLU ÜNİVERSİTESİ

JÜRİ VE ENSTİTÜ ONAYI

Mevlüt GÜRBÜZ'ün **"Production and Characterization of 94NBT-6BT Piezoelectric Single Crystal Materials"** başlıklı **Seramik Mühendisliği** Anabilim Dalındaki, Doktora Tezi 10/04/2013 tarihinde, aşağıdaki jüri tarafından Anadolu Üniversitesi Lisansüstü Eğitim-Öğretim ve Sınav Yönetmeliğinin ilgili maddeleri uyarınca değerlendirilerek kabul edilmiştir.

	Adı-Soyadı	**İmza**
Üye (Tez Danışmanı)	**: Prof. Dr. AYDIN DOĞAN**	**.....**
Üye	**: Prof. Dr. SERVET TURAN**	**.....**
Üye	**: Prof. Dr. A. SAVAŞ KOPARAL**	**.....**
Üye	**: Doç.Dr. CEM SEVİK**	**.....**
Üye	**: Yrd. Doç. Dr. METİN ÖZGÜL**	**.....**

Anadolu Üniversitesi Fen Bilimleri Enstitüsü Yönetim Kurulu'nun …… tarih ve …… sayılı kararıyla onaylanmıştır.

Enstitü Müdürü

ÖZET

Doktora Tezi

94NBT-6BT PİEZOELEKTRİK TEK KRİSTAL MALZEMELERİN ÜRETİLMESİ VE KARAKTERİZASYONU

Mevlüt GÜRBÜZ

Anadolu Üniversitesi
Fen Bilimleri Enstitüsü
Seramik Mühendisliği Ana Bilim Dalı

Danışman: Prof. Dr. Aydın DOĞAN

2013, 162 sayfa

Kurşun içeren ve kurşunsuz piezoelektrik tek kristal malzemelerin geliştirilmesi bu malzemelerin mükemmel domain diziliminden dolayı 1997'den günümüze birçok araştırmacının dikkatini çekmiştir. 2000'li yıllardan sonra yeni nesil piezoelektrik tek kristal malzemeler oldukça hızlı gelişen elektronik teknolojisine bağlı olarak yüksek performanslı cihaz üretimi için daha çok tercih edilmektedir. Fakat yakın bir gelecekte kurşun esaslı malzemelerin kullanımı proses esnasında yüksek buharlaşmadan dolayı çevresel düzenlemeler tarafından yasaklanacaktır. Son yıllarda sodyum bizmut titanat-baryum titanat ($94Na_{0.5}Bi_{0.5}TiO_3$-$6BaTiO_3$) (94NBT-6BT) tek kristalleri yüksek piezoelektrik özelliklerinden dolayı kurşunsuz piezoelektrik malzemeler için uygun bir adaydır. Son zamanlarda NBT esaslı tek kristallerin piezoelektrik performansını geliştirmek için dikkate değer araştırma çalışmaları yapılmıştır. Bu tezde $BaTiO_3$, katkısız ve Li, Fe, Mn katkılı 94NBT-6BT tek kristalleri eriyikten büyütme tekniği ile başarılı bir şekilde üretilmiştir. Ek olarak 94NBT-6BT seramikleri ve çok kristal matriks içine gömülmüş tek kristal çekirdekler katı hal (CS) ve spark plazma sinterleme (SPS) teknikleri ile katı hal tek kristal büyütme çalışması için sinterlenmiştir. Büyütülen kristallerin ve seramiklerin morfolojileri stereo ve taramalı elektron mikroskobu ile karakterize edilmiştir. Elemental analizleri enerji saçılımlı X- ışını (EDX) ve X-ışını fluresans (XRF) metoduyla belirlenmiştir. Tek kristallerin ve seramiklerin kristal fazları X-ışını difraktometresi tekniğiyle belirlenmiştir. 94NBT-6BT tek kristallerin sıcaklık ve frekansa bağlı dielektrik ve sızıntı akımı özellikleri, piezoelektrik ve ferroelektrik özellikleri empedans yük analizörü, LCR metre, d_{33} metre ve AIXACT (aixPES/CMA) piezeoelektrik-ferroelektrik analizörü ile ölçülmüştür.

Anahtar Kelimeler: Tek kristal, piezoelektrik, sodyum bizmut titanat-baryum titanat, karakterizasyon, dielektrik, sızıntı akımı

ABSTRACT

Ph.D. Dissertation

PRODUCTION AND CHARACTERIZATION OF 94NBT-6BT PIEZOELECTRIC SINGLE CRYSTAL MATERIALS

Mevlüt GÜRBÜZ

Anadolu University
Graduate School of Science
Ceramic Engineering Program

Supervisor: Prof. Dr. Aydın DOĞAN
2013, 162 pages

Development of the lead based and lead free piezoelectric single crystals has attracted more attention by various scientists from 1997s to the present due to their perfectly aligned domains. After 2000s, new generation piezoelectric single crystals are more preferred to produce high performance devices due to the rapidly developing electronic technology. However, the use of lead based materials will be prohibited by environmental regulations due to their high volatilization during processing in near future. In recent years, sodium bismuth titanate-barium titanate ($94Na_{0.5}Bi_{0.5}TiO_3$-$6BaTiO_3$) (94NBT-6BT) single crystals considered to be suitable candidate as lead free piezoelectric material because of their strong piezoelectric properties. Recently, considerable research efforts have been devoted to enhance piezoelectric performance of the grown NBT based single crystals. In this thesis, $BaTiO_3$, undoped and Li, Fe, Mn doped 94NBT-6BT single crystals were successfully grown by flux growth technique. Moreover, 94NBT-6BT ceramics and embedded single crystal seed in polycrystalline NBT-BT matrix were sintered by conventional (CS) and spark plasma sintering (SPS) techniques for solid state single crystal growth study. Morphology of the grown crystals and ceramics were characterized by stereo and scanning electron microscopy (SEM). Elemental analysis were performed with energy dispersive X-ray (EDX) and X-ray fluorescence (XRF) methods. Crystalline phase of the single crystals were analyzed by X-ray diffraction (XRD) techniques. Temperature and frequency-dependent dielectric and leakage current properties, and also piezoelectic and ferroelctric properties of the 94NBT-6BT single crystals and ceramics were measured by impedance/gain phase analyzer, LCR meter, d_{33} meter and AIXACT (aixPES/CMA) piezoelectric and ferroelectric analyzer.

Keywords: Single crystal, piezoelectric, sodium bismuth titanate-barium titanate, characterization, dielectric, leakage current

ACKNOWLEDGEMENTS

At the end of my thesis I would like to special thank all those people who made this thesis possible and an unforgettable experience for me.

First of all, I am deeply grateful to my advisor Prof. Dr. Aydın Doğan, who offered his continuous advice, helpful suggestions and encouragement throughout the course of this thesis. I thank him for the systematic guidance and great effort he put into training me in the scientific field.

I would like to special thanks to thesis committee, Prof. Dr. Servet Turan, Prof. Dr. A. Savaş Koparal, Assoc. Prof. Dr. Cem Sevik, and Assist. Prof. Dr. Metin Özgül for their support and helpful suggestions.

I am thankful to Prof. Dr. Erdem Koç and all members of the Ondokuz Mayıs University Mechanical Engineering Department for their support and tolerance. I also want to thank Ondokuz Mayıs University for financial support during thesis.

I am thankful to my friends and colleagues, Dr. Burçak Atay, Dr. Göktuğ Günkaya, Ali Bıyıklı, Nebahat Bıyıklı, Mert Gül, Ayşe Gül Akyürekli, Duygu Yılmaz Çakta, Tayfun Toktaş, Mustafa Bağırgan, Esra Erdoğan, Çağdaş Aslan, Emre Tüfekçioğlu, Aslan Gencer, Erhan Ayas, and Pınar Uyan for the help and support during thesis.

I wish to thank my parents, Ismahan and Hüseyin Gürbüz, Zehra and Adem Uyan, Şerife and Muzaffer Akkan, Sevgi and Fatih Gürbüz, and all family members. Their love provided my inspiration and was my driving force. I am thankful to my wife, Dr. Zuhal Gürbüz, whose love and encouragement allowed me to finish and achieved this thesis.

Finally, I would like to dedicate this work to my nieces İrem Akkan and Sinem Gürbüz. I hope you will do better.

May, 2013

TABLE OF CONTENTS

LIST OF FIGURES

LIST OF TABLES

LIST OF SYMBOLS AND ABBREVIATIONS

PZT: Lead zirconium titanate ($Pb(Zr,Ti)O_3$)

KNN: Potassium sodium niobate ($K_{0:5}Na_{0:5})NbO_3$

NBT: Sodium bismuth titanate ($Na_{0.5}Bi_{0.5})TiO_3$

SBT: $SrBi_2Ta_2O_9$

SBN: $SrBi_2Nb_2O_9$

BZT: Barium zirconium titanate

PMN-PT: Lead magnesium niobate-lead titanate ($Pb(Mg_{1/2}\ Nb_{2/3})O_3$-$PbTiO_3$)

PZN-PT: Lead zinc niobate-lead titanate ($Pb(Zn_{1/2}\ Nb_{2/3})O_3$-$PbTiO_3$)

BT: Barium titanate ($BaTiO_3$)

NBT-BT: Sodium bismuth titanate -barium titanate ($Na_{0.5}Bi_{0.5})TiO_3$-($BaTiO_3$)

NBLT-BT: Li doped sodium bismuth titanate -barium titanate

NBFT-BT: Fe doped sodium bismuth titanate -barium titanate

NBMT-BT: Mn doped sodium bismuth titanate -barium titanate

SSCG: Solid state single crystal growth method

CS: Solid state sintering method

SPS: Spark plasma sintering

ε_r: Dielectric constant

tanδ: Dielectric loss

d_{33}: Piezoelectric coefficient

k_p: Mechanical coupling coefficient

Q_m: Mechanical quality factor

T_c: Curie temperature

P_r : Remanent polarizasyon

E_c : Coercive field

NBT–BKT: Sodium bismuth titanate-bismuht potasium titanate

TSSG: Top seeded solution growth

SEM: Scanning electron microscopy

XRD: X-ray diffraction method

EDX: Energy dispersive X-ray

XRF: X-ray fluorescence spectroscopy

1. INTRODUCTION

Ceramic materials are widely used in the field of communication, energy conversion and storage, electronic and automation technologies due to their electrical, optical and magnetic properties as well as the mechanical and thermal stability. Therefore use of them is increasing day by day. Historical development of electroceramic materials is in parallel with the emergence and development of new technologies. Piezoelectric materials are one of the most popular electro ceramics which are developed depending on new technologies [1]. If piezoelectric materials are classified with respect to the process; the classes are piezoelectric ceramics (lead zirconium titanate, barium titanate), piezoelectric single crystals (quartz, lithium niobate, potassium sodium niobate, etc.), the piezoelectric thin films (zinc oxide, lead zirconium titanate), piezoelectric polymer films (viniylidene floride). These materials are widely used in the field of energy harvesting applications, medical device applications, defense, aviation and aerospace industry, acoustic device applications, sensor technologies, actuator, transducer and generator applications for many years due to its piezoelectric effect [2,3].

Especially lead containing crystal lead zirconium titanate (Pb (Zr, Ti) O_3)-PZT) is widely used for the mentioned application areas due to its superior piezoelectric properties. On the other hand, polycrystal piezoelectric materials do not provide the new technological requirements in today. Because of the fact that fabrication of new generation piezoelectric materials is essential instead of common piezoelctric materials. Since the year 2000, a number of studies have been accomplished about the production of piezoelectric single crystals due to superior piezoelectric properties of lead and lead free systems for the development of high performance devices [4,5]. Examples of lead free piezoelectric materials can be given as potassium sodium niobate $(K_{0:5}Na_{0:5})NbO_3$ (KNN), sodium bismuth titanate $(Na_{0.5}Bi_{0.5})TiO_3$ (NBT), $SrBi_2Ta_2O_9$ (SBT), $SrBi_2Nb_2O_9$ (SBN), barium zirconium titanate (BZT) [6,7]. As an example for lead containing systems, lead magnesium niobate-lead titanate ($Pb(Mg_{1/2}Nb_{2/3})$ O_3-$PbTiO_3$) PMN-PT, lead zinc niobate-lead titanate or lead zirconium niobate- lead titanate PZN-PT, ($Pb(Zn_{1/2}NB_{2/3})$ O_3-$PbTiO_3$) can be given [8,9].

The use of materials containing heavy metals and lead based piezoelectric materials will replace with lead free piezoelectric materials in the near future due to worldwide environmental and legal regulations. Therefore, the number of studies for the production of environmentally friendly lead free piezoelectric single crystal materials is increasing recently. One of the most studied materials is sodium bismuth titanate ($Na_{0.5}Bi_{0.5}$) TiO_3 (NBT) based materials due to their high ferroelectric and the Curie temperature. But the investigations focuced on NBT and its solid solution such as NBT-BT single crytsals are limited and not systematic. Also, reported electrical measurement of grown crystals are quite different even if the same growing method and same composition. Therefore, the resarchers have focused on the fundamental understandig of NBT based single crystals [10].

As a result, especially in the last few years, to meet the expectation of the rapid development of electronic technology and environmental organizations, it is started that lead containing polycrystal piezoelectric materials are replaced by lead free piezoelectric materials and devices with a single crystal structure.

In this thesis, because of these conciderations growth of barium titanate ($BaTiO_3$), sodium bismuth titanate-barium titanate 94($Na_{0.5}Bi_{0.5}$)TiO_3-6($BaTiO_3$), (94NBT-6BT) piezoelectric single crystals using flux growth method were purposed , and the characterization of grown single crystals were performed.

To summarize the thesis presented apart from the theoretical part, the main lines can be grouped under four main headings. The first part consists of the synthesis and characterization of $BaTiO_3$, undoped(pure) and Li, Fe, Mn doped 94NBT-6BT powders with solid state synthesis method. The second part is about the growth and characterization of $BaTiO_3$, 94NBT-6BT single crystals by flux growth method. In the third part, for the production of 94NBT-6BT system via solid state single crystal growth method (SSCG), studies of conventional solid state sintering (CS) and spark plasma sintering (SPS) methods are performed. In the last section, electrical characterization of 94NBT-6BT single crystals and CS/SPS sintered ceramics are performed.

2. GENERAL INFORMATION

2.1. Piezoelectric Materials and Their Properties

Piezoelectric property was discovered as a result of a study performed by Jacques and Pierre Curie in 1880. According to their studies, when the mechanical forces applied on crystals such as quartz, zincblende and tourmaline, it causes generation of electrical charge in these crystals. The concept Piezo is derived from a Greek word “piezein” means compress, pressing. In other words, they are polarized as a result of dimensional changes due to a mechanical or electrical influences; this effect is known as the piezoelectric effect [11,12,13].

If a mechanical stress is applied to some materials, it generates an electrical charge in proportion to the stress or if an electric field applied, a mechanical deformation is occurred. One side of material have negative charge and the other side have positive (Figure 2.1a). This effect because of the electric field or mechanical stress is called as the piezoelectric effect. When a mechanical pressure is applied to the material, the distance between the poles is reduced and the surface electric potential occurs in measurable quantities. Piezoelectric materials have a charge difference due to the remanent pole pairs. Pressure force reduces the distance between the charge centers and creates a voltage. This condition is defined as the direct piezoelectric effect (Figure 2.1b). When the electric field is applied, applied voltage leads to the mechanical deformation at very low levels. Energy arising from mechanical deformation creates a polarization and the electrical energy emerges. This condition is defined as the converse piezoelectric effect (Figure 2.1c). Because of the applied voltage alters the size of the distance between the charge centers, it causes deformation for size and electrical effect is transformed into a mechanical magnitude. The piezoelectric effect is a reversible effect and if applied force is removed, polarization is also removed. Therefore, a piezoelectric property varies depending on the direction. For example, when a compressive stress applied in the direction of quartz (100), there is a polarization, if it is in the direction (001), there is no polarization [14]. Direct and converse piezoelectric effect are referred as in order of generator and motor, and expressed in simple equations given below [15].

$$D = dE + \varepsilon^T E \quad \text{(generator)} \tag{2.1.}$$

$$S = s^E T + dE \quad \text{(motor)} \tag{2.2.}$$

In the equation, D is the dielectrical displacement, S is the strain, T is the stress, E is the electric field, d is the piezoelectric coefficient (inverse of elasticity modulus), s is material compliance and ε is the dielectric constant. The values given in the equations have the properties depending on the direction and defined by subscript as given in Figure 2.2. Piezoelectric coefficient (d) is associated with polarization, and piezoelectric coefficients are indicated with respect to polarization axes. These polarization axes are on the basis of 3 main orthogonal axes and called as 1, 2 and 3 and indicated by 2 sub numbers. The direction of polarization and the direction of the electric field applied are indicated by the first sub number whereas the second sub number indicates the related stress and elongation. For example, definition for d_{33} is that a piezoelectric material having the piezoelectric coefficient polarized in the direction of 3 and also elongation in the direction of 3. Piezoelectric coefficient related with stress perpendicular to the direction of polarization is expressed as d_{31}. In some applications, the electric field can be applied perpendicular to the polarization axis and so this application leads to the shear stresses formation around 2 axis. Elongations or the voltage in these applications is expressed as "15" and given as d_{15}. There is relationship between piezoelectric charge constant d and the piezoelectric voltage constant g as g = d / ε. Here ε refers to the dielectric permittivity of the material [16-19].

The equation above is as follows if it is written as a simple equation based on d.

$$D_3 = d_{33} T_3 \text{ (direct effect)} \tag{2.3.}$$

$$S_3 = d_{33} E_3 \text{ (converse effect)} \tag{2.4.}$$

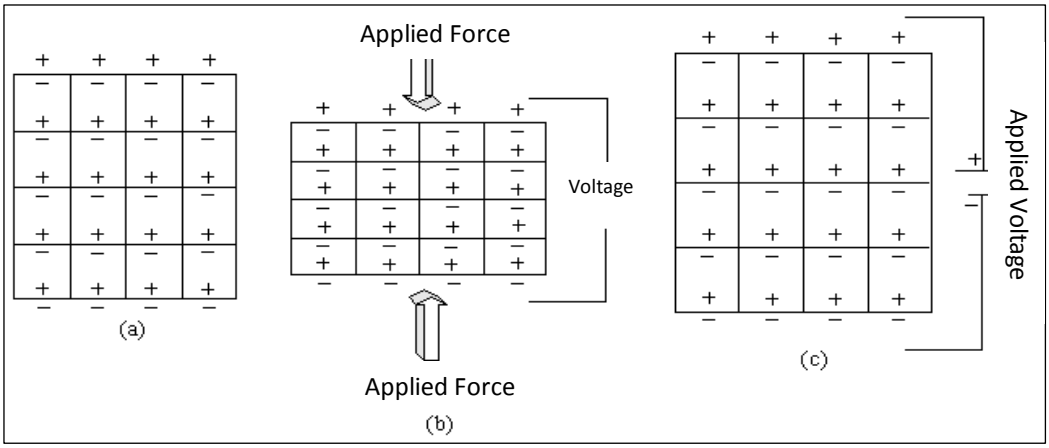

Figure 2.1. The charge difference of piezoelectric materials due to their remanent pole pairs (a), the direct piezoelectric effect (b), the converse piezoelectric effect (c) [19]

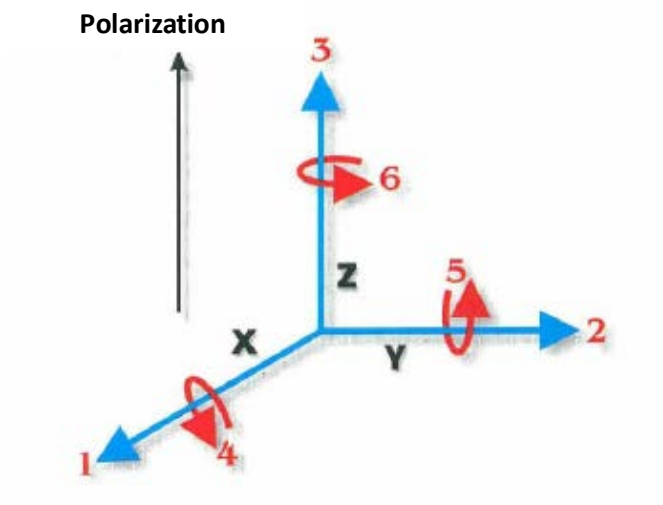

Figure 2. 2. Directions of forces acting on the piezoelectric element [12]

The direct and converse piezoelectric effects mentioned above are occurred if the crystal has no center of symmetry. As an explanation for this, one side of the molecules of crystals is positively and the other side is negatively charged and so these are called as domains. As shown in Figure 2.3a, domains of single crystal materials have the arrangement in one direction (single polar axis). Ceramics generally have the polycrystal structure and these crystals distribute randomly. Therefore, domains in polycrystals align randomly due to randomly distributed grains (Figure 2.3b). This situation negatively affects the electrical

properties of the material. For this reason, polycrystalline ceramics are needed to be polarized to provide the orientation of domains in order to gain piezoelectric property. To do this, polycrystalline materials are heated under the high electric field at specific temperatures to have oriented domains in the same direction (Figure 2.4) [20].

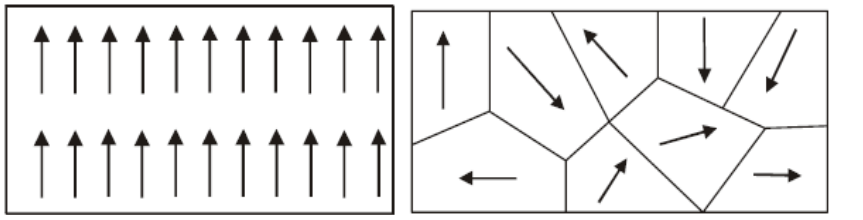

a) Single crystal domain distribution b) Polycrystal domain distribution

Figure 2.3. Domain distribution of (a) single crystal and (b) polycrystal materials [20]

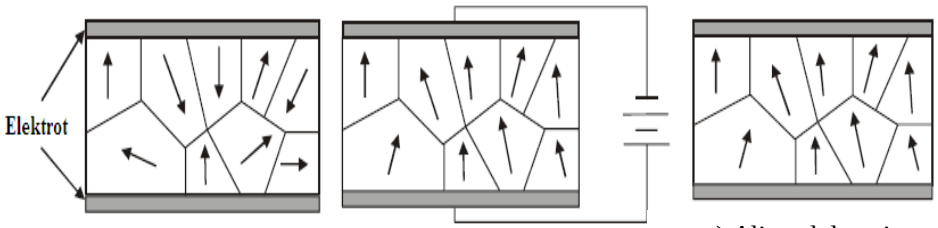

a) Randomly distributed domains b) Polarization c) Aligned domains

Figure 2.4. Alignment of domains to create piezoelectric element [20]

As stated above, there must not be a center of symmetry to have piezoelectric property. For center of symmetry, as if thought that there is line passes through the center of a crystal, it will be observed that there is an intersection observed on the other surface with another line. This symmetry formed by this line is called as center of symmetry and a simple cube can be given as an example. For the structure of tetrahedral, this is not the case and there is no center of symmetry formed. All crystals are divided into 32 different classes, or point groups (Figure 2.5). These 32 sub-groups are divided into seven main sub-systems. These are triclinic, monoclinic, orthorhombic, tetragonal, rhombohedral, hexagonal and cubic. 21 out of 32 point groups have no center of symmetry (prerequisite for piezoelectricity) and 20 of them have piezoelectric properties [11,14].

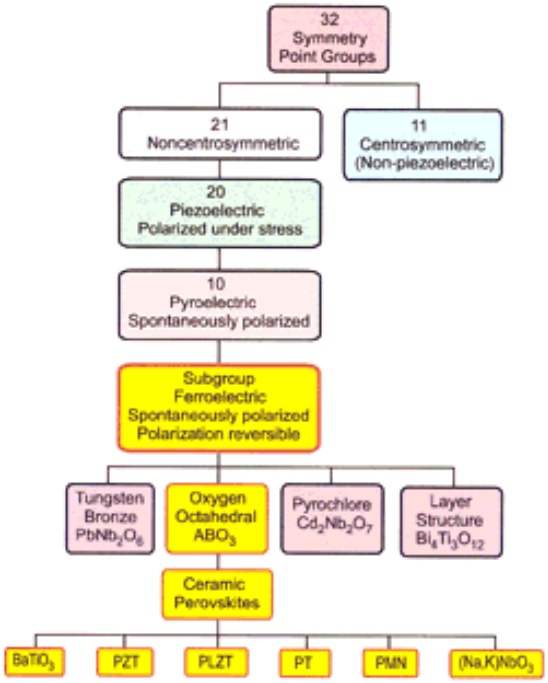

Figure 2.5. The symmetry point groups and electrical properties of sub-groups depending on symmetry [11]

Piezoelectric materials can be classified based on production processes as in Figure 2.6. It is possible to produce the piezoelectric materials, some examples of which are given in figure, as in the form of generally polycrystal, single crystal, thin film and polymer film [21].

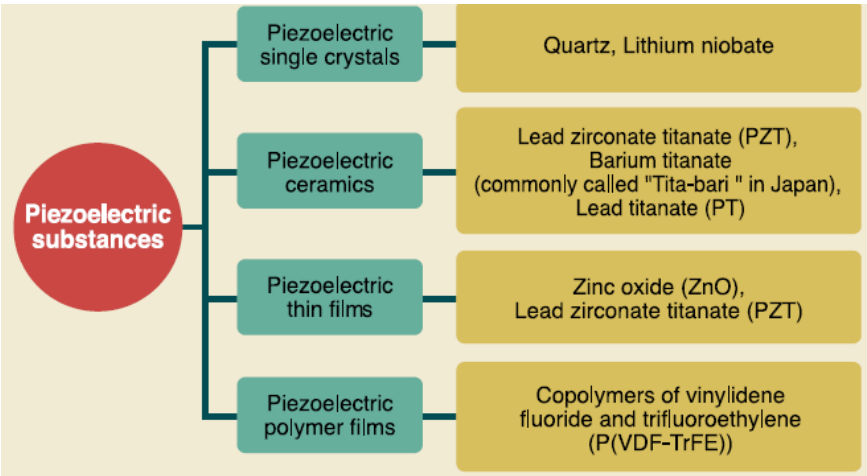

Figure 2.6. General classification of piezoelectric materials [21]

Lead zirconium titanate and barium titanate with perovskite structure are widely used as piezoelectric materials. The general formula for these structures is ABO_3 (Figure 2.7). A simple cube can be seen with large cations located in the edges ('A', Pb, Ba, Ca, K, Na, etc.), smaller cations ('B' Ti, Nb, Mg, Zr, etc.) and oxygen atoms in the center of surface. The best example can be given as $BaTiO_3$ for the structure of ABO_3.

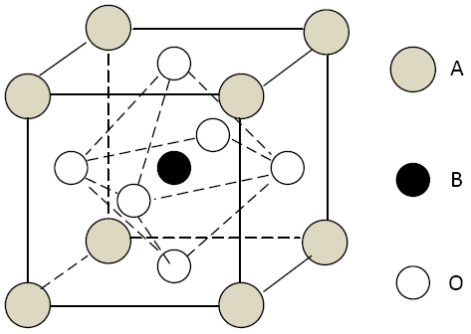

Figure 2.7. Schematic representation of the perovskite structure of ABO_3

Barium titanate has a high dielectric coefficient and shows ferroelectric characteristics. $BaTiO_3$ has the curie (Curie) temperature of 130°C, and it is the first piezoelectric ceramic material developed. The transition temperature can be changed by the addition of dopants to the A and B sides. Cubic-tetragonal and orthorhombic-rhombohedral transitions can be observed at normal operating temperature. But tetragonal-orthorhombic transition takes place close to the normal operating temperature level. Lead, calcium and barium additions result in lowering transition temperature and they are useful for controlling the ferroelectric properties at 0°C [17,19].

Lead zirconium titanate (Pb (Zr, Ti) O_3)-PZT) can be given as an example of ceramics with piezoelectric perovskite structure and it is widely used in practice. PZT ceramics are produced using lead oxide (PbO), zirconium oxide (ZrO_2) and titanium oxide (TiO_2) powder. The PZT structures are formed because of equal divalent Pb^{+2} and four valence Zr^{+4}, Ti^{+4} cations in powders. In other words, PZTs with perovskite structure are obtained from binary system alloys of lead zirconate ($PbZrO_3$) and lead titanate ($PbTiO_3$). It is determined that PZT solid

solution composed of $PbTiO_3$ and $PbZrO_3$ has high piezoelectric properties at morphotropic phase boundary (MPB). Because this boundary is almost independent of temperature, it is possible to obtain high piezoelectric effect. PZT ceramics are approximately twice in terms of piezoelectric properties compared to the barium titanate and due to the fact that they have no phase transformation in a wide temperature range (-50°C to 200°C). So, they are used in place of barium titanate. Phase equilibrium diagram of solid solution of $PbTiO_3$ and $PbZrO_3$ is helpful for the explanation of superior dielectric and piezoelectric properties of PZT. Figure 2.8 shows the equilibrium phase diagram of $PbTiO_3$ and $PbZrO_3$ solid solution. Here, T_c line separates the high temperature paraelectric cubic crystal structure from low-temperature ferroelectric crystal structure. Morphotropic phase boundary (MPB) is divided the ferroelectric field into two regions. The first of these is rhombohedral $PbZrO_3$ with 8 oriented field level along <111> and second is tetragonal $PbTiO_3$ with 6 oriented field level along <100>. Morphotropic phase boundary is obtained if Zr / Ti ratio is 52/48 at room temperature. PZT solid solution has several advantages compared with barium titanate. These advantages can be given as higher electromechanical coupling coefficient, higher Curie temperature and easier polarization of PZT in comparison to $BaTiO_3$ [1,17,19].

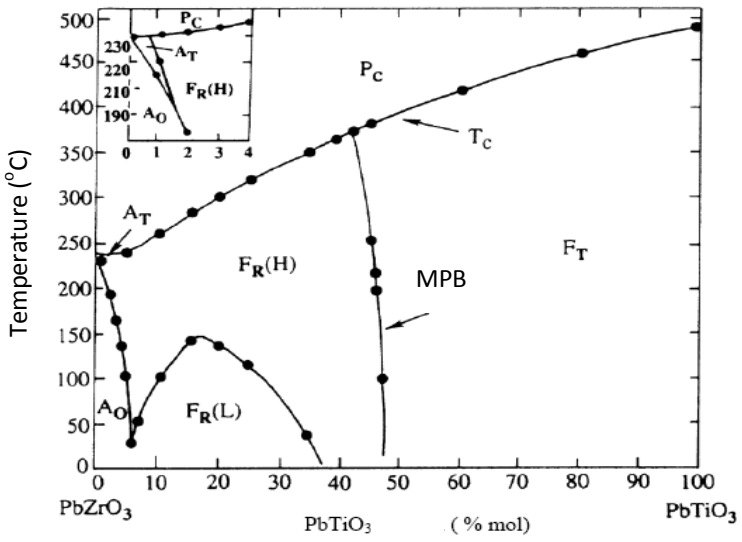

Figure 2.8. Equilibrium phase diagram of solid solution of $PbTiO_3$ and $PbZrO_3$ [17]

Modification of piezoelectric properties of PZT is provided by solid solutions obtained via additives. These additives are called as donor, acceptor, isovalence and multivalence. Donors such as Nb^{+5} (instead of Zr^{+4}) and La^{+3} (instead of Pb^{+2}) can be compensated with cation gaps. They have high piezoelectric coefficient provided because of easy motion of oriented field walls as a result of metal ion gap formation. These PZT solid solutions are called as soft PZT. For acceptor additives, charge of additive cation is lower than replaced ions. For example, Fe^{+3} is replaced with Zr^{4+} or Ti^{+4} and charge imbalance is compensated by oxygen vacancy. This oxygen vacancy causes formation of acceptor-vacancy dipoles and prevents re-organization of domains by these dipoles. Thus, these ceramic known as "hard PZT" are characterized by high coercive field, low piezoelectric coefficients, highly asymmetric hysteresis loop, high mechanical quality factor and low dielectric losses. Isovalence dopant group is composed of Ba^{+2} or Sr^{+2} replaced with Pb^{+2} and Sn^{+4} replaced with B side cations. These aditives prevent the re-orientation of the domains, decrease the Curie temperature and dielectric loss. Multi valence dopants are replaced with Ti^{+4} or Zr^{+4} and operate in the direction of reducing aging effect [17].

As mentioned above, modified piezoelectric materials are used generally in the field of energy harvesting applications, medical applications, defense, aviation and aerospace industry, acoustic device, sensor applications due to their direct and converse piezoelectric effect. Figure 2.9 shows the application fields of piezoelectric materials. To give more specific examples, as indicated in figure, they are used for ignition mechanisms, acceleration, pressure and shock sensors, piezoelectric pump and ultrasonic motors, depth meter, underwater systems, transformers, filters and resonators [21,22].

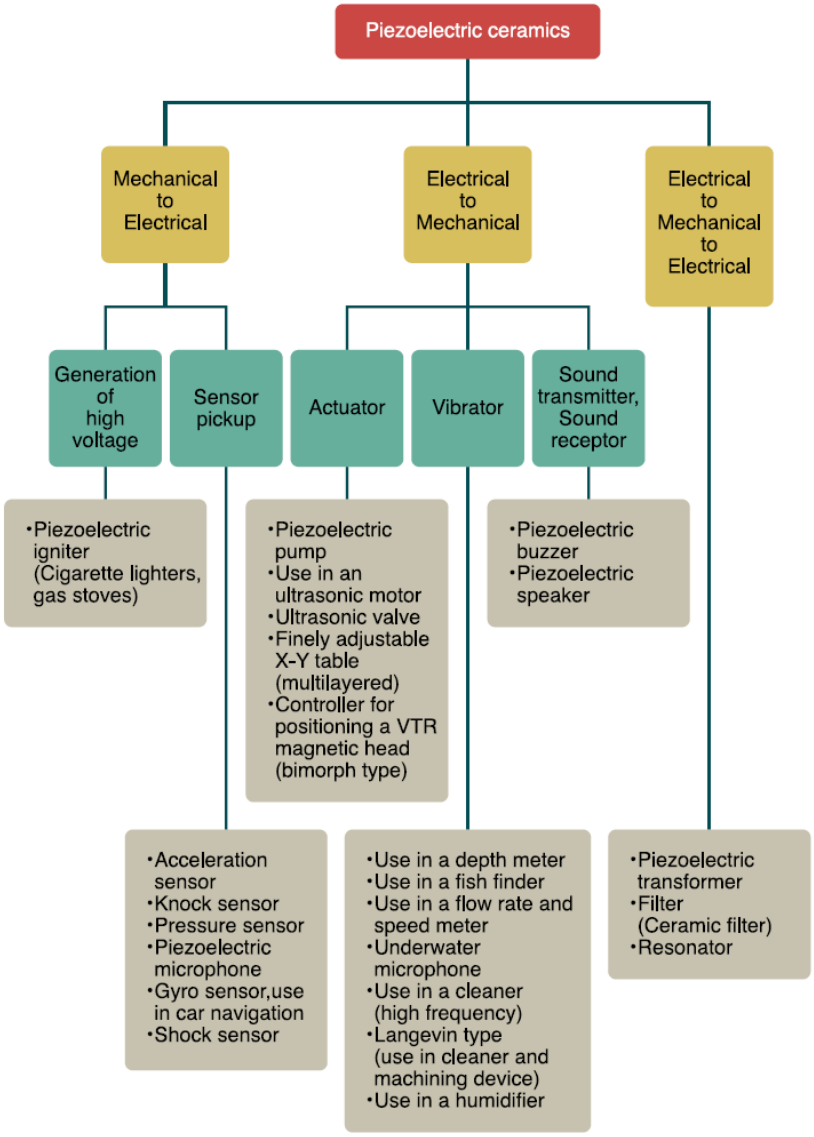

Figure 2.9. Applications of piezoelectric materials [21]

But in recent years, development of new piezoelectric materials with superior properties has became mendatory due to the unavailability of expected performance of piezoelectric materials in the devices. Because of these requirements, the numbers of studies for the development of lead and lead free single crystal piezoelectric materials are increasing each passing day. However, in recent years, studies on lead free single crystal materials has gained speed due to the environmental restrictions and regulations on lead based materials.

2.2. Ferroelectric Properties

Ferroelectric materials are located in a subclass of pyroelectric materials, and also some of the piezoelectric materials show ferroelectric properties at the same time. 10 of 20 units of symmetry point group having piezoelectric property show pyroelectric properties. This group of materials possesses the unusual characteristic of being permanently polarized within a given temperature range. For a ferroelectric classification materials should have a permanent polarization and the change in the direction of polarization is required to be achieved [11,19].

Orientation of domains of ferroelectric material is referred as polarization. When an electric field is applied to a ferroelectric material, domains within the structure are excited and the material are polarized via electric field in the same direction with the field. As can be seen in the Figure 2.10, there are four types of polarization as atomic, ionic, dipolar (molecular, directional) and space charge polarization. Polarization types are closely related with the dielectric constant of the material. Electronic polarization is seen in all dielectric materials. Electrons around the nucleus are switch with the electric field in the direction of positive electrode and so is the nucleus in the direction of negative electrode. With removal of the electric field, they go back to original state. Depending on the electric field, ionic polarization takes place by displacement of anion and cation in the opposite direction. Dipolar polarization is due to the permanent dipole moment. When the electric field is applied, dipoles are aligned with the electric field. If the electric field is removed, the dipoles remain oriented. In the case of space charge polarization, electron or cation travel long-distance path. As result of presence of impurities in the material, charges move in the case of presence of electric field in the interfaces between the phases [23,24].

As shown in Figure 2.11, polycrystalline ferroelectric ceramics have the domains which are separated by 180° and 90° domain walls. As a result of ferroelectric behavior of piezoelectric materials, domain conversions occur because of electric field as well as applied mechanical force. Domains, as stated above, are directed along the electric field. Some domains return back to the original state by the removal of the electric field, whereas some of them do not.

Polarization formed by these domains is defined as remanent polarization (P_r). Polarization value of ferroelctric materials is zero at certain electric field value. This value is called as coercive field (E_c). These values are very important for the characterization of ferroelectric materials [23].

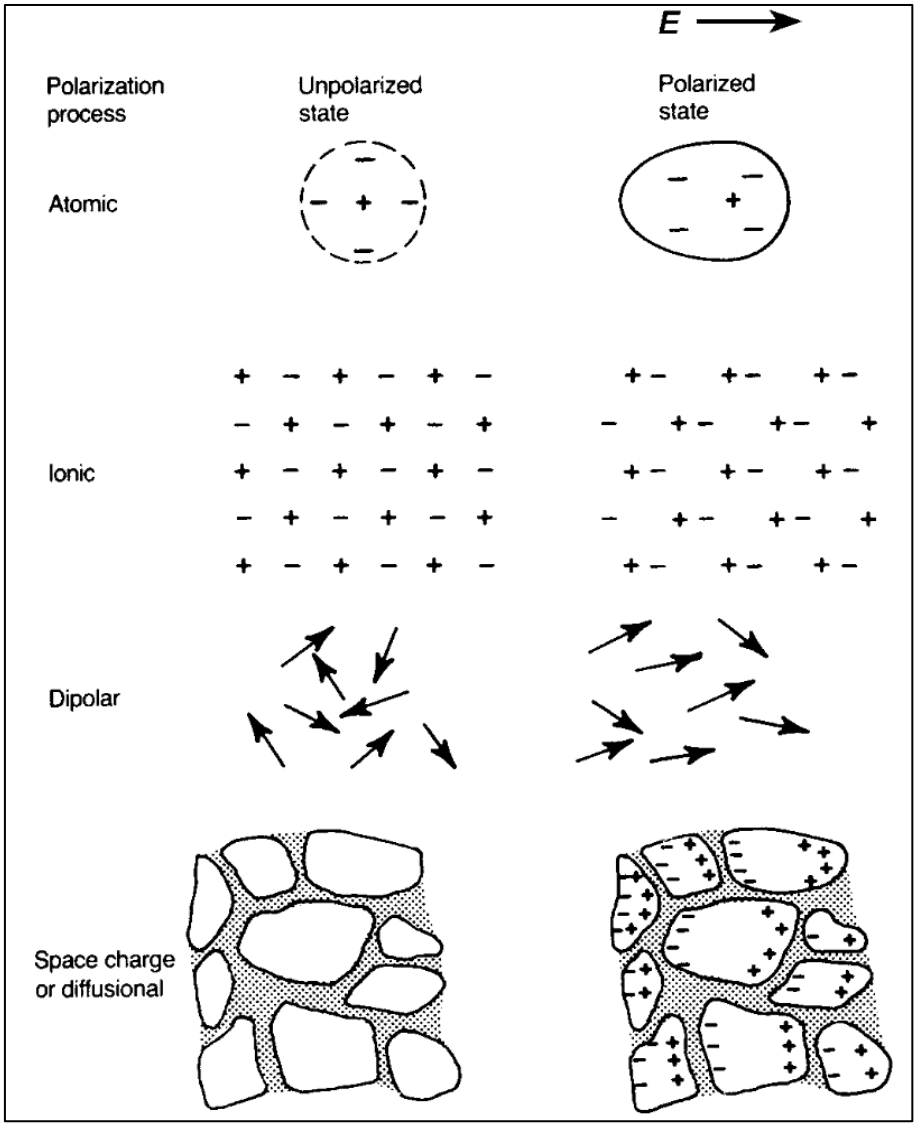

Figure 2.10. Different polarization mechanisms [1]

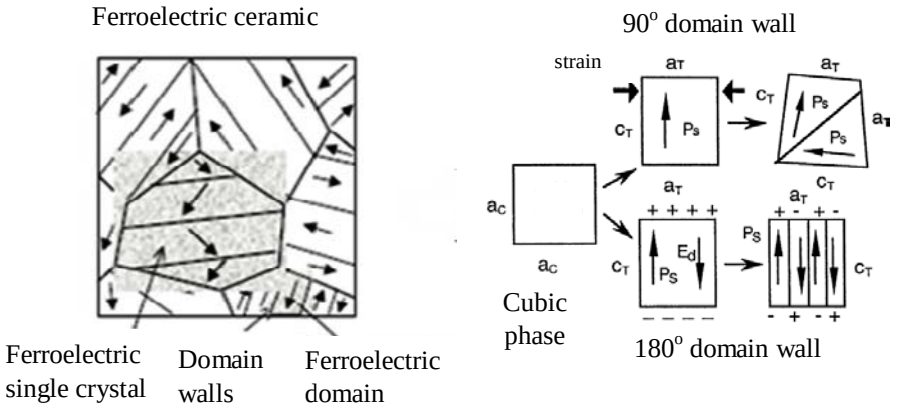

Figure 2.11. Domain and domain walls for ferroelectric materials [25-26]

2.3. Electrical Characterization of Piezoelectric / Ferroelectric Materials

The electrical properties of piezoelectric materials must be known to use them in any application. In general, the dielectric constant (K_T or ε_r) and loss (tanδ), piezoelectric coefficient (d_{33}), mechanical coupling factor (k_p), mechanical quality factor (Q_m) and the curie temperature (T_c) must be known for any piezoelectric material.

Dielectric constant is defined as the charge storage capability of piezoelectric materials or the degree of polarizability of material. Electrons are accumulated on the electrodes by applying voltage to the two conductive parallel plates having distance between them and there is a charge density formed proportional to the electric field. The ratio of the resulting charge density to the electric field is called dielectric constant and calculated by the following formula. Wherein, ε^* is the materials permitivity, ε_o is the permittivity of vacuum, (8.85×10^{-14} F / m) [23].

$$K^T = \frac{Kmaterials}{Kvacuum} = \frac{\varepsilon^*}{\varepsilon_0} \qquad (2.5.)$$

Dielectric loss is the amount of energy lost in the reversible phase of alternating current. This is usually in the form of heat at the time of use. When the alternative electric field is applied to an ideal dielectric material, current is leading

to the voltage as the phase angel of π/2 (90˚). However, at the time of process, the phase angle between current and voltage is not exactly 90˚ and the angle of lag is expressed as δ and the amount of lag becomes tanδ. *K*' represents relative dielectric constant and K'' is defined as relative loss factor [19].

$$tan\delta = \frac{K''}{K'} \tag{2.6.}$$

Electromechanical coupling coefficient (k_{eff}) are used to measure efficiency of conversion of electrical energy to mechanical energy or mechanical energy to electrical energy. In other words effective electromechanical coupling coefficient describes the ability of the ceramics to convert one from energy to another. This coefficient is defined as the material resonance (f_r) and antiresonance frequencies (f_a).

k^2_{eff} = mechanical energy converted to electrical energy / input mechanical energy

k^2_{eff} = electrical energy converted to mechanical energy / input electrical energy

$$k_p \approx \frac{f_a^2 - f_r^2}{f_r^2} \tag{2.7}$$

Mechanical quality factor (Q_m) is a dimensionless unit, and it defines the quality of piezoelectric element as the component of vibration. For the piezoelectric samples, the minimum impedance (Z_m), capacitance (C), the resonance (f_r) and anti resonance (f_a) frequencies are estimated using impedance gain phase analyzer, and Qm value for ceramic elements is calculated using the following formulations.

$$Q_m = \frac{{f_a}^2}{2\pi c Z_m f_r \left({f_a}^2 - {f_r}^2 \right)} \tag{2.8.}$$

For a piezoelectric material, conversion of the mechanical effect to the electrical polarization or electric field to mechanical strain can be defined as piezoelectric coefficient. Because piezoelectric constants are dependent upon electric field and mechanical effect, they are indicated with to subscripts as "dij".

The first subscript gives the direction of the electric field and changes from 1 to 3. The second subscript is the direction of strain obtained and changes from 1 to 6. Piezoelectric constants are derived from the following formulas [15,23].

$$d_{33} = k_{33}\sqrt{\varepsilon_0 K_3^T s_{33}^E} \tag{2.9.}$$

$$d_{31} = k_{31}\sqrt{\varepsilon_0 K_3^T s_{11}^E} \tag{2.10.}$$

Electrical properties of ferroelectric materials are characterized by the hysteresis and butterfly loop. As can be seen in Figure 2.12, when the low electric field is applied, there is a linear relationship between the electric field and polarization. As the electric field increases, randomly oriented domains are directed into the electric field orientation. At the point B, material will be saturated in parallel with the increase of polarization and most of the domains are directed in parallel with the electric field. After saturation, polarization of the ferroelectric crystalline decreases with the reduction of electric field as shown by curve BC. With the removal of electric field, a portion of the domains in the structure revert to their original state whereas the other portion remains as oriented. Therefore, the value of polarization at the point of C is defined as remanent polarization (P_r). Polarization decreases when the direction of electric field is changed and as can be seen from CEF curve it will be saturated again with reach of electric field to a certain value. As can be seen from the curve, the polarization value is zero at the points of E and G. The electric field at this point is called as coercive field (E_c). The resulting curve is called the hysteresis loop [23,27].

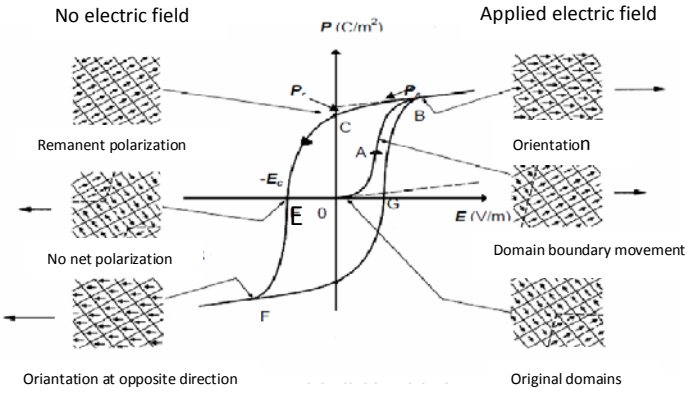

Figure 2.12. Hysteresis loop for ferroelectric materials [23]

In Figure 2.13, the amount of deformation exhibited for ferroelectric material is obtained depending on electric field. As can be seen, depending on the increased field, deformation is increased linearly whereas after a certain value there is no increase observed due to the domain conversions.

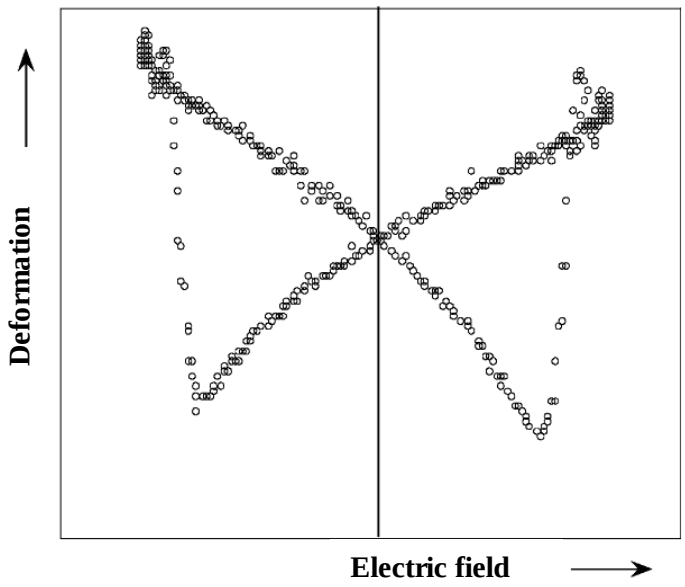

Figure 2.13. Butterfly cycle for ferroelectric materials [28]

3. INNOVATION FOR PIEZOELECTRIC MATERIALS

Chronological development stages of ferroelectric and piezoelectric materials starts from the 1800s and continue to the present day. To summarize in general, in the 1800s, it is discovered that Rochelle salt (sodium potassium tartrate tetra hydrate) have had pyro electric and piezoelectric properties. In the 1940s, capacitors with a high dielectric constant and perovskite barium titanate ($BaTiO_3$) material with the structure of ABO_3 has been developed. In the middle of 1950s, the lead zirconium titanate (Pb (Zr,Ti)O_3-PZT), and at the end of the 1960s, lead lanthanum zirconium titanate (PLZT) structures have been obtained. At the 1970s and 1980s, ferroelectric composites and lead magnesium niobate (PMN) relaxor ceramics have improved. In the 1990s, Moonie and Rainbow has provided the production of ferroelectric films on silicon devices via piezo devices [11].

As noted, lead containing (heavy metal) materials are used in piezoelectric applications. PZT composition consists of approximately 60% lead based materials. Especially after the 2000s, with some of the regulations and institutions in the process of the European Union (Waste Electrical and Electronic Equipment, WEEE, Restriction of Hazardous Substances, RoHS, etc.), there are restrictions on the use of lead based materials because of their toxic effects and evaporation during processing [29].

There are some attempts to develop alternative material systems for PZT systems due to limitations mentioned above. In this field, studies on lead free piezoelectric materials have increased after the year 2000. As examples of lead free piezoelectric materials, potassium sodium niobate ($K_{0.5}Na_{0.5}$) NbO_3 (KNN), sodium bismuth titanate ($Na_{0.5}Bi_{0.5}$) TiO_3 (NBT), barium zirconium titanate (BZT) can be given. As can be seen in Figure 3.1, especially alkali niobium systems and bismuth alkali containing systems are the most widely studied systems [30,31].

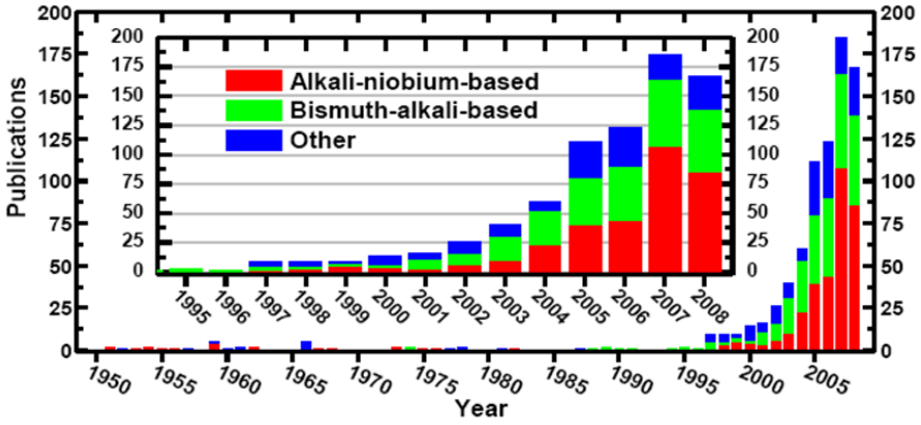

Figure 3.1. Number of publications by year related with lead-free piezoelectric materials [30]

In addition to the prohibition of lead, when electrical properties of poly crystal lead free ceramics compared with PZT systems, it is observed that the desired electrical properties is not satisfied. For this reason, ever since the late nineties, studies related with the development of piezoelectric single crystal as well as polycrystal piezoelectric materials has been accelerated. Especially today, PMN-PT, PZN-PT, NBT and KNN-based single crystal materials are widely studied. However, the prohibition of the use of lead made it necessary to study of lead free piezoelectric single crytstal materials [11]. Very recent studies on lead-free polycrystal and single crystal piezoelectric materials are summarized below.

3.1. Lead Free PolyCrystal Piezoelectric Ceramics

Because of excellent piezoelectric properties of lead based lead zirconium titanate structure, they are widely used in different areas. This feature is explained by the closeness of composition to the morphotropic phase line. However, due to the toxicity of lead oxide is limited in some applications. Especially, lead oxide evaporation during processing, accumulation of lead in environment and organisms cause damage to the brain and nervous system. Some of performed studies have confirmed the lead transfer (leakage) from PZT to water in the case of PZT left into water. Because of these reasons, the studies are directed to the new lead free systems with excellent piezoelectric characteristics [32-33].

One of the lead free piezoelectric materials is alkali niobate ($KNbO_3$, $NaNbO_3$, $KNaNbO_3$) systems. $KNbO_3$ ceramics displays the phase transition similar to that of barium titanate structure. Transition occurs from cubic structure to tetragonal at 435^oC'de, from tetragonal to orthorhombic at 225^oC and from orthorhombic to rhombohedral at -10^oC. All of tetragonal, orthorhombic and rhombohedral phases are ferroelectric. Potassium niobate systems have weak piezoelectric effect. Therefore, $KNbO_3$ and $NaNbO_3$ solid solutions have better piezoelectric property depending on the composition (d_{33} = 160 pC/N). Dielectric constant has been found as 400 at room temperature. The main disadvantage of these systems with the conventional sintering methods, production of fully dense ceramics cannot be achieved. One of the reasons for this case is that the phase stability is very limited. Phase stability is 1040^oC for $KNbO_3$, while 1140^oC for potassium sodium niobate. Therefore, high temperature sintering is not possible. In addition, even if very little change in the composition structure causes the formation of new phases. Sintering temperature for $KNbO_3$ is in between 950 and 1030^oC and so is for ($K_{0.5}Na_{0.5}$) NbO_3 (KNN) in between 1090 and 1120^oC. So far, pure $KNbO_3$ system has theoretical density of 90-95% (4.62 g/cm^3), but the same theoretical density is not eligible for KNN (4.51 g/cm^3) [31-33].

As an example for other lead free piezoelectric ceramics, ($Na_{0.5}Bi_{0.5}$)TiO_3 (NBT) can be given. Due to high Curie temperature (T_c = 320^oC) and strong ferroelectric feature at room temperature, it is a candidate material to be one of the lead free piezoelectric materials. However, evaporation and volatility of Bi ions is higher for sintering at the temperature above 1130^oC. Therefore, it is difficult to polarize this material due to the high conductivity. In order to eliminate these problems; additives such as La, Li, K, Zn, Nb, Mg and Zr additives are used for the improvement of NBT system. Recently, it is determined that sodium bismuth titanate, among these solid solutions, potassium bismuth titanate (1-x) $Bi_{0.5}Na_{0.5}TiO_3$-x$Bi_{0.5}K_{0.5}TiO_3$ (NBT-BKT) system has an increase for electromechanical properties at morphotropic phase boundary when x = 0.18. However, in many practical applications, piezoelectric properties of this system are not sufficient. Therefore, the new NBT based ceramic systems need to be developed [34].

Because of high ferroelectric properties that they owned; $SrBi_2Ta_2O_9$ (SBT), $SrBi_2Nb_2O_9$ (SBN), $SrBi_4Ti_4O_{15}$ (SBTI), some of lead free bismuth based perovskite structured materials, are being studied as an alternative to PZT. SBT oxides are usually prepared by grinding and calcination of carbonates and oxides. However, this method has some disadvantageous due to lack of homogeneity, high impurity and continuously repeated processes. In addition, high temperature treatment as a result of solid state reaction of these systems is not suitable in the sense of ferroelectric properties. Synthesis of powder at high temperature caused the formation of undesirable phases, and this adversely affects the electrical properties. It is clear that novel synthesis methods such as combustion synthesis are necessary due to the being of this process used for this time consuming and the need for high energy. It is possible that very reactive and homogeneous powders can be produced using this method at faster rates and desired stoichiometry. However, there are some drawbacks such as very low production rate, expensive raw materials to be used because of soluble salts contents of the materials used in the process and the releasing of toxic gases during the production [35].

Results of studies in the literature related with electrical characteristics are summarized in Table 3.1. As can be seen in the table, in general, piezoelectric coefficient of lead free piezoelectric materials is lower, and electromechanical coupling coefficient are almost close to lead based materials. It obvious from the results of studies conducted that the lead containing materials still have higher results than lead free systems.

Table 3.1. Comparison of lead free piezoelectric materials with lead based systems

Materials	**T_C (^oC)**	**d_{33} pC/N**	**$k_{t\ (\%)}$**	**$k_{p\ (\%)}$**	**ε_r**	**tanδ**	**Q_m**
$BaTiO_3$ [36]	115	190	-	36	1700	0.005	-
PZT 5H	-	620	43	65	-	0.027	72
PZT 4 [36]	328	289	58	-	1300	0.004	-
PZT802	-	215	39	-	-	-	-
PZT552 [37]		580	51				
$(Na_{0.5}K_{0.5})NbO_3$ (NKN) [38]	460	200	45	-	-	-	-
$(Na_{0.5}K_{0.5})NbO_3$ (NKN) [39]	-	160	-	45	420	0.014	-
(NKL)$(Sb_{1-x}Nb_x)O_3$ NKL: Na,K,Li [40]	397	230	7	37	612	0.026	520
$KNbO_3$ [41]	-	98	48	17	-	-	-
$(K_{0.5}Na_{0.5})0.97Li_{0.03}(Nb_{0.9}Ta_{0.1})O_3$ (KNLNT) [42]	>300	245	42	-	890	-	-
$K_{0.5}Na_{0.5}NbO_3$-$LiTaO_3$ [36] KNN-LT	320	230	-	51	1256	0.016	-
$0.90(Bi_{1/2}Na_{1/2})TiO3$-$0.05(Bi_{1/2}K_{1/2})TiO_3$-$0.05BaTiO_3$ (BNT-BKT-BT5) [37]	-	150	49	-	-	-	-
BiNT-BiKT-BT: $Bi_{0.5}Na_{0.5}TiO_3$-$Bi_{0.5}K_{0.5}TiO_3$-$BaTiO_3$	301	191	-	33	1141	-	84
SBTT3(0.3): $Sr_{0.3}Bi_{3.7}Ti_{2.7}Ta_{0.3}O_{12}$ [36]	540	14.6	-	4	188	0.016	1243
$(1-x)(Na_{0.5}K_{0.5})NbO_3$–$xBiAlO_3$ (NKN–BA) [43]	372	202	-	46	-	-	-
$(Bi_{1/2}Na_{1/2})TiO_3$ $Ba(Ti,Zr)O_3$ (BNT-BZT) [44]	244	147	-	-	881	0.026	-
$Bi_{0.5}(Na_{1-x-y}K_x\ Li_y)0.5TiO_3$ (BNKLT) [45]	-	231	50.5	41	-	-	-

Apart from the mentioned studies; the study performed by Saito and colleagues on the composition of KNN is best in the literature. From Figure 3.2 and Table 3.2, it is obvious that significant results comparable with PZT are observed from the study. As can be seen, modified KNN based systems (LF4T)

have piezoelectric coefficient, Curie temperature and electromechanical coupling factor are almost the same as PZT based materials [46].

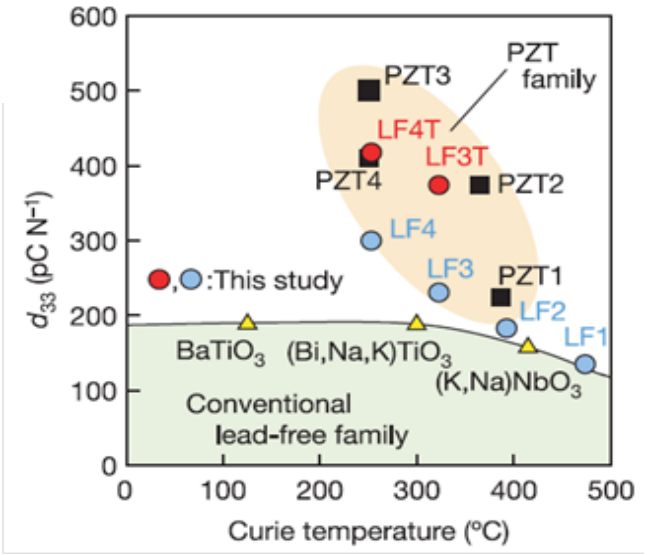

Figure 3.2. Comparison of piezoelectric coefficient of lead free materials with that of PZT [46]

Table 3.2. Comparison of electrical properties of modified KNN piezoelectric material with PZT4 material [46]

Properties	**LF4T (Modified KNN)**	**PZT4**
Curi Temperature (^{o}C)	253	250
Piezoelectric coupling coefficient (k_p)	0.61	0.60
Piezoelectric coefficient (d_{33}) (pC/N)	416	410
Piezoelectric voltage constant(g_{33}) (10^{-3}Vm/N)	29.9	20.2
Dielectric constant	1570	2300

As a result, the polycrystal lead free piezoelectric materials are still produced with high performance. Moreover, the production of single crystal lead free piezoelectric materials instead of polycrystal is the subject of future studies.

Production of high performance lead free devices and lead free single crystal having higher electrical properties are the main subject for future trend.

3.2. Piezoelectric Single Crystal Materials

Studies on the production of single crystal piezoelectric materials is one of the major field today due to the need for faster movement, higher temperature limits, a longer service life and high performance in many application in which piezoelectric materials are used. Single crystal piezoelectric materials are started to be used instead of polycrystal structures because of their desired piezoelectric properties and excellent domain orientation. By fabrication of single crystal materials, applications such as acoustic, optical, wireless communication, actuator, diagnostic and therapeutic medical devices are also improved. In addition, as can be seen in Figure 3.3, a lot of company (American Piezo Comp., Ceracomp, etc.) experienced in piezoelectric materials are planning their research and development activities on the production of high performance devices using single crystal piezoelectric materials. In addition, developmental scheme for the future piezoelectric materials are given in Figure 3.3. As can be seen here, today, polycrystal ceramic materials cannot provide the required performance for the devices. For this reason, the production of high performance devices by the use of single crystal and further that of lead free devices by the usage of lead free single crystalline are the main goals of the studies. In Figure 3.4, the stages in the development of materials by the years can be seen. Especially in the 2000s, due to high electrical properties, single crystals containing lead (PMN-PT and PZN-PT) are used, whereas nowadays due to environmental restrictions, lead-free piezoelectric single crystal has been studied intensively [47-48].

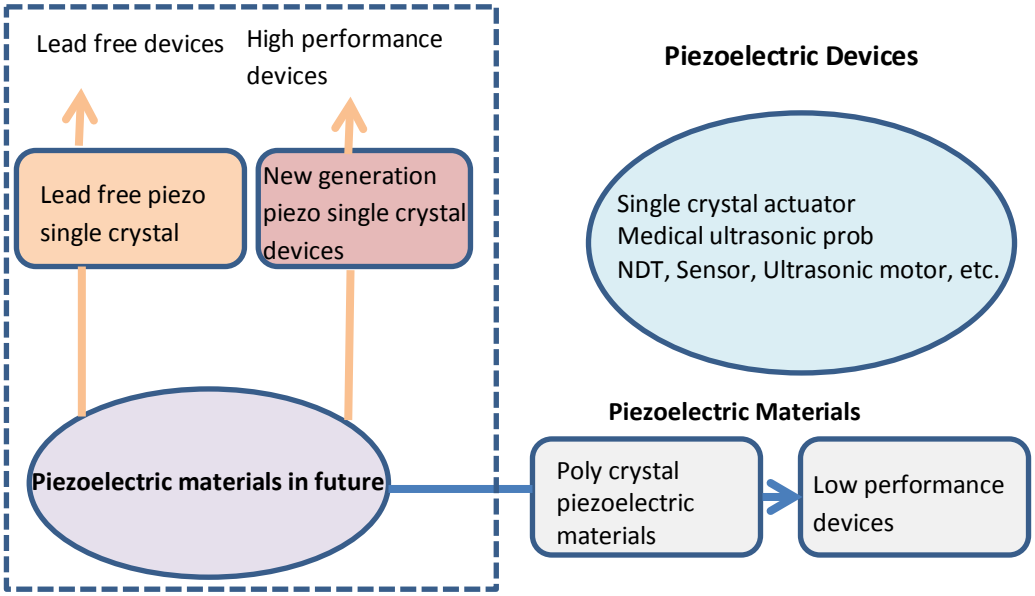

Figure 3.3. Developmental scheme for the future piezoelectric materials [48]

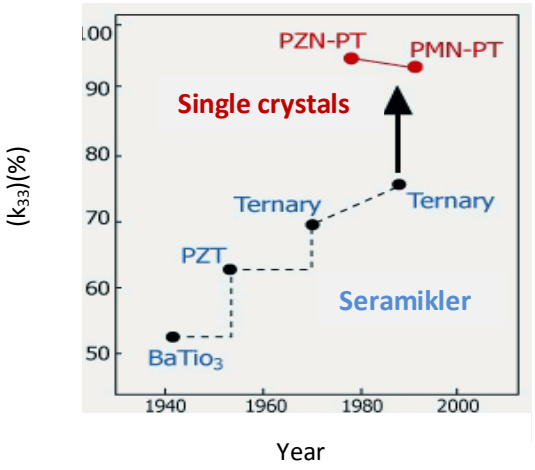

Figure 3.4. Developmental stages of electromechanical coupling coefficient of piezoelectric materials [48]

Properties of $BaTiO_3$, $(NKL)(SB_{1-x}Nb_x)O_3$ lead free piezoelectric materials, PZT-5H polycrystal piezoelectric material and PMN-PT relaxor-PZT single crystals are compared in Table 3.3. PMN-PT and relaxor-PZT (CeraPSC) single crystals have higher dielectric constant, piezoelectric coefficient and electro mechanical coupling coefficient than $BaTiO_3$, (NKL) $(SB_{1-x}Nb_x)O_3$. For this reason, it is preferred as an alternative to common PZT. In addition, it is observed that lead free polycrystal piezoelectric structures do not have the properties of

PZT and also single crystal structures. But, it is observed that the PMN-PT single crystal systems have lower T_C, T_{RT} and E_C than PZT-5H (polycrystal) and relaxor-PZT single crystal systems. Low T_C and E_C cause depoling during operation and, low T_{RT} narrows the application temperature. For the purpose of making single crystal such as PMN-PT and PZN-PT have high piezoelectric coefficient, high electromechanical coupling factor and high dielectric constant value as well as much higher T_C, T_{RT} and E_C, relaxor-PZT single crystals are improved via SSCG technique. Thus, in the case of comparison of single crystal relaxor-PZT with single crystal PMN-PT and PZN-PT systems, all of its properties are higher and it has the ability to be used at high temperature applications [36,40,49]

Table 3.3. Comparison of the electrical properties of PMN-PT single crystals, relaxor-PZT single crystals, lead-containing and lead-free piezoelectric materials.

	$BaTiO_3$ [50,49]	**$(NKL)(Sb_{1-x}Nb_x)O_3$ Lead free piezo** [40]	**PZT-5H Polycrystal**	**PMN-30PT Single crystal (001)**	**CeraPSC2-1 Relaxor-PZT Single crystal (001)**	**CeraPSC2-1 Relaxor-PZT Single crystal**	
						(001)	**(110)**
Dielectric Constant [$\varepsilon_{33}^T/\varepsilon_o$]	1700	612	3500	5000	6500	6000	5000
Dielectric Loss [tanδ, %]	0.005	0.026	<2	<0.5	<0.5	<0.5	<0.5
Curie Temperature [T_C,°C]	115	397	190	145	200	200	200
Romb-Tet. Phase Trans. Temp. [T_{RT}, °C]	-	-	190	90	105	120	120
Coupling coefficient [k_{33},%]	36	37	75	90	92	90	90
Piezoelectric constant [d_{33},pC/N]	190 d_{15}=270(çk) d_{15}= 587(tk)	230	600	1500	2000	2000	-
Coercive Field [E_C,kV/cm]	-	-	8.5	2.5	5.5	5.5	5.5

Studies on lead containing and lead free piezoelectric single and polycrystal structures are compared at Table 3.4. As can be seen in the Table, lead magnesium niobate-lead titanate, PMN-PT ($Pb(Mg_{1/2}NB_{2/3})O_3$-$PbTiO_3$), lead zinc niobate-lead titanate or lead-zirconium niobate- lead titanate PZN-PT, ($Pb(Zn_{1/2}NB_{2/3})O_3$-$PbTiO_3$) are examples of such piezoelectric single crystal materials. The reason for the preference of single crystal piezoelectric material instead of common polycrystal lead zirconium titanate (PZT) is that it has high

dielectric constant, piezoelectric and the coupling coefficient. In general, the piezoelectric coefficient and electromechanical coupling factor are 2000-2500 pC/N, 60-90%, respectively. These values are quite high as compared to that of common PZT. However, the use these materials is restricted because of the fact that Curie temperature (T_C), phase transition temperature from rhombohedral to tetragonal structure (T_{RT}) and the coercive electric field (E_C) are low. Therefore, T_C, T_{RT} and E_C are required to be higher than that of piezoelectric single crystals. For this subject, PYbN-PT, PIN-PT and $BiScO_3$-$PbTiO_3$ crystals particularly with high T_C are produced by some researchers but crystal size are not higher than a few millimeters. In addition, the quality of the crystals obtained is not homogeneous. PMN-PT and PZN-PT single crystal piezoelectric structures are considered as candidates in the future for the use for high performance medical ultrasound imaging probes, sonar in order for underwater communication, high precision sensor and actuators due to their high electrical characteristics [50-52].

But today, the restrictions on the use of lead will stop the production of these materials. For this reason, the importance of lead free single crystal materials has increased. As can be seen in the Table, because of the restrictions on the use of lead in the future, there is a rapid increase for studies related with the development of lead free piezoelectric materials. Materials such as potassium sodium niobate $(K_{0.5}Na_{0.5})NbO_3$ (KNN), sodium bismuth titanate $(Na_{0.5}Bi_{0.5})TiO_3$ (NBT), $SrBi_2Ta_2O_9$ (SBT) or $SrBi_2Nb_2O_9$ (SBN), barium zirconium titanate (BZT) can be given as examples for lead free piezoelectric materials. These materials are preferred due to the high ferroelectric properties and high Curie temperature, whereas their piezoelectric properties are lower than the lead containing systems due to their alkali evaporation, low density and hard poling(high conductivity [44,46]. Recently, Fe, Mn, Zr doped NBT-BT based structures have similar properties with that of PZT. Especially at nearly morphotropic phase boundary, d_{33} value is 283 and 360 pC / N and it is reached the value of 483 pC/N with the addition of Mn. Also k_p value (> 50%) is high as comparable with that of PZT. Dielectric properties are also very close to that of some PZT composition [62].

Table 3.4. Comparison of polycrystal and single crystal piezoelectric materials

	Materials	T_C (°C)	d_{33} pC/N	$k_{p(\%)}$	ε_r	tanδ	Q_m
POLYCRYSTAL MATERIALS	$BaTiO_3$ [36]	115	190	-	170	0.00	-
	PZT 4 [53]	328	289	71	1300	□.004	-
	PZT 5H [50]	190	600	75	3500	0.02	-
	PZT 8 [53]	300	225	64	1000	0.004	-
	PZ 54 [53]	225	500	71	2500	0.004	-
	BNT [54]	310	64	-	302	-	-
	94BNT-6BT [54]	288	122	-	625	0.013	-
	BNT-BT (Mn katkılı) [54]	243	160	-	2300	-	-
	BNT-BT(Zr katkılı) [54]	244	147	-	8814	-	-
SINGLE CRYSTAL MATERILAS	PZN-PT [55]	-	3000	-	6670	0.0049	-
	PZN-4.5PT [56]	166	2200	94	8000	0.01	50
	PMN-30PT [50]	□□5	1500	90	5000	0.005	-
	PMN-28%PT [57]	125	1900-2100	9□-92	4500-5500	<0.01	-
	PMN-30%PT [57]	135	2200-2500	92-94	7500-9000	<0.01	-
	PMN-33%PT [57]	166	2820	94	8000	<0.01	-
	PMN-PT-Epoxy 1-3 Kompozit [58]	-	1030	90.1	2300	-	10.39
	$BSPT66\ (1-x)BiScO_{3-x}PbTiO_3$ [59]	460	200	73	-	0.5	-
	$Pb(In_{1/2}Nb_{1/2})O_3$-$PbTiO_3$ (PIN-PT) [60]	>250	700	78	-	-	-
	$(NKL)(Sb_{1-x}Nb_x)O_3$ [40]	397	230	37	612	0.026	-
	$[Bi_{0.5}(Na_{1-x}K_x)_{0.5}]TiO_3$ [61]	365	160	-	-	-	-
	$0.96Na_{0.5}Bi_{0.5}TiO_3$–$0.04BaTiO_3$ [62]	310	283	50	1230	0.018	-
	$0.94Na_{0.5}Bi_{0.5}TiO_3$–$0.06BaTiO_3$ [62]	305	360	62	-	-	-
	Mn katkılı Na0.5Bi0.5TiO3–BaTiO3 [62]	320	483	56	1090	0.019	-

As a result, the studies planned at future for the production of piezoelectric single crystals can be summarized briefly as follows.

A) Production of new piezoelectric single crystals

- Production of piezoelectric single crystals with high T_C and Q_m
- The development of doped PMN-PT single crystals
- The development of tetragonal PMN-PT single crystals
- The development of PZT based single crystals

B) The production of lead free piezoelectric single crystals

- The development of NBT-BT single crystals
- The development of KNN single crystals

C) Production of new piezoelectric single crystals using SSCG method

D) The development of single crystal composites

E) The development of piezoelectric devices using piezoelectric single crystal and composites

- Piezoelectric single crystal actuators
- Piezoelectric single crystal sensors
- Piezoelectric single crystal transducers

However, as indicated above, due to the restrictions on the use of lead, they are replaced by alternative materials such as lead free KNN and NBT and devices produced by the use of these materials in the future. Especially in recent times, due to the fact that results of NBT based studies are the alternative for that of PZT, and so studies on this material is accelerated.

4. SINGLE CRYSTAL PRODUCTION METHODS

Grain boundaries of polycrystal materials have adverse effect on mechanical, physical and electrical properties. For this reason, single crystal material production is important for some application without grain boundary. Single crystal materials are used for many optical and electronic applications because of their superior properties better than that of polycrystal materials. Growth of these materials as single crystal material depends on melting temperature, the desired composition, crystal structure of the material and the desired properties for the application. Crystal growth techniques for the materials are determined by their characteristic phase diagram. Figure 4.1 shows the fields in which the single crystalline material used at the 2000s. As can be seen in this figure, semiconductor materials such as silicon (Si), gallium arsenide (GaAs), indium phosphate (InP), gallium phosphate (GaP) have a large market share. [63].

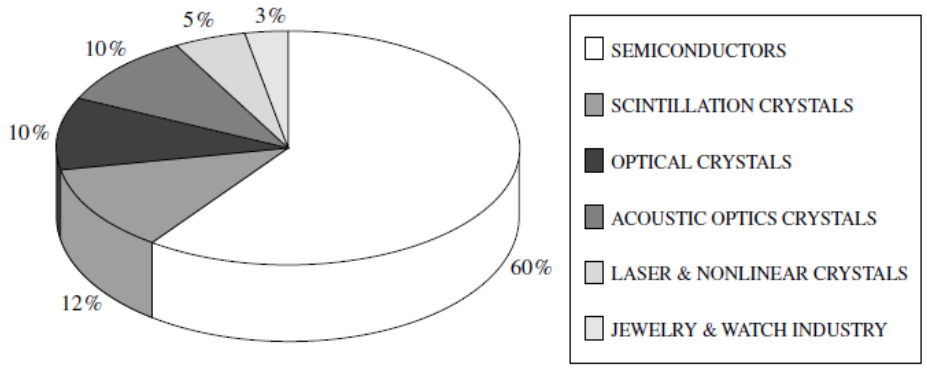

Figure 4.1. Single crystal material applications and market shares for 2000s [64]

From optical and electronic applications, it is observed that single crystal materials are used commonly. Especially in the semiconductor industry, silicon single crystals are being growth up to 20 cm diameter. Single crystal sapphire materials are used for laser applications. Turbine blades are produced as single crystal for metallic materials at high temperature applications. Czochralski method is preferred in particular among the common methods. In recent years, because of the preference of single crystal materials due to their superior

properties in piezoelectric applications, single crystal growth studies are performed, details of which is given below [63,65].

4.1. Growth of Single Crystal Materials and Theory

Production of a single crystal material is often very difficult and much more expensive than polycrystal materials. Quality of produced crystal varies depending on impurity and production conditions. In general, growth of crystal has stages of transformation from gas or liquid to solid or from liquid to solid. Atomic structures of liquid have random sequence, but they are transformed into regular structure during crystal growth [1].

The most important factor determining the crystal growth of material from the melt is the phase diagrams of the material. For growth of crystal from melt, congruently and incongruently melting of material or decomposition of all material without melting is the most important point to be considered. In an ideal case, the material melts congruently and crystal grows via solidification of melt. On the other hand, if material melts incongruently, crystal and melt will have different compositions and thus, composition of mixture should be adjusted carefully to have high quality single crystal production. The growth rate for this type of melting is very slow. If the crystal decomposes without melting, crystal growth is provided by using another fluxing agent which have lower melting point or vapor phase [66].

Single crystal production is a difficult process. It can be explained by general principle of thermodynamics given below. Growth of single crystal is a reversible process under isothermal conditions and Gibbs energy G must be constant [1].

$$\Delta G=0=\Delta H-T\Delta S \qquad (4.1.)$$

Where, H is enthalpy, S is entropy, and T is the thermodynamic temperature. Thus the formula is as follows.

$$\Delta S=0=\Delta H/T \quad (4.2.)$$

If $\Delta H = L_a$ (L_a is a latent heat for every single atom), Jackson dimensionless parameter α is determined by the following equation. For equation, k is the Boltzmann constant, T_{CR} is the temperature of the change of state, and α is the decrease of entropy for transition from disordered structure in liquid state to a regular lattice structure of the solid state [1].

$$\alpha = \Delta S/k = L_a/kT_{CR} \quad (4.3.)$$

If α <2, the crystal grows without any direction (facet) and the shape of it is defined by the melt isotherm. Many metals such as iron and lead are included in this category. When 2< α <10, it covers bulk material and the formation of direction is observed. Germanium and silicium are given as examples for single crystal growth. If α > 10, it is observed that there is an easy nucleation and it is difficult to avoid the formation of polycrystal structure. For the growth of ice from water vapor, α = 20 at 0°C. At this value, there is snow formation with very low density and polycrystal feature. On the other hand, when α = 2.7, large crystals are formed for growth of high density ice from water [1].

A driving force for the start of crystal formation and growth is required. Heat and mass transfer are effective for the driving force and the degree of influence depends on the phase of the media. Equilibrium is reached when heat and mass transfer is zero between the interface of two phases of the starting material and the product. In this case neither growth nor dissolution of crystal takes place. Because of this reason, it is required to diverge from equilibrium. In this case the degree of divergence from equilibrium depends on the driving force and at his point there is a growth or dissolution at the interface between the ambient phase and crystal [67].

The degree (S) of driving force for crystal growth from vapor phase is expressed as follows. Where, p_∞ is the equilibrium vapor pressure and p is the growth pressure.

$$S = p/p_\infty \quad (4.4)$$

For the solution growth, the driving force is related with the difference between concentration at the equilibrium temperature and at the growth temperature as explained below [67].

$$\Delta C = C_{\infty} - C \tag{4.5.}$$

For growth from melt, driving force is defined as the difference between equilibrium temperature and the growth temperature as given by the equation [67].

$$\Delta T = T - T_{\infty} \tag{4.6.}$$

Degree of driving force can be generalized by the difference of chemical potential between the two phases indicated in the following equation [67].

$$\Delta\mu = \mu^{(g)} - \mu_{\infty}^{(g)} = \mu^{(g)} - \mu_{\infty}^{(c)} \tag{4.7.}$$

Where, $\mu^{(g)}$, $\mu_{\infty}^{(g)}$ ve $\mu_{\infty}^{(c)}$ define chemical potentials of super saturated vapor, saturated phase and the solid phase, respectively. Here, the general driving force can be explained as shown by the following equation. In the equation, k is the Boltzmann constant and T_B is the absolute temperature. For crystal growth driving force is associated with $\Delta\mu/kT$ [67].

$$\Delta\mu = kT_B ln(p/p_{\infty}) = kT_B lnS \tag{4.8.}$$

As seen in the comments, driving force is associated with chemical potential as well as heat and mass transfer. Condensation process is required for the phase of diluted media and mass transfer is effective. Heat transfer plays an important role for the crystallization at melt-like condensed phase [67].

Crystal growth process can be analyzed in three stages. The first of these is being of super saturated or super cooled state in the presence of driving force. Second one is being of nucleation stage. In other words, a nucleus for the growth as the crystal needs to reach a critical size. As can been in Figure 4.2, the nucleolus is formed by atom clusters smaller than the critical radius. As the

critical size is reached, the nucleation phase begins. The final stage is the stage of nucleation, i.e. growth, depending on the increase in the critical radius. In Figure 4.2, the relationship between free energy change (ΔG) and radius during solidification of a material is given [65].

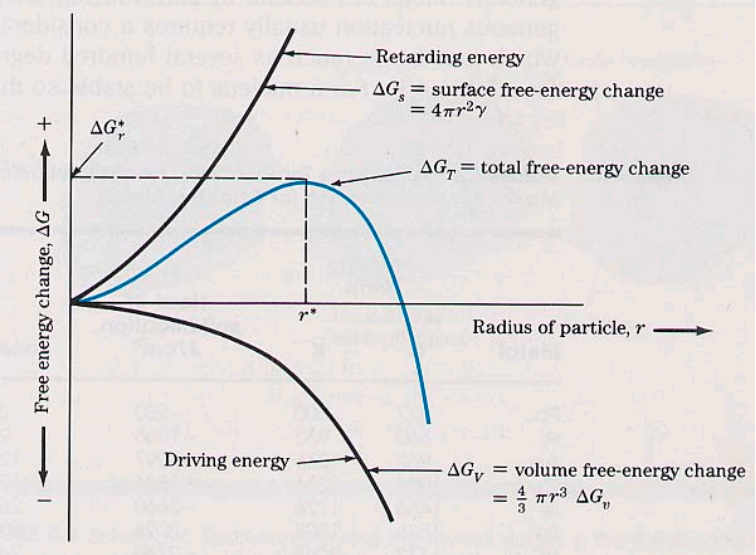

Figure 4.2. The relationship between the critical radius and the free energy change of materials during solidification [65]

As can be seen in the figure, there are two types of energy. First is the volume free energy released during conversion liquid to solid, the second is the surface free energy necessary for formation of solid surfaces of particles during solidification. For example, if a metal is cooled under equilibrium solidification temperature, energy providing the conversion from liquid to solid is the ΔG_V difference between the volume free energies of liquid and solid. Free energy change for a spherical nucleus with the radius r is expressed as $4/3\pi r^3 \Delta G_v$ due to the fact that sphere has the volume of $4/3\pi r^3$. But on the other hand, there is different energy preventing the formation of the nucleolus and the nucleus. This energy is ΔG_s required for the formation of surfaces of spherical nucleus and nucleolus. This energy is the multiplication of the specific surface free energy γ of the spherical particle and the surface of ($4\pi r^2$) sphere. The middle curve given by the figure is the total free energy. This energy is the sum of volume free energy

required for the formation of the nucleus or nucleolus at critical radius and surface free energy and given by following equation [65].

$$\Delta G_T = 4/3\pi r^3 \Delta G_v + 4\pi r^2 \gamma \quad (4.9.)$$

The derivative of the equation given above gives the correlation between free energy of surface and volume with the critical radius. Equation is as follows [65].

$$d(\Delta G_T)/dr = d/dr\,(4/3\pi r^3 \Delta G_v + 4\pi r^2 \gamma) = 12/3\,\pi r^{*2} \Delta G_v + 8\pi r^* \gamma = 0 \quad (4.10.)$$

$$r^* = -2\gamma/\Delta G_v \quad (4.11.)$$

There are two types of nucleation as homogeneous and heterogeneous nucleation. Critical energy for nucleation is defined as the free energy between surface and nucleus and the driving force. The easier the nucleation is provided for lower the critical energy. Therefore, impurities, dissolved small particles, scratches or roughness in the container in which growth is performed causes enhancement of heterogeneous nucleation. For this reason, crystal growth via heterogeneous nucleation using the seed crystal is common. As mentioned in previous sections, relationship between the driving force $\Delta\mu/kT$ and the growth rate (R) provides information on the growth mechanisms. As can be seen in Figure 4.3, crystal growth mechanism can be classified as adhesive type, two-dimensional nucleation growth and spiral growth [67].

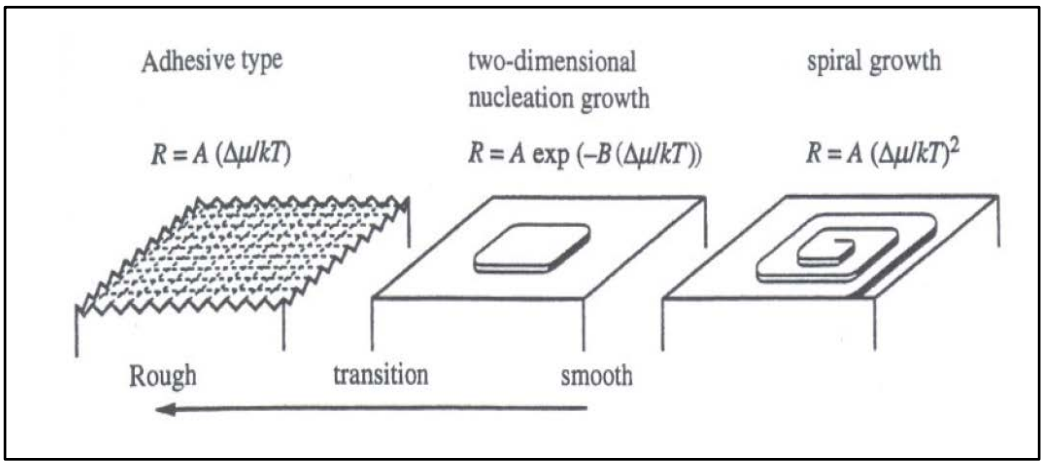

Figure 4.3. The effects of the growth rate and the driving force on growth mechanism models [67]

The effect of the crystal growth rate on the growth models and crystal morphology depending on the driving force is given in Figure 4.4. As shown in the figure, roughness of interface is increasing with the increase in the driving force (Δμ / kT). Thus, curve have variation on the points of Δμ/kT * and Δμ/kT**. Interface interaction becomes rough when the driving force is bigger than Δμ/kT** and so adhesive type growth mechanism takes place. The morphology of growing crystalline has the dendritic structure. When the driving force is below the point of Δμ/kT*, interface becomes more flat and smooth and thus the spiral growth mechanism becomes effective. The growing crystal has the polyhedral structure. When the driving force is in between Δμ/kT* and Δμ/kT**, the interface becomes smooth and nucleation mechanism at two dimensions become effective. The morphology of the growing crystal is in the form funnel (hopper). If the driving force value is extremely high, nucleation is increased and crystal start to aggregate. In the figure given below Δμ/kT* and Δμ/kT** values are different for different crystal directions [67].

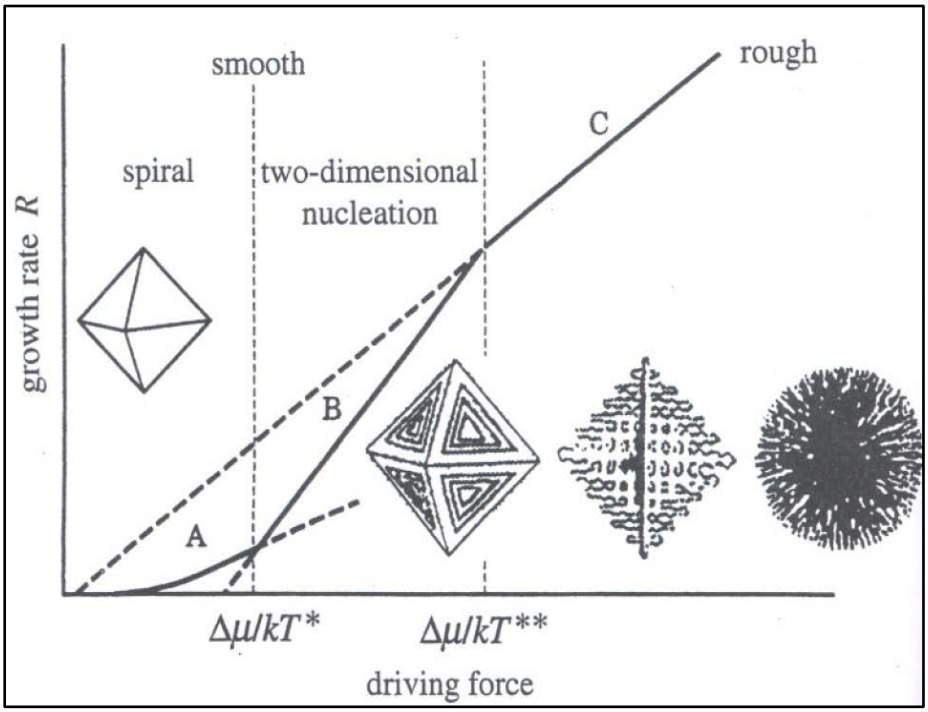

Figure 4.4. Growth models and crystal morphologies depending on the driving force and the growth rate [67]

4.2. Piezoelectric Single Crystal Production Methods

In general, single crystals are produced using melt for the production of single crystal from many material compositions. From the literature, Czochralski, Bridgman, growth from melt (Flux Growth), solid state single crystal growth method (SSCG) and top seeded solution growth (TSSG) methods can be found as a new generation methods for the production of single crystal piezoelectric materials [14,48,68].

4.2.1.Czochralski method

This method is generally used for the production of single crystals with quite high optical quality such as alumina, for the growth of semiconductor single crystal (silicon, germanium, gallium arsenide, etc.), for the growth of some single-crystal metal (palladium, platinum, silver, gold) and for the production of single crystal piezoelectric materials ($Ca_3Ga_2Ge_4O_{14}$ (CGG), $La_3Ga_5SiO_{14}$ (LGS), $La_3Ga_5{:}_5Nb_0{:}_5O_{14}$, (LGN) and $La_3Ga_5{:}_5Ta_0{:}_5O_{14}$ (LGT) $LiNbO_3$).

Czochralski method is technique for pulling crystal from the melt. In this technique, as can be seen in Figure 4.5 and Figure 4.6, seed is rotated and pulled slowly by dipping into the crucible where the crystal melt is obtained. In this technique, in general, chemically inert platinum or iridium crucibles having high mechanical strength are used because of high temperature working condition. This technique is not cost effective because of the need for special furnace systems for very high temperature melting and the high cost of crucibles [68-71].

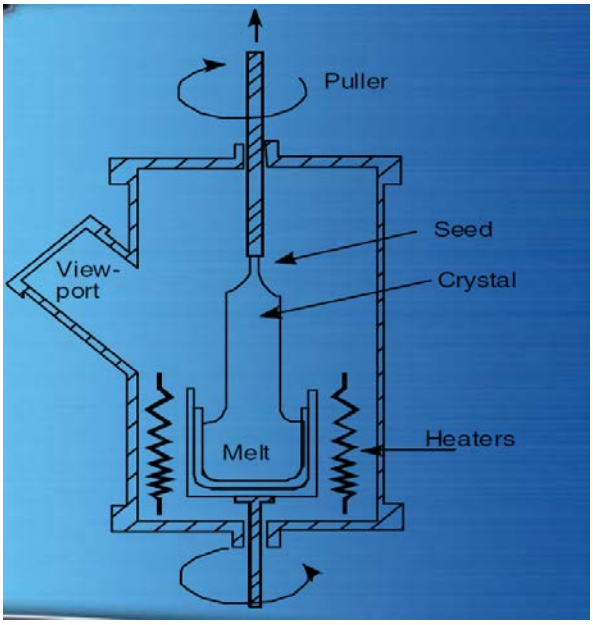

Figure 4.5. The furnace design used in Czochralski method [71]

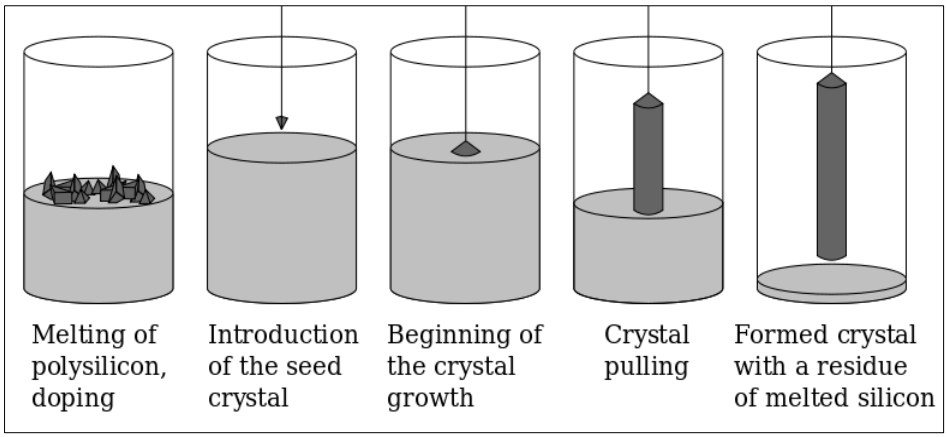

Figure 4.6. Single crystal production stages in Czochralski method

4.2.2. Bridgman method

The use of seed crystal and crucible are needed also for this method. Either horizontal or vertical design of the furnace is performed. Directional solidification takes place and the temperature differences are needed. Temperature changes must be controlled very well. The growth rate of this technique is usually 1mm/h. Crucibles are usually for single use only. As can be seen in Figure 4.7, there is a contact between seed and melt, and the seed gradually grows. This method is used

for the growth of piezoelectric single crystal such as $Sr_3Ga_2Ge_4O_{14}$ (SGG), $La_3Ga_5SiO_{14}$ (LGS, langasite), $(Na_{1/2}Bi_{1/2})TiO_3$, $(Na_{1/2}Bi_{1/2})TiO_3$-$BaTiO_3$ [71,72].

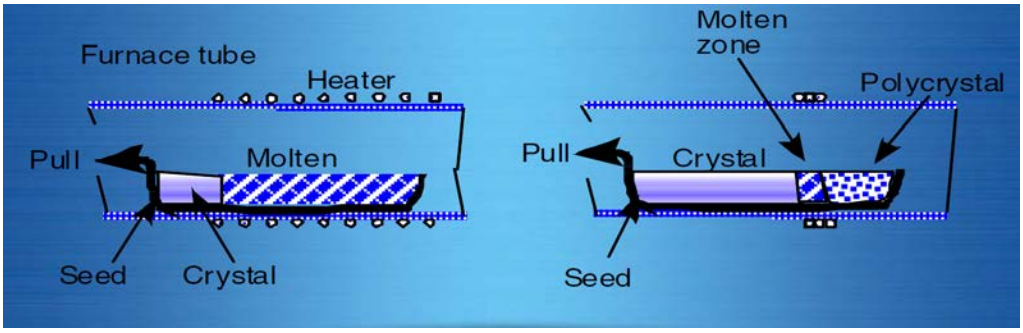

Figure 4.7. Single crystal production with Bridgman method [71]

4.2.3. The method for single-crystal growth from the melt (Flux Growth)

In this method, raw materials weighed at certain composition and proportions are milled homogeneously via ball mill after the addition of fluxing agent. Homogeneous mixture are placed in platinum crucibles and then covered so as not to leak, at the end crucibles are place in alumina crucibles. Prepared crucibles are placed into furnace. For a certain period of time they must be in the furnace at high temperature. Melt is gradually cooled from melting temperature to room temperature and hold on a certain periods of time at each level. In this technique, considering the time passing to hold (wait) for reaching the temperature of melting and cooling, it takes quite a long time. Amount and the type of fluxing agent for the crystal growth are very important. Usually fluorine based fluxing agents (such as KF) are mostly preferred.

With this method, single crystal piezoelectric materials such as $[Bi_{0.5}(Na_{1-x}Kx)_{0.5}]TiO_3$(BNTK), $BiFeO_3$-$PbTiO_3$, Pb $[(Sc_{1/2}Nb_{1/2})\ 0.58Ti_{0.42}]\ O_3$ (PSN-PT) are produced. Figure 4.8 shows the furnace design for this method and the crystals formed after growth. As can be seen in the figure, the main crystal, parasitic, satellit and pyrochlore crystals are observed in the lead-containing materials after growth stage [73-75].

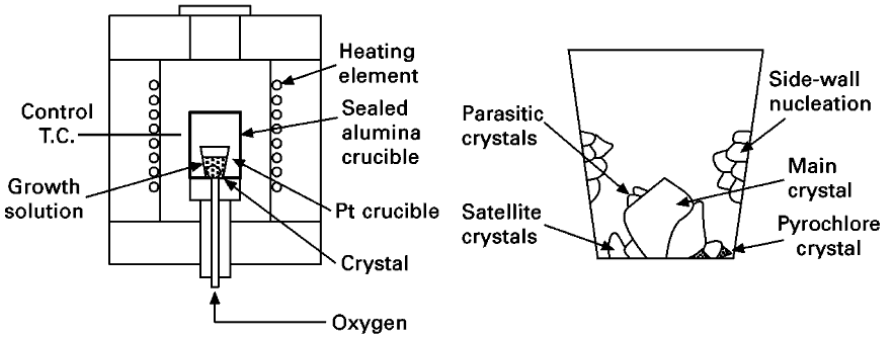

Figure 4.8. Furnace design for single-crystal growth from the melt and produced crystals after growth [75]

4.2.4. Solid state single crystal growth method

Solid state single crystal growth method is preferred in recent years especially for the production of piezoelectric single crystals. As shown in Figure 4.9, small single crystal seed is embedded into polycrystal structure or powder and then pressed. After that pressed samples are subjected to heat treatment with suitable temperature. With the heat treatment seed is grown within the polycrystal structure. This process is known as the solid state single crystal growth method [48].

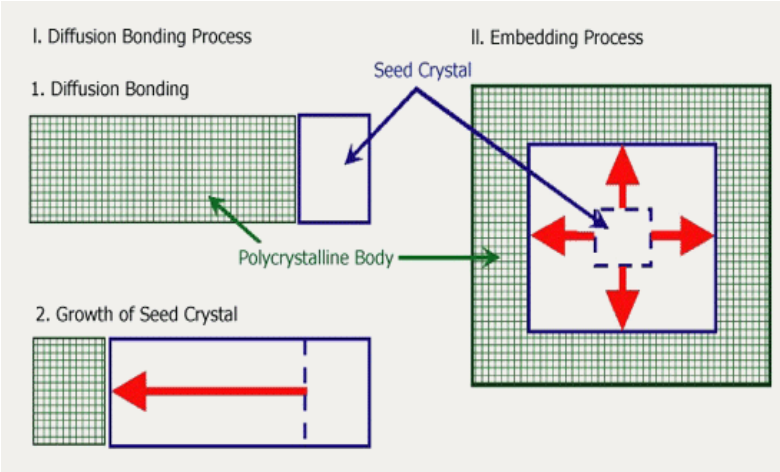

Figure 4.9. The stage of solid state single crystal growth (SSCG) method [48]

One of the most important factors for growth via SSCG method, the average particle size of the matrix (R) must be bigger than the critical size (R_c) needed to abnormal grain growth, but should be less than 2 times of this critical size. Thus, When $R_c<R<2R_c$, abnormal grain growth is stopped and so a continuous single-crystal growth takes place. When these conditions are provided, the number of density (ND) of abnormally grown particles, i.e. the number of particles per unit area, is "0". One of the growth factors is that the seed should have the same crystallographic structure with the polycrystal. In addition, the size and shape of porosity in polycrystal structure should be controlled carefully. Because existing of porosity in the system have a negative impact on the quality of produced single crystal and also the seed matrix interface connection is weak. In SSCG method, sintering atmosphere effects substantially the crystal growth and the quality. Sintering atmosphere effects not only porosity and abnormal grain growth but also crystal growth and quality as well [76]. The study on NBT-BT shown in Figure 4.10 indicates that, growth is processed together with interface reaction and diffusion mechanism in accordance with the theory of crystal growth as can be seen below. From that information, the driving force of the seed (Δg_{seed}) must be greater than Δg_c and that of the matrix must be smaller than Δg_c. By the provision of these conditions, seed grows in matrix and is transformed from polycrystal structure to single crystal structure [77].

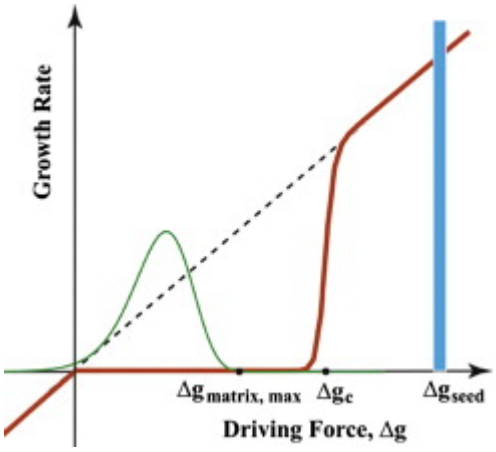

Figure 4.10. The interaction between the driving force and the growth rate for SSCG method [77]

The advantages of this method;

- This method is similar to a conventional sintering process and also it is quite cost effective method.
- It is possible to develop new compositions with high T_C, T_{RT}, and E_C.
- It is suitable for the production of net shaped single crystals without any mechanical processing.
- Repeatable production is possible.
- There is no melting during crystal growth, it is an effective method for the production of relaxor-PZT.
- There are no composition differences for the grown single crystal.
- Process temperature is low and there is no need Pt crucibles.
- Ring or tube-shaped single crystals can be produced [48,77]

This method is used for the production of especially PMN-PT, PZN-PT, PMN-PZT, relaxor-PZT, $BaTiO_3$, KNN and NBT-BT. In particular, PMN-PT and PZN-PT single crystals have been used for instead of polycrystal PZT due to their high piezoelectric coefficient (d_{33}> 2000 pc/N) and electromechanical coupling coefficient (k> 90%). As stated in previous sections, low Curie temperature (T_C), a rhombohedral to tetragonal structure transition temperature (T_{RT}) and the coercive electric field (E_C) are drawbacks for these materials. Some of the recent studies show that it is possible to produce single crystal piezoelectric materials such as high T_C (Relaxor-PZT), $BaTiO_3$, Ba $(Ti,Zr)O_3$ and PMN-PT by using SSCG method. Approximately 6cm in size and chemically homogeneous relaxor-PZT single crystals can be produced via SSCG method. Electrical properties can be given as K_T> 5000, T_C> 200°C, T_{RT}> 120°C, and E_C> 5 kV / cm. It is obvious that relaxor-PZT single crystal has higher T_C, T_{RT} and E_C as compared to PMN-PT and PZN-PZT single crystals [50]. For this reason, it is the best candidate for medical transducer and actuator applications.

4.2.5. Top seeded solution growth method

In recent years, top seeded solution growth (TSSG) method is preferred for especially in the production of big sized NBT-BT and PZN-PT piezoelectric single crystals. This crystal growth method is a combination of flux(melt) growth and Czochralski method. As can be seen in Figure 4.11 seed with a few millimeters is in contact with the melt on which it is rotated with the speed of rotation being very slow. In this method, the correct selection of the composition of the melt, control of the pulling speed, control of thermal changes resulting from the furnace heat, the melting container are the main desired crystal growth control parameters. Single crystal materials with about 40 mm in diameter and 10 mm thick are produced with this method [68,79].

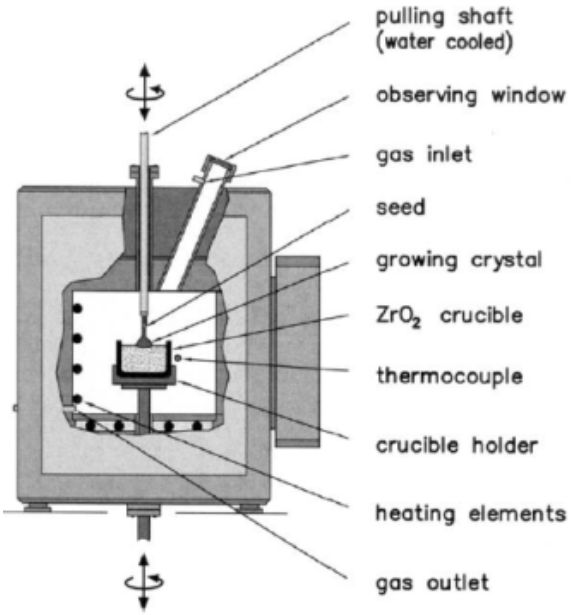

Figure 4.11. Furnace design for TSSG method and elements [80]

5. SODIUM BISMUTH TITANATE PIEZOELECTRIC MATERIALS

As mentioned in previous sections, today the most widely used piezoelectric ceramic is lead zirconium titanate (Pb[ZrxTi1-x]O_3) (PZT). Because of the excellent piezoelectric properties of these materials, they have been widely used for many years. These materials contain a large proportion of lead which is heavy metal that easily evaporates during the process and so diffuses to the atmosphere. Because of this situation it has become detrimental to the environment and health. Especially in recent years, the use of heavy metals have been restrics by the European Union, so development of lead-free piezoelectric materials instead of lead-based piezoelectric materials have great importance by researchers. One of the materials used in the development of lead-free piezoelectric materials is sodium bismuth titanate ($Na_{0.5}Bi_{0.5}$) TiO_3 (NBT)-based structures [23,54,81].

5.1. NBT Based Piezoelectric Materials and Properties

NBT based lead free materials are studied by Smolensky and colleagues in 1960 for the first time, but lead free materials has not had enough attention in those years as much as today. In the 1990s for NBT systems some of the dielectric and optical properties was designated. In addition, structure property relationship of these materials was not clearly defined. By the 2000s, it was understood that this material is in rhombohedral *R*3*c* space group under the temperature of 255^{o}C, but it is transformed by heating to the structure of tetragonal under 400-500^{o}C, cubic and tetragonal under 500-540^{o}C and fully cubic structure above the temperature of 540^{o}C in *P*4*bm* tetragonal space group. Figure 5.1 shows the crystal structure of the NBT system having pseudo-cubic structure [81,82].

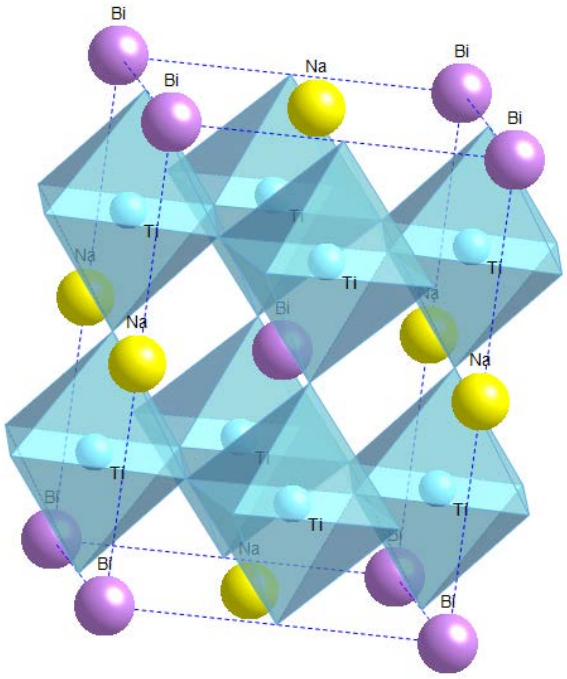

Figure 5.1. The crystal structure of NBT based perovskite materials [81]

As noted above, the material shows strong ferroelectric features when it has a rhombohedral structure. When the temperature is rises above 200^{o}C, it is transformed from the structure of ferroelectric rhombohedral to antiferroelectric tetragonal. By the reaching to the Curie temperature, structure is transformed into paraelectric cubic phase. NBT system has Curie temperature (Tc) of 320^{o}C, remanent polarization of P_r = 38μC/cm^2 and coercive field of E_c = 73kV/cm. But the structure of these materials consists alkali, and so it causes evaporation during sintering with the result of condensation problem. For this reason, high electrical field necessary for the polarization of these materials, so they have lower piezoelectric features than lead-based systems. In addition, high conductivity features of material causes some problems during polarization. By the addition of elements such as La, K, Nb, Zr, either piezoelectric properties or polarization and condensation problems are tried to be eliminated [81,83].

Table 5.1 shows the effects of certain additives on electrical properties of NBT system. NBT system without additive has Curie temperature of 310^{o}C, piezoelectric coefficient of 64 pC/N and dielectric constant of 302. By the addition of barium titanate, bismuth potassium titanate, barium zirconate into the structure, there is a small decrease observed for Curie temperature, whereas the

piezoelectric coefficient and dielectric constant increases. For example, addition of barium titanate (BT) into the structure, both the dielectric constant and piezoelectric coefficient is doubled [54].

Table 5.1. The electrical properties of NBT composition with additive and without additive [54]

System	Composition	T_c (°C)	d_{33} (pC/N)	K
BNT	$(Bi_{0.5}Na_{0.5})TiO_3$	310	64	302.6
BNT–BT	$(Na_{0.5}Bi_{0.5})_{0.92}Ba_{0.08}TiO_3$	280	125	625
BNT–BT–Nb_2O_5	$(Na_{0.5}Bi_{0.5})_{0.92}Ba_{0.08}TiO_3 + xNb_2O_5$	250	149	1230
BNT–BT–CeO_2 + La_2O_3	$(Na_{0.5}Bi_{0.5})0.94–6BaTiO_3$ + 0.5 mol% CeO_2 + 0.5 mol% La_2O_3	–	162	831
BNT–BT–$MnCO_3$	$(Na_{0.5}Bi_{0.5})_{0.92}–Ba_{0.08}TiO_3 + x$ mol% $MnCO_3$	243	160	–
BKT–BT–$MnCO_3$		174	117	2300
BNT–BK–BT	$(Bi_{0.5}Na_{0.5})TiO_3–(Bi_{0.5}K_{0.5})TiO_3–BaTiO_3$	125	150	–
	$(1–3x)$BNT–$2x$BKT–BT			
BNT–BZT	$(Bi_{0.5}Na_{0.5})TiO_3–Ba(Ti,Zr)O_3$	244	147	8814
BNT–BKT–$SrTiO_3$	$Bi_{0.5}(Na_{0.84}K_{0.16})_{0.5}TiO_3 + xSrTiO_3$	292	185	868
BNKLi–BT	$Bi_{1-z}(Na_{1-x-y-z}K_xLi_y)]_{0.5}Ba_zTiO_3$	210	205	1040
	$(BN–x/y/z)$ BN–0.15/0.075/0.02			

Table 5.2 shows the effect of BT addition to NBT material with different composition and different additives. As can be seen here, at the time of the addition of barium titanate 6% in mole (when 94NBT-6BT) especially at the morphotropic phase boundary, it shows higher piezoelectric property. In the case of the addition of BT (x <0.06 and x> 0.06) below and above of morphotropic phase boundary, piezoelectric coefficient decreases. Therefore, the maximum piezoelectric property is obtained at morphotropic phase boundary [54].

Table 5.2. Electrical properties of NBT-BT composition [54].

Composition	d_{33} (pC/N)	Tan δ (%)	K	T_c (°C)
$(Na_{0.5}Bi_{0.5})_{0.94}Ba_{0.06}TiO_3$	125	1.3	625	288
$(Na_{0.5}Bi_{0.5})_{0.92}Ba_{0.08}TiO_3$	125	–	–	280
$(1–x)(Na_{0.5}Bi_{0.5})TiO_3–x\ BaTiO_3$				
$x = 0.02$	78	1.73	402	–
$x = 0.04$	87	2.07	445	–
$x = 0.06$	122	1.79	601	–
$x = 0.08$	112	2.04	841	–
$x = 0.1$	94	2.39	764	–
$(Na_{0.5}Bi_{0.5})TiO_3–6BaTiO_3$	117	2.5	776	–

Table 5.3 shows the effect of lanthanum titanate ($LaTiO_3$) and sodium niobate ($NaNbO_3$) addition to NBT system on electrical properties. As can be seen here, $LaTiO_3$ addition causes an increase on piezoelectric coefficient as from 64 pC/N to approximately 90 pC/N. Moreover, it has increasing effect on Curie temperature and the dielectric constant. However, the increasing addition of $NaNbO_3$ decreases the piezoelectric coefficient but increases the dielectric constant. Therefore, addition of neither $NaNbO_3$ nor $LaTiO_3$ increases the piezoelectric coefficient as much as barium titanate. Thus, the addition of BT is more suitable to improve piezoelectric property [54].

Table 5.3. The effect of the addition of $NaNbO_3$ and $LaTiO_3$ into NBT system [54]

Composition	d_{33} (pC/N)	Tan δ (%)	K	T_c (°C)
$(Bi_{0.5}Na_{0.5})_{(1-1.5x)}La_xTiO_3$	92	0.04	560	
$x = (0–0.6$ mol%)				
$x = 1$	80	0.015	375	370
$x = 1.72$	91	0.04	550	345
$x = 2$	89	0.033	495	335
$x = 3$	–	0.036	770	365
$(Bi_{0.5}Na_{0.5})TiO_3$–$NaNbO_3$				
$x = 0.01$	80	5.60	637	–
$x = 0.02$	88	5.90	624	–
$x = 0.03$	60	5.96	754	–
$x = 0.04$	50	6.26	753	–
$x = 0.05$	32	5.40	801	–

As a result, the addition of BT to NBT system at morphotropic phase boundary allows acquiring superior piezoelectric properties as compared to other additives. Therefore, for the preparation of polycrystal powder to produce single crystal crystal, $0.94(Na_{0.5}Bi_{0.5})$ - $0.06BaTiO_3$ (94NBT-6BT) composition is preferred.

5.2. Recent Studies (2008-2012) for The Production of NBT-BT Single Crystal

In recent years, single crystal growth studies in order to improve the piezoelectric properties of NBT-BT based ceramics is also increasing. In addition, due to lack of systematic result on the production and characterization of single crystal material, difference of the obtained results and insufficiency of establishment of structure-property relationships, studies are performed using the many different single crystal production method. From studies conducted particularly in 2008-2012, method of crystal growth from melt (flux growth), top seeded solution growth (TSSG), solid state single crystal growth method (SSCG) are preferred for NBT and NBT-BT system.

Electrical properties of polycrystal and single crystal NBT based materials are compared in Table 5.4. Dielectric properties of polycrystal NBT systems are higher by the addition of Mn and Zr. On the other hand, piezoelectric coefficient is not as high as that of PZT. For structure produced as single crystal, lead containing systems have high piezoelectric coefficient, electromechanical coupling coefficient and dielectric constant. In the near future it will be replaced with lead free systems due to the restrictions to be on the lead containing materials. Therefore, NBT-based structures is started to gain features similar to PZT by the contribution of additives (Fe, Mn, Zr, $BaTiO3$, etc.). Especially at the morphotropic phase boundary, ($0.94Na_{0.5}Bi_{0.5}$ TiO_3-$0.06BaTiO_3$) d_{33} value of 283 and 360 pC/N. It is increased to about 483 pC/N by the addition of Mn. Also k_p value (> 50%) is as high as comparable with that of PZT. Dielectric properties are very close to some of the PZT compositions [62].

Table 5.4. Comparison of NBT based materials with PZT and other lead free materials

	Materials	T_C (^oC)	d_{33} pC/N	$k_{p(\%)}$	ε_r	tanδ
POLYCRYSTAL STRUCTURES	PZT 5H [50]	190	600	75	3500	0.02
	BNT [54]	310	64	-	302	-
	KNN [84]	-	126	42	590	-
	94BNT-6BT [54]	288	122	-	625	0.013
	BNT-BT (Mn doped) [54]	243	160	-	2300	-
	BNT-BT(Zr doped) [54]	244	147	-	8814	-
SINGLE CRYSTAL STRUCTURES	PMN-30%PT [57]	135	2200-2500	92-94	7500-9000	<0.01
	KNN [YAZ flasb]	423	160	-	240	0.02
	0.5% Mn doped KNN[85]	416	270	-	730	0.03
	$(NKL)(Sb_{1-x}Nb_x)O_3$ [40]	397	230	37	612	0.026
	$[Bi_{0.5}(Na_{1-x}K_x)_{0.5}]TiO_3$ [61]	365	160	-	-	-
	$0.96Na_{0.5}Bi_{0.5}TiO_3$– $0.04BaTiO_3$ [62]	310	283	50	1230	0.018
	$0.94Na_{0.5}Bi_{0.5}TiO_3$– $0.06BaTiO_3$ [62]	305	360	62	-	-
	Mn doped Na0.5Bi0.5TiO3–BaTiO3 [62]	320	483	56	1090	0.019

According to the studies, especially in 2008-2012, for the NBT and NBT-BT single crystal system, the method of single crystal growth from melt (flux growth), top seeded solution growth method (TSSG), solid state single crystal growth method (SSCG) are used. Studies in this area are summarized below.

Studies on the production of NBT based single crystals from the melt (flux growth) are summarized in Table 5.5. In this method, the raw materials and certain fluxing agents are milled after weighing at definite composition and proportions. After drying the homogeneous mixture are milled, it is placed in platinum crucible and covered not to have any leakage and then crucible are placed in the alumina crucibles. Prepared crucibles are placed in the furnaces to reach high temperature and waited certain period of time in the furnace. Melt is cooled gradually at the melting temperature and waited certain periods of time at each level. Because the time needed to reach the melting temperature and also that for cooling process is very long, the process takes a long time considering the waiting time. In recent years, according to studies in general, process performed especially on the oxygen atmosphere has substantial effect on the dielectric and

ferroelectric properties. In addition, the crystal size produced does not exceed a few millimeters.

Table 5.5. Recent studies for flux growth method

Publications	Explanation	Properties
M.Suzuki et al. 2010 [86]	NBT single crystals were grown using Bi_2O_3 and NaF fluxing agent at 1250^oC for 20h under high oxygen pressure.	Remanent polarisation values were measured as 31, 44 and 55μC/cm^2 for [100], [110] and [111] directions, respectively
R.Dhanasekaran et al. 2009 [87]	NBT-BT single crystals were grown by flux growth method in (001) ve (100) plane. Grown crystals were annealed under oxygen and nitrogen atmosphere. Effect of the oxygen and nitrogen atmosphere were investigated on dielectric and ferroelectric properties of grown crystal.	The crystal quality and dielectric properties of annealed single crystals were positvely effected under oxygen and nitrogen atmosphere due to the oxygen vacancy
R.Dhanasekaran et al. 2008 [88]	NBT-BT single crystals were grown by flux growth using different fluxing systems. Compositional variation were analyzed after crystal growth	From the X-ray rocking curve analyses, the crystal quality was enhanced using different fluxing systems. Also, acording to Curi-Weiss rules, different fluxing methods were improved ferroelectric properties of grown crystals.

In recent years, NBT-based single crystals are grown by top seeded solution growth method (TSSG). This method is quite similar with the method of production of single crystal from melt. The only difference is that after melt is produced in a certain stoichiometry, they contact with the surface of melt using single crystal seed oriented in a specific direction and the sample obtained is pulled up by rotating in a certain rotation speeds in the melt. One of the biggest advantages of this method is that the single crystals in large scale can be produced

according to the plane of the used seed. As can be seen from Table 5.6, the studies done particularly in recent years, it can be said that studies are performed for compositions near the NBT-BT morphotropic phase boundary. The piezoelectric coefficient is changed in the range of 280 and 483 pC/N, and k_p factor is in the range of 50-70% for crystals produced in particular at (001) plane. In addition, it is determined that the piezoelectric properties are improved with the addition of Mn to the NBT-BT system. Moreover, it can be deduced from the results that the crystals grown at (001) plane have better properties as compared to that of ones growth at the other directions.

Table 5.6. Recent studies for TSSG method

Publications	Explanation	Properties
Q.Zhang et al. (2011) [62]	<001> oriented NBT-BT single crystals were grown by TSSG for various compositions. NBT-BT seed crystal were used to grow the single crystals	Dielectric constants of produced NBTBT95/5, NBTBT94/6 and NBTBT93/7 single crystals at 1kHz were measured between 900 to 1100. Piezoelecteric coefficient(d_{33}) of single crystals were measured as 420, 400, 373 pC/N, respectively. Coupling coefficient (k_t) of sampels were changed between 66 to 70%.
Q.Zhang et al. (2010) [89]	<001> oriented NBT-BT single crystal seed were used to fabricate 96NBT-4BT single crystals from its melt.	From the results, d_{33} and k_t values were 283 pC/N and 50%
Q.Zhang et al. (2010) [90]	94NBT-6BT compositions were prepared and single crystals were grown using <001> oriented NBTBT seeds.	d_{33} and k_t values of fabricated single crystals were measured as 360pC/N and 62%, respectively.

Table 5.6. Recent studies for TSSG method (continuation)

Q.Zhang et al. (2009) [91]	1% Mn doped 90NBT-10BT compositions were prepared, and single crystals were grown from their melt using <001> oriented NBT-BT seed crystal	d_{33} and k_t values of 1% Mn doped 90NBT-10BT single crystals were measured as 483pC/N and 56%
W.Ge et al. 2009 [92]	<001>, <110>, <111> oriented 96NBT-4BT single crystals were grown with TSSG	Dielectric constant of grown single crystals were calculated as 650, 740 and 400 at room temperature. d_{33} of <001>, <110> oriented single crystals was measured as 146 ve 117 pC/N.
W.Ge et al. 2008 [93]	0.95NBT-0.05BT single crystals were grown with TSSG using excess sodium carbonate and bismuth oxide.	d_{33} values of and <111> oriented grown single crystals were found as 280pC/N and 90 pC/N . <001> oriented grown crystal shoved better electrical properties than other orientation.
W.Ge et al. 2008 [94]	Single crystal compositions were selected as 0.94NBT-0.06BT and 0.98NBT-0.02BT. Excess sodium carbonate and bismuth oxide were used to provide homogeneous melt. The single crystals were grown using Pt wire. Grown single were pulled out at slow rotational speed.	The grown single crystals were nearly 25mmx10mm in size. d_{33} values of <001>, <110> and <111> oriented 0.98NBT-0.02BT single crystals were measured as 60,65 ve 30 pC/N.

Instead of single crystal production methods known in recent years, solid-state single-crystal production method (SSCG) has been started to be used. For other methods of producing crystal, crystal is produced by solidification of the melt, but for this method there is no melt used. Short crystal production time, cheapness and simplicity are the biggest advantage of this method as compared to others. There is very limited number of study especially for NBT-BT system. In the literature so far, there is only one article on NBT-BT material as of 2012.

According to the study performed, powder is synthesized as to be 95NBT-5BT. The single crystal of $SrTiO_3$ is embedded into synthesized powder at (110) plane then the single crystal is produced by applying heat treatment at 1200°C for 10 hours to 10 days. Electrical characteristics of the single crystal produced are measured as piezoelectric coefficient of 207 and electromechanical coupling factor of 50% [77].

In this method, the most significant parameters determining the crystal quality and electrical properties are the densification of matrix material and matrix-seed interface interaction. In general, at the beginning of the problems encountered, pores in the matrix material are swept into single crystal during crystal growth. Therefore, the interaction of the seed with matrix should be optimized prior to single crystal growth.

6. OBJECTIVES AND METHODS

Piezoelectric materials are used for many years at the fields of health, medical, energy, defense, aerospace and aviation as for sensor, actuator and transducer applications. Completely eliminating the use of lead containing materials used in these areas in the near future, production of new generation lead free piezoelectric materials are needed necessarily.

The studies on the new generation piezoelectric materials have focused on lead free polycrystal and single crystal structures. Lead free polycrystal piezoelectric materials could still not replaced with common PZT materials. In the case of piezoelectric single crystal studies, KNN and NBT based structures are widely studied. It is observed that piezoelectric feature of single crystals especially having 94NBT-6BT composition at morphotropic phase boundary can be improved with the addition of different additives. However, from the experimental data obtained from performed studies, it is observed that results obtained from single crystals produced even with the same method and compositions are not consistent and reproducible. For this reason, the structure-property correlation of this composition is still not clear.

For these reasons, the aim of this thesis is the production of single crystals from flux growth method and characterization of new generation sodium bismuth titanate barium titanate lead zirconium titanate 94 ($Na_{0.5}Bi_{0.5}$) TiO_3-6$BaTiO_3$ (94NBT -6BT) piezoelectric crystal materials with and without additive as an alternative to polycrystal zirconium titanate (Pb (Zr, Ti) O_3) - (PZT) materials.

To briefly summarize the studies in this thesis;

1. $BaTiO_3$ powder synthesis, and crystal growth studies by the method of single crystal growth from melt (flux growth) and their characterization.
2. The production of undoped and doped (Li, Fe, Mn, etc.) polycrystal sodium bismuth titanate-barium titanate 94 ($Na_{0.5}Bi_{0.5}$) TiO_3-6$BaTiO_3$ (94NBT-6BT) based ceramic powder and characterization.
3. The growth of 94NBT-6BT piezoelectric single crystals with flux growth
4. CS and SPS assisted solid state single crystal production studies for 94NBT-6BT compositions.

5. Characterization of electrical properties of grown 94NBT-6BT single crystals with flux growth materials, and electrical characterization of sintered samples with CS/SPS sintering method for solid state single crystal growth studies.

In the first part of the study, the production of polycrystal barium titanate ($BaTiO_3$) and sodium bismuth titanate-barium titanate $94(Na_{0.5}Bi_{0.5})TiO_3$-$6BaTiO_3$ (94NBT-6BT) based ceramic powders were performed. Polycrystal powders were prepared according to the stoichiometric recipe and then the homogeneous mixtures were obtained by grinding. $BaTiO_3$ and $94(Na_{0.5}Bi_{0.5})TiO_3$-$6BaTiO_3$ based ceramic powders were produced with solid state reaction method. In addition, the effects of addition of different elements such as Li, Fe, and Mn to the composition of 94NBT-6BT on the electrical properties were investigated. Microstructure, crystal structure, elemental analysis and thermal properties of powders were determined using both microscopic and non-microscopic techniques such as scanning electron microscopy (SEM), X-ray diffraction (XRD), energy dispersive X-ray analysis (EDX), X-ray fluorescence spectroscopy (XRF) and thermal analysis devices (TG / DTA, heat microscopy), respectively.

Growth of $BaTiO_3$, doped and undoped 94NBT-6BT piezoelectric single crystals was grown by flux growth method in the second part. KF was used as fluxing agent to grow $BaTiO_3$ at 1200℃ for 15h. After heat treatment, the melt was cooled to room temperature quite slowly. On the other hand, synthesized 94NBT-6BT polycrystal powders were placed into platinum crucibles by the addition fluxing agent ($NaCO_3$ and Bi_2O_3). Platinum crucibles were subjected to heat treatment at the temperature of above 1300^oC for 5-10 hours by insulating the surround and sealed to have any leakage. Ensuring the quite slow cooling, growth of the crystals were performed. Grown single crystal samples were characterized by SEM, XRD, XRF and EDX.

For the third part of the study, studies were performed for solid state single crystal production. In this method, matrix-interface interaction was increased using spark plasma sintering method (SPS) instead of hot pressing. Both microstructure and electrical properties were compared for polycrystal materials produced via solid state sintering (CS) and SPS methods.

In the last part of the study includes electrical properties of 94NBT-6BT piezoelectric single crystals, and CS/SPS sintered polycrystal materials for SSCG method. Electrical properties such as piezoelectric coefficient (d_{33}), temperature and frequency-dependent dielectric constant (ε_r) and dielectric loss ($\tan\delta$), hysteresis loops and leakage current densities were determined for both grown single crystal samples and polycrystal samples. In Table 6.1, all characterization methods and instruments used in the study are summarized.

Table 6.1. Characterization methods used in this thesis

Methods/Devices-Model	Objectives
Particle size and surface charge measurement device (Zeta Sizer)/ Malvern Nano ZS	Particle size distrubition of synthesized powders
Scanning electron microscopy (SEM)/ Zeiss Evo 50 EP	Microstructural caharacterization of synthesized powders and grown single crystals
EDX analysis/ Bruker AXS XFlash	Chemical analysis of synthesized powders and grown single crystals
X-Ray diffraction/ Rigaku Rint ve Bruker Advanced D8	Determination of crystal phase of synthesized powders and grown single crystals
X-Ray fluorescence spectroscopy (XRF)/ Rigaku ZSX Primus	Determination of changes in the composition and oxide compounds depend on the process
The heating microscope/Misura Flex	Analysis of deformation behaviour of synthesized powders and grown single crystals
Thermal analysis (TG/DTA) Netzch	Analysis of decomposition temperature of raw materials for crystal growth
Piezoelectric coefficient measurement devices (d_{33} metre)/APC	Measurement of d_{33} value
Empedance/ Gain phase analyzer HP-4194A and Agilent 4294A	Measurement of dielectric and piezoelectric properties as a function of frequencies
Piezoelectric and ferroelectric measurement analyzer / Aixact aixPES/CMA	Determination of hysteresis curve and leakage current density of the grown crystals
LCR metre/GW Instek LCR 8101	Measurement of dielectric properties as a function of temperature and frequencies

7. EXPERIMENTAL

7.1. Synthesis of Polycrystal Powders via Solid State Synthesis Method

Powders were produced via solid state synthesis with desired compositions for the production of barium titanate and sodium bismuth titanate single crystals using flux growth method. The most important advantages of this method are usability of simple and cost effective production devices (ball milling, drying in oven or evaporator) during powder synthesis. But for this method, large particle size distribution, the formation of large particles, the formations of residue during grinding are the main disadvantages. As can be seen in Figure 7.1, highly sensitive grinding process, optimization of applied temperature and time are very important. In the figure, it is obvious that insufficient temperature and time leads to incomplete reaction, whereas extreme temperature and the waiting time cause strong bonds between the particles [95].

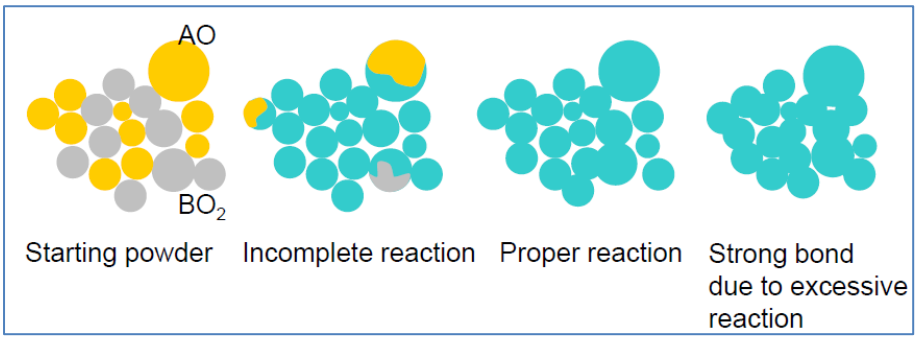

Figure 7.1. Solid state synthesis and reaction related formations [95]

In addition, the size of used starting material during solid state synthesis effects the structure of powders produced after reaction. As can been in Figure 7.2, if the particles size of powder is large, there can be unreacted starting materials within the structure after reaction. When the small sized powders are used, homogeneous powder synthesis is achieved. In the case of not homogeneous milling and insufficient milling time, because there is no homogenous mixture obtained and there exist large sized particle within the mixture.Also, starting raw materials or intermediate phase is formed at the end of the reaction. Because of

these reasons, optimization of grinding conditions in terms of temperature and time is very important [95,96].

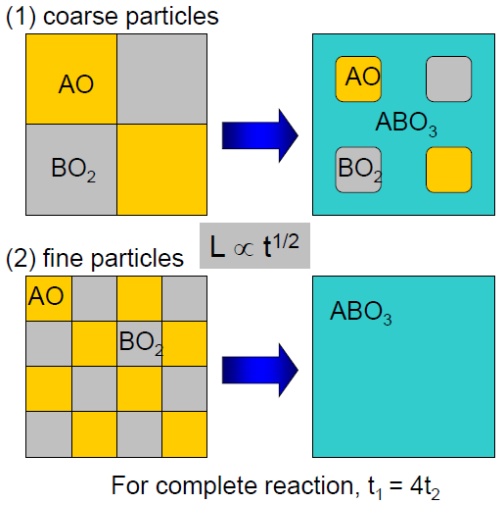

Figure 7.2. The effect of particle size on reaction [95]

Taking into account the mentioned factors, codes and descriptions of powder synthesized in accordance with the solid state reaction used in the thesis are given in Table 7.1.

Table 7.1. Codes and descriptions of polycrystal powders synthesized by solid state reaction

MATERIALS CODES	EXPLANATION
BT	Barium titanate ($BaTiO_3$)
NBT	Sodium bismuth titanate ($Na_{0.5}Bi_{0.5}TiO_3$)
NBLT	Li doped sodium bismuth titanate (Li-$Na_{0.5}Bi_{0.5}TiO_3$)
94NBT-6BT	$94Na_{0.5}Bi_{0.5}TiO_3$ -$6BaTiO_3$ with a composition of sodium bismuth titanate- barium titanate
94NBLT-6BT	$94Na_{0.5}Bi_{0.5}TiO_3$ -$6BaTiO_3$ with a composition of Li doped sodium bismuth titanate- barium titanate
94NBFT-6BT	$94Na_{0.5}Bi_{0.5}TiO_3$ -$6BaTiO_3$ with a composition of Fe doped sodium bismuth titanate- barium titanate
94NBMT-6BT	$94Na_{0.5}Bi_{0.5}TiO_3$ -$6BaTiO_3$ with a composition of Mn doped sodium bismuth titanate- barium titanate

7.1.1. Synthesis of barium titanate powders

$BaCO_3$ and TiO_2 are used as starting material to produce polycrystal $BaTiO_3$ powder via solid state synthesis. According to the flow diagram given in Figure 7.3, in order to increase the interaction between the powders, it is aimed to reduce the size of $BaCO_3$ first. Therefore, $BaCO_3$ was milled using plenatory mill in an aqueous medium for 1-4 hours. Drying step was performed by placing powder milled into the freeze dryer. The dried powder of $BaCO_3$ was mixed with alcohol homogeneously in an ultrasonic dispersant. On the other hand, TiO_2 powders about 30 nm in size were prepared similarly. The two prepared solutions were mixed and stirred in ethanol using ultrasonic homogenizer. After dried at 80^{o}C, obtained homogeneous mixture was calcined at 550-750 -950-1050^{o}C for 2-10 hours. Size distribution, crystal structures, decomposition behavior and morphological analysis of materials were investigated using laser diffraction, the X-ray diffraction method (XRD), thermo gravimetric analysis (TG/DTA), and scanning electron microscopy (SEM) methods, respectively. In Table 7.2, the codes and proportion of prepared TiO_2-$BaCO_3$ systems in different ratios is given.

Table 7.2. Ti/Ba molar ratios in the synthesis of barium titanate

Materials Codes	Ti/Ba ratio
BTS100	1.00
BTS103	1.03
BTS111	1.11
BTS143	1.43
BTS200	2.00
BTS334	3.34
BTS989	9.89

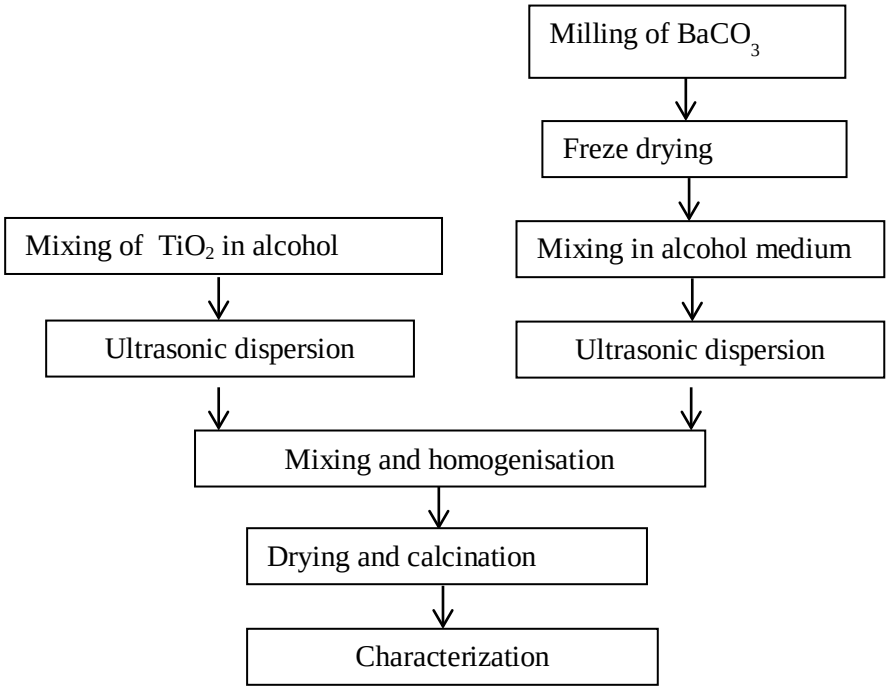

Figure 7.3. Flow chart for the synthesis of barium titanate powder using solid state synthesis method

Particle size distributions of powder milled in aqueous medium for 1-4 hours and then dried in a freeze dryer for the reduction of $BaCO_3$ powder size is given in Figure 7.4. It is clear from the particle size distrubition graph and scanning electron microscope (SEM) image given in Figure 7.4a and Figure 7.5 that $BaCO_3$ powder is rod like shaped structure and has the size distribution varying between 1-3µm. Depending on the increasing milling time, these rod like shaped structures are broken as to be the sizes of about 620 nm after 4 hours grinding. It can be seen that in Figure 7.4b and Figure 7.6, size distribution of milled powder for 1-2 hours decrease below 600 nm after freeze drying process, but increasing particle size (875 nm) of dried powder is observed at the end of the 4 hour grinding. This is because of the agglomeration tendency of the powder due to its electrostatic attraction force at nano scale after 4 hours grinding. In addition, in Figure 7.4a and 7.4b, the narrow size distribution is observed for 1^{st} and 2^{nd} hour after drying process subsequent to beginning and end of 1^{st} hour, whereas,

despite the decrease in size especially at the end of the 4th hour, dried powders have wider particle size distrubition. This situation increases the tendency to agglomeration with reduction of particle size,

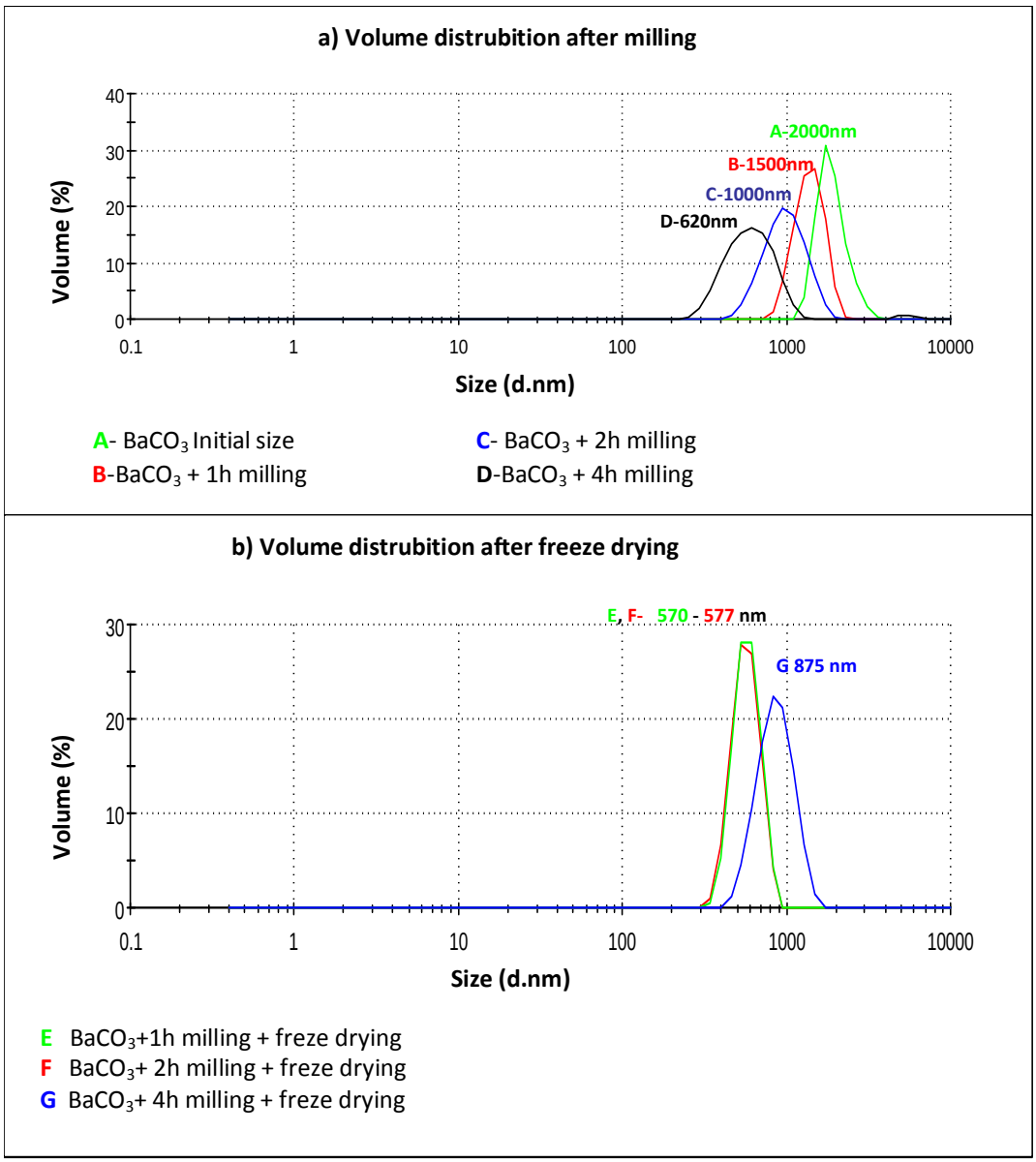

Figure 7.4. Size distribution of barium carbonate ($BaCO_3$) powder, after grinding (a) and after freeze drying (b).

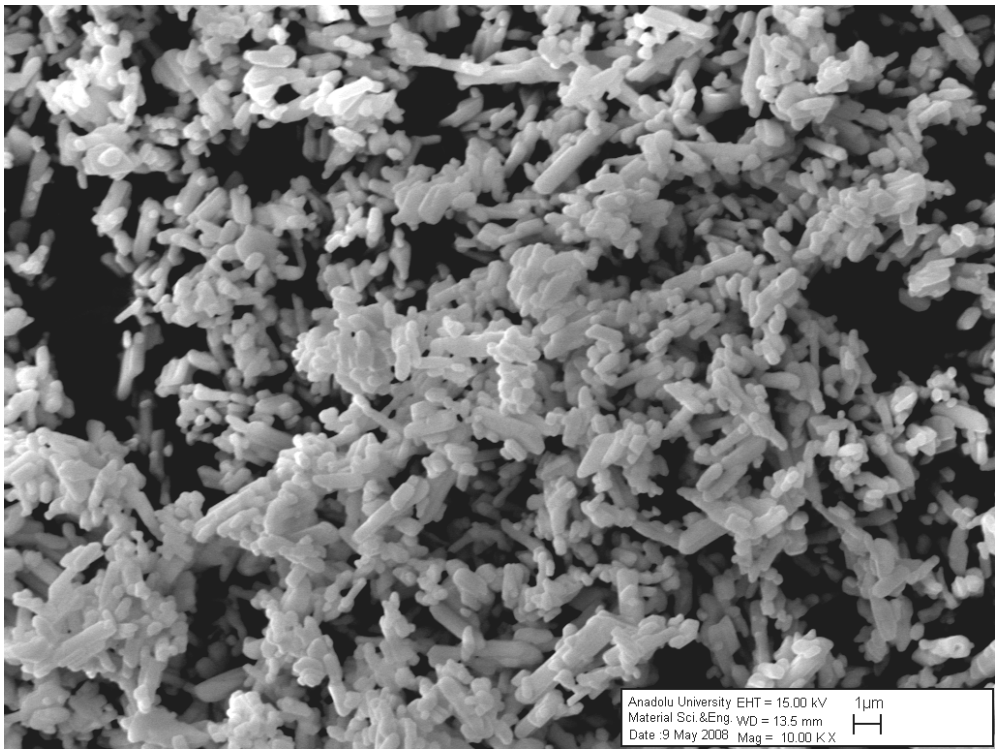

Figure 7.5. Scanning electron microscope image of unmilled (initial) $BaCO_3$ powder

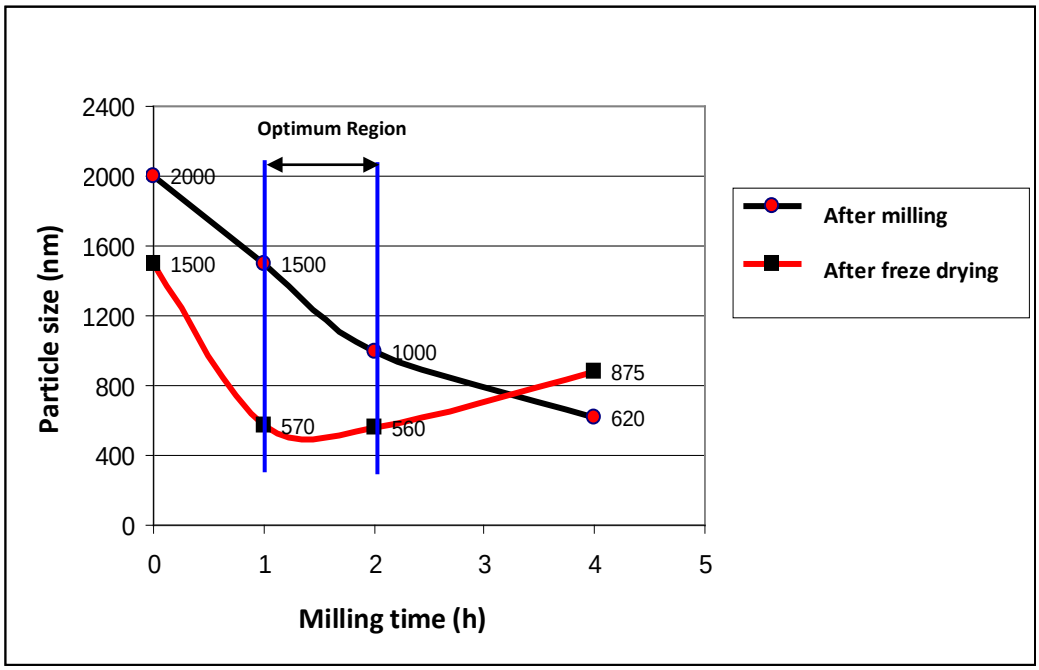

Figure 7.6. Comparison of size distribution after grinding and freeze drying

As a result, $BaCO_3$ powder can be reduced under 600 nm wtih plenatory mill and freeze drying. Despite the decrease in size depending on the increase on milling time, increase in attraction forces with decrease in distance between powder particles depending on increasing surface area cause agglomeration after drying process.

Effect of composition, calcination temperature (550-750-950-1050^oC) and calcination time (2-10h) on $BaTiO_3$ powder formation are investigated by mixing of $BaCO_3$ and TiO_2 powder. Ti/Ba ratio were selected between 1 to 9.89 using $BaCO_3$(nearly 600 nm) and TiO_2 (nearly 30nm) powders. TG curve of initial and freeze dried $BaCO_3$ powder is given in Figure 7.5. As can be seen from the curve, decomposition temperature of the unmilled powder begins over 1000^oC. On the other hand, decomposition temperature of freeze dried $BaCO_3$ powder is above 550^oC, and decomposition begins at a temperature significantly lower as compared to the initial material. If large particles, large and small particle mixing are used for synthesis, large particles do not react with other particles. Therefore, it causes to incomplete reaction and undesired interphase. Also, high temperature and time are required to complete the reaction. Therefore, reducing the size of $BaCO_3$ is very important to interact with nanosized TiO_2 for a homogeneous $BaTiO_3$ formations.

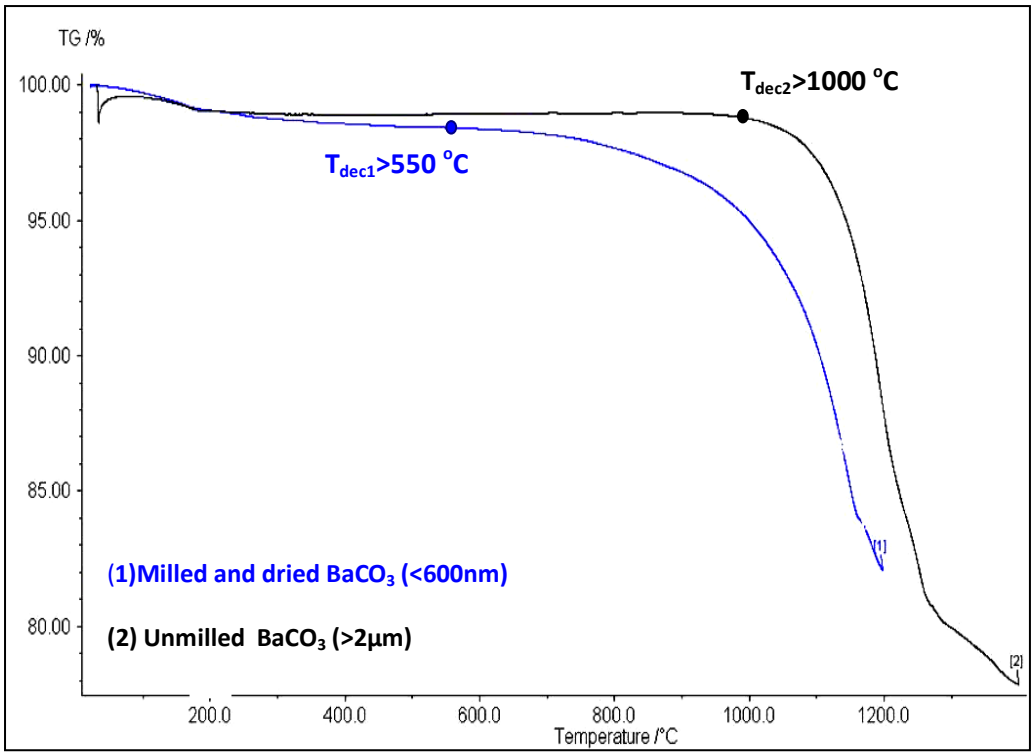

Figure 7.7. TG curves of barium carbonate before and after milling

To determine the effect of powder composition and calcination temperature on the formation of $BaTiO_3$, heat treatment was performed at different temperatures (550-750-950-1050^oC) using $TiO_2/BaCO_3$ powders with different in proportions of mixed homogeneous composition. Crystal structure of the heat treated powder was analyzed by using XRD method. Figure 7.8 shows XRD pattern of calcined powder at 550 and 750℃ for 2 hours for powder. From XRD peaks of powders calcined at 550℃ given in Figure 7.8, it has been observed that there exist $BaCO_3$ for all compositions and TiO_2 for anatase and rutile structures. It has also been observed that $BaCO_3$ does not decompose completely and fully interact with TiO_2. The formation of a very small amount $BaTiO_3$ (o $BaTiO_3$, 2θ = 31. 699) has been observed. From the XRD pattern of powders coded as BTS989 and BTS100, depending on the increasing TiO_2 and decreasing $BaCO_3$ amount, intensity of TiO_2 increases. As a conclusion, this temperature is not a suitable temperature for the formation of $BaTiO_3$.

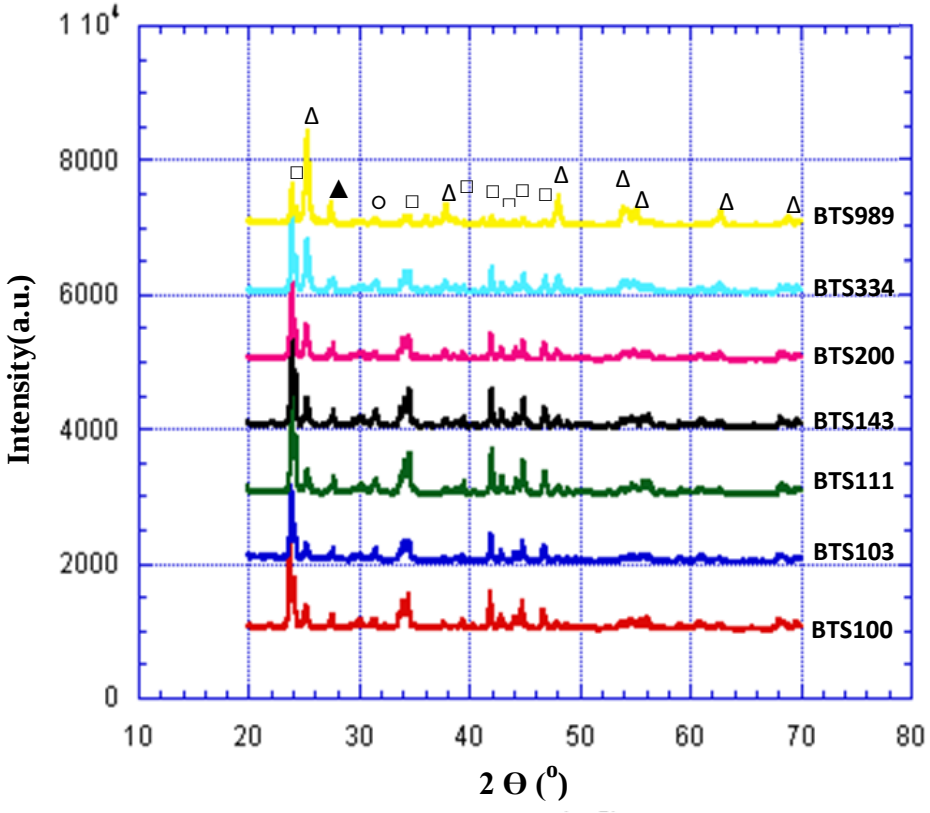

Figure 7.8. XRD pattern of powders, calcined at 550°C for 2 hours, with the ratio of different Ti/Ba (○$BaTiO_3$ ▲Rutile TiO_2 Δ Anatase TiO_2 □$BaCO_3$)

As can be seen in Figure 7.9, when the calcination temperature is 750°C, depending on the increasing temperature formation of $BaTiO_3$ is observed for all compositions. But for all the compositions there are unreacted $BaCO_3$ observed. By XRD results, intensity of $BaCO_3$ decreases with increasing Ti/Ba ratio (□ $BaCO_3$, $2\theta = 24^o$). The reason for this situation is indicated by dominant phase appearing with the increasing TiO_2 amount within the structure. Almost all of BTS100 coded (Ti / Ba = 1:1) powder sample has been transformed into $BaTiO_3$ for this temperature. However, even if a small amount of $BaCO_3$ (□ $BaCO_3$, $2\theta = 24^o$) residue is observed in the structure. The reason for this is insufficient calcination time. In addition, a higher transformation rate of BTS100-coded into $BaTiO_3$ as compared to others confirms BaO-TiO_2 phase diagram at this rate. As a reason, from the phase diagram, when the Ti: Ba = 1:1, the structure under 1460°C is cubic barium titanate. As a result, when the Ti: Ba ratio is 1, the

complete formation of $BaTiO_3$ structure is observed. Due to presence of TiO_2 in the structure with the increased Ti ratio, there is partial formation of $BaTiO_3$ structure. Therefore, for the synthesis of $BaTiO_3$, Ti: Ba ratio should be 1.

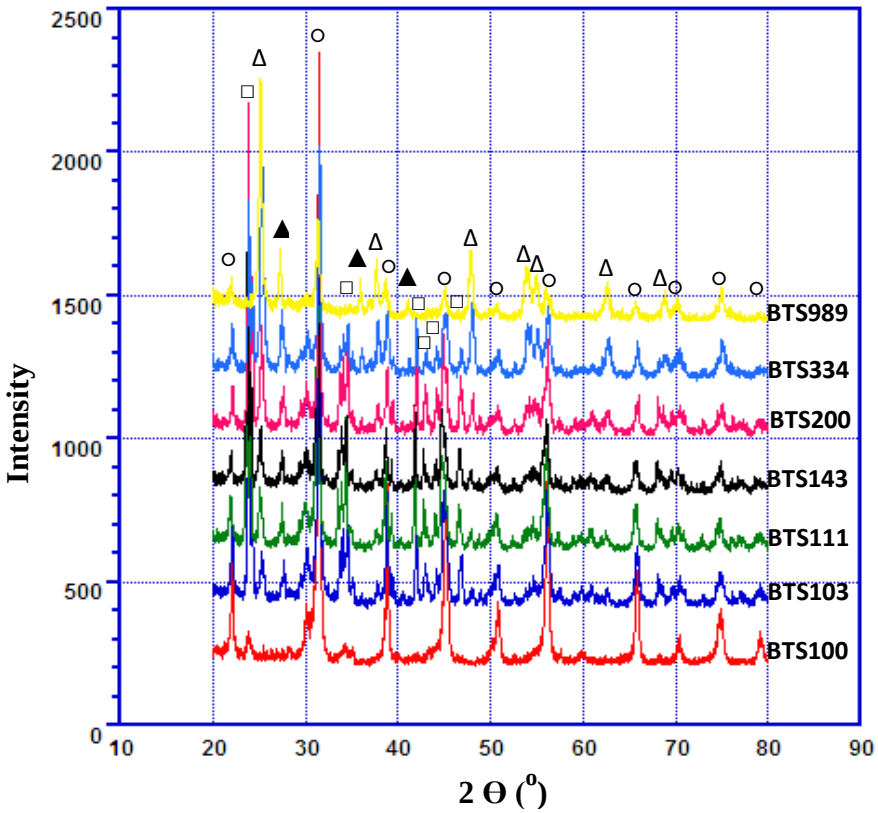

Figure 7.9. XRD pattern of BTS coded powders, calcined at 750°C for 2 hours, with the ratio of different Ti/Ba (○$BaTiO_3$ ▲Rutile TiO_2 ΔAnatase TiO_2 □ $BaCO_3$)

In Figure 7.10, phase analysis of BTS100 coded powders with Ti / Ba = 1 for calcination at 550-1050°C for 2 hours is given. As can be seen here, there is no any reaction occurred completely within the structure at 550°C. The starting materials are used for the formation of $BaTiO_3$ exists within the structure. In addition, this temperature is a temperature insufficient for the decomposition of $BaCO_3$. When the calcination temperature is 750-950°C, structure is converted to $BaTiO_3$, but there remains a small amount of $BaCO_3$ residue within the structure. When the temperature is set at 1050°C, complete decomposition of $BaCO_3$ is observed whereas having not enough time causes formation of Ba_2TiO_4 interphase within the structure. Therefore, the calcination time at this temperature should be increased.

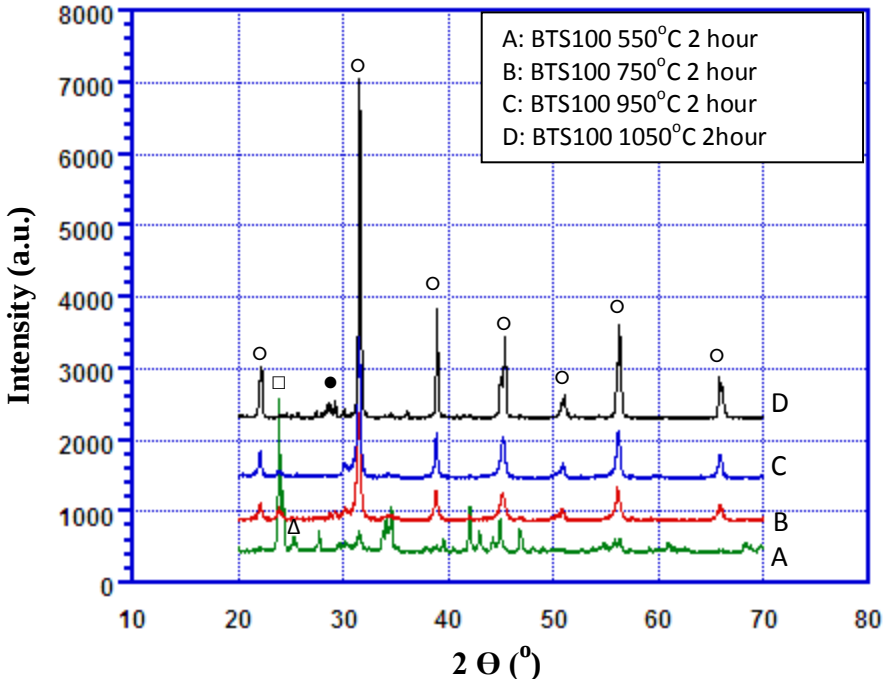

Figure 7.10. XRD pattern of BTS100 coded powders, calcined at 550-750-950-1050°C for 2 hours, with the ratio of Ti/Ba=1 (○$BaTiO_3$●Ba_2TiO_4▲Rutile TiO_2 Δ Anatase TiO_2 □ $BaCO_3$)

To see the effect of calcination time, heat treatment is applied for BTS100 coded powder with Ti / Ba = 1 at 1050°C for 2, 5, and 10 h. According to the XRD analysis (Fig. 7.11) after calcination at different time intervals, not only formation of $BaTiO_3$ phase but also Ba_2TiO_4 interface are observed for 2 and 5 hours duration. For this reason, 10 hour calcination is performed at constant calcination temperature, and thus it is observed that the structure is fully transformed into $BaTiO_3$. Similar XRD pattern are observed after heat treatment at 1100 ° C for 5 hours.

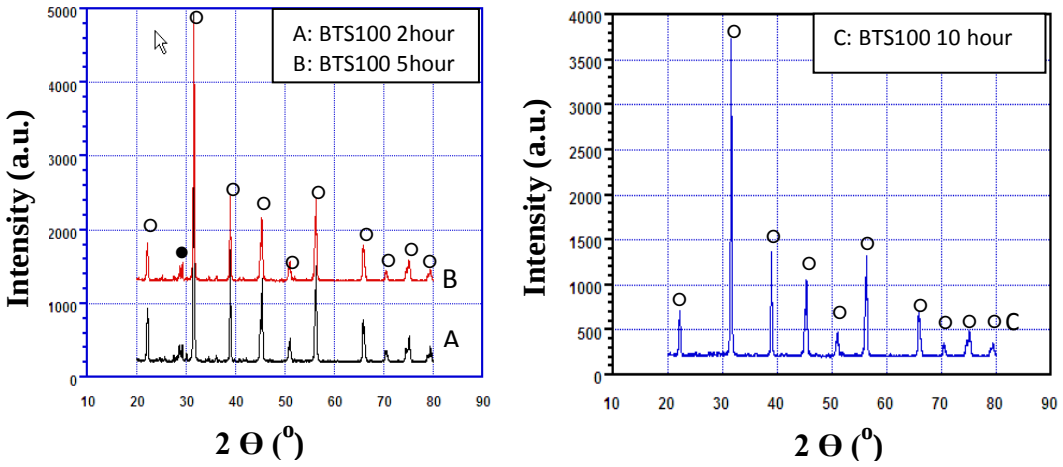

Figure 7.11. XRD pattern of BTS100 coded powders, calcined at 1050°C for 2-5-10 hours, with the ratio of Ti/Ba=1 (○$BaTiO_3$ ●Ba_2TiO_4)

SEM images with different magnification before and after calcination are given in Figure 7.12. In Figure 7.12a, powder is mixed homogeneously before calcination. In Figure 7.12b and Figure 7.12c, SEM images with different magnification are observed after calcination. As can be seenfrom SEM analysis, $BaTiO_3$ powders are produced in the size of smaller than 200 nm.

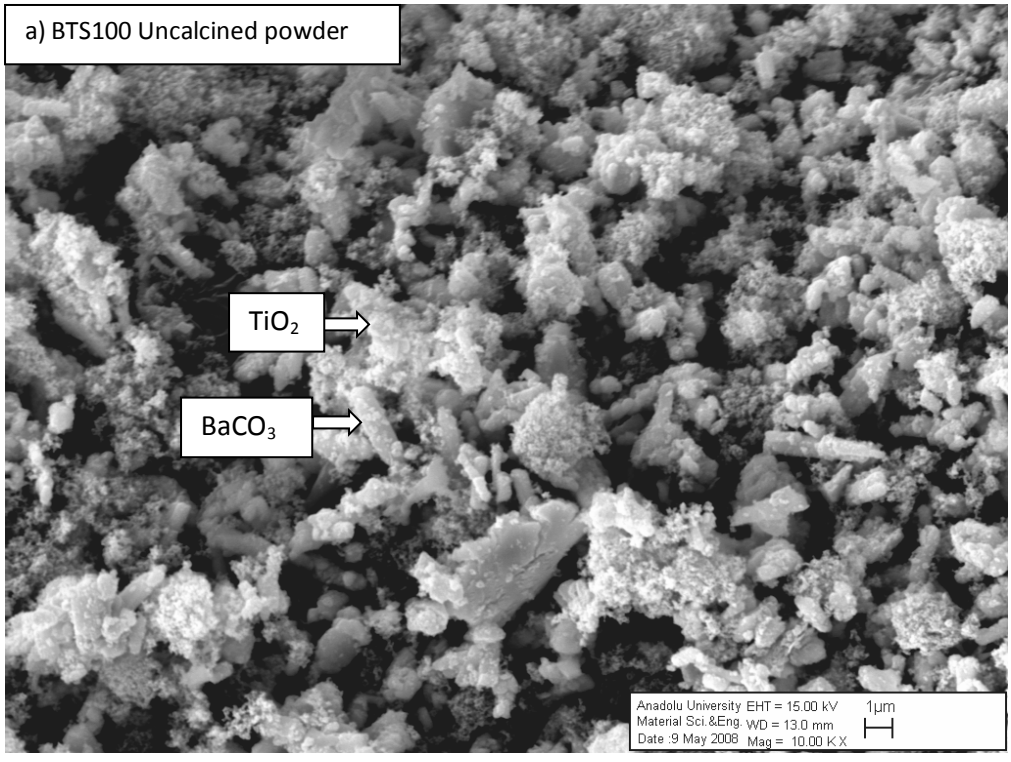

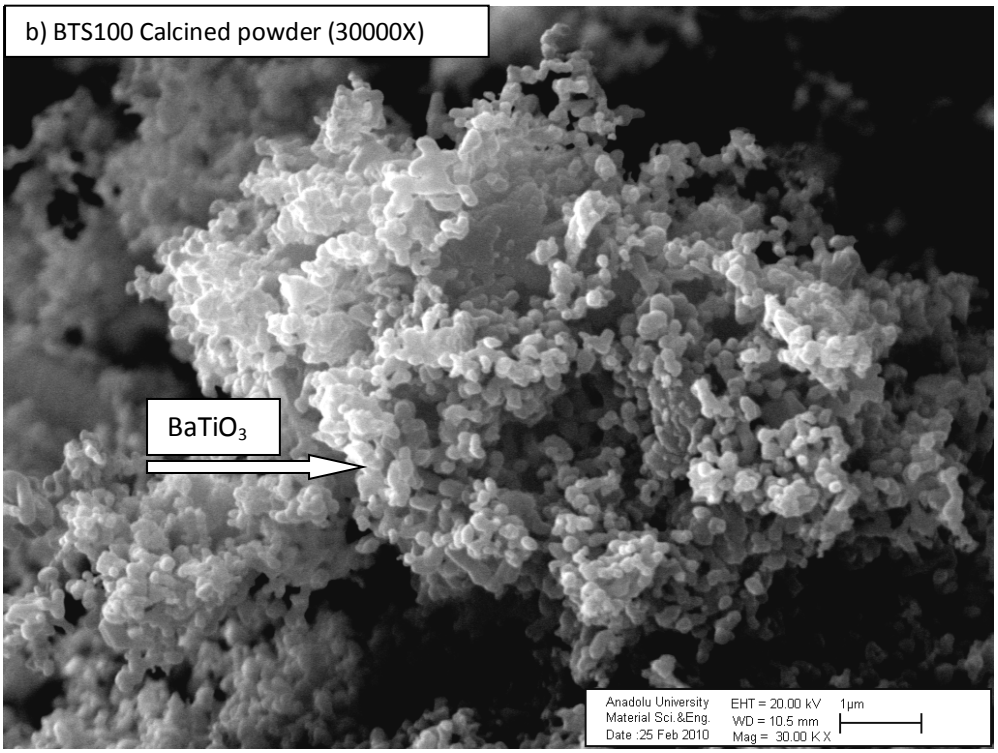

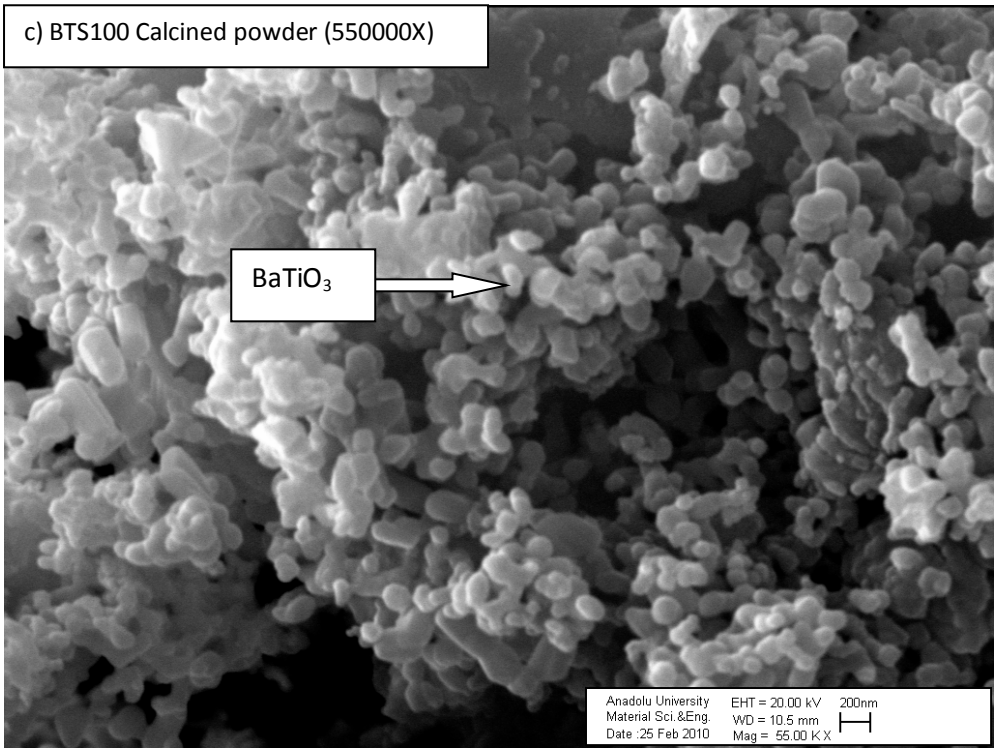

Figure 7.12. SEM images of BTS100 coded calcined powders, with Ti/Ba = 1; a)10.00KX, b) 30.00KX and c) 55.00KX

7.1.2. Synthesis of NBT-BT based powders

Bismuth oxide (Bi_2O_3), sodium carbonate (Na_2CO_3), titanium dioxide (TiO_2) and barium carbonate ($BaCO_3$) were used as starting material for the solid state synthesis of 94NBT-6BT powder. Li_2CO_3, Fe_2O_3 and MnO_2 were used to modify the 94NBT-6BT composition. As given flow chart in Figure 7.13, starting powders were mixed homogeneously and milled with zircona balls in ethanol approximately 15 hours. Obtained powder mixtures after grinding were dried at 80^oC and calcined at 900^oC for about 3-5 hours. Particle size of calcined powders was reduced by milling similarly in the ethanol medium. After milling, dried powders were sieved under 100 microns. Crystal structure and microstructure of the synthesized powder has been characterized with X-ray diffraction (XRD) technique and scanning electron microscope (SEM).

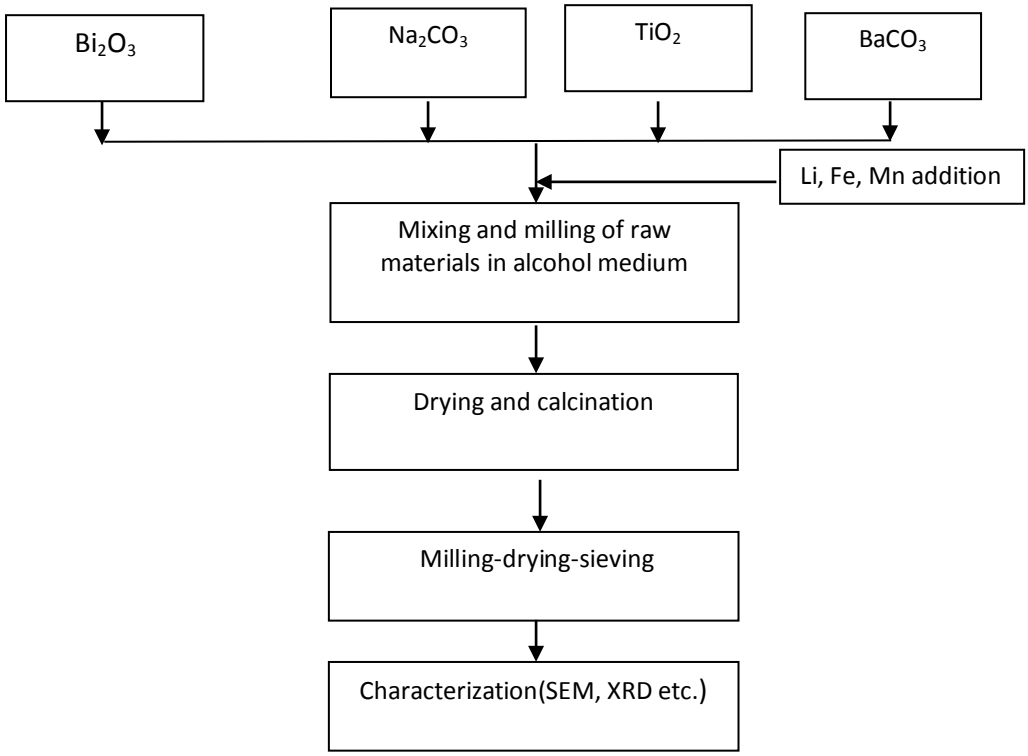

Figure 7.13. Flow chart for the production of 94NBT-6BT composition

In Figure 7.14, it is obvious that all of produced powders as undoped and Li, Fe and Mn doped are converted to the perovskite structure as can be seen from the XRD patterns of powders. Within the structure there are no undesired intermediate phase and unreacted structures.

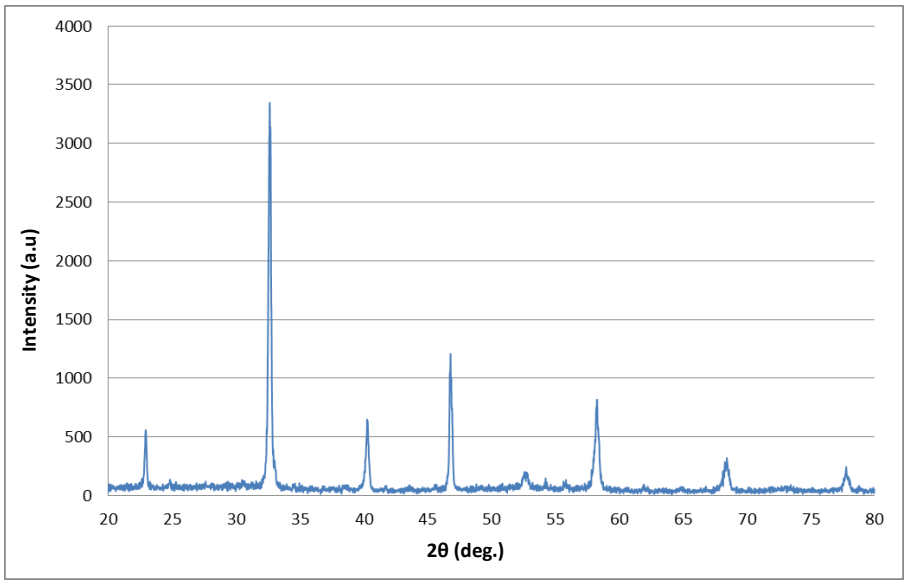

Figure 7.14. XRD pattern of 94NBT-6BT based powder

In Figure 7.15, scanning electron microscope images of undoped and Li, Fe, and Mn-doped 94NBT 6BT powders are given. From morphologies of produced powders, undoped powders have sharp-edged structure and Li doped powders appear to have structure quite close to the rounded corners and a cubic structure (Figure 7.15 a-b). Considering the microstructures of Fe and Mn doped powders, it is clear that powders have spherical shape (Figure 7.15c-d). From the edge lengths of the undoped and Li doped powders, it can be said that size of some particles is as much as 2 micron, but in general appears to be under 2 microns. It is obvious that Fe and Mn doped powders with spherical morphology have the size smaller than 500 nm.

a) 94NBT- 6BT

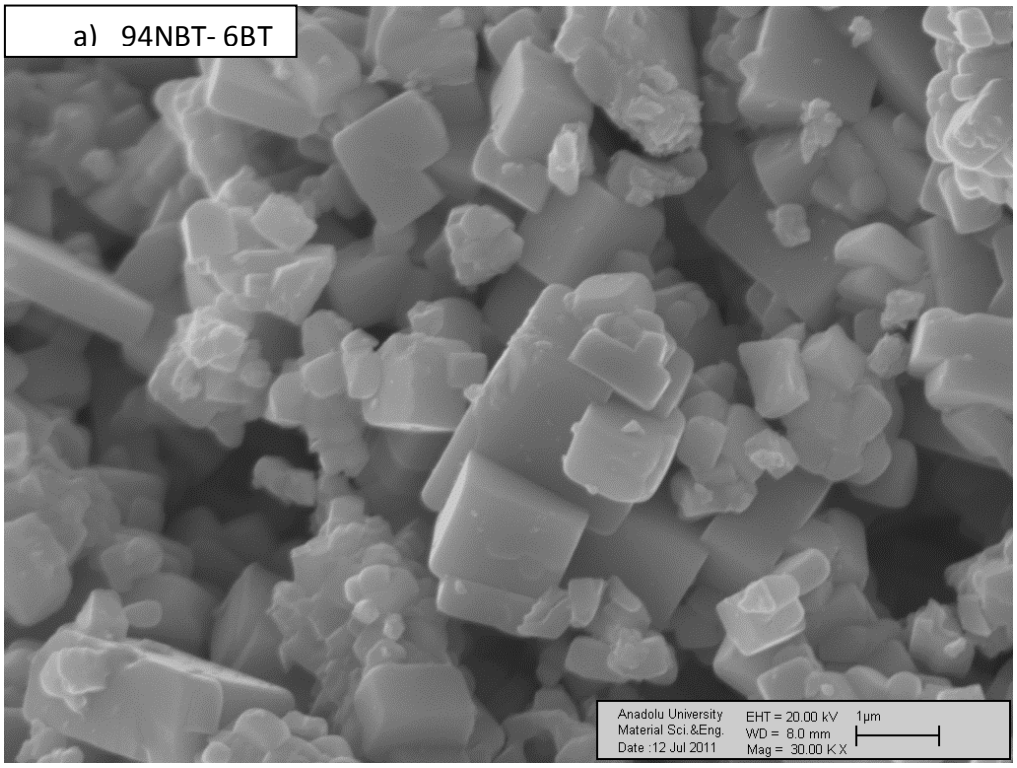

b) 94NBLT- 6BT

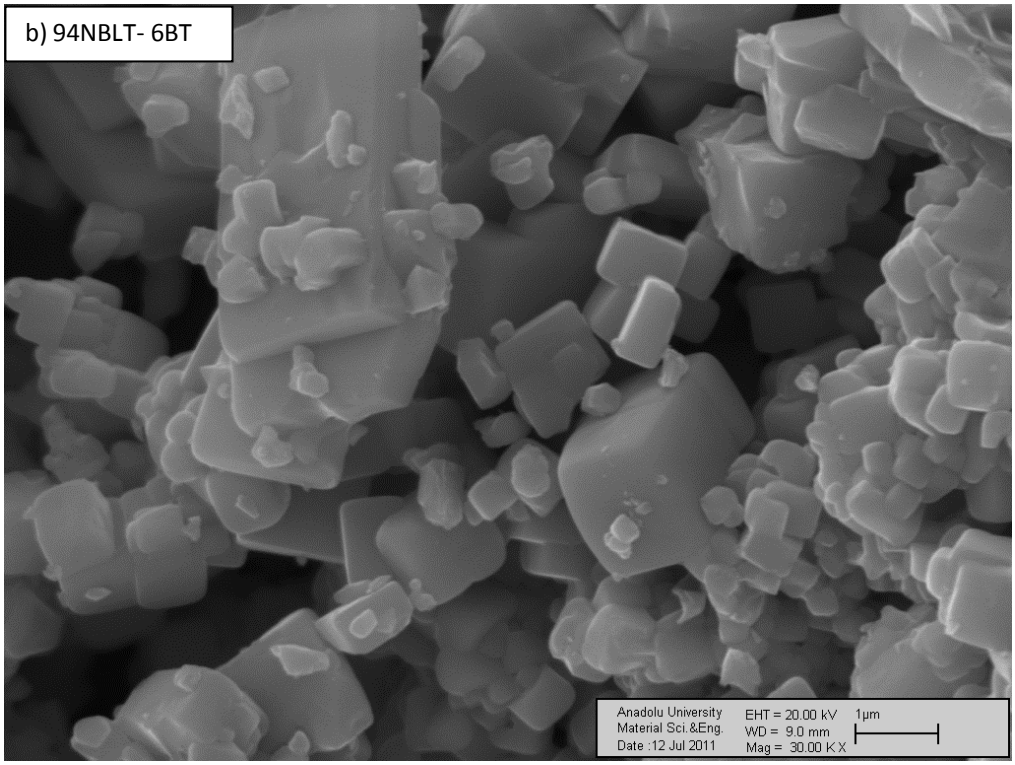

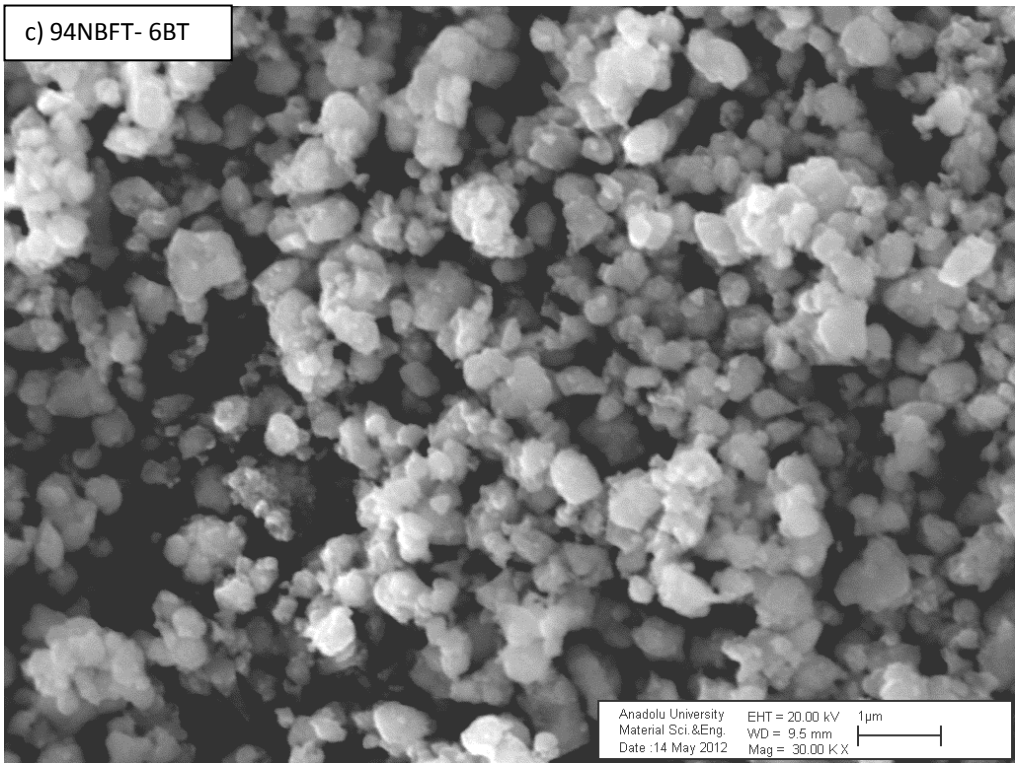

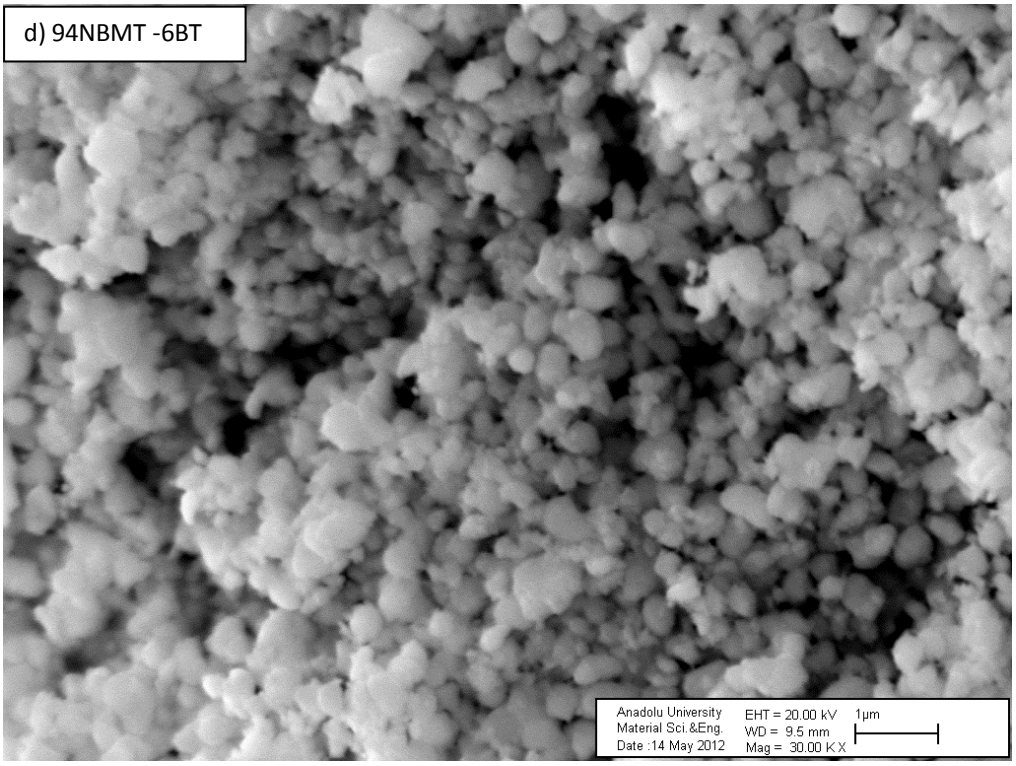

Figure 7.15. SEM images of powders with a composition of 94NBT-6BT: undoped (a) and Li, Fe and Mn doped (b-c-d)

8. SINGLE CRYSTAL GROWTH OF BT AND NBT-BT BY FLUX GROWTH METHOD

8.1. Barium Titanate Single Crystal Production

Barium titanate ($BaTiO_3$) (BT) single crystals were fabricated with flux growth method using BT polycrystal powder which were produced by solid state synthesis method as given by flow chart in Figure 8.1. KF (fluxing agent) was added into the powders, and then placed into a sealed Pt container for heat treatment at 1200^{o}C for15 hours. After very slow cooling process, the melt was cooled to 900^{o}C and then cooled to room temperature. Obtained single crystals were characterized by removing from crystal growth container after the cooling process. Produced single crystal materials were analyzed via stereo microscope, scanning electron microscope (SEM), energy dispersive X-ray technique (EDX) and X-ray diffraction (XRD).

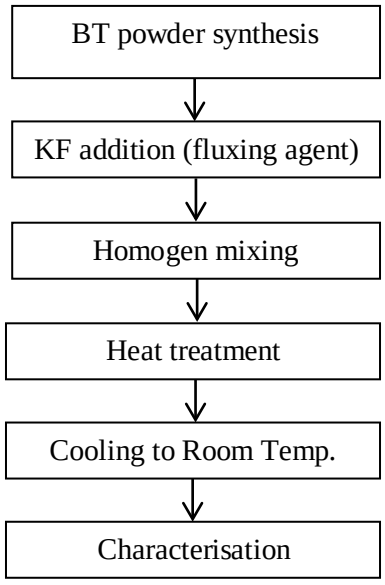

Figure 8.1. Flow chart for the production of BT single crystal

As given in the stereo microscope and SEM images in Figure 8.2, BT crystals have polyhedron structure. Produced crystals are in size smaller than

1mm. From the highly magnified SEM image of samples, grain boundaries are not observed (Figure 8.2c)

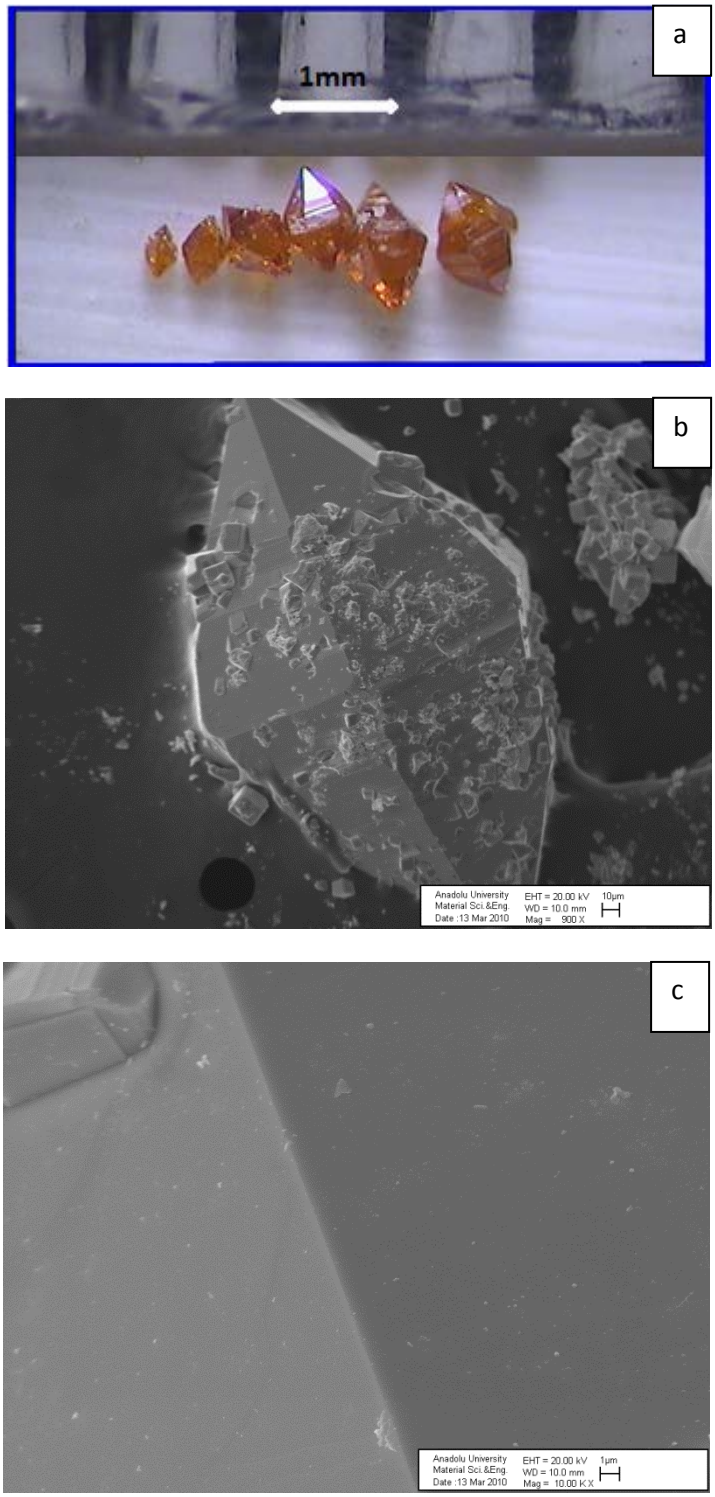

Figure 8.2. Stereo (a) and SEM (b-c) images of BT single crystals

To determine the crystal structure and chemical composition of the grown single crystals, XRD and EDX analysis were performed as given below. From XRD pattern, the structure is determined as perovskite $BaTiO_3$ (Figure 8.3).

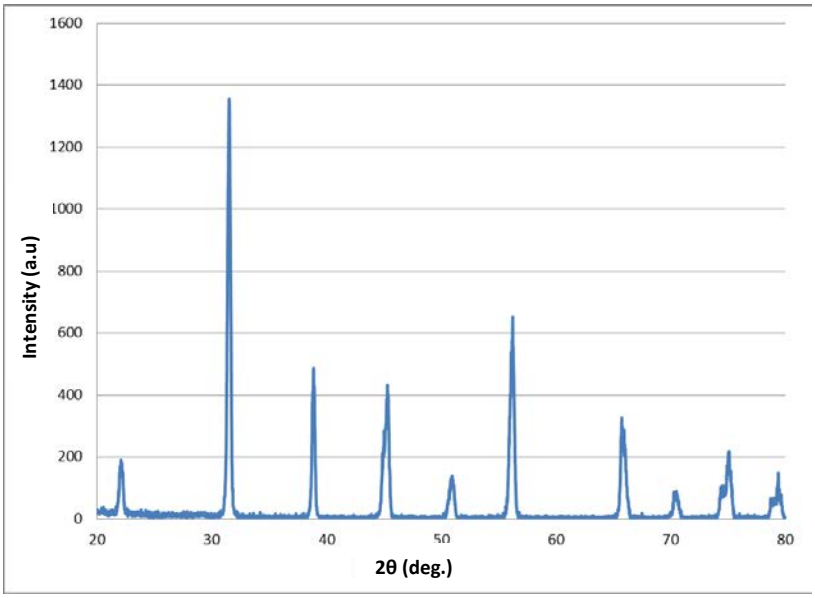

Figure 8.3. XRD pattern of BT single crystal powders

In addition, as can be seen by EDX analysis, there exist O, Ba and Ti peaks as expected within the structure. By the detailed look on EDX peaks, it can be clearly seen that Ba and Ti peaks are overlapped (Figure 8.4a-b). In Table 8.1, from chemical analysis of single crystals, they are determined as close to the expected values.

Table 8.1. Elemental analysis of BT single crystal materials

Element	BT Composition Expected values (Atom C. %)	Grown BT single crystal Experimental EDX results (Atom C. %)
Ba	**20**	**18.90**
Ti	**20**	**21,03**
O	**60**	**60.07**

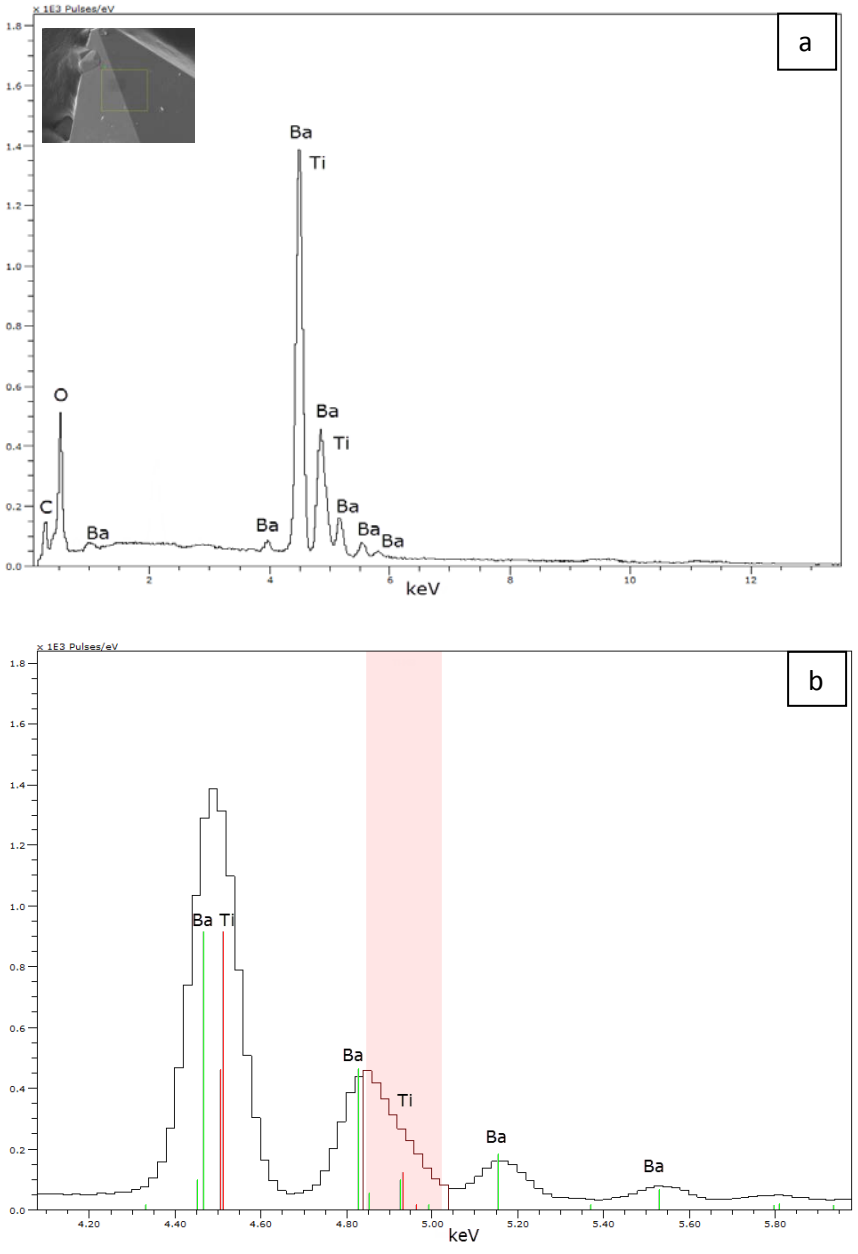

Figure 8.4. EDX analyses of BT single crystal

As a result, 1mm in size BT single crystals were produced by flux growth method. Due to very small size of the produced crystals; the electrical properties could not be investigated.

8.2. Production of 94NBT-6BT Based Single Crystal Materials

Polycrystal powders which are necessary for the production of 94NBT-6BT single crystals from their melt (flux growth). Powders were produced using bismuth oxide (Bi_2O_3), sodium carbonate (Na_2CO_3), titanium dioxide (TiO_2) and barium carbonate ($BaCO_3$) as starting material via solid state synthesis method. Li_2CO_3, Fe_2O_3, MnO_2 were used as dopant materials.

Single crystal production method was performed as given in Figure 8.5 for doped and undoped 94NBT-6BT composition. As can be seen in the figure Li, Fe, and Mn were added into the synthesized powders. After calcination process of powder, 20% by weight $NaCO_3$ and Bi_2O_3 fluxing agent were added. The reason for the addition is to reduce losses due to evaporation at high temperature and to prevent the stoichiometry change. Homogeneously ground and mixed raw materials were placed into the platinum crucible after the application of drying and sieving. Crucible cover cap were sealed with alumina cement to prevent leakage problem. Undoped and Li doped powders were also weighed after the addition of fluxing agent at the desired chemical composition, and ground homogeneously. The powders were directly fed in platinum crucible without calcination. To obtain the melt the temperature was determined as 1380^{o}C and it was kept at this temperature for approximately 5-10 hours with respect to composition. And then it was cooled to 900^{o}C at the cooling rate of 1^{o}C/hour. After this temperature it cooled to room temperature in the rate of 100^{o}C/hour and by this way doped and undoped 94NBT-6BT single crystals were produced. Crystal structures and elemental composition of produced single crystals were analyzed using XRD, EDX, XRF technique.

Piezoelectric properties, dielectric properties depending on temperature and frequency, coercive field and remanent polarization values and result of leakage current densities are given in chapter 10 and compared with each other.

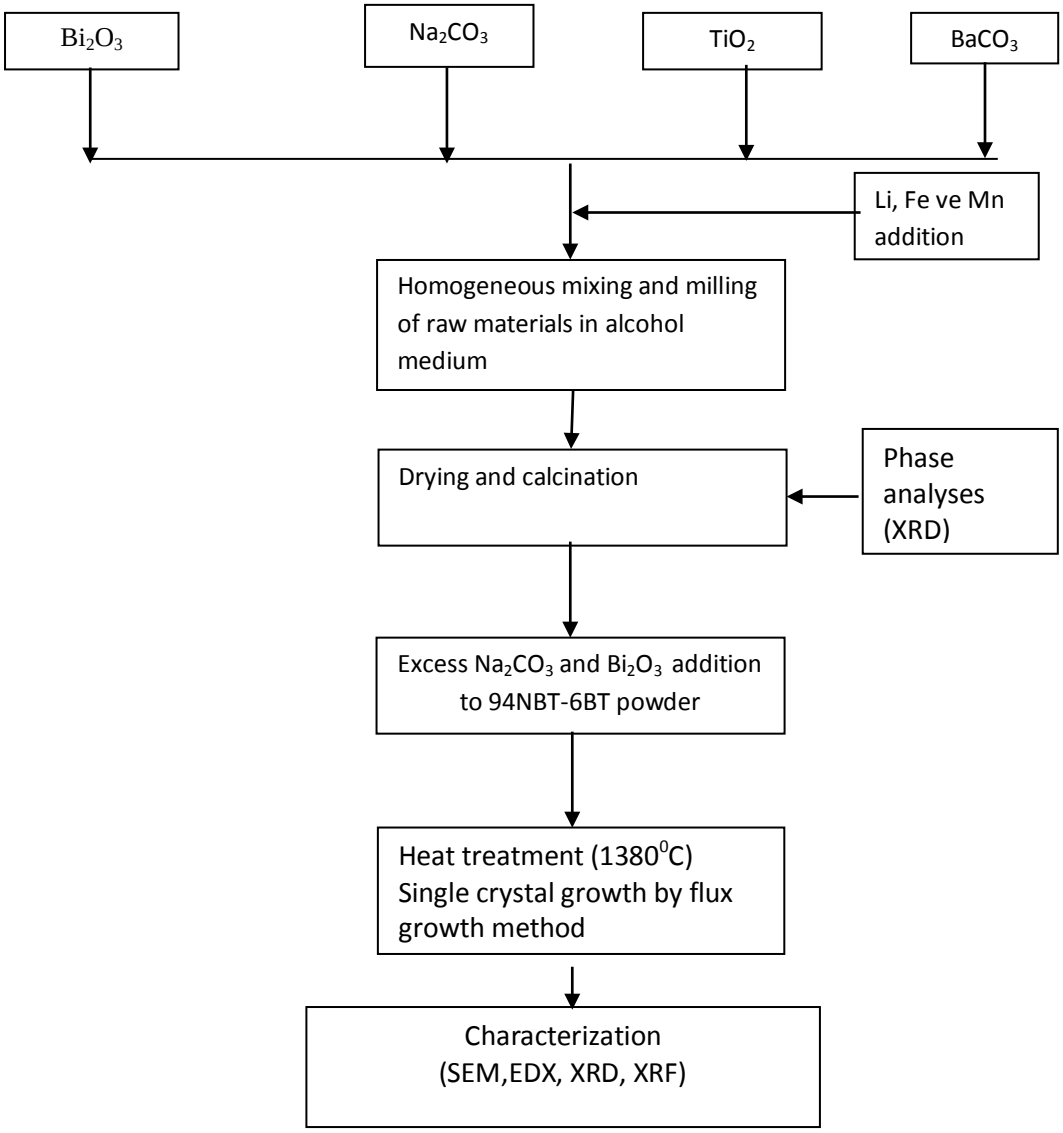

Figure 8.5. Flow chart for the production of 94NBT-6BT single crystal

Codes and explanation of processes of single crystal materials are given in Table 8.2. As seen in the table, six different single crystal materials were produced for composition of 94NBT-6BT. RW-coded single crystals were grown using uncalcined powder. KAL-coded single crystals were grown using solid state synthesized powders.

Table 8.2. Elemental analysis of BT single crystal materials

MATERILAS CODES	EXPLANATION
94NBT-6BT RW	$94Na_{0.5}Bi_{0.5}TiO_3$-$6BaTiO_3$ single crystals were grown using uncalcined powder.
94NBT-6BT KAL	$94Na_{0.5}$ $Bi_{0.5}$ TiO_3 -6 $BaTiO_3$ single crystals were grown using calcined powder at 900^oC
94NBLT-6BT RW	Li doped $94Na_{0.5}Bi_{0.5}TiO_3$-$6BaTiO_3$ single crystals were grown using uncalcined powder
94NBLT-6BT KAL	Li doped $94Na_{0.5}Bi_{0.5}TiO_3$-$6BaTiO_3$ single crystals were grown using calcined powder at 900^oC
94NBFT-6BT KAL	Fe doped $94Na_{0.5}Bi_{0.5}TiO_3$-$6BaTiO_3$ single crystals were grown using calcined powder at 900^oC
94NBMT-6BT KAL	Mn doped $94Na_{0.5}Bi_{0.5}TiO_3$-$6BaTiO_3$ single crystals were grown using calcined powder at 900^oC

8.2.1. Thermal analysis studies for the production of 94NBT-6BT based single crystal

Determination of melting temperature is important for the melting of powder to perform single crystal growth from NBT-BT-based powders. Melting point was analyzed using DSC (differential scanning calorimeter) and heat microscope for the growth of powder from 94NBT-6BT melt. As can be seen in Figure 8.6 there was endothermic peak observed at about 1288^{o}C for powder. This temperature is melting point of the powders because materials takes the heat during melting.

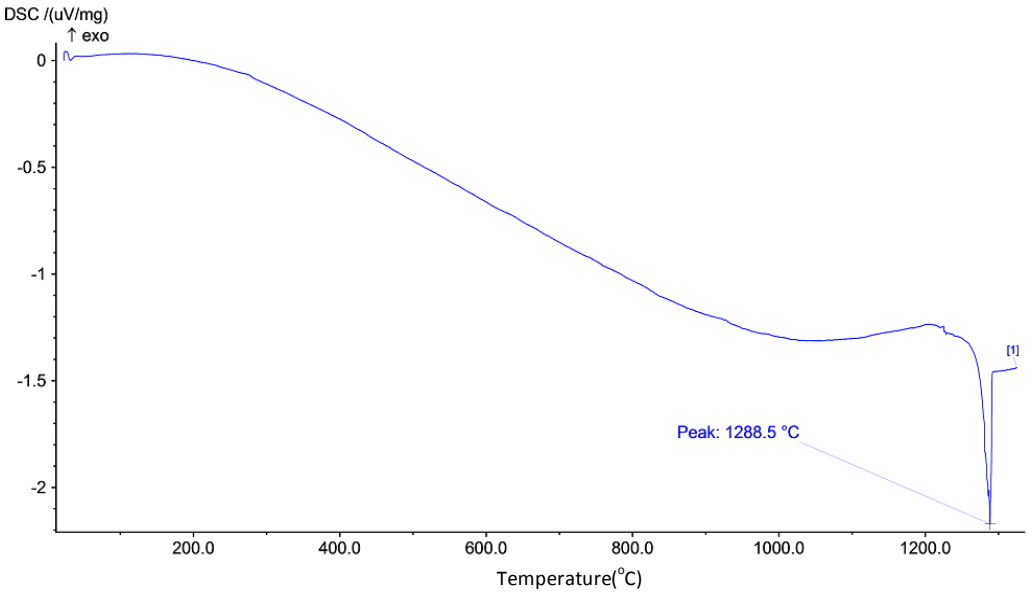

Figure 8.6. DSC analysis of 94NBT-6BT composition

Also, heat microscopy analyzes were carried out to verify the melting point. As shown the figure, the size of powder based samples starts to decrease at approximately around 1000^{o}C. There is a dimensional expansion at 1250^{o}C the material starts to be soften and it is completely melted at approximately 1280^{o}C (Fig. 8.7a). In Figure 8.7b it can be seen that produced powders were pressed and subjected to heat treatment at 1150^{o}C. As can be seen, dimensional change is quite low up to 1250^{o}C; it started softening just before this temperature and then melting. The thermal microscopy images in Figure 8.8 also confirm the mentioned

results. Material has saved its structure up to 1250°C but there is a deformation on the structure and at just after 1270°C it is completely melted. As a result, results from DSC and heat microscopy analysis confirm each other for the determination of melting point. For single crystal growth from the melt, the melting temperature was chosen as 1380°C which is above 100°C of the melting point of the powder.

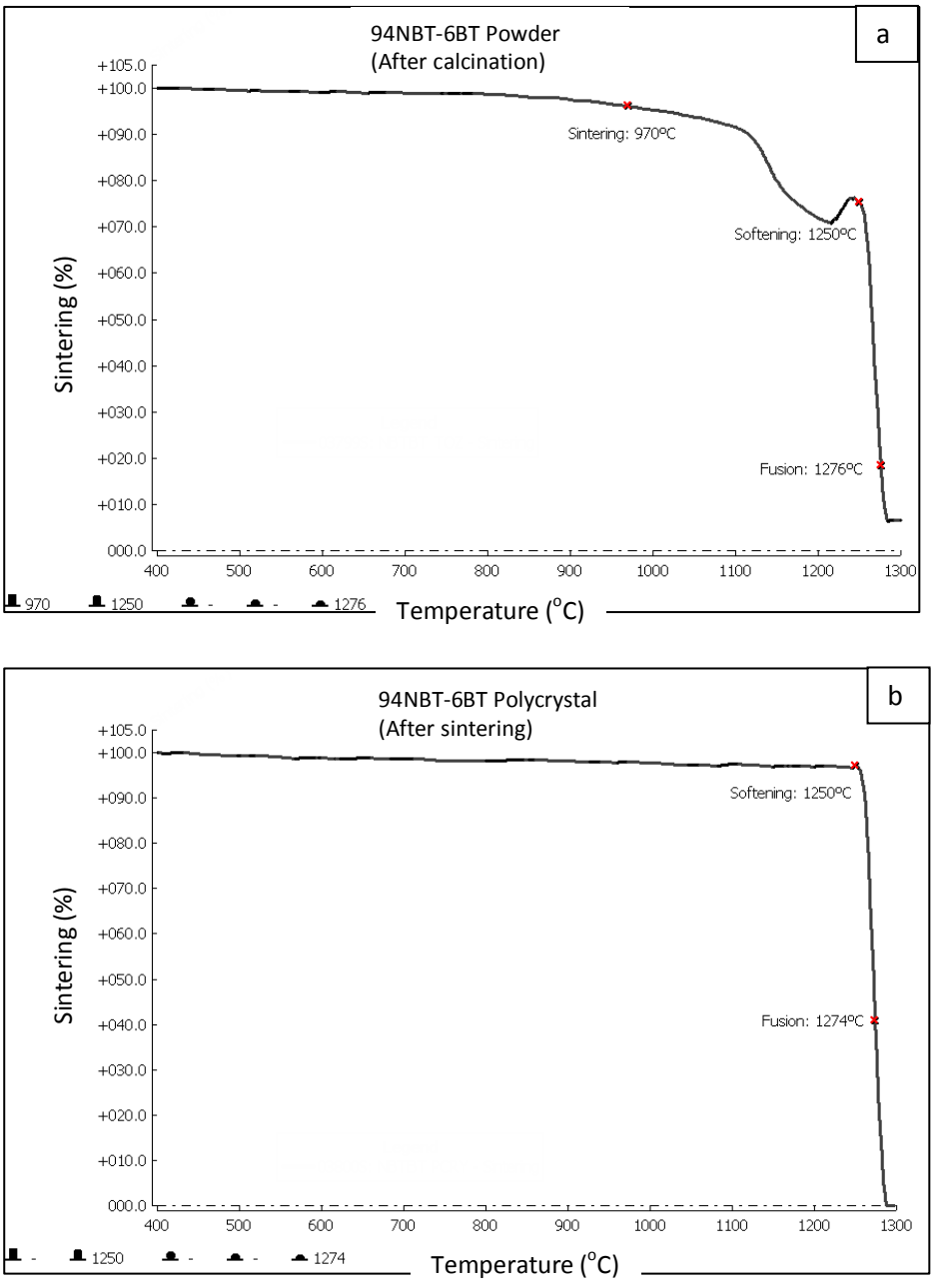

Figure 8.7. Heat microscopy analysis of 94NBT-6BT in the form of powder (a) and pellet (b)

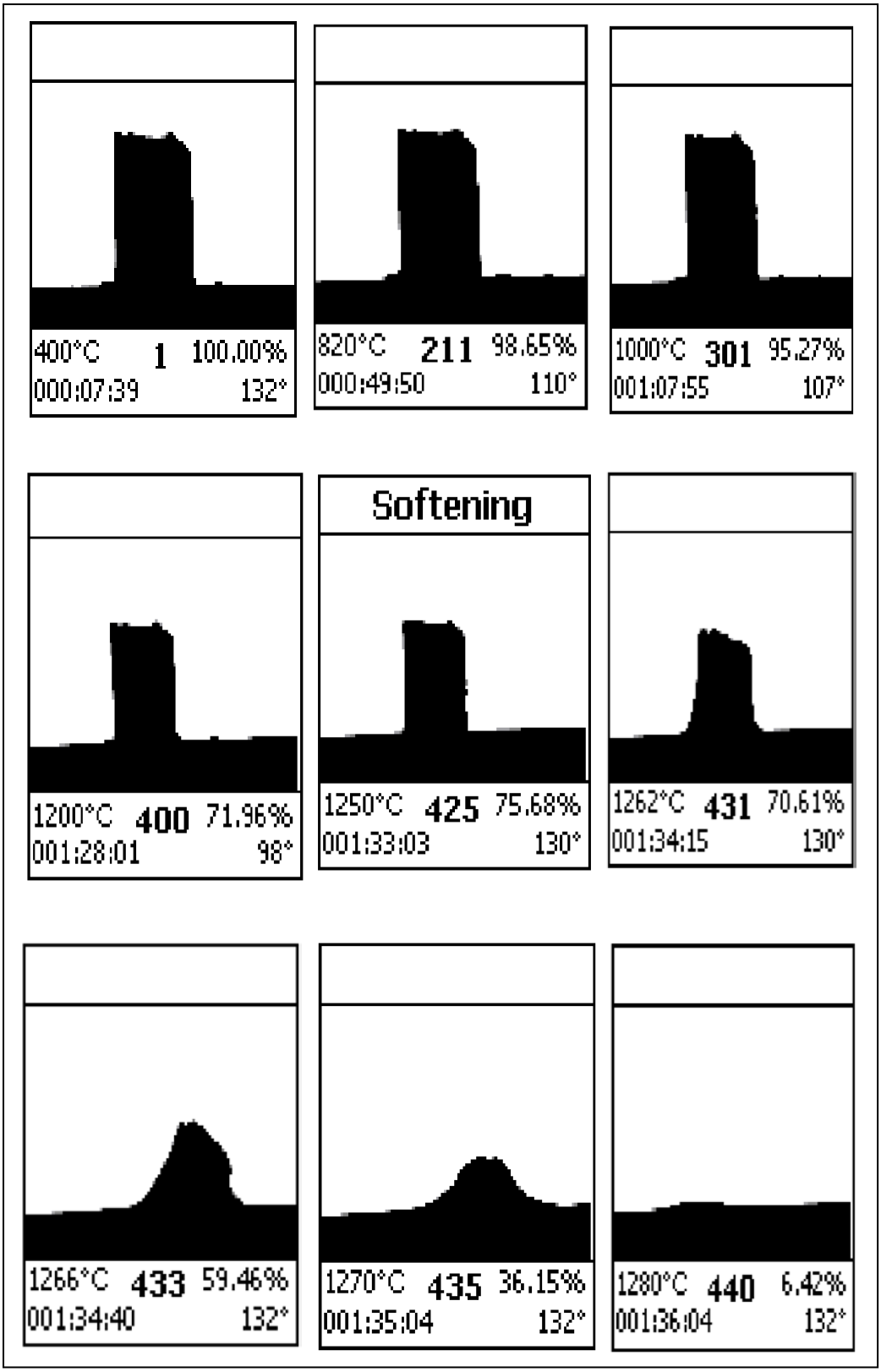

Figure 8.8. Temperature dependent heat microscopy analysis of the 94NBT-6BT powder

8.2.2. 94NBT-6BT based single crystal growth and characterization

As stated in the previous section, all of compositions based on 94NBT-6BT were melted at 1380^{o}C for 5-10 hours in the platinum crucible and cooled at very slow cooling rates to 900^{o}C firstly and then to room temperature. At the end of the cooling, dimensions of 94NBT-6BT KAL and 94NBT-6BT RW coded single crystals produced was measured approximately as 3x3x3 mm (Figure 8.9a-b). In Figure, as can be seen, the samples are transparent after the polishing, and there is no residues in crysttals. For both the fracture surface and polished surface of the produced crystals, SEM analysis were performed (Figure 8.10). Particles and grain boundaries for polycrystal 94NBT-6BT KAL material are observed clearly, whereas gain boundary for fracture surface of single crystal samples are not observed. Any deformation or failure is not observed as a result of SEM analysis for polished samples (Fig. 10b-c).

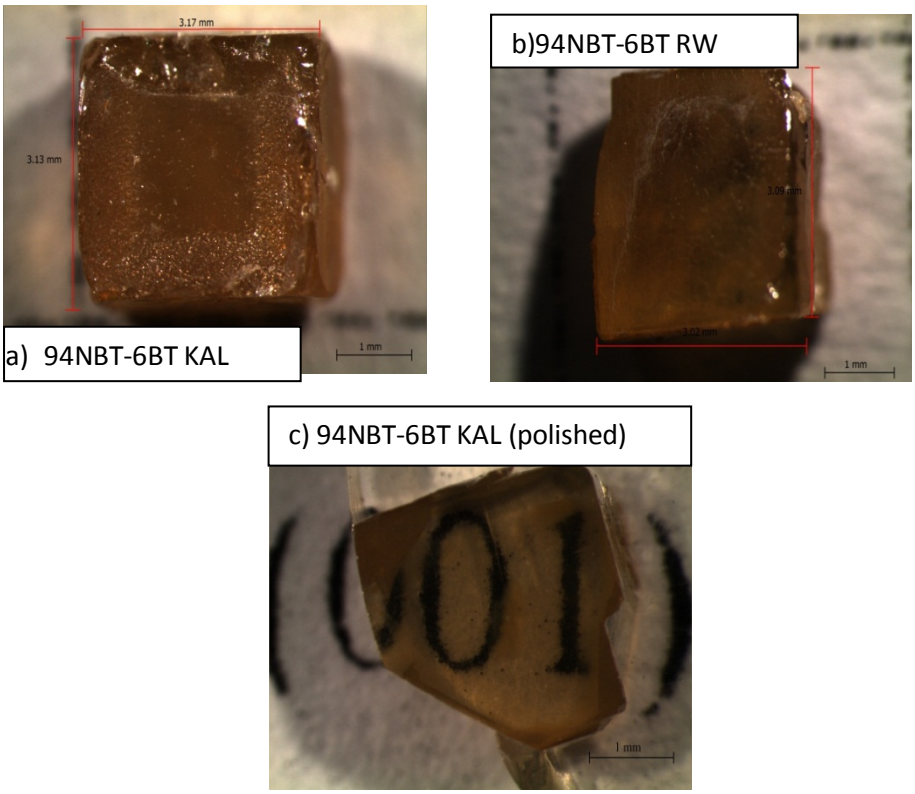

Figure 8.9. Stereo microscope images of 94NBT-6BT based single crystals before polishing (a-b) and after polishing (c)

a) 94NBT-6BT KAL Polycrystal Fracture Surface

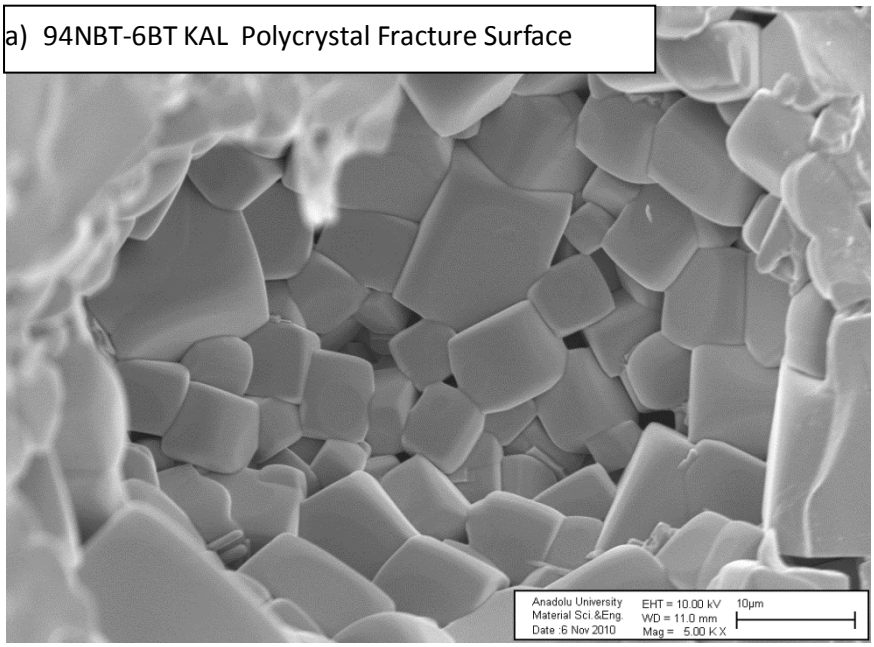

b) 94NBT-6BT KAL Single Crystal Fracture Surface

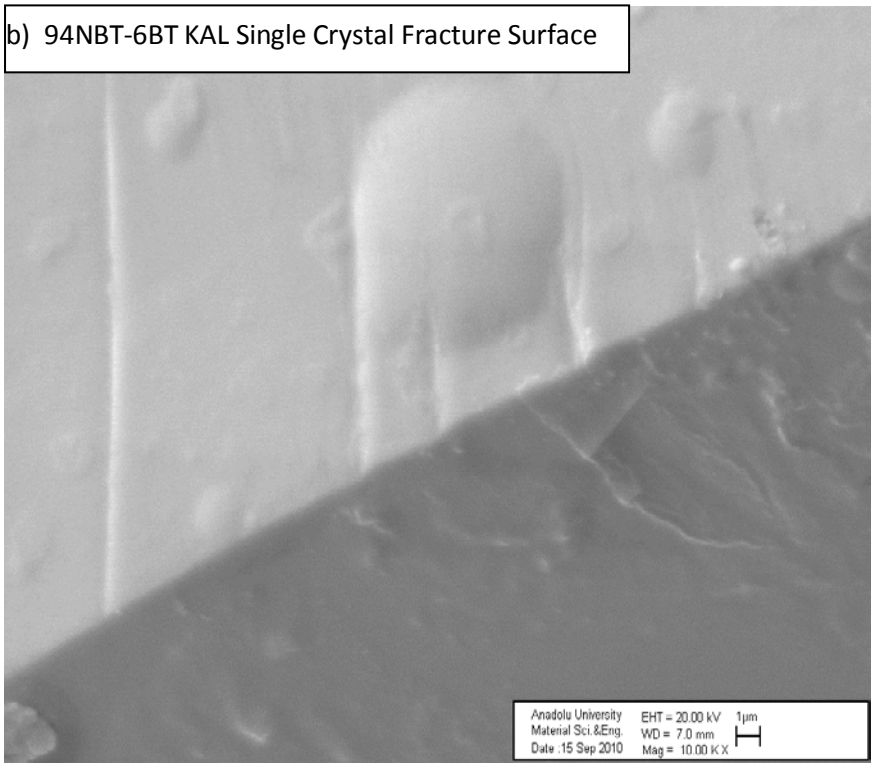

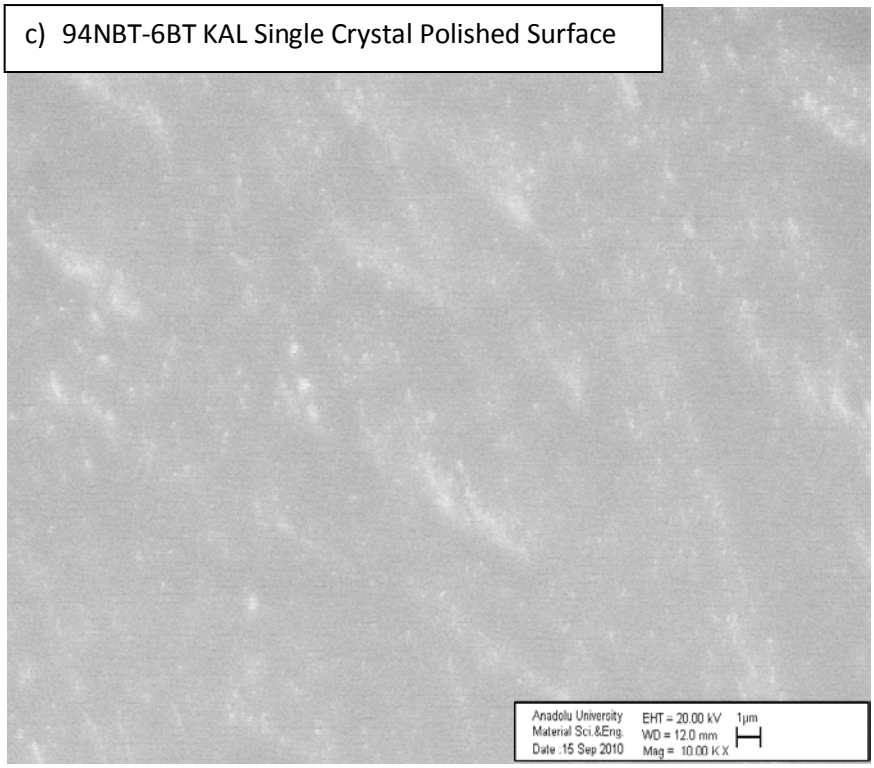

Figure 8.10. SEM images of the fracture surface for polycrystal (a) and fracture and polished surface (b-c) 94NBT-6BT single crystals

XRD analyzes were performed to determine whether 94NBT-6BT KAL system to be single crystal or not. In Figure 8.11a, XRD pattern for 94NBT-6BT KAL coded polycrystal can be seen. As can be seen here, the diffractions from all planes are obtained. It is determined that crystal structure has the structure of 94 $(Na_{0.5}Bi_{0.5})$ TiO_3-6$BaTiO_3$. Similarly, the produced single crystal materials were ground to get powder form, and XRD analysis was performed. As can be seen in Figure 8.11b, the same diffraction patterns are observed with the polycrystal powder. It is observed that single crystal samples in powder form and calcined powder have completely perovskite structure and also there are no undesired phases. When XRD analysis is performed for polished sample in a oriented direction, it is observed that there is diffraction from only one plane (Figure 8.11c). This is the strongest indication that the produced sample is single crystal.

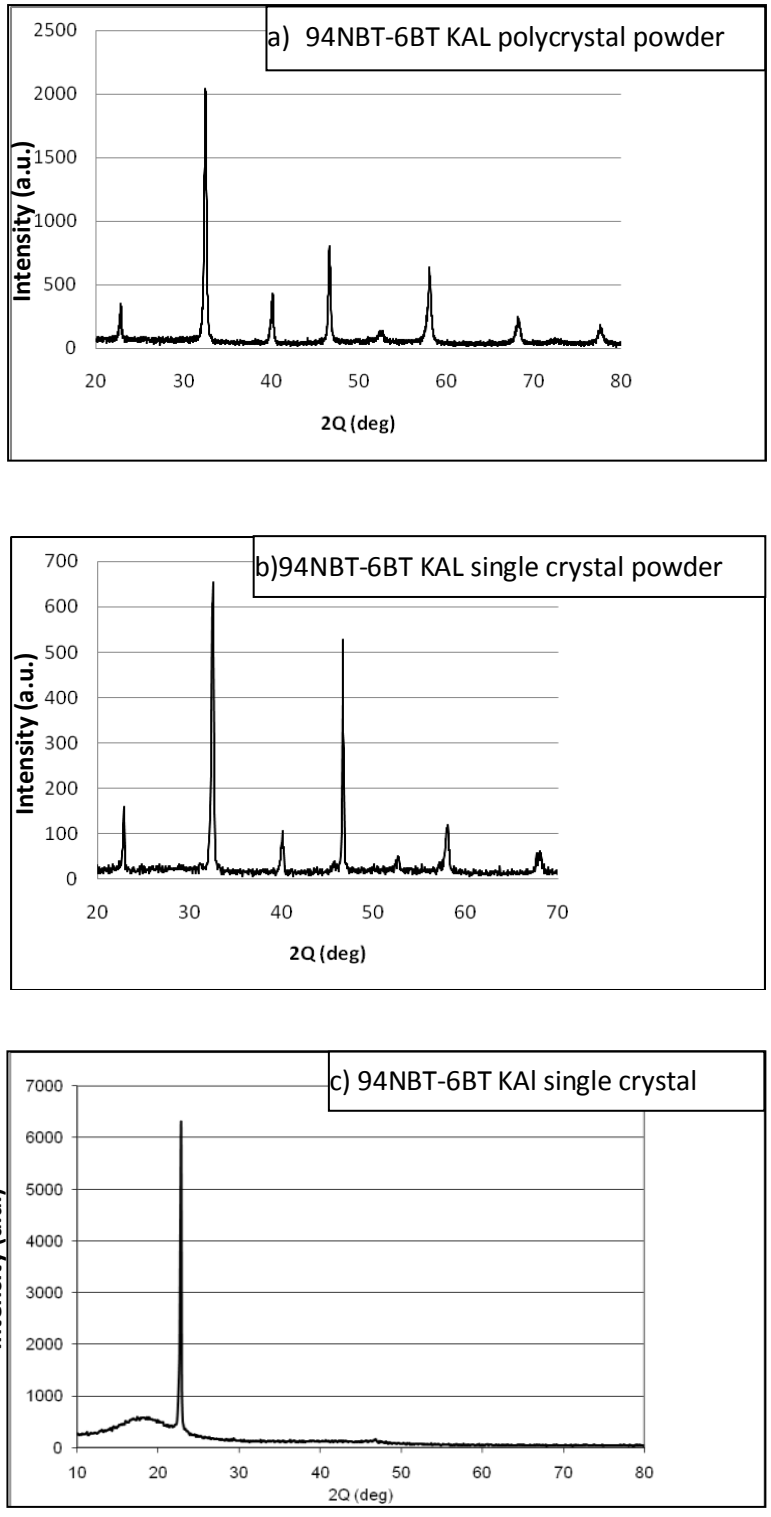

Figure 8.11. XRD pattern for polycrystal powder (a) single crystal powder from a single crystal structure (b) and the bulk single crystal (c) with a composition of 94NBT-6BT KAL

NBT and BT crystal possessed rombohedral and tetragonal symmetry at room temperature. When the BT concentration increases, NBT-BT crystal includes both rombohedral and tetragonal phase. Peak siplitting were investigated to determine rhombohedral structure $(Na_{0.5}Bi_{0.5})TiO_3$ or tetragonal $BaTiO_3$, by measurement of peaks between 39-41^o and 45-48^o via slow XRD rate (Figure 8.12). As shown in the figure, (003) and (021) siplitting are observed from (111) peak. This peak siplitting is specific to the rhombohedral NBT structure. Similarly, the (200) peak is separated from (002) peak. This peak siplitting is specific for tetragonal BT [91,97]. This result confirms that the structure has composition of NBT-BT.

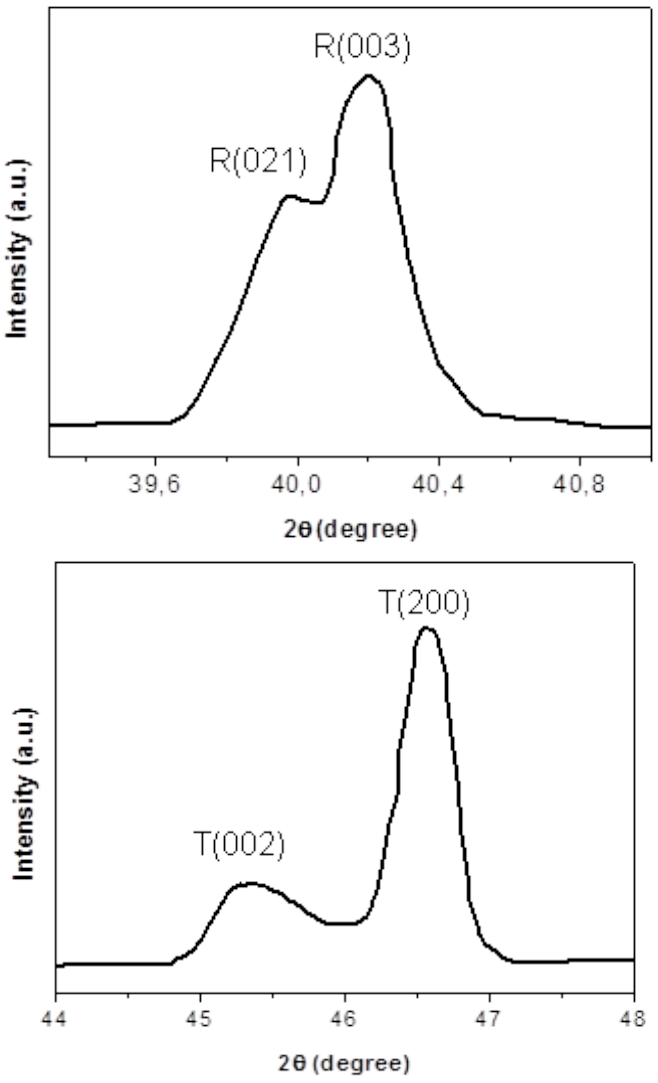

Figure 8.12. Peak siplitting for (111) and (200) diffraction in the case of 2θ = 39-41^o and 45-48^o

Figure 8.13 shows the undoped and Li, Fe, and Mn doped single crystals. Grown samples with dimensions ranged from 3x3x1 and 5x5x1 mm after polishing. Undoped and Li doped crystals of crystals are yellowish in color, whereas Fe and Mn doped crystals are dark brown and blackish in color.

a) 94NBT-6BT RW SCRY

b) 94NBT-6BT KAL SCRY

c) 94NBLT-6BT RW SCRY

d) 94NBLT-6BT KAL SCRY

Figure 8.13. Photos of undoped and Li, Fe, and Mn doped 94NBT-6BT-based single crystals

Figure 8.14 and 8.15 shows the XRD pattern of grown crystals in a certain direction and single crystal powder, respectively. As can be seen, all compositions are preferentially oriented at (001). The powdered samples for all crystals have no other undesired phases, it incudes completely perovskite structure.

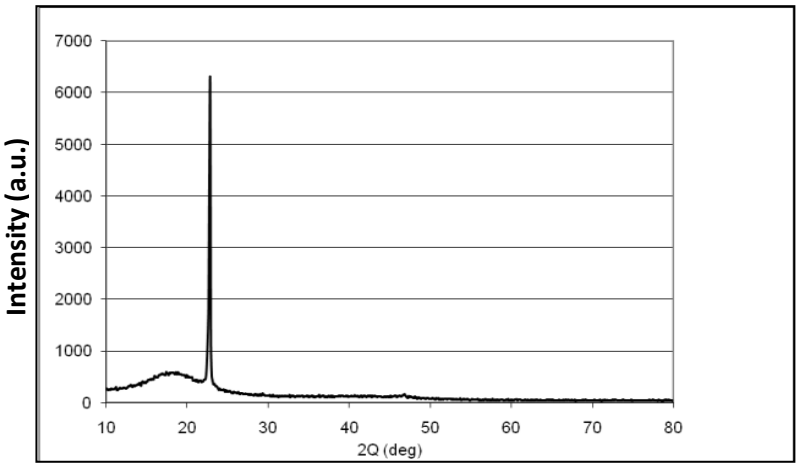

Figure 8.14. XRD pattern of oriented 94NBT-6BT based single crystal

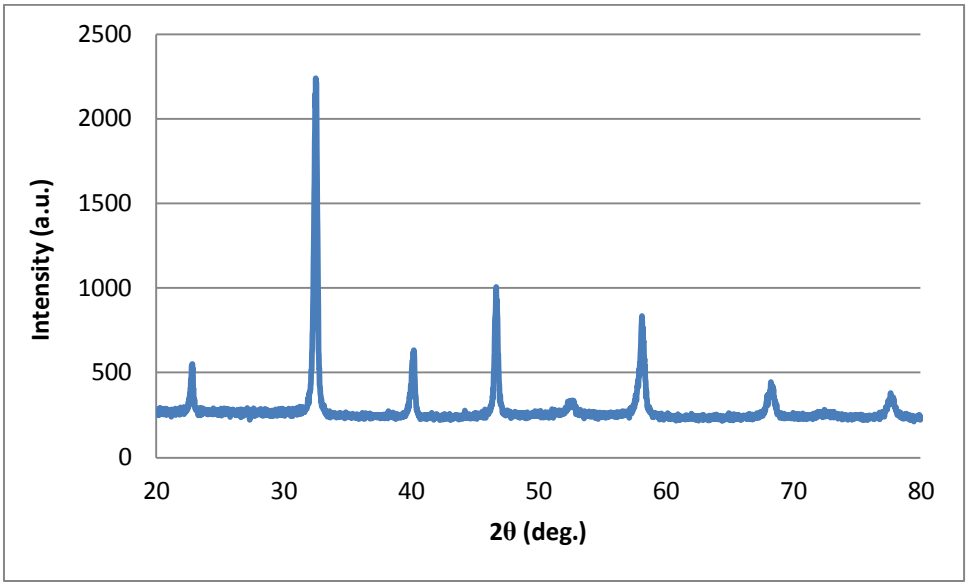

Figure 8.15. XRD pattern of 94NBT-6BT based single crystal powder

EDX and XRF analysis were performed to understand if any loss due to evaporation for crystals grown and if any differences in chemical composition. As can be seen in Figure 8.16, according to the EDX result, Na, Bi, Ti, Ba and O are observed for undoped 94NBT-6BT compositions. Fe and Mn peaks are shown as well as Na, Bi, Ti, Ba and O for doped crystals. The peaks of lithium did not appear in EDX spectra due to the light mass of lithium. In addition, from EDX and XRF result given in Table 8.3 and Table 8.4, the expected values and experimental values of composition and grown crystals are quite close to each other, especially for KAL codded single crystals. However, the desired atomic percentages could not be reached for RW-coded samples. It can be explained that, when the uncalcined powders are used for crystal growth, evaporation tendency of uncalcined powder increases. It can be concluded that evaporation loss can be compensated by excess $NaCO_3$ and Bi_2O_3 addition for KAL coded samples.

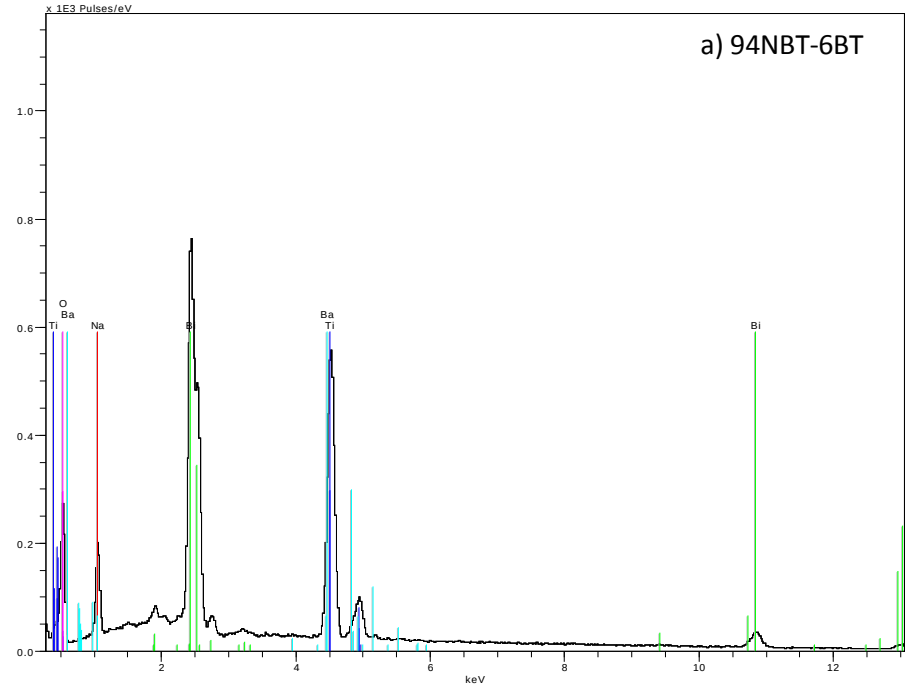

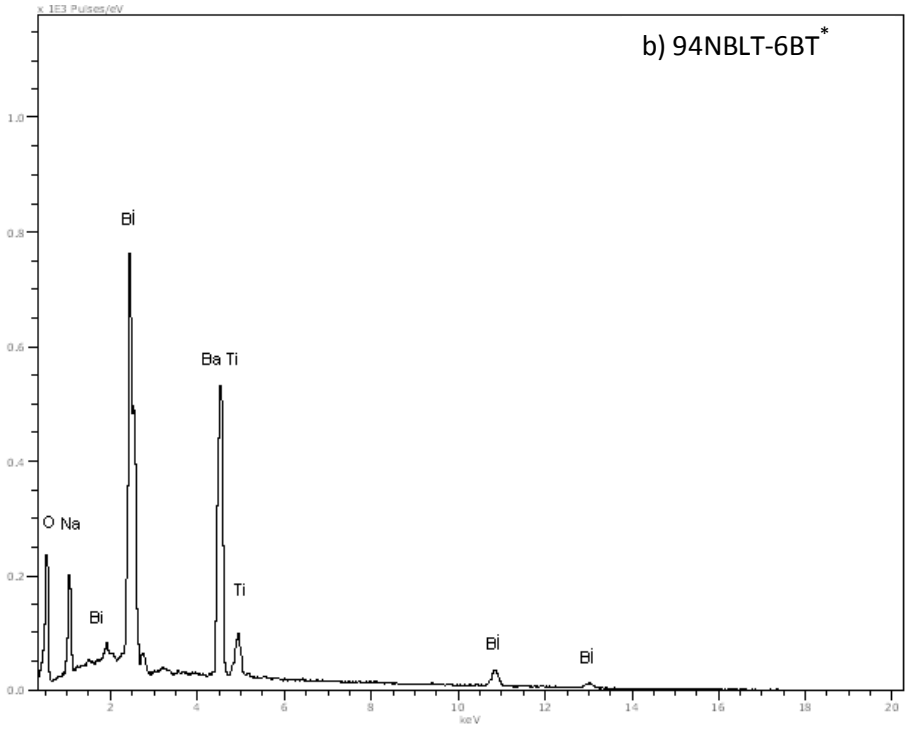

* The peaks of lithium does not appear in EDX spectra due to the light mass of lithium

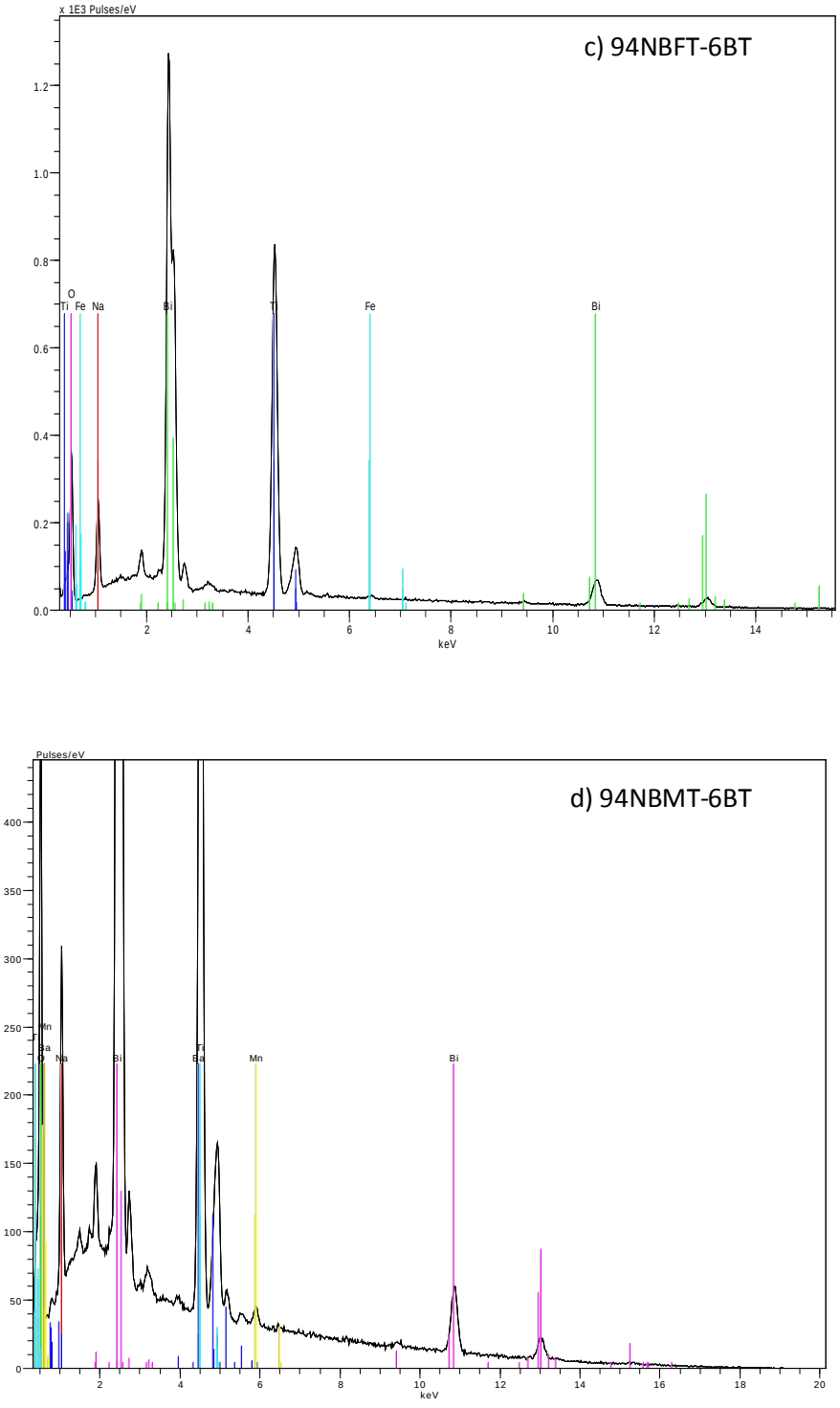

Figure 8.16. EDX analysis of undoped and Li, Fe, Mn 94NBT-6BT doped single crystals

Table 8.3. Elemental analysis of undoped and Li, Fe, Mn doped 94NBT-6BT single crystals

COMPOSITIONS		ATOMIC (%)							
		Na	Bi	Ti	Ba	O	Li	Fe	Mn
94NBT-6BT	Expected	9,4	9,4	20	1,2	60	-	-	-
94NBLT-6BT	Expected	9,17	9,4	20	1,2	60	0,235	-	-
94NBFT-6BT	Expected	9,17	9,4	20	1,2	60	-	0,235	-
94NBMT-6BT	Expected	9,17	9,4	20	1,2	60	-	-	0,235
94NBT-6BT RW	Experimental	7,69	10,23	20,75	0,31	61,01	-	-	-
94NBT-6BT KAL	Experimental	10,33	10,4	19,22	0,94	59,11	-	-	-
94NBLT-6BT RW	Experimental	7,95	10,11	20,85	0,38	60,6	*	-	-
94NBLT-6BT KAL	Experimental	9,62	9,85	20,25	1,05	59,22	*	-	-
94NBFT-6BT KAL	Experimental	9,35	10,45	19,8	0,98	59,2	-	0,215	
94NBMT-6BT KAL	Experimental	9,32	10,20	19,42	0,96	59,88	-	-	0,221

* The lithium can not analyzed in EDX spectra due to the light mass of lithium

Table 8.4. XRF analysis of undoped and Li, Fe, Mn doped 94NBT-6BT crystals

MATERIALS CODES	Bi_2O_3	Na_2O	TiO_2	BaO	Li_2O	Fe_2O_3	MnO_2
94NBT-6BT Expected	51,62	7,31	37,44	3,94	-	-	-
94NBLT-6BT Expected	51,73	7,13	37,52	3,94	0,088	-	-
94NBFT-6BT Expected	51,55	7,11	37,38	3,94	-	0,442	-
94NBMT-6BT Expected	51,66	6,51	37,46	3,94	-	-	0,24
94NBT-6BT RW Exp.	51,98	6,52	37,58	3,87	-	-	-
94NBT-6BT KAL Exp.	53,66	7,85	34,64	3,78	-	-	-
94NBLT-6BT RW Exp.	51,80	6,52	37,58	3,87	*		
94NBLT-6BT KAL Exp.	51,78	7,44	36,85	3,21	*		
94NBFT-6BT KAL Exp.	51,62	8,75	35,59	3,52	-	0,57	-
94NBMT-6BT KAL Exp.	52,31	6,79	37,6	3,20	-	-	0,09

*The lithium can not analyzed with XRF due to the light mass of lithium

9. STUDIES FOR SOLID STATE SINGLE CRYSTAL GROWTH

According to the performed studies, when NBT-BT-based piezoelectric materials are produced as single crystal, the piezoelectric properties are improved. As given in the previous sections; Czochralski, Bridgeman, top seeded solution growth (TSSG), flux growth are used for crystal growth. These methods are based on high temperature and the melt base process, because of these reasons these methods are not cost effective. In addition, the control of chemical homogenity of produced crystals is difficult due to the evaporation during processing.

In recent years, solid state single crystal production (SSCG) method has been used as a new method for production of piezoelectric NBT-BT single crystals. This method is quite similar with conventional ceramic sintering method, and it is easier and more economical method as compared to others. Basically, single crystal seed is embedded into polycrystal powder and shaped under hot press. Produced material as a result of hot pressing is exposed to heat treatment at a suitable temperature and time to start single crystal growth. Structure consists of small pores during hot pressing, but this causes decrease in the density of the matrix material, weak interaction between matrix and seed and the existing of small pores in the structure at the end of the growth. To eliminate these problems, spark plasma sintering technique (SPS) has been used recently for piezoelectric materials [98,99]. In Figure 9.1, according to the working principle of the SPS method, sintering is taken place by passing of high current density direct electric current via graphite mold through powder. The biggest advantage of this method is that heating and cooling may be carried out very fast depending on current due to the fact that there is no other special heater. Also with the SPS method, sintering can be performed at lower temperatures than common sintering method. Highly dense materials can be produced via SPS at lower temperature and shorter sintering times [100,101].

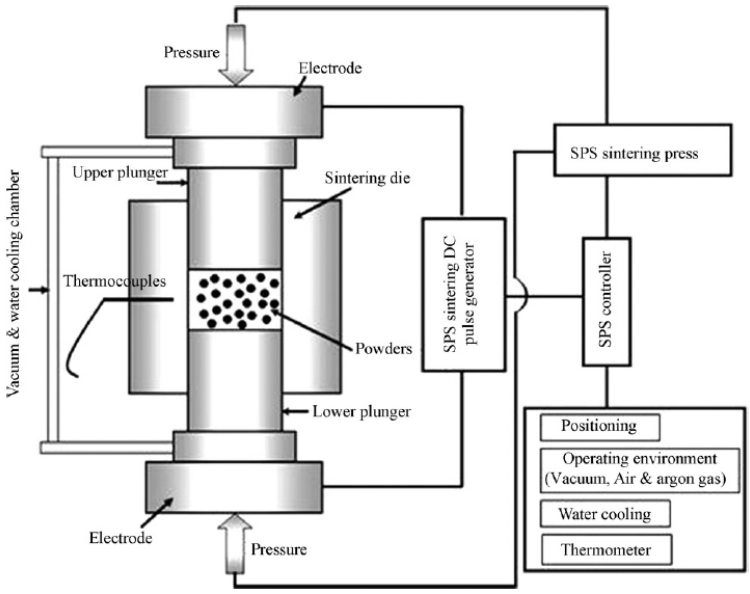

Figure 9.1. A schematic view of SPS method [101]

There is no a lot of study performed by the SPS supported SSCG method. So far, a study was conducted on PMN-PT. According to the study, polycrystal matrix materials were obtained with nearly 100% theoretical density and strong connections between matrix-seed interface has achieved [99]**.** On the other hand, there is almost no study about SPS assisted SSCG of piezoelectric lead free materials. In Figure 9.2, in relation to the method of the SSCG, Kang et al. have studied on NBT-BT, and Fisher et al. have focused on KNN. According to these studies it has been observed that residual pores within polycrystal matrix has been entrapped within the single crystal. This is the biggest disadvantage of the SSCG method [77,98]**.**

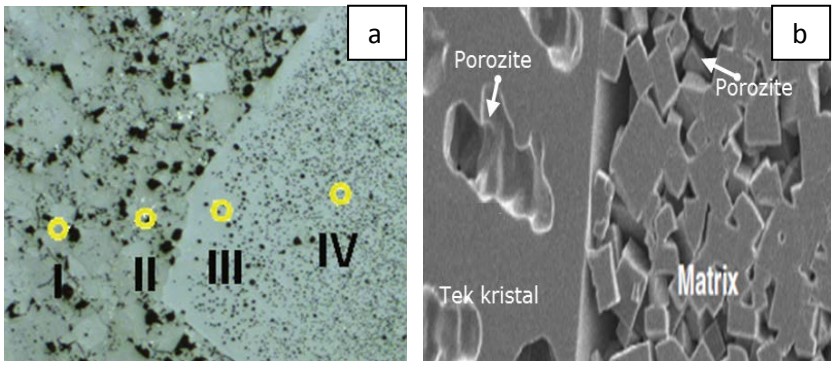

Figure 9.2. Grown NBT-BT (a) and KNN (b) single crystals with SSCG method [77,98]

It is thought that mentioned problems can be eliminated by using SPS method. SPS method can be used for NBT-BT single crystal production because of providing the production of highly dense polycrystal matrix material and increasing attachment of dense matrix phase to the single crystal interface. Therefore, the NBT based powders, codes of which are given in Table 9.1. These powders were sintered with solid state sintering (CS) and SPS method. Effect of sintering on the density of matrix material was compared for these methods. In addition, single crystal seed material was embedded into the structure using both of these two methods and so matrix interface connection was compared. Piezoelectric, dielectric and leakage current density of these materials are given in Chapter 11 in this thesis.

Powders were produced using solid state synthesis method as given in Chapter 7. Calcined and granulated powders were used for conventional solid state sintering method (CS), whereas calcined and ungranulated powders were used for spark plasma sintering (SPS) method. The granulated and ungranulated powders were sieved under 75 microns and 100 microns, respectively. Studies related to the sintering of NBT-based powders via CS and SPS are given below,the results are compared.

Table 9.1. Codes and description for powders used in CS and SPS methods

MATERIALS CODE	EXPLANATION
NBT	$Na_{0.5}$ $Bi_{0.5}$ TiO_3 powder which is synthesized with solid state powder synthesis method at 900 ^oC
94NBT-6BT	$94Na_{0.5}Bi_{0.5}TiO_3$-$6BaTiO_3$ powder which is synthesized with solid state powder synthesis method at 900 ^oC
NBLT	Li doped $Na_{0.5}$ $Bi_{0.5}$ TiO_3 powder which is synthesized with solid state powder synthesis method at 900 ^oC
94NBLT-6BT	Li doped $94Na_{0.5}Bi_{0.5}TiO_3$-$6BaTiO_3$ powder which is synthesized with solid state powder synthesis method at 900 ^oC

9.1. Sintering of NBT-Based Powder via CS and SPS Method and Microstructure Characterization

NBT, NBLT, 94NBT-6BT, 94NBLT-6BT powders were calcined using solid state synthesis method at 900^{o}C for 4 hours. In Figure 9.3, sintering process steps performed via CS and SPS method are given. For sintering via CS, 3% polyvinyl alcohol (PVA) was added to calcined powder. PVA containing dried powders were sieved under 75 micron and then they became disk shaped by the application of 4 ton press. As a last part the 300 MPa pressure was applied using cold isostatic pressing. The formed samples after pressing were sintered at 1130, 1150 and 1180^{o}C for 2 hours using CS method. For SPS sintering method, powders were grounded using agate mortar after calcination without PVA addition and sieved under 100 microns. They were sintered at different pressures (30-50MPa) at 900 and 950^{o}C for 5 minutes. Carbon resulting from graphite mold has been removed by application of 1000^{o}C on samples sintered for 3-5 hours.

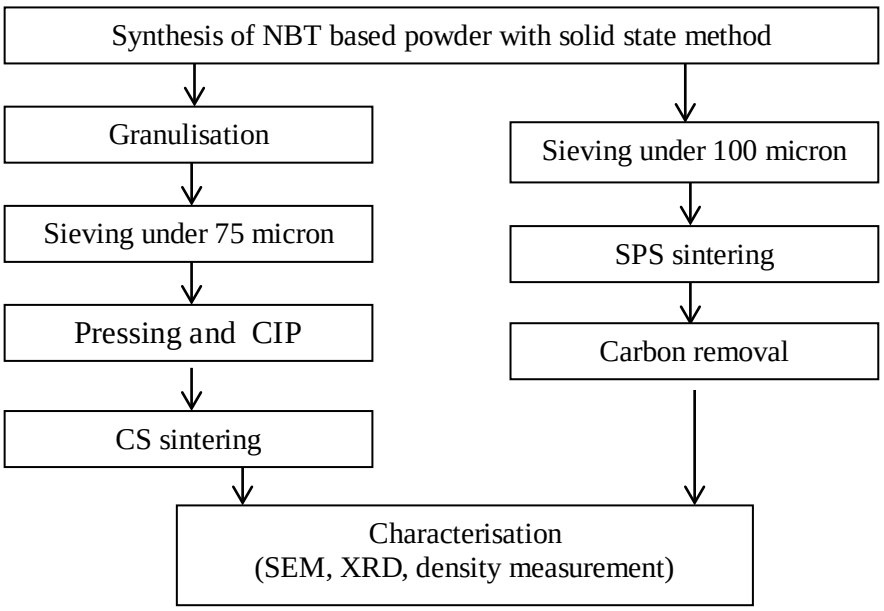

Figure 9.3. Flow diagram of CS and SPS sintering methods

In Figure 9.4 shows the low and high magnification SEM images of powders can be seen for both CS and SPS method after calcination. In general, from produced powder morphology, they have almost cubic structure.

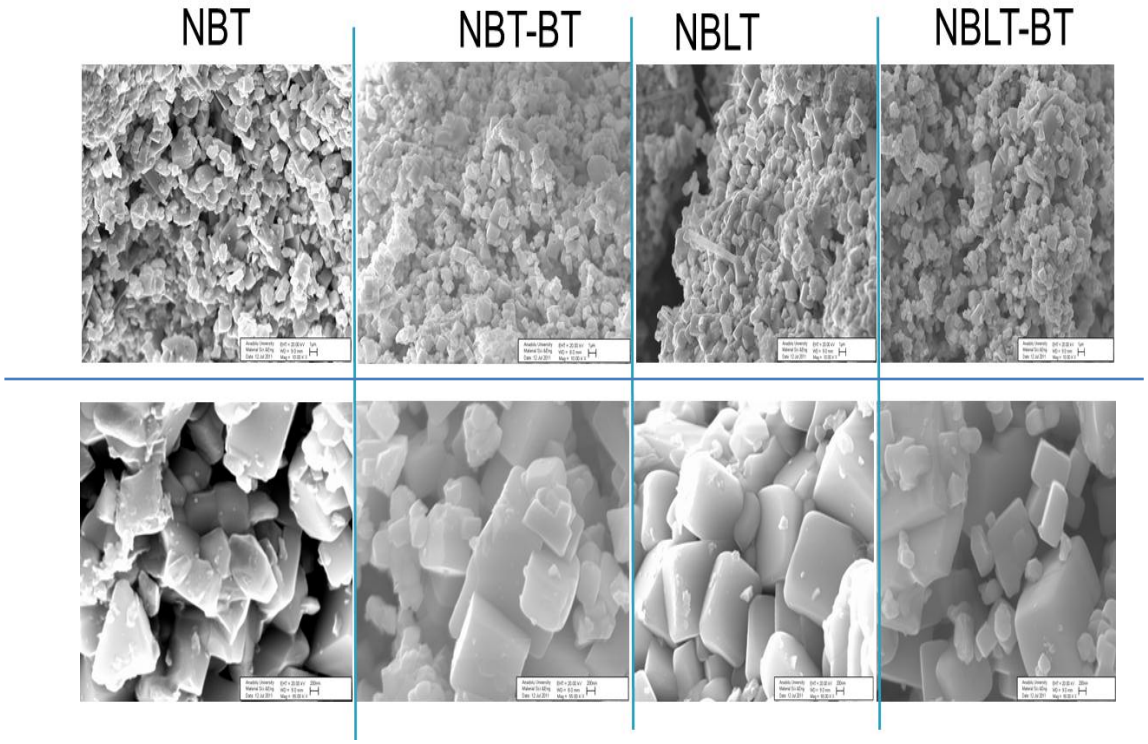

Figure 9.4. SEM images of NBT based powders after calcination

The synthesized powders were sintered at 1130, 1150 and 1180^{o}C for 2 hours. The calcined powders similarly were sintered via spark plasma sintering method at 900-950^{o}C for 5 minutes. The theoretical density of the samples sintered via CS method and the SPS method are given below (Figure 9.5).

With respect to density measurement 98% theoretical density has been achieved for NBT at 1150^{o}C via solid state sintering. For sample sintered at 950^{o}C at 50 MPa for 5 minutes via SPS, almost 100% theoretical density has been achieved. At sintering temperature 200^{o}C lower and at shorter sintering time, highly dense samples are obtained (Figure 9.5a). For NBT-BT system, maximum 96% theoretical density is obtained but density is decreased with increasing the sintering temperature. For SPS samples, quite high density value is achieved. This

result is also the indication of prevention of alkali evaporation by obtaining high-density at low temperature (Figure 9.5b). For Li doped NBLT, the theoretical density of 98% is reached for each of the three temperatures. However, the samples obtained via SPS have bigger values (Figure 9.5c). For NBLT-BT approximately 98% theoretical density is obtained at 1180^{o}C'de, higher density is reached at the lower temperature for SPS samples (Figure 9.5d).

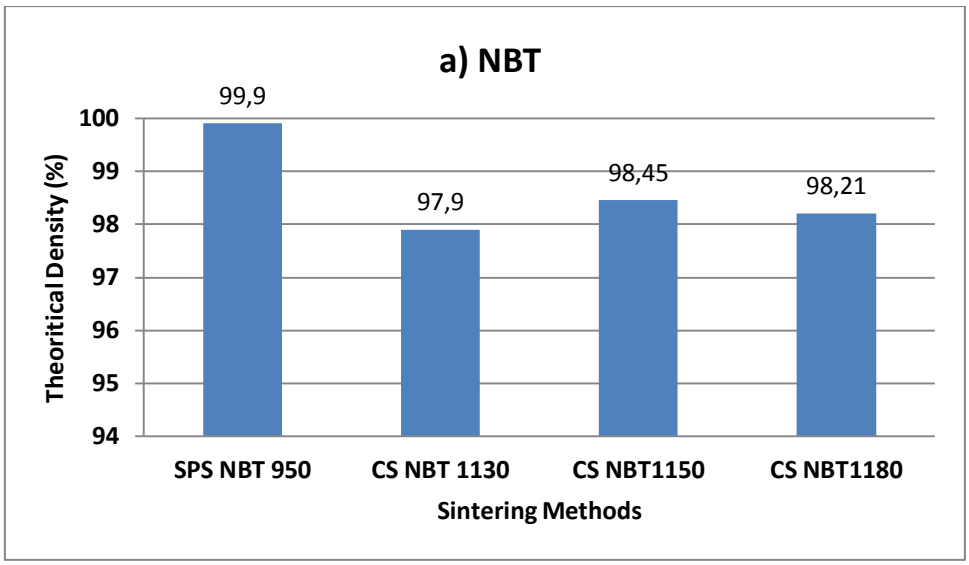

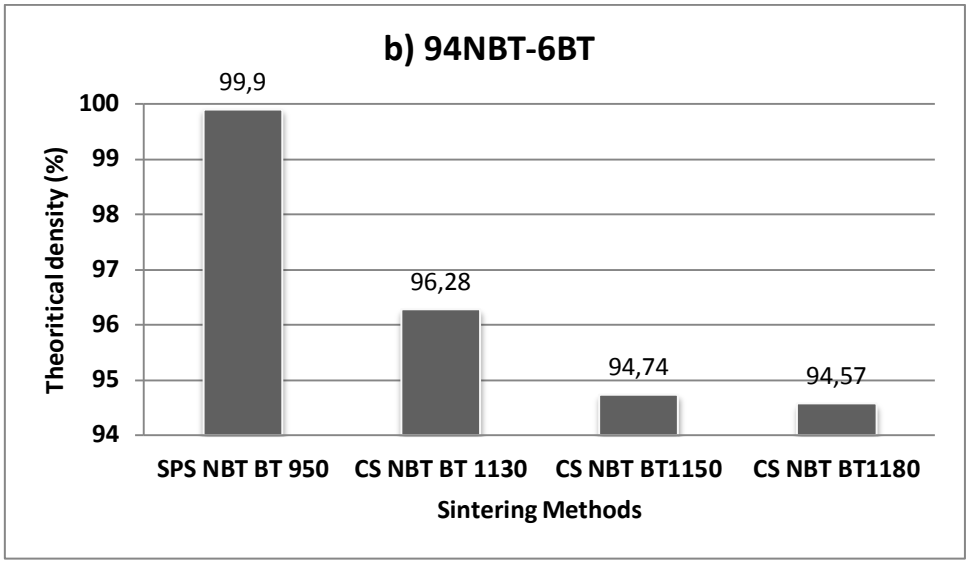

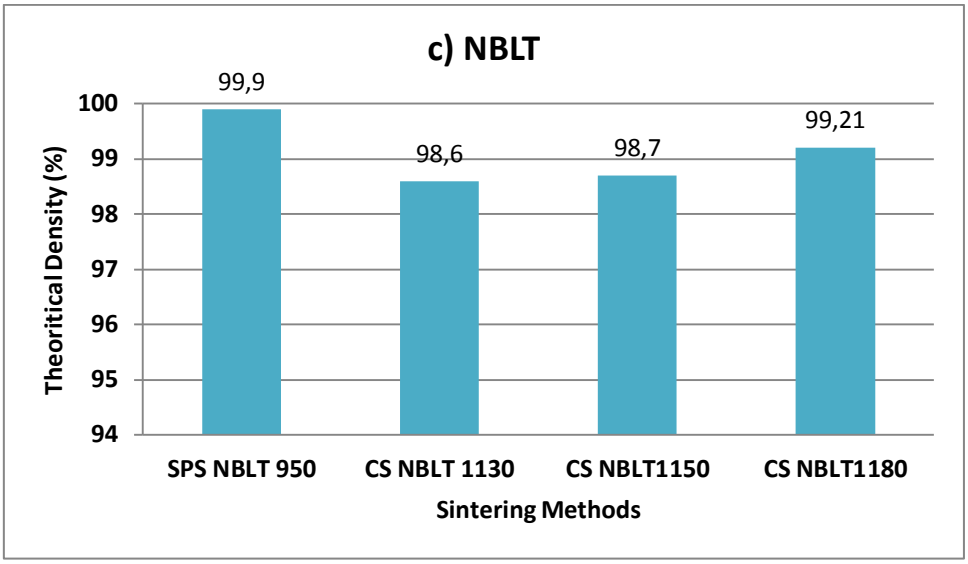

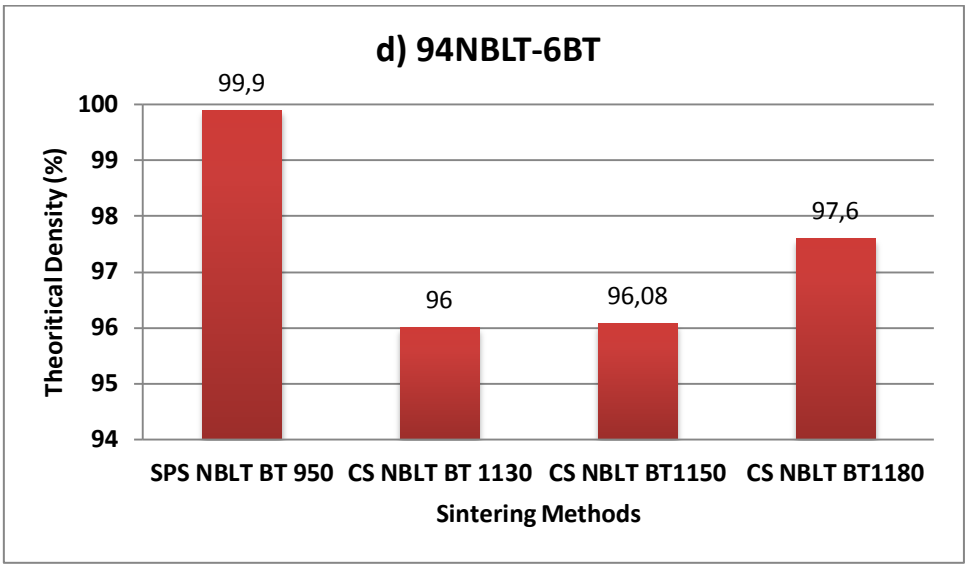

Figure 9.5. Comparison of the densities of the NBT based samples sintered via CS and SPS

Images of the microstructure of NBT-based samples sintered at 1130, 1150 and 1180^{o}C for 2 hours via solid state sintering are given below (Figure 9.6). From SEM images of microstructures, all of the compositions have porosity observed for all sintering temperatures. This reduces the density of the material.

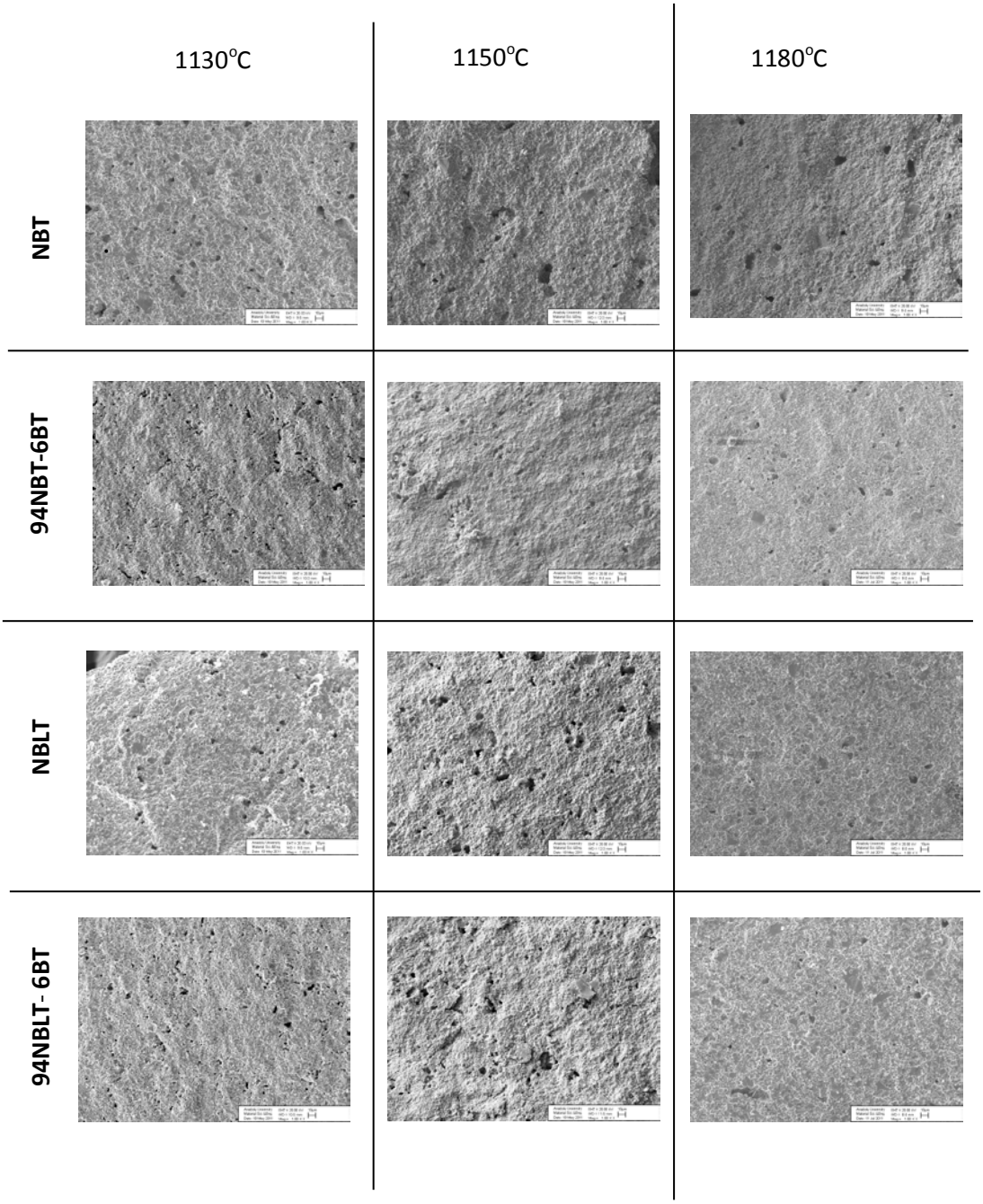

Figure 9.6. Microstructures of NBT-based ceramics sintered via CS method

High magnification SEM images of samples with the highest density values given above for the composition of NBT are given below (Figure 9.7). As can be seen from microstructure, bonding between the particles is quite good especially for NBT, 94NBLT-6BT as a result of sintering at 1150°C for 2 hours. This value is 1180°C for NBLT composition. However, as a result of sintering at

1130°C for 2 hours for the composition of NBT-BT, a maximum theoretical density value of 96% has been reached but with respect to other samples there has been weak particle bonding observed. In general, except for the composition of 94NBT-6BT, the neck formation is observed at 1150 and 1180°C. But these samples have porosity as can be seen in the low magnification SEM images.

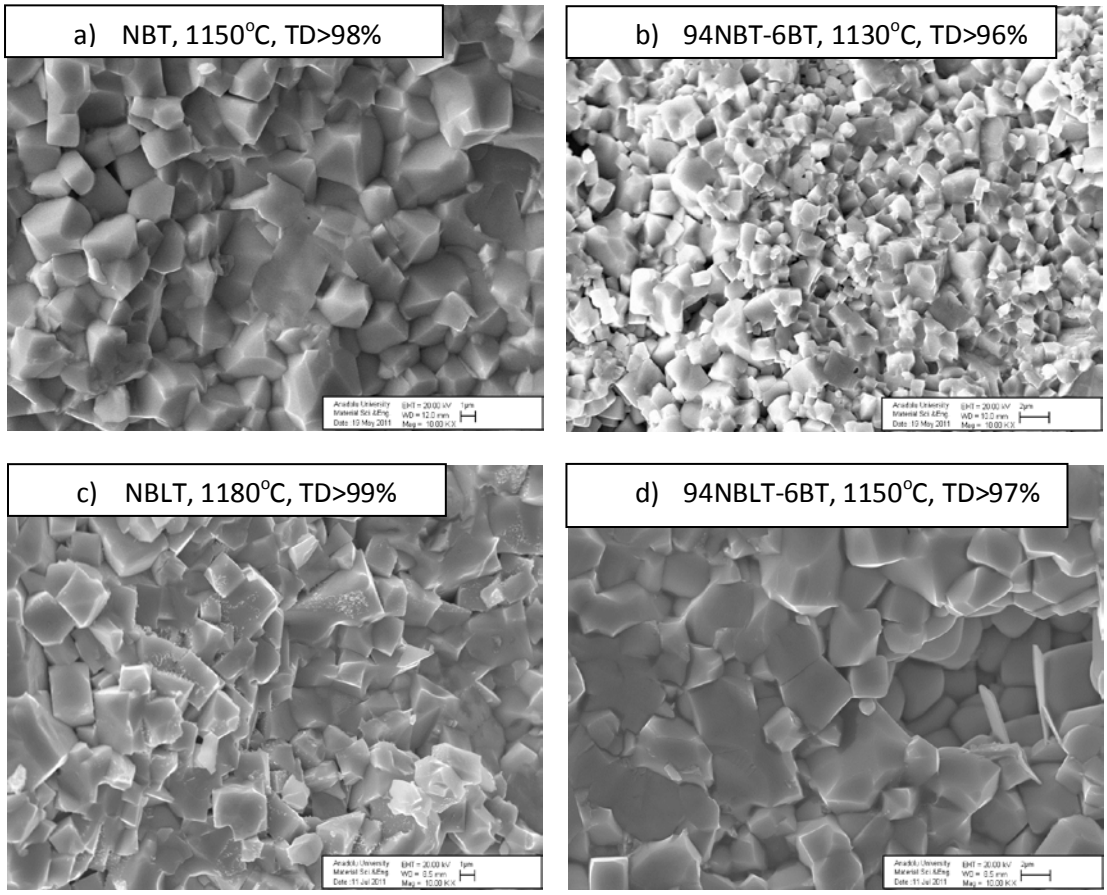

Figure 9.7. Microstructures of (a) NBT, (b) NBT-BT, (c) NBLT, (d) NBLT-BT at high magnification for maximum densities of NBT-based samples

NBT based samples were sintered at 900°C and 30MPa for 5 minutes with SPS method. In Figure 9.8, fractures and pores are observed in the structure as a result of SEM images given in different magnification ratios. Particle bonding can not be achieved fully. This reduces the density of the sample.

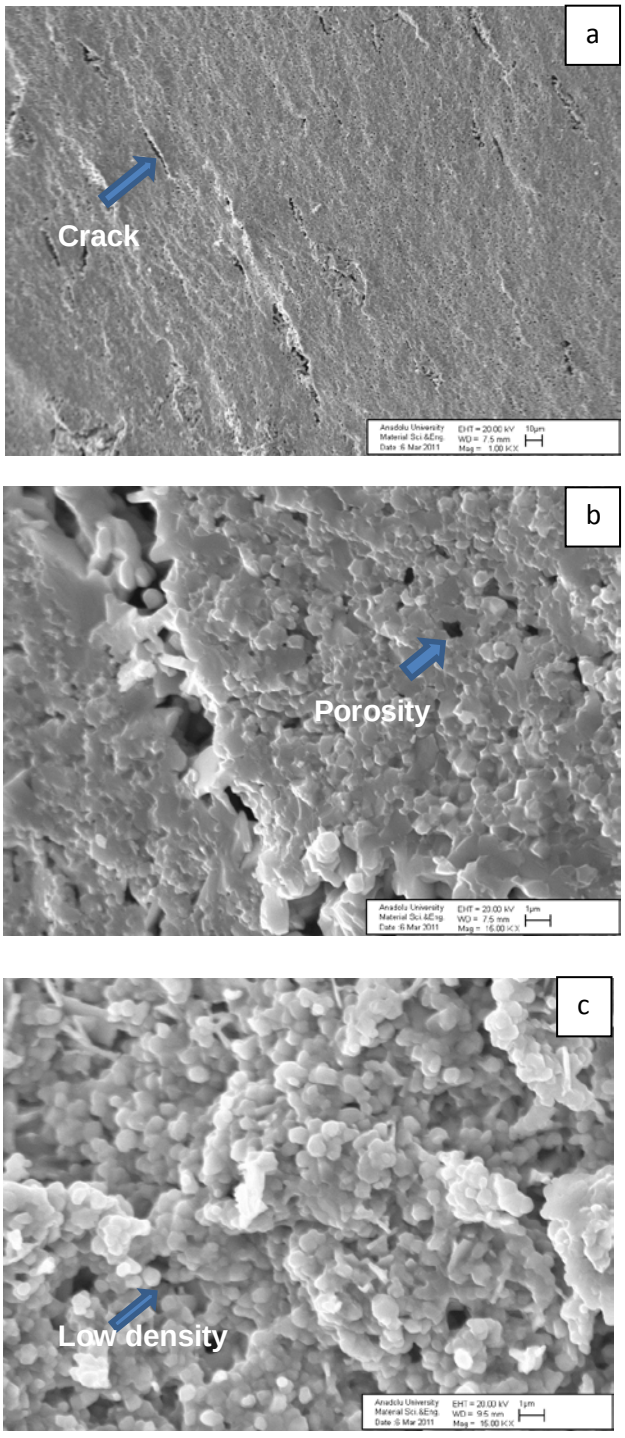

Figure 9.8. The microstructure images of the NBT based sample after SPS sintering under 30MPa; (a) 1000X, (b) 15000X, (c) 15000X

In Figure 9.9, the SPS pressure has been performed at 50 MPa, and sintered at 900 and 950^{o}C for 5 minutes. From the microstructure analysis of the

sintered samples, it can be concluded that there is no porosity in the structure at both temperature for low magnification images. In addition, high magnification SEM images were obtained for 950°C. As shown in the analysis of whole NBT systems, it can be observed that there is a good bonding between particles and non porous structure is produced. The SEM and density measurement results support the obtained results.

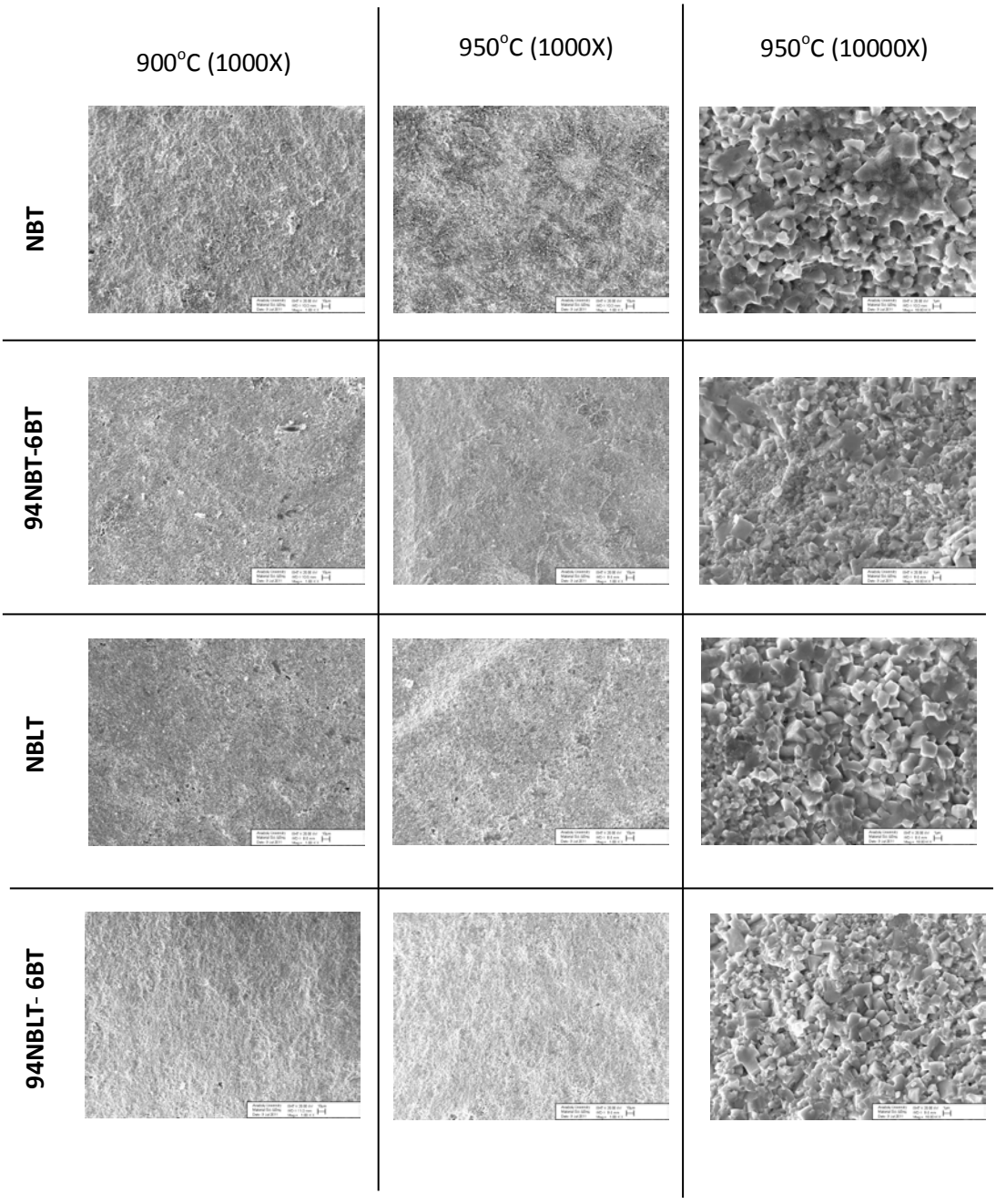

Figure 9.9. SEM analysis of the NBT based samples sintered by SPS at different temperatures

In addition, structures of crystal produced via SPS are determined as perovskite from XRD analysis. It is also observed that there are no undesired phases in the structure. (Figure 9.10).

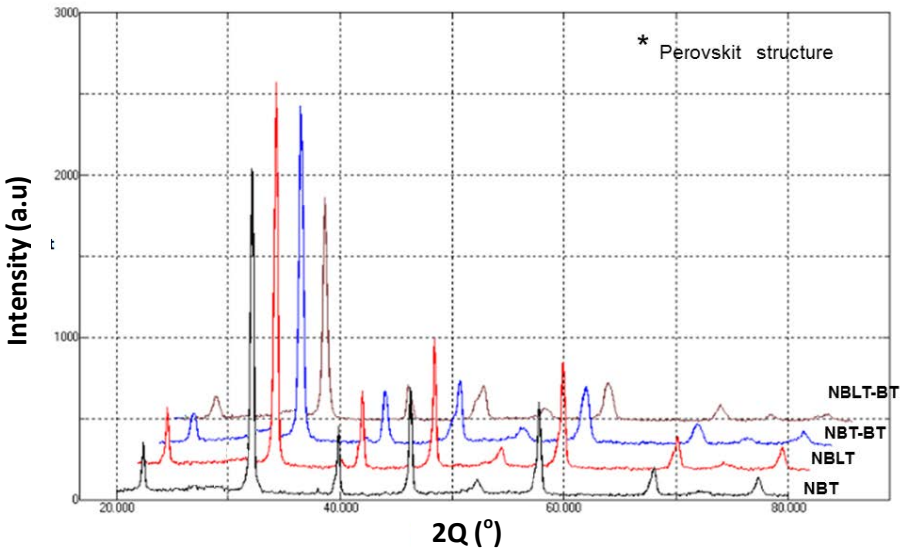

Figure 9.10. XRD pattern of SPS sintered NBT based samples

To summarize the results, high density materials are produced via SPS sintering at lower temperature and faster sintering time than that of solid state sintering method. This method provides considerable advantageous especially in terms of the time of single crystal growth via SSCG method to produce high density matrix also strong seed- interface bonding. In addition, the evaporation of alkali materials can be reduced with SPS when compared CS method. The effect of sintering methods on matrix-seed interface are compared and the results given below.

9.2. Comparison of Matrix-Seed Interface Interactions for CS and SPS Sintering Methods

As mentioned in previous sections for solid state single crystal method, formation of pore must not be taken place for matrix material and seed- matrix interface bonding must be strong. Effect of CS and SPS on material intensity was examined at previous section and it wa determined that samples sintered via SPS have higher density as compared to that of CS method. Therefore, at this part,

effect of these methods on matrix-seed interface bonding via using CS and SPS method. As given stereo microscope images in Figure 9.11, heat treatment was applied for both of sintering methods by embedding seed crystal materials in the powders with 94NBT-6BT composition.

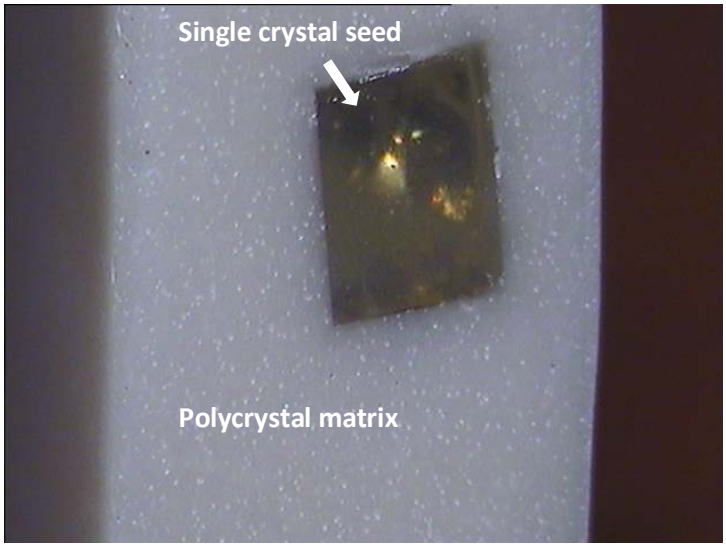

Figure 9.11. Stereo microscope image of single crystal seed material embedded in polycrystal matrix

Seed material was embedded in granulated powder for CS method and then 4 tons of pres were applied for pre-shaping. Later, isostatic pressing was applied via applying 300 MPa press. Shaped samples were sintered at 1130^{o}C for 2 hours at which maximum density was reached. SEM images of sintered samples via CS method are given in Figure 9.12. As can be seen from images, there are lots of pores in matrix material for CS sintered samples. Due to existing of their pores and thus sweeping of them into growing crystal at the crystal growth step, quality of crystal will be adversely effected (Figure 9.12a). Looking at the high magnification SEM images, it is obvious that matrix-seed interface bonding is quite weak (Figure 9.12b-c).

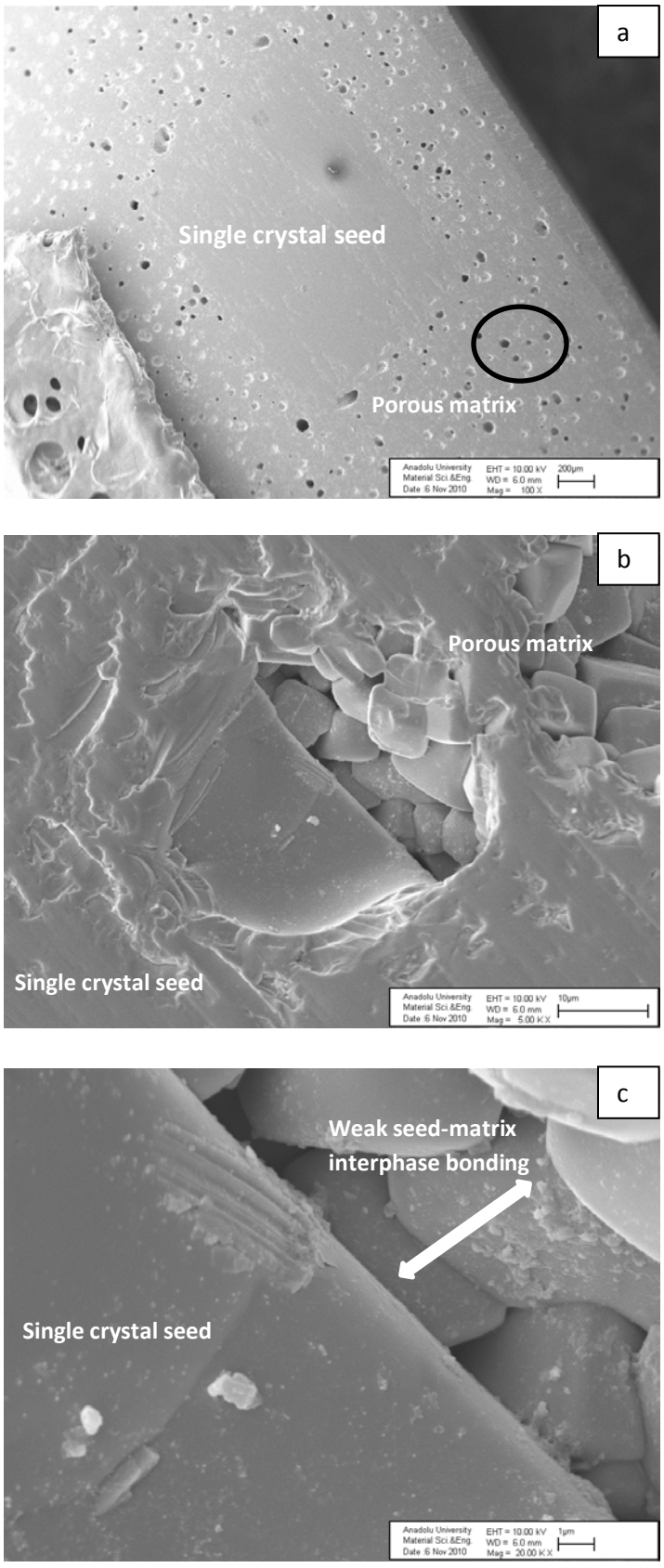

Figure 9.12. SEM images of samples sintered with CS method at different magnification ratio (a) 100x, (b) 5000x, and (c) 20000X)

Ungranulated powders were used for the study of SPS sintering method and sintering conditions was arranged as given previous parts, 50 MPa press, 950^{o}C for 5 minutes. In Figure 9.13, SEM images of the sintered samples are given. As can be seen both low and high magnification SEM images, quite dense matrix structures are produced. It is also observed that there is strong and homogeneous binding between the seed -matrix interface

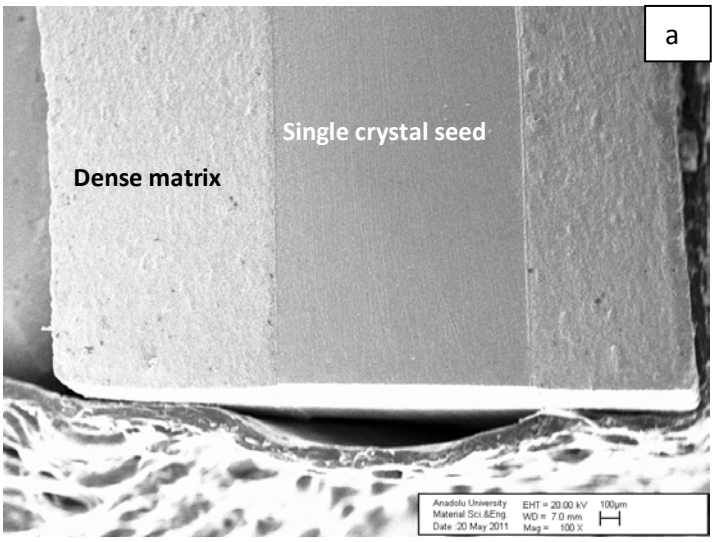

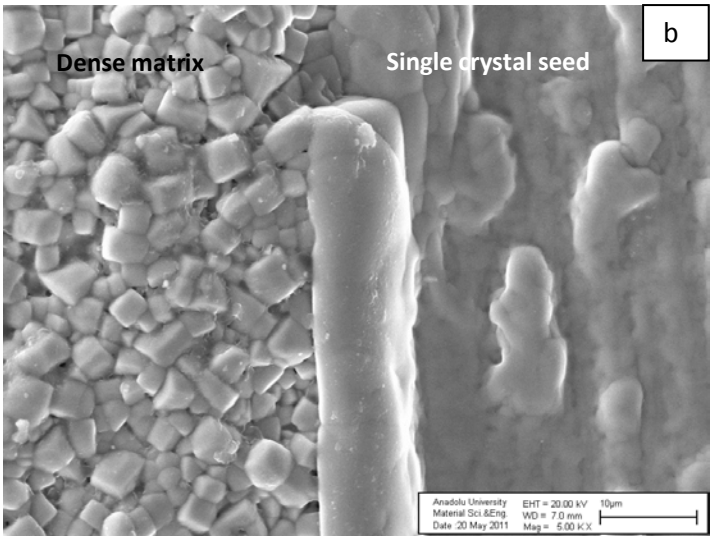

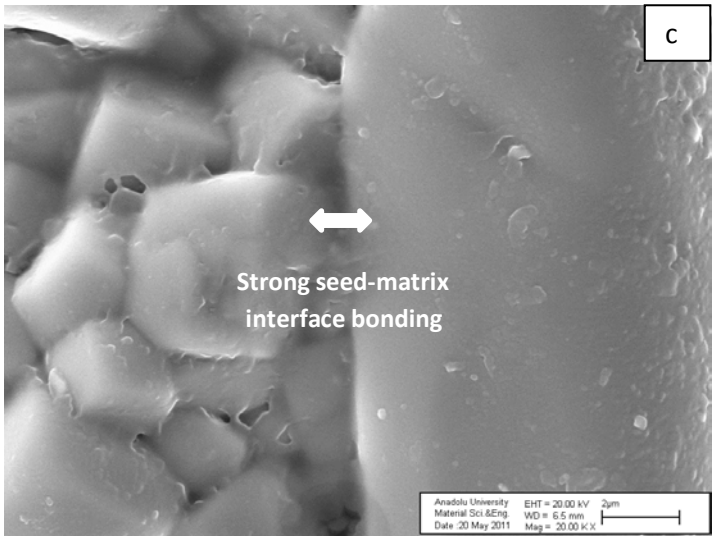

Figure 9.13. SEM images of samples sintered via SPS method at different magnification ratios (a) 100x, (b) 5000x, and (c) 20000X

As a result, as the most important requirements of SSCG method, nonporous polycrystal structure and strong seed-matrix interface bonding was achieved at the temperature below almost 200-250^{o}C as compared to common sintering methods. This is also very important because it prevents alkali evaporation during processing at high temperatures.

10. ELECTRICAL CHARACTERIZATION OF NBT-BT BASED SINGLE CRYSTALS

Electrical measurement flow chart for 94NBT-6BT single crystalline and for polycrystal materials sintered via CS and SPS methods are given in Figure 10.1.

For electrical measurements, thickness of both 94NBT-6BT based grown single crystals at <001> orientation and sintered via CS and SPS samples were polished to be the size of about 1mm. Both sides of samples were electroded using silver paste by applying heat treatment at 580^{o}C for 10 minutes.

Samples were polarized under the condition of DC electric field of 0-5 kV/mm and in silicon oil at the temperature of 80 -100℃ for 20 minutes. Dielectric constant (ε_r) and dielectric loss (tanδ) were investigated depending on polarization electric field (0-5kV/mm) and frequency (0.1-10kHz) via Agilent4294A impedance gain phase analyzer. Dielectric constants of samples were calculated using capacitance, thickness, area of materials. Piezoelectric coefficient (d_{33}) was measured after 24h with Pennebaker (model 8000) piezo-d_{33} (American Piezo) test device. d_{33} values of samples were measured after the calibration of the device with reference materials having known piezoelectric constant. Dielectric properties of produced materials were performed via GW-INSTEK LCR-8101 as depending on temperatures (R.T.-450^{o}C) and frequency (1-10-100kHz). Temperature dependent dielectric properties were calculated similarly through determining of capacitance values at defined frequency and placing these values into the formula of dielectric property. Hysteresis loop and leakage current density of materials as a function of temperature were obtained by using AIXACT (aixPES/CMA) ferroelectic and piezoelectric analyzer.

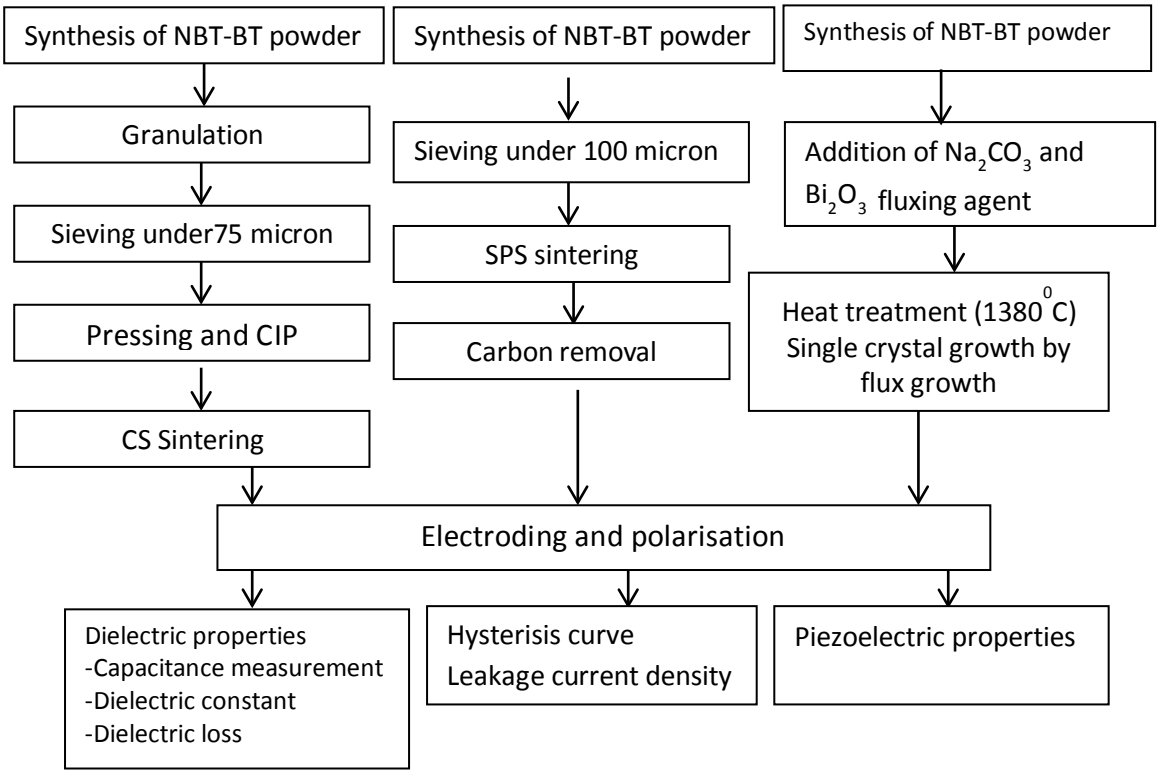

Figure 10.1. Flow chart of electrical property measurement

Codes and descriptions of 94NBT-6BT single crystals are given in Table 10.1. As can be seen in the charts, RW coded samples stands for uncalcined powder for undoped and Li doped 94NBT-6BT compositions, KAL coded samples for produced crystals from calcined powders.

Table 10.1. The codes and descriptions of 94NBT-6BT-based single crystal samples

MATERILAS CODE	EXPLANATION
94NBT-6BT RW	$94Na_{0.5}Bi_{0.5}TiO_3$-$6BaTiO_3$ single crystals which are grown using uncalcined powders
94NBT-6BT KAL	$94Na_{0.5}Bi_{0.5}TiO_3$-$6BaTiO_3$ single crystals which are grown using calcined powders
94NBLT-6BT RW	Li^{+1} doped $94Na_{0.5}Bi_{0.5}TiO_3$-$6BaTiO_3$ single crystals which are grown using uncalcined powders
94NBLT-6BT KAL	Li^{+1} doped $94Na_{0.5}Bi_{0.5}TiO_3$-$6BaTiO_3$ single crystals which are grown using calcined powders
94NBFT-6BT KAL	Fe^{+3} doped $94Na_{0.5}Bi_{0.5}TiO_3$-$6BaTiO_3$ single crystals which are grown using calcined powders
94NBMT-6BT KAL	Mn^{+4} doped $94Na_{0.5}Bi_{0.5}TiO_3$-$6BaTiO_3$ single crystals which are grown using calcined powders

10.1. Frequency Dependent Dielectric Properties of 94NBT-6BT Based Single Crystals at Room Temperature

Dielectric constant (ε_r) and dielectric loss factor (tanδ) at room temperature depending on frequency of 94NBT-6BT based undoped and Li, Fe and Mn doped single crystal materials are given in Figure 10.2. If frequency is in between 0-1000Hz, dielectric constant decreases due to the increasing frequency. As can be seen in Figure 10.2a, the Fe doped 94NBFT-6BT KAL single crystal has the highest dielectric constant. Dielectric constant is approximately 1160 at 100 Hz, whereas this value decreases to 1082 at 1000 Hz. Mn containing 94NBMT-6BT

KAL system has the second highest dielectric constant and this value is 1135 at the beginning but decreases to 1030 with increasing frequency. Pure (undoped) 94NBT-6BT KAL and 94NBT-6BT RW crystals have lower dielectric constant when compared Fe and Mn doped systems. 94NBT-6BT KAL crystals have dielectric constant of 1080 at 100 Hz but decreases to 1015 with increasing frequency. These values are 1055 and 980 respectively for 94NBT-6BT RW. Li doped 94NBLT-6BT KAL and 94NBLT-6BT RW crystals have the lowest dielectric constant. 94NBLT-6BT KAL has the dielectric constant of 1015 at the beginning but decreases up to 950 with increasing frequency. These values for 94NBLT-6BT RW are 1000 and 940 respectively. As given above, dielectric properties differs depending on powder production process. As can be seen in the figure, when 94NBT-6BT was calcined (94NBT-6BT KAL), it has higher dielectric feature as compared to the powder fed directly (94NBT-6BT RW). Similarly, crystals (94NBLT-6BT KAL) produced using powder after calcination has higher dielectric feature as compared to crystals (94NBLT-6BT RW) fed directly. Value of dielectric constant continues to decrease with increasing frequencies (higher). For the dielectric constant of crystals containing Fe and Mn, there is a decrease up to 860 and 830, for pure (undoped) and Li doped systems there is a decrease up to 800 and 770 (Figure 10.2b). As a result, Fe doped crystal has the highest, and Li doped the lowest dielectric constant.

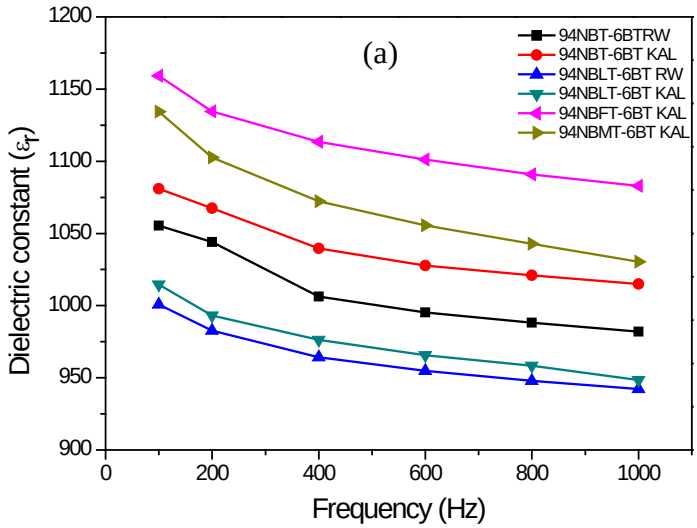

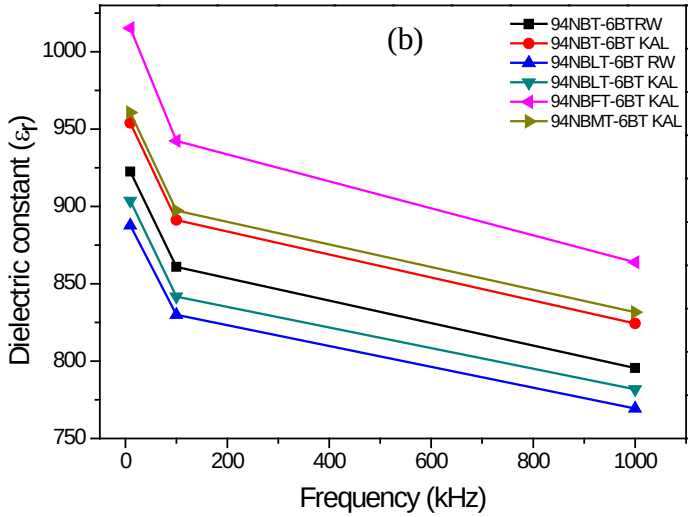

Figure 10.2. Low (a) and high (b) frequency dependent dielectric constants of 94NBT-6BT composition at room temperature

In Figure 10.3, according to the frequency dependent dielectric loss values, Mn containing system has the highest dielectric loss. This value is 0,05 for low frequencies, but reaches 0,059 for higher frequencies. Fe containing system has the values of 0,042 for lower frequency, but increases up to 0,067. Dielectric loss for materials produced using calcined powder for undoped crystals starts from 0,042 and reaches up to 0,06 with increasing frequency. For crystals produced using uncalcined powders, this value starts from 0,043 and reaches to 0,061 with increasing frequency. While dielectric loss is 0,039 for Li doped crystals for the production of which calcined powder are used, this loss reaches to 0,057 for high frequencies. Dielectric loss for crystals using uncalcined powder Li doped powder differs between 0,037 and 0,058 as the frequency changes.

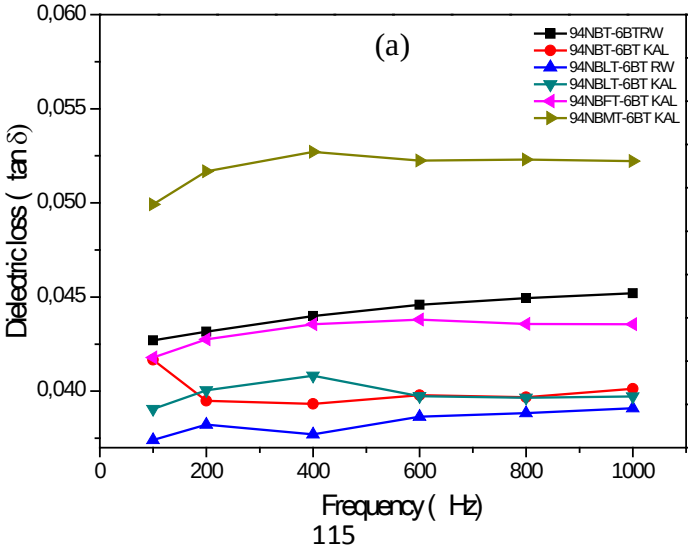

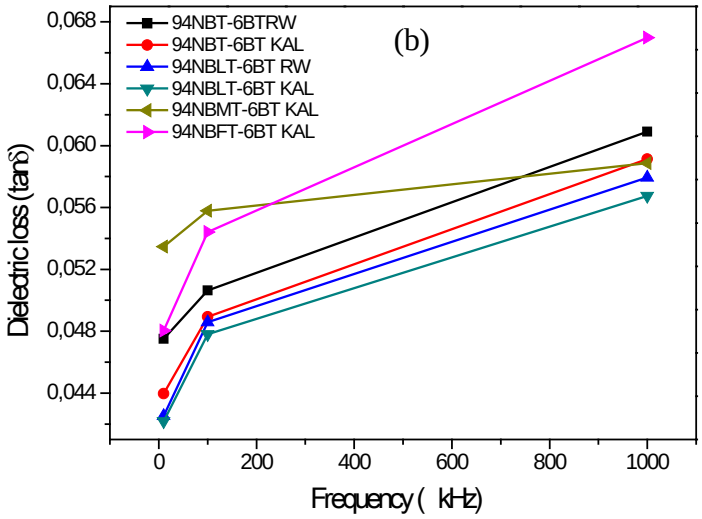

Figure 10.3. Dielectric loss values for 94NBT-6BT composition at room temperature depending on low (a) and high (b) frequency

10.2. Dielectric and Piezoelectric Properties of Produced Crystals Depending on Polarization Electric Field

Piezoelectric properties of grown crystals were conducted at 90^{o}C in oil for 20 minutes under different polarization electric field. In Figure 10.4, piezoelectric constant values dependent on different polarization electrical field for 94NBT-6BT material is given. As can be seen here, the d_{33} value was 65 pC / N under the field of 3kV/mm, whereas this value increases up to 115 pC / N with increasing polarization. Material loses its dielectric property (breakdown) after the application of polarization electric field of 5kV/mm. The biggest problem for the NBT based materials is the ability of polarization. These materials have a high conductivity due to alkali within the structure. Conductivity of the single crystals increases depending on the increasing polarization voltage and leakage current. Therefore, polarization of the crystals is difficult due their conductive nature. In Figure 10.5, effect of polarization electric field on dielectric properties is given. Dielectric constant decreases from 1030 to 800 with the increasing polarization electric field. Moreover, the dielectric loss varies between 0,40 to 0,50.

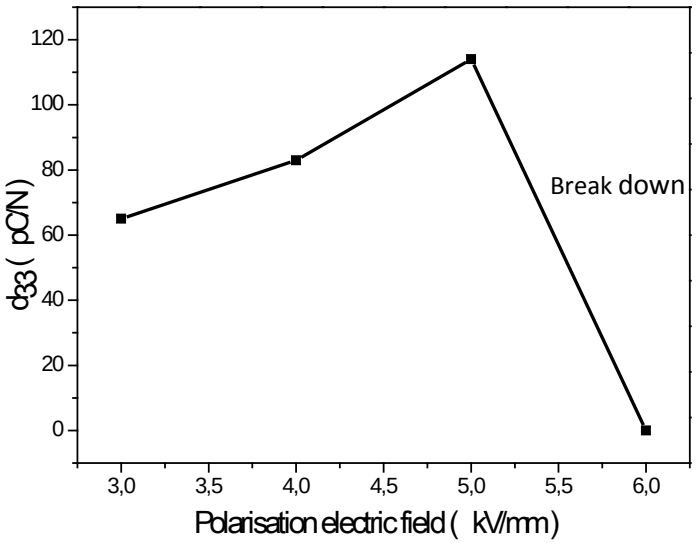

Figure 10.4. d_{33} chart depending on the polarization electric field of 94NBT-6BT composition

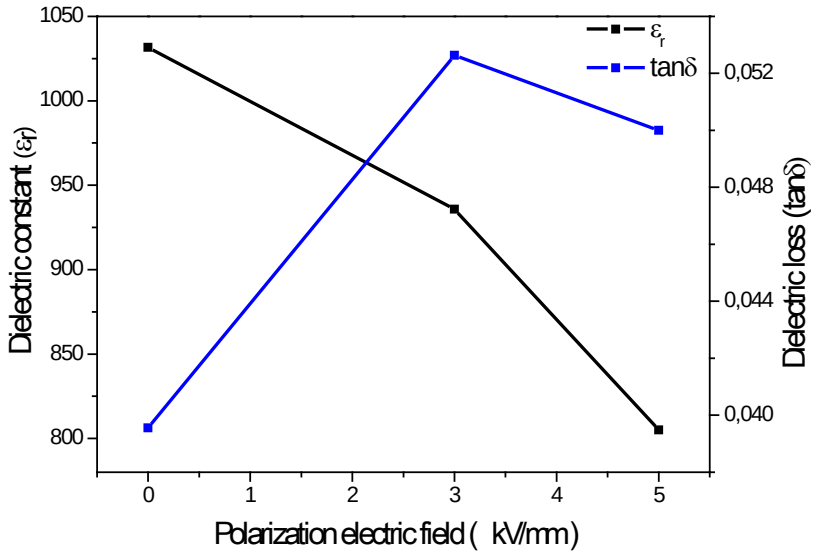

Figure 10.5. Dielectric constant and dielectric loss chart for 94NBT-6BT compositions depending on polarization electric field

10.3. Determination of Temperature and Electric Field Dependent Hysteresis Graphics for Single Crystals

Temperature dependent hysteresis loops were obtained to determine why the polarization of crystals under electric field was difficult. In the charts given below (Figure 10.6a-f), hysterisis curve of grown crystals as a function of temperature are given. As can be seen from figures, there is an expansion on hysteresis loop with increasing temperature for all samples. Produced crystals shows a different behavior depending on temperature as compared to a ferroelectric material. In general, the contraction of hysteresis loop is expected for a ideal ferroelectric material depending on the temperature. Another reason for this is the leakage current density due to electrical conductivity of the material as a result of the existing of alkali within the structure.

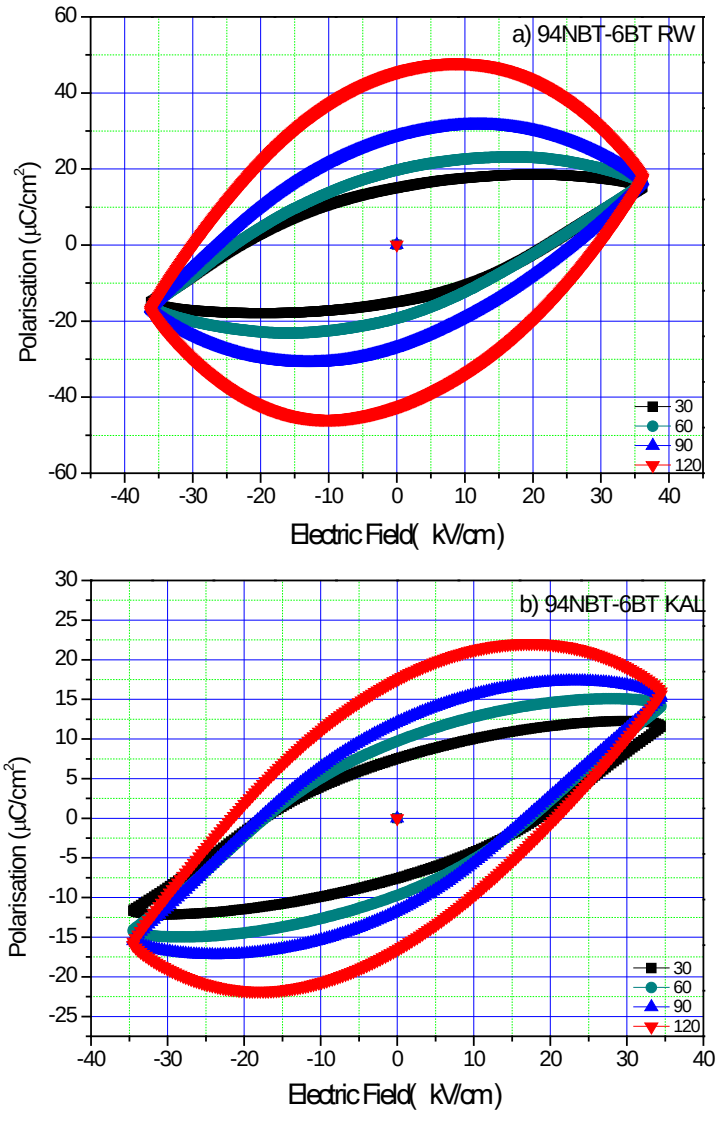

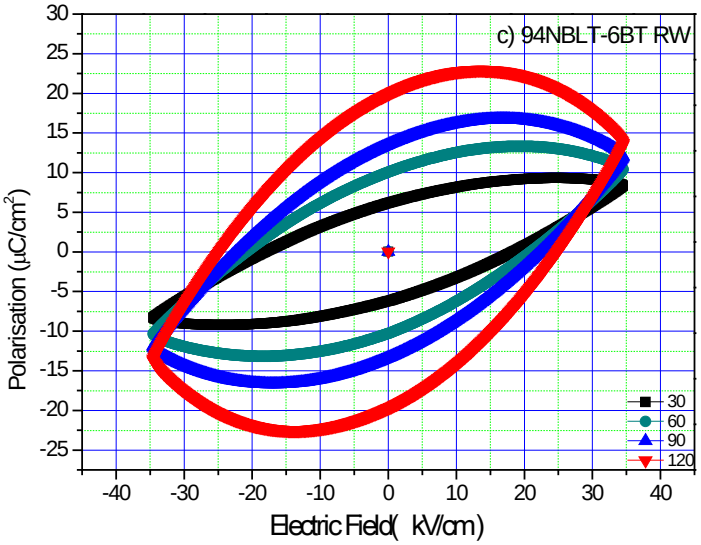

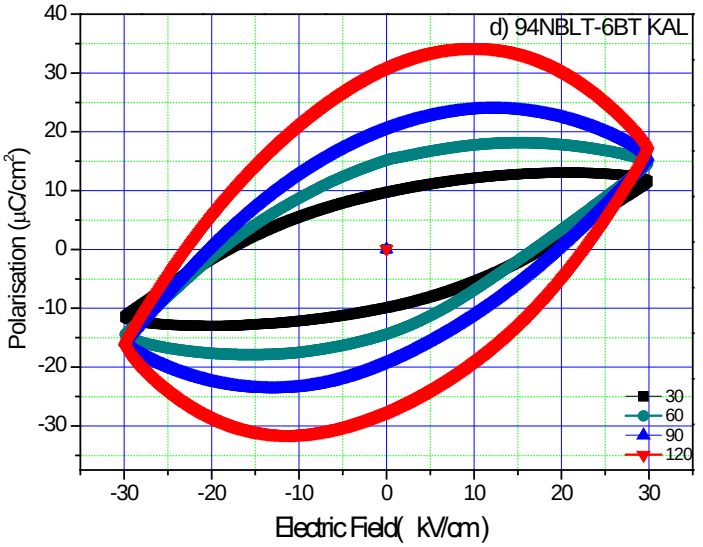

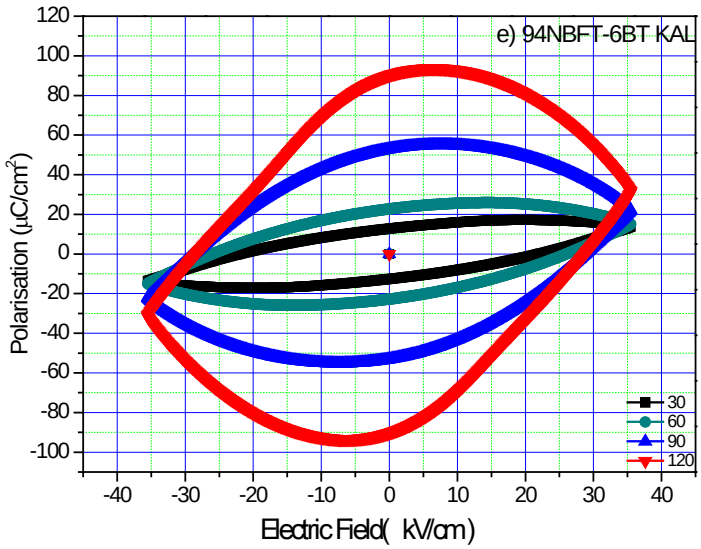

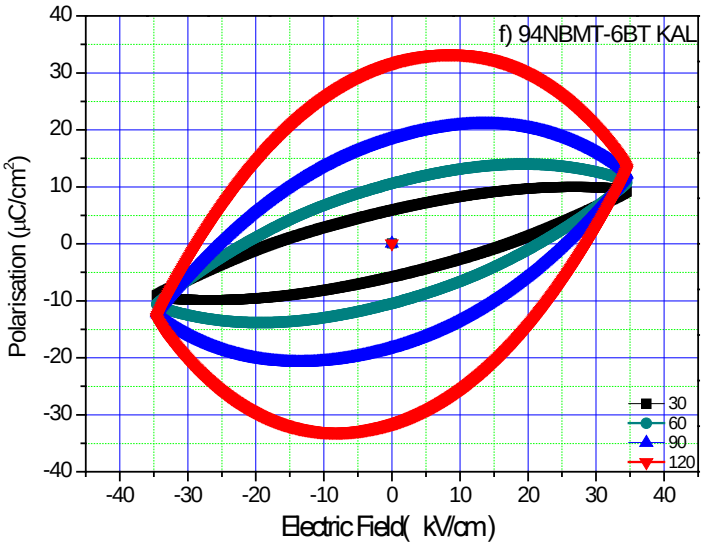

Figure 10.6. The temperature dependent hysteresis loop for 94NBT-6BT-based single crystals

In Figure 10.7, remanent polarization (P_r) and the coercive field (E_c) values are determined as depending on temperature according to the curves given above. As can be seen in the graph, the Fe containing 94NBFT-6BT KAL single crystals have the highest value of remanent polarization with increasing temperature. Undoped single crystals 94NBT-6BT KAL have the lowest value of the remanent polarization (Figure 10.7a). Similarly, coercive field value increases depending on the temperature. Similarly coercive field values is the highest for Fe containing 94NBFT-6BT KAL single crystals, whereas the lowest for undoped 94NBT-6BT KAL single crystals (Figure 10.7b).

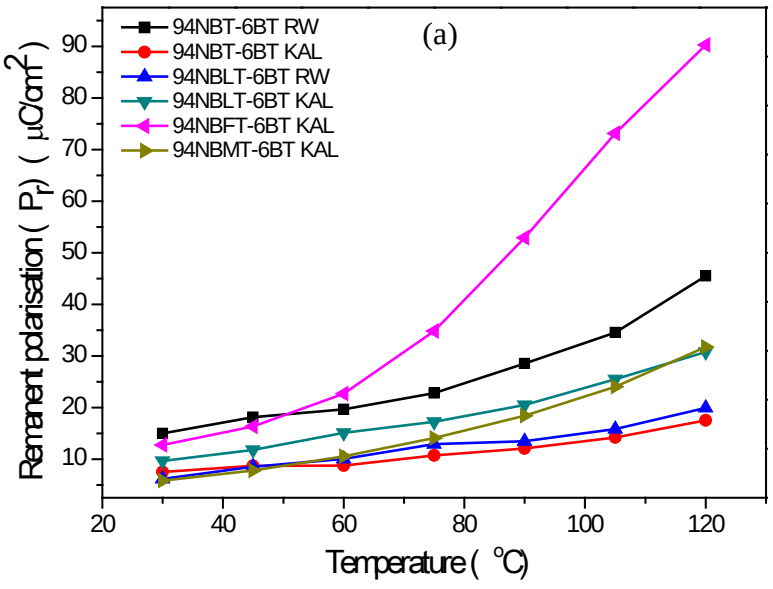

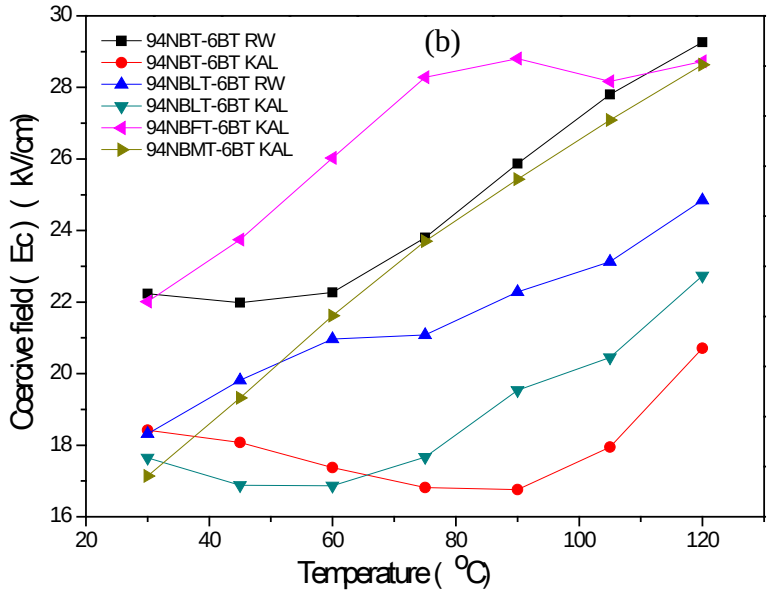

Figure 10.7. The temperature dependent P_r (a) and E_c (b) changes for 94NBT-6BT-based single crystals

Electric field dependent hysteresis loops were obtained at room temperature. Hysterisis curve of grown crystals as a function of electric field are given in Figure 10.8. As can be seen from figures, hysteresis curves of all grown crystals are expanded with increasing electric field.

As can be seen from figures, increasing of P_r and E_c values with increasing temperature and electric field can explained by conductivity of crystals, it is related with the high leakage current density. Therefore, leakage current densities of pure (undoped) and doped single crystals were analyzed as follows.

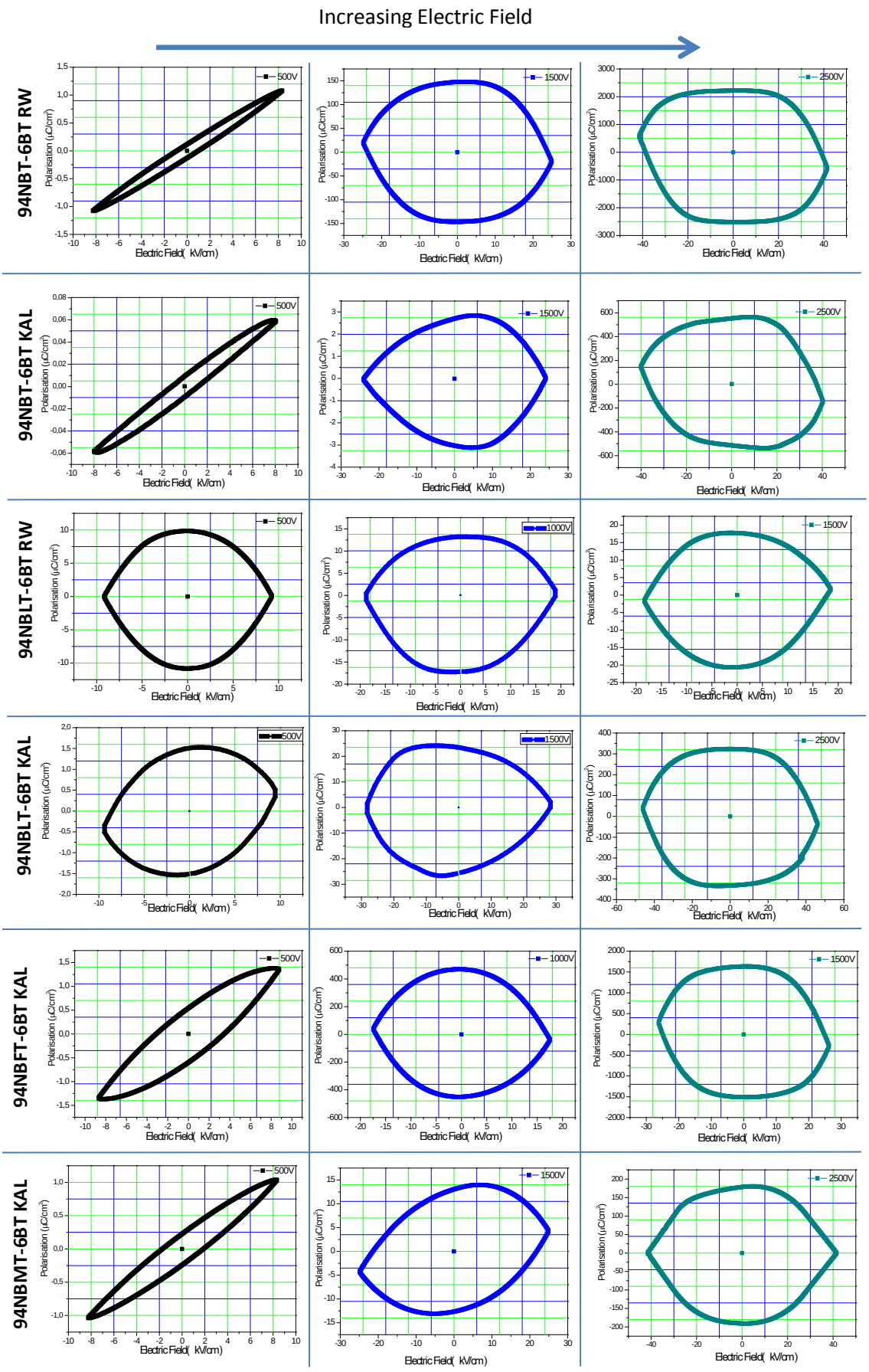

Figure 10.8. The electric field dependent hysteresis loop for 94NBT-6BT-based single crystals

10.4. Determination of Temperature Dependent Leakage Current Densities of Single Crystals

As noted above, polarization capabilities of single crystals are dependent on temperature and applied electric field. As can be seen above, a remanent polarization and coercive electric field have an increasing tendency with temperature and electric field. Thus, due to the increasing polarization voltage both hysteresis loops and polarization graphs are effected by leakage current. High leakage current at a certain polarization temperature increases conductivity of material and so polarization of produced crystal is difficult. In Figure 10.9a-f, leakage current densities of single crystals is given. As can be seen in the figure, especially between the temperature of 30-120^{o}C the leakage current densities for all single crystals increases as depending on the electric field and temperature.

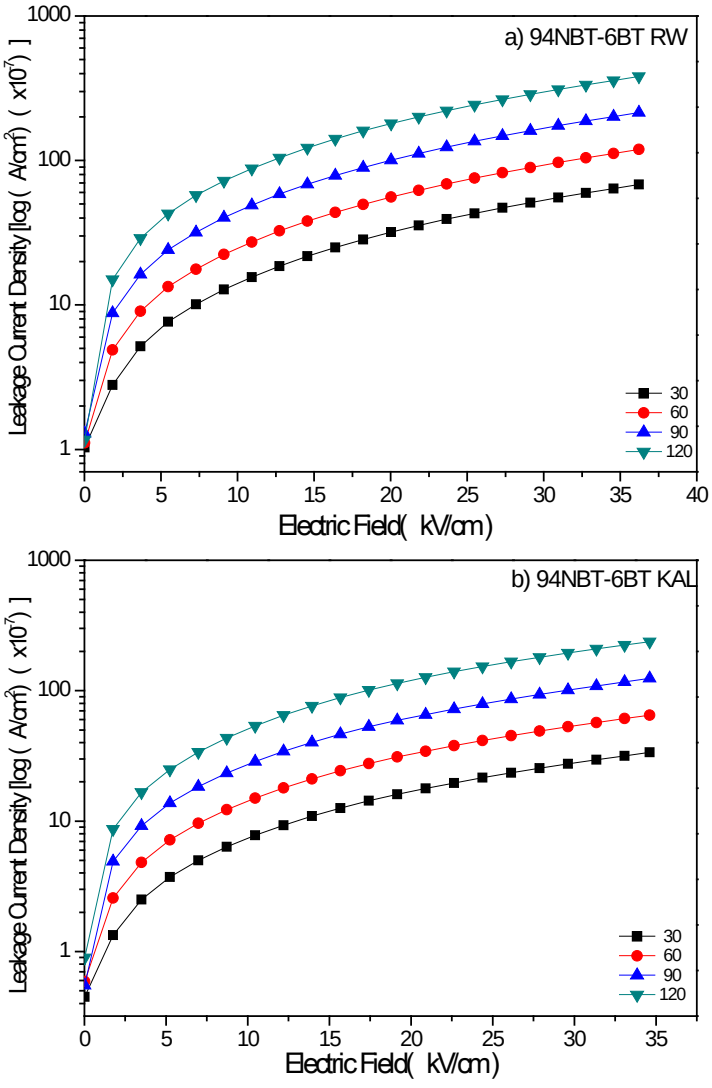

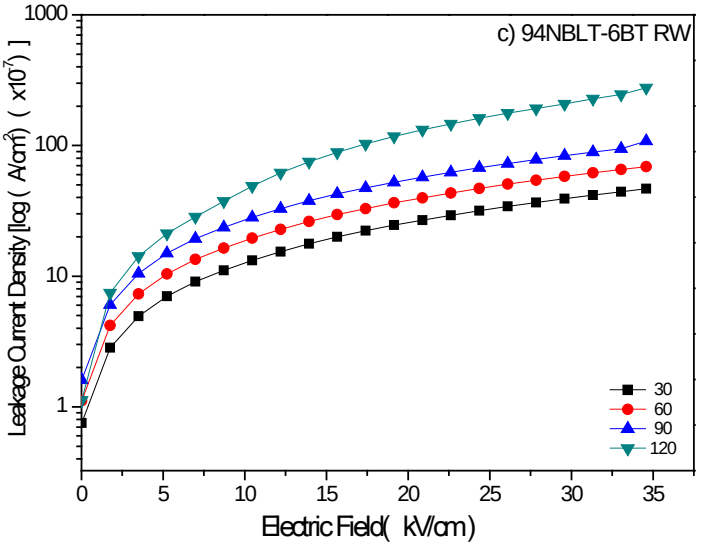

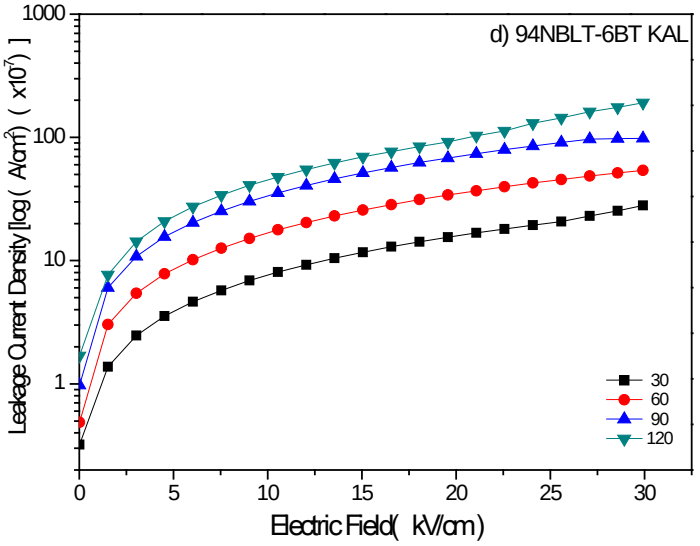

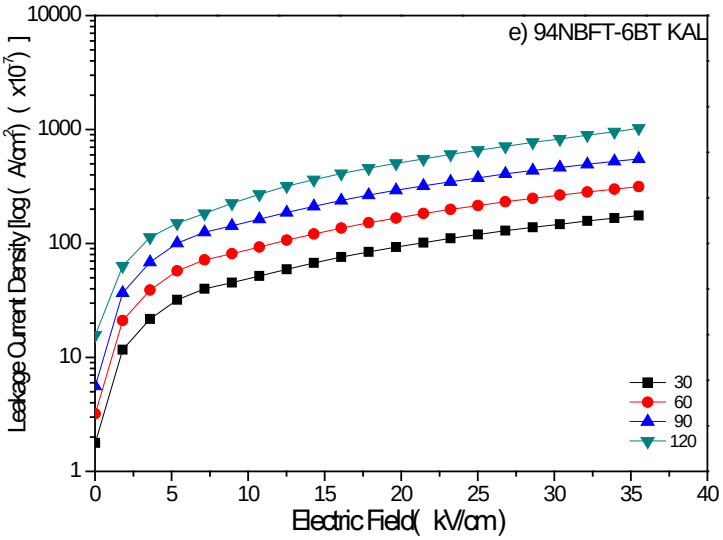

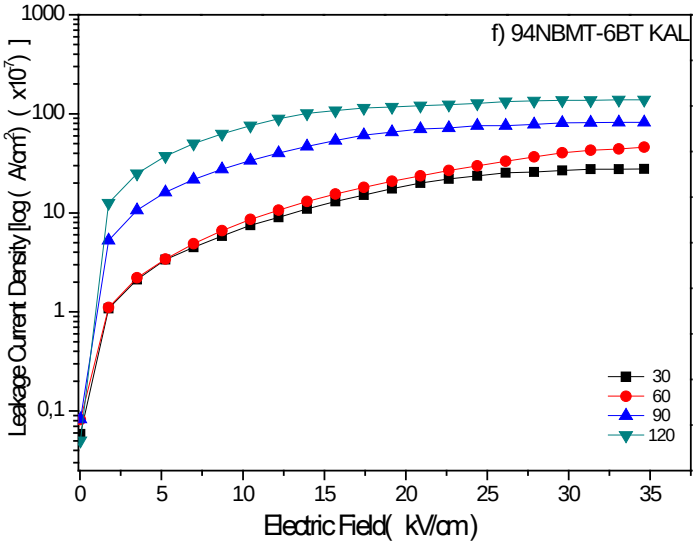

Figure 10.9. The temperature dependent leakage current densities of 94NBT-6BT based single crystals

In Figure 10.10, maximum leakage current density chart of 94NBT-6BT-based single crystals are given at different temperatures. According to the graph, the maximum leakage current density also increases with the increasing temperature. As seen in the figure, Fe containing 94NBFT-6BT single crystals has the highest leakage current density whereas Mn containing 94NBMT-6BT single crystals has the lowest. Also pure(undoped) and Li containing 94NBT-6BT KAL and 94NBLT-6BT KAL single crystal materials using calcined powder has lower leakage current density as compared with 94NBT-6BT RW, 94NBLT-6BT RW single crystals. In conclusion, powder processing has agreat affect on the leakage current density. From the results, when the calcined powder is used to grow the single crystals, lower leakage current density is obtained.

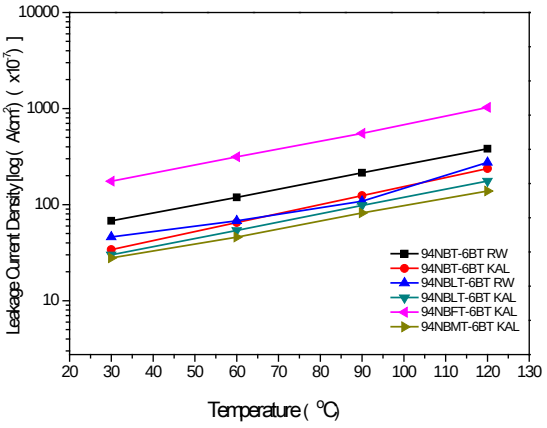

Figure 10.10. Temperature dependent maximum leakage current densities of 94NBT-6BT based single crystals

In Figure 10.11, leakage current densities of crystals are compared for the polarization temperature at 90°C. As shown in the figure, 94NBT-6BT KAL crystals have approximately 1,6 times lower leakage current density than that of 6BT 94NBT-RW samples. Similarly, for systems containing lithium, leakage current density of 94NBLT-6BT KAL crystals is lower than 94NBLT-6BT RW single crystals. For Fe containing crystals, leakage current density is 7,5 times higher than that of Mn containing crystals.

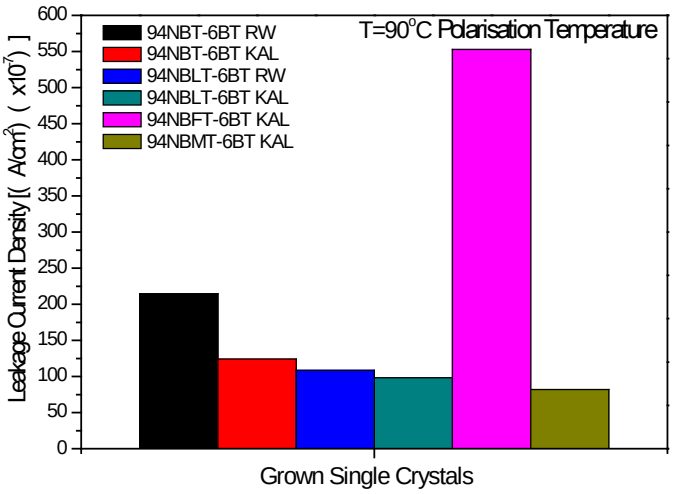

Figure 10.11. Comparison of leakage current densities of 94NBT-6BT based single crystals at 90°C

According to the results, polarization capability of Mn doped 94NBMT-6BT KAL single crystals is bigger due to the low leakage current density. In addition, the leakage current density of single crystals varies according to the process during the production of single crystals. Applying calcination to the powder for the production of single crystal provides lower leakage current.

10.5. Temperature and Frequency Dependent Dielectric Properties

Temperature dependent dielectric properties of unpolarized 94NBT-6BT based single crystals were compared for 1-10-100 kHz. Dielectric constant and dielectric loss of 94NBT-6BT RW and 94NBT-6BT KAL single crystals are given in Figure 10.12 and Figure 10.13. From 94NBT-6BT RW and 94NBT-6BT KAL single crystals, it is obvious that crystals produced using calcined powders

have higher dielectric strength. Especially, for 1 kHz, 94NBT-6BT RW sample has the dielectric constant of approximately 1430 and dielectric loss of 0,042 at room temperature. These values increase up to 19410 and 1,14 with increasing temperature, respectively, (Figure 10.12 a-b).

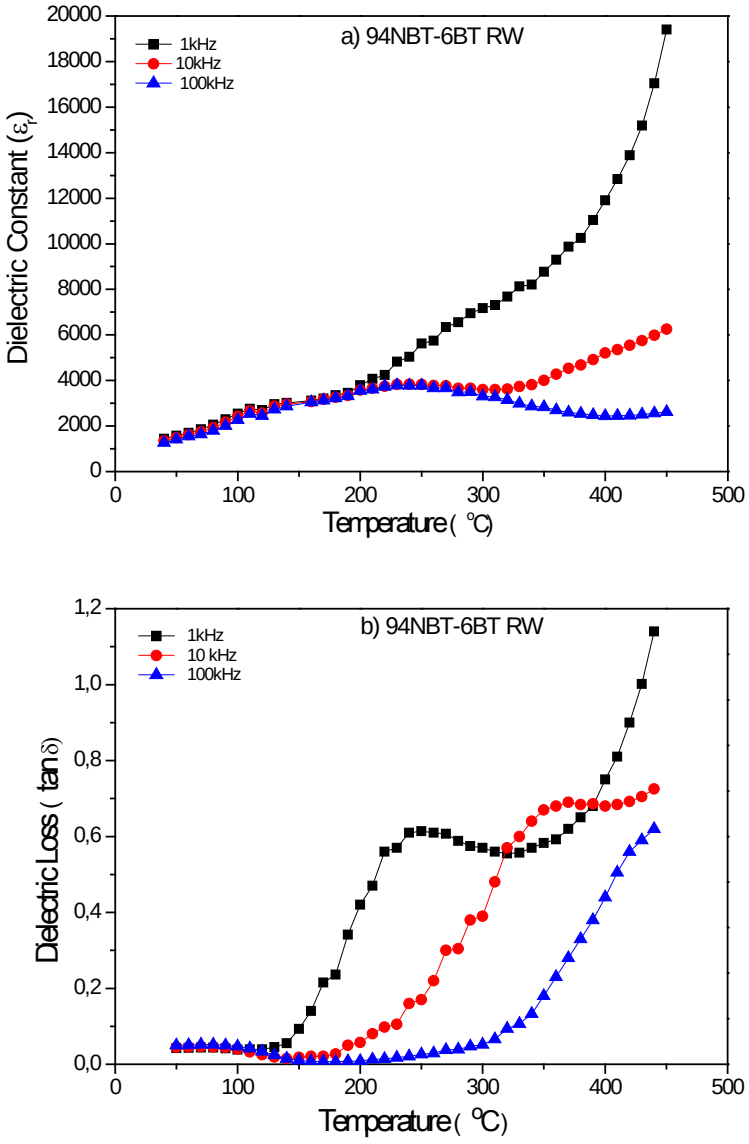

Figure 10.12. Temperature and frequency dependent dielectric constant (a) and dielectric loss (b) values for 94NBT-6BT RW single crystals

In Figure 10.13, pure (undoped) 94NBT-6BT KAL single crystals produced using calcined powder have higher dielectric constant and lower

dielectric loss for 1 kHz. Dielectric constant and dielectric loss values at room temperature are 1430 and 0.037, whereas for the maximum temperature 28310 and 1.05, respectively (Figure 10.13ab).

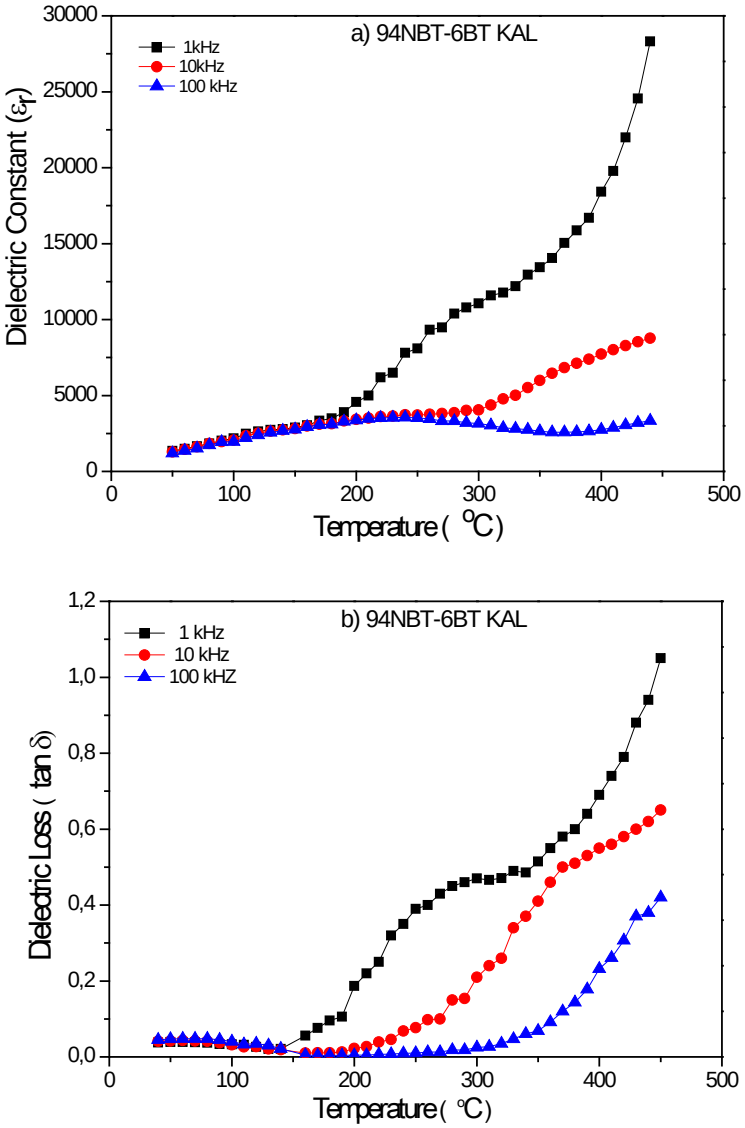

Figure 10.13. Temperature and frequency dependent dielectric constant (a) and dielectric loss (b) values of 94NBT-6BT KAL single crystals

Dielectric constant and dielectric loss of Li doped 94NBLT-6BT RW single crystal used without calcined powder are given at different frequencies in Figure 10.14. Dielectric constant and dielectric loss values are 1125 and 0,33 for 1

kHz, respectively. Dielectric strength and dielectric loss values increases up to 10810 and 0,76 with increasing temperature (Figure 10.14a-b).

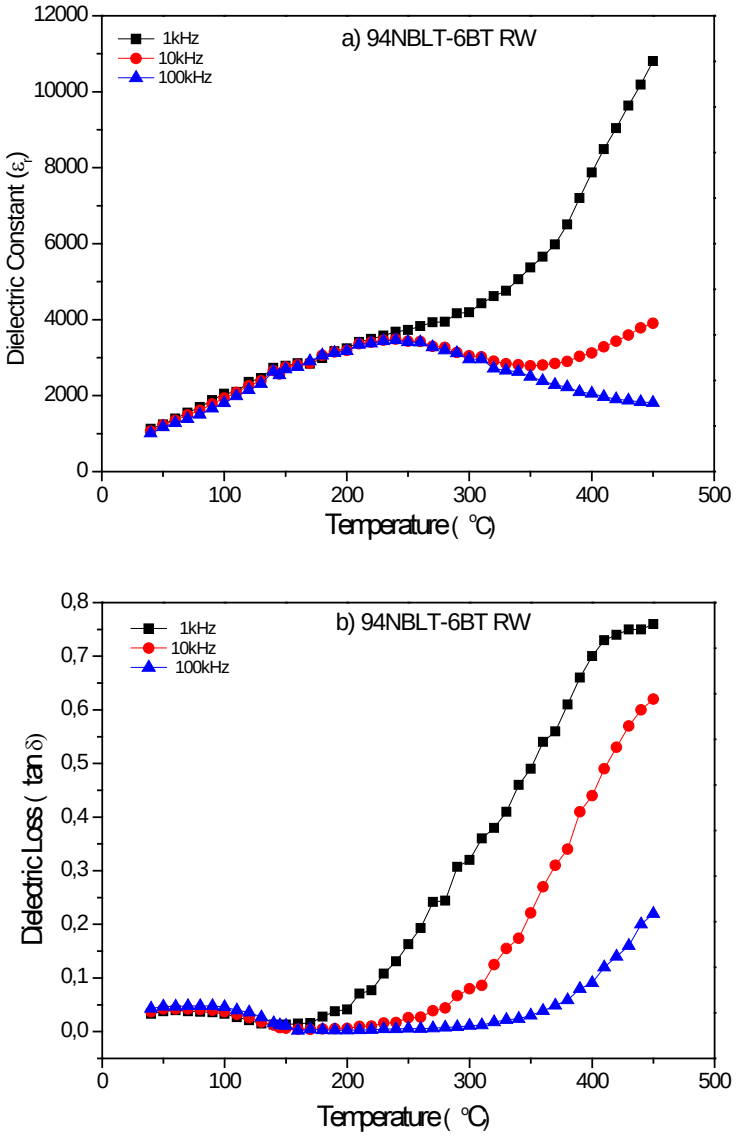

Figure 10.14. Temperature and frequency dependent dielectric constant (a) and dielectric loss (b) values for 94NBLT-6BT RW single crystals

Temperature and frequency dependent dielectric constant and dielectric loss values for 94NBLT-6BT KAL single crystals produced form calcined powders are given in Figure 10.15. Single crystals produced from calcined powder in similar way with undoped single crystals have the higher dielectric constant, whereas the electric loss value is almost the same. Dielectric strength at

room temperature is 1285 and the dielectric loss value is 0,037. These values are 22630 and 0,078 at high temperature (Figure 10.15a-b).

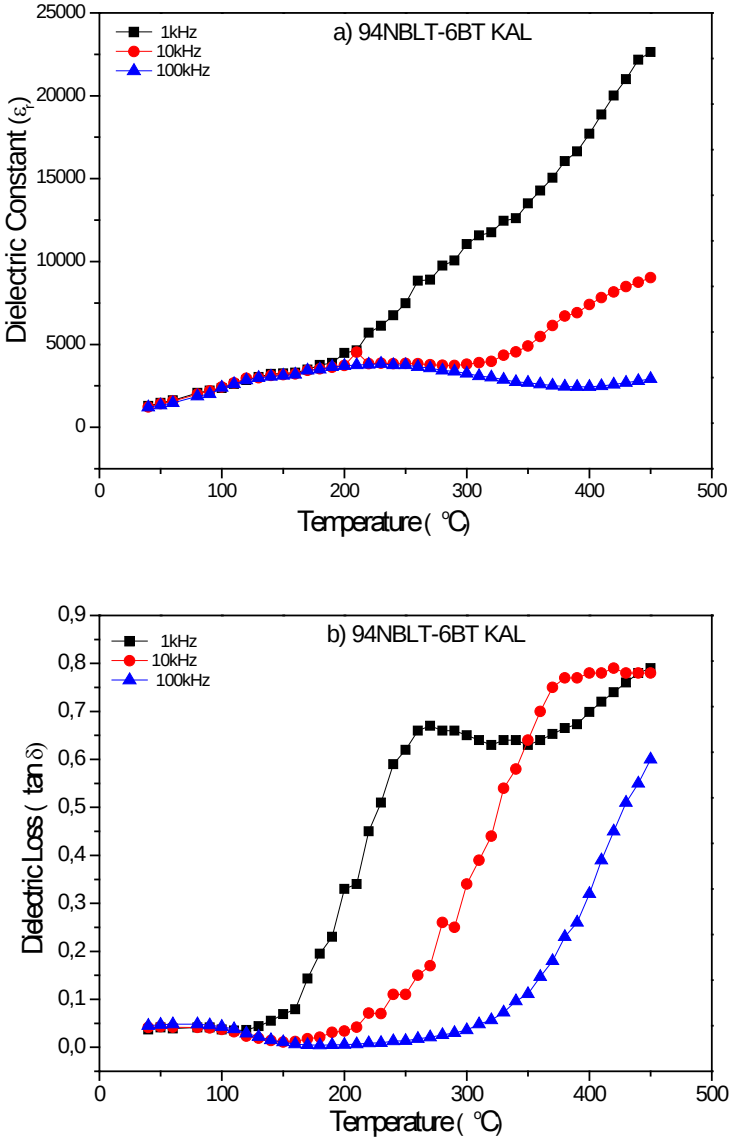

Figure 10.15. Temperature and frequency dependent dielectric constant (a) and dielectric loss (b) values for 94NBLT-6BT KAL single crystals

Dielectric constant and dielectric loss values for 94NBF-6BT KAL single crystals produced form Fe-doped powders are given in Figure 10.16. With the addition of Fe, dielectric constant value is initially about 1575 especially for 1 kHz and increases up to 37580 with increasing temperature. Dielectric loss values

are 0.04 for lower temperature but 1,29 for maximum temperature (Figure 10.16ab).

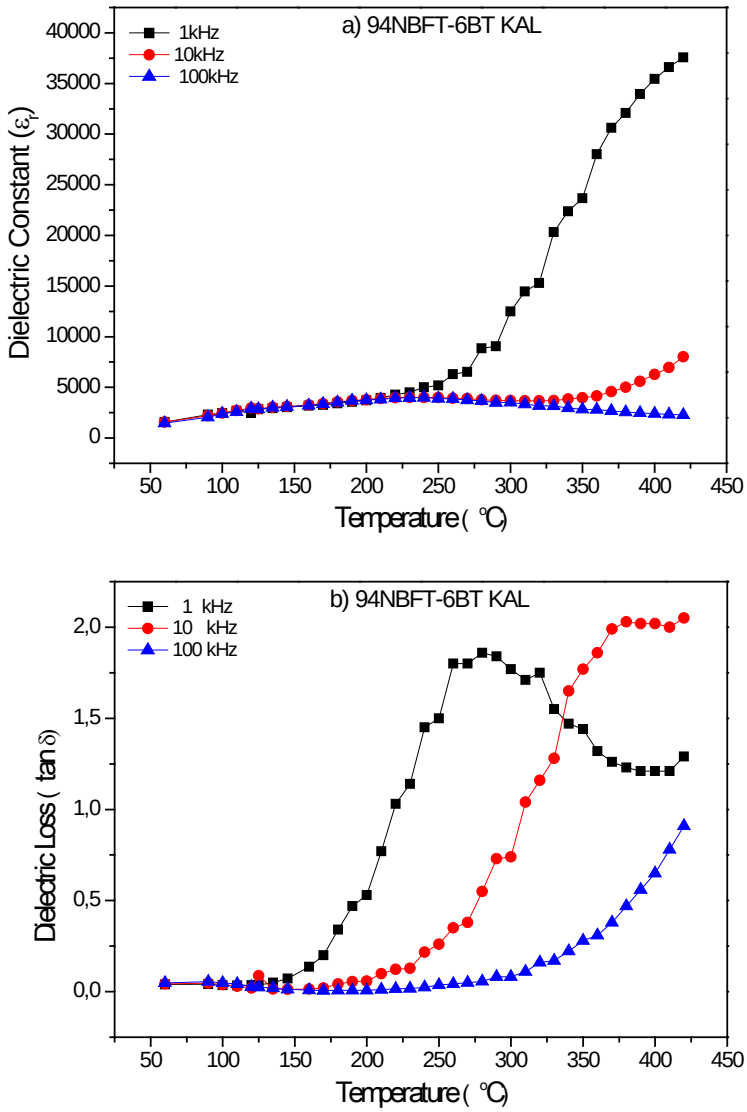

Figure 10.16. Temperature and frequency dependent dielectric constant (a) and dielectric loss (b) values for 94NBFT-6BT KAL single crystals

Finally, dielectric properties of 94NBMT-6BT KAL single crystals produced using Mn doped calcined powder is given in Figure 10.17. If dielectric properties of Mn doped crystals are compared with that of others, it is understood that it has reached the maximum value at 1 kHz with increasing temperature. Similarly, the dielectric loss has reached higher values with increasing temperature as compared to the other crystals. Dielectric constant is 1330 at the

beginning but has reached the values of 125000 with increasing temperature. The dielectric loss value varies between 0,028 and 7 (Figure 10.17a-b).

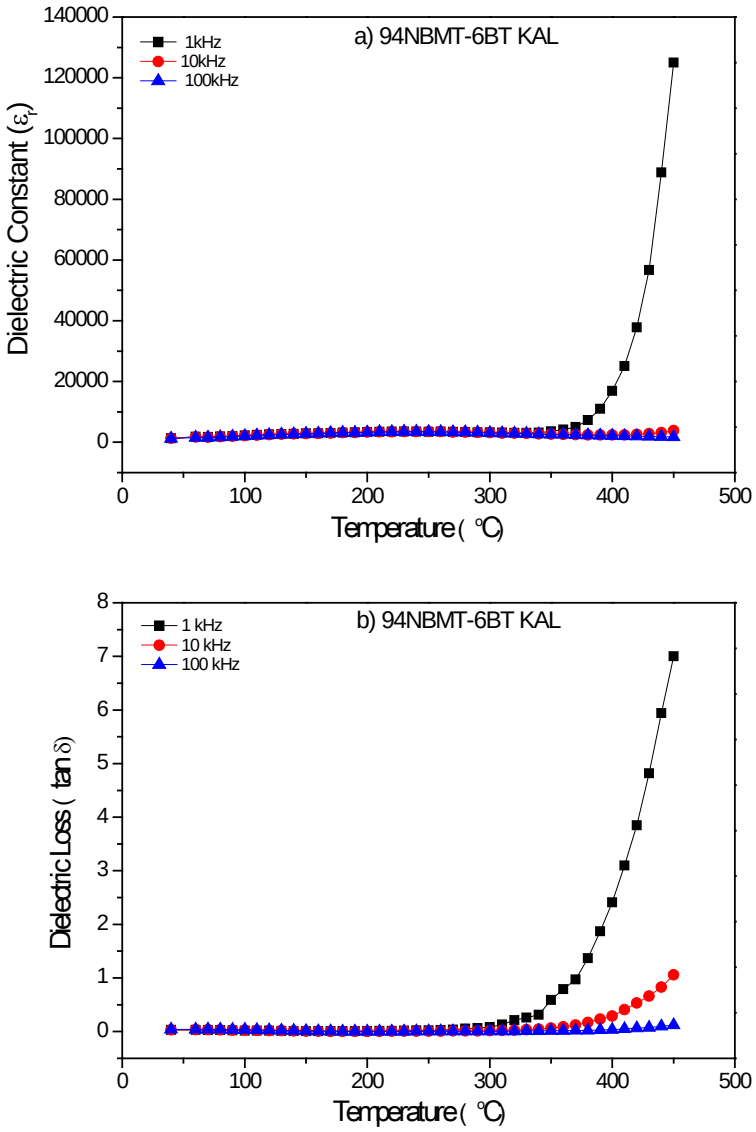

Figure 10.17. Temperature and frequency dependent dielectric constant (a) and dielectric loss (b) values for 94NBMT-6BT KAL single crystals

As a result, the dielectric properties vary depending on whether calcined powder is used or not. It is determined that the single crystals produced using the calcined powders have higher dielectric constant. In addition, Mn doped single crystals have higher dielectric constant with increasing temperature as compared to that of others.

11. ELECTRICAL CHARACTERIZATION OF 94NBT-6BT CERAMICS SINTERED WITH CS and SPS METHODS

Materials having 94NBT-6BT compositions were produced using calcined powder via solid state sintering method (CS) and spark plasma sintering method (SPS) for solid state single crystal growth studies. 300 MPa press was applied using cold isostatic press after pre-shaping process for sintering via CS, later shaped samples were sintered at 1130, 1150 and 1180^{o}C for 2 hours. These samples were sintered at 950^{o}C for 5 minutes at 50 MPa for sintering via SPS method. Electrical characterization of the materials produced by the method of CS and SPS are discussed below. Codes and descriptions of materials used are given in Table 11.1.

Table 11.1. Materials and their codes used at CS and SPS method

MATERIALS CODE	EXPLANATION
CS 94NBT-6BT UNPOLED	$94Na_{0.5}$ $Bi_{0.5}$ TiO_3-$6BaTiO_3$ polycrystal ceramics which are produced from calcined powder using CS method (Before polarization)
CS 94NBT-6BT POLED	$94Na_{0.5}$ $Bi_{0.5}$ TiO_3-$6BaTiO_3$ polycrystal ceramics which are produced from calcined powder using CS method (After polarization)
SPS 94NBT-6BT UNPOLED	$94Na_{0.5}$ $Bi_{0.5}$ TiO_3-$6BaTiO_3$ polycrystal ceramics which are produced from calcined powder using SPS method (Before polarization)
SPS 94NBT-6BT POLED	$94Na_{0.5}$ $Bi_{0.5}$ TiO_3-$6BaTiO_3$ polycrystal ceramics which are produced from calcined powder using SPS method (After polarization)

CS and SPS samples for electrical measurements to be approximately 1 mm thickness were polished and surface of them was electroted using silver paste.

The samples were polarized under 4 kV / mm DC electric field within oil at the temperature of 90^{o}C for approximately 20 minutes. Frequency dependent dielectric constant and dielectric loss before and after polarization at room temperature were compared with impedance gain phase analyzer as being dependent on capacitance values. Piezoelectric coefficients (d_{33}) of polarized samples were measured with d_{33} meter. Mechanical quality factor (Q_m) and coupling coefficient (k_p) were calculated by the determination of difference of resonance and anti-resonance frequency using gain phase analyzer. Temperature (0-450^{o}C) and frequency (1-10-100 kHz) dependent dielectric property measurements of CS and SPS materials were measured via LCR meter. Results of hysteresis loop and leakage current density of CS and SPS samples were characterized using AIXACT (aixPES / CMA) device.

11.1. Frequency Dependent Dielectric Properties of 94NBT-6BT Samples Produced with CS and SPS at Room Temperature

In Figure 11.1, dielectric constants of 94NBT-6BT materials produced via CS and SPS method at room temperature as a function of frequencies were given before and after polarization. Dielectric constant is high for both low (Figure 11.1a) and high frequencies (Figure 11.1b) before polarization, but decreases with increasing frequencies. A slight decrease in the dielectric constants is observed after polarization. As can be seen in Figure 11.1, sintering method has also effect on dielectric properties. Samples sintered via SPS have higher dielectric properties for all frequencies as compared to CS method. In Figure 11.1a, dielectric constant of samples produced via SPS is 785 before polarization, whereas decreases up to 740 with increasing frequency. In Figure 11.1b, dielectric constant decreases at high frequencies up to around 640. After polarization, dielectric constant decreases at low frequencies up to 700 starting from 730. The dielectric constant at high frequencies is around 600. Dielectric constants of samples produced via CS method are very low before and after polarization depending on frequency as compared to SPS method. In Figure 11.1a, the dielectric constant before polarization is started from 530 but decreased up to 485 with the increasing frequency. At higher frequencies, this value decreased up

to 400. After polarization at low frequencies, it is started from 445 and decrease up to 420, but higher frequencies it decreases up to 360. As a result, the ability of polarization, frequency, sintering method affects the dielectric properties. Samples produced via SPS method have quite high dielectric strength as compared to that of samples produced via CS method.

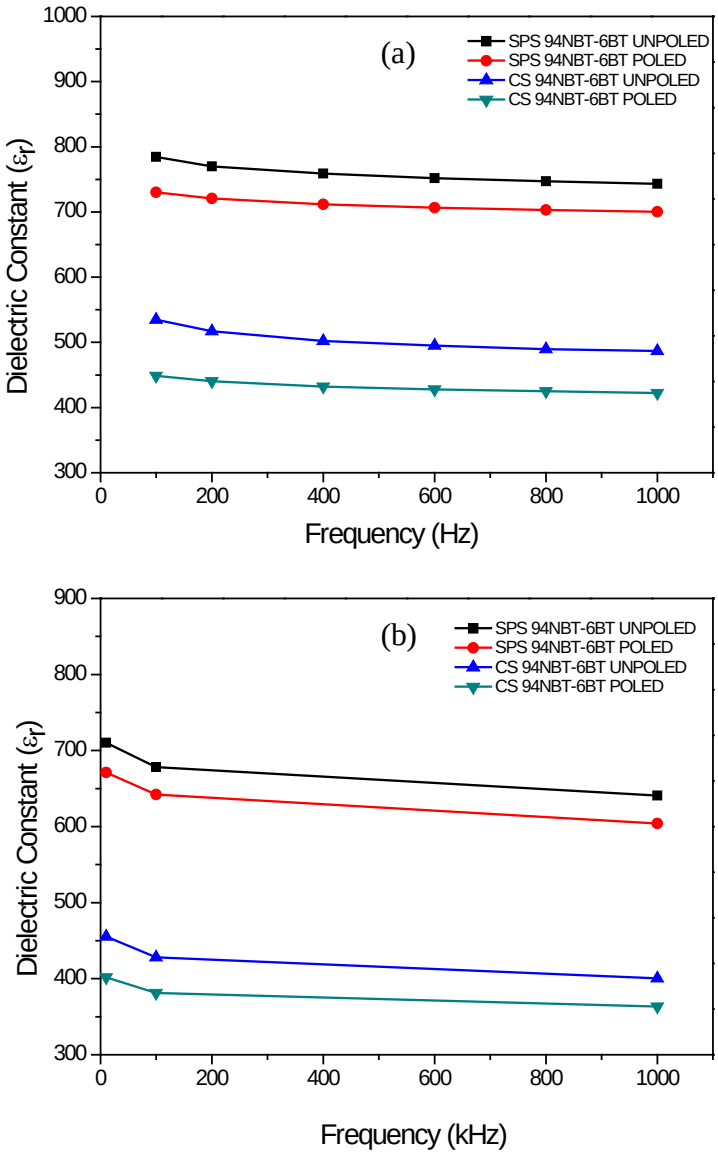

Figure 11.1. Dielectric constants of 94NBT-6BT ceramics produced via CS and SPS method before and after polarization at low (a) and high (b) frequency

In Figure 11.2, dielectric loss of samples produced via CS and SPS method at room temperature values are compared for low and high frequency. As can be seen from figure, samples sintered via SPS method at lower frequencies have lower dielectric loss values before and after polarization as compared to materials sintered via CS method.

Dielectric loss value was approximately 0,28 at lower frequencies before polarization but there is not much difference after polarization. For higher frequencies, dielectric loss before polarization is changed between 0,032 and 0,065 but after polarization ranged from 0,055 to 0,030 (Figure 11.2b). For materials sintered via CS method, this value is started from 0,062 and decreased up to 0,055 before polarization. However, after polarization, it is decreased from 0,05 to 0,038 (Figure 11.2a). For higher frequencies, dielectric loss is changed between 0,046 and 0,056 before polarization and it changes 0,036 and 0,050 after polarization (Figure 11.2b).

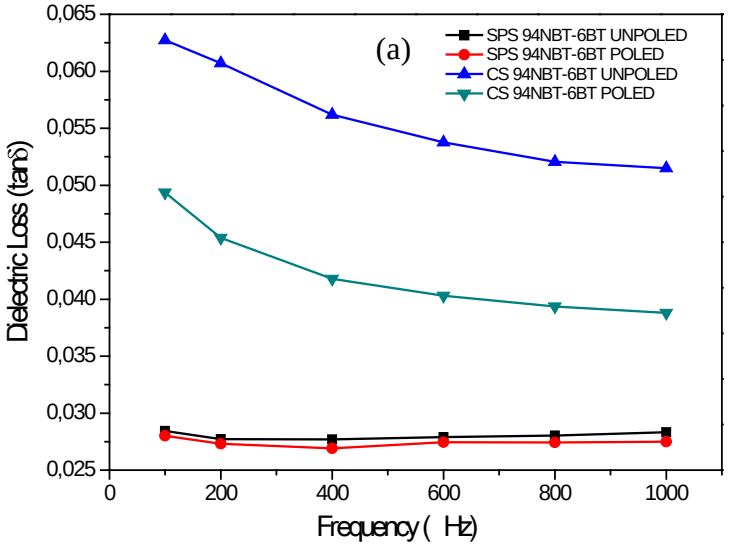

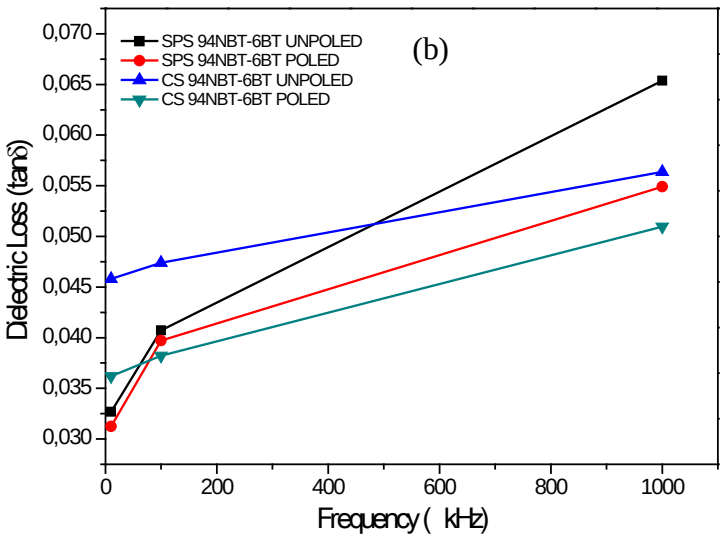

Figure 11.2. Dielectric loss of 94NBT-6BT ceramics produced via CS and SPS method before polarization at low (a) and high (b) frequencies

11.2. Piezoelectric Properties of 94NBT-6BT Ceramics Produced via CS and SPS Methods

Dielectric and piezoelectric properties of 94NBT-6BT ceramics produced via CS and SPS method at room temperature are summarized in Table 11.2. As seen in the table, materials produced via SPS method have superior properties as compared to materials produced via CS method. As given in table, dielectric constant of material sintered via SPS is higher that of material sintered via CS method, but dielectric loss value is lower. For the comparison of CS and SPS method, mechanical coupling factor (k_p) for materials sintered via SPS are twice and quality factor (Q_m) is four times higher as compared to that of material produced via CS method. piezoelectric coefficients are nearly same for both of two sintering methods.

The reason for the higher values of the samples sintered by SPS can be explained by having high density under 1000^{o}C and relatively short waiting time at this temperature and thus prevention of evaporation of alkali. Using of higher sintering temperature and longer waiting time for CS method increases alkali

evaporation and so decreases density of materials. Therefore, this has adverse effects on electrical properties of final product.

Table 11.2. Piezoelectric properties of 94NBT-6BT ceramics sintered via CS and SPS method

Materials	ε_r	**tanQ**	k_p	Q_m	d_{33}
CS 94NBT-6BT	544	0,031	12	48	70
SPS 94NBT-6BT	742	0,027	20	205	75

As a result, highly dense material can be produced at lower temperature via spark plasma sintering method as compared to common solid state sintering method. According to the results, ceramics with pure 94NBT-6BT composition produced via SPS method has superior piezoelectric feature. Because of these reasons, piezoelectric properties can be improved with SPS method using certain additives. In addition, the high density and strong matrix single crystal seed interface can be achieved via SPS as given previous sections, these materials can be used for SSCG method.

11.3. Determination of Temperature Dependent Hysteresis Charts for 94NBT-6BT Samples Produced by CS and SPS

Temperature dependent hysteresis loops for 94NBT-6BT samples produced via CS and SPS method are shown below. In Figure 11.3, hysteresis loop at different temperatures depending on electric field of samples are given. As seen in the shapes, remanent polarization and coercive field values of all specimens vary depending on increasing temperature and electric field. As shown in the figures, hysteresis loop reaches saturation point with increasing temperature especially after 90^oC. Coercive field decreases with the increasing temperature while remanent polarization values increases. This reveals the ability of the material to be polarized at lower electric field with increasing temperature.

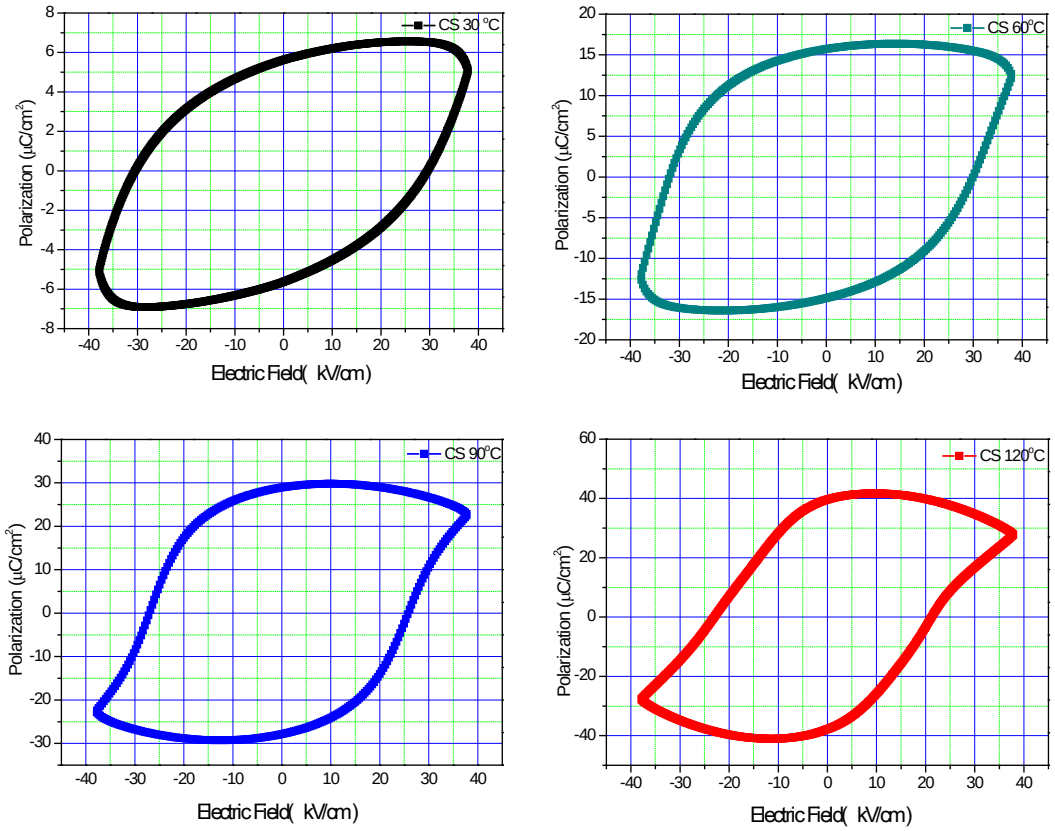

Figure 11.3. The temperature dependent hysteresis loop of 94NBT-6BT ceramics sintered with CS method

In Figure 11.4, hysteresis loops for materials produced via SPS method are given. Similar to CS method, remanent polarization value increases with increasing temperature but coercive field decrease depending of electric field and temperature. In addition, for SPS method, remanent polarization and coercive field values depending on temperature are lower as compared to that for CS method.

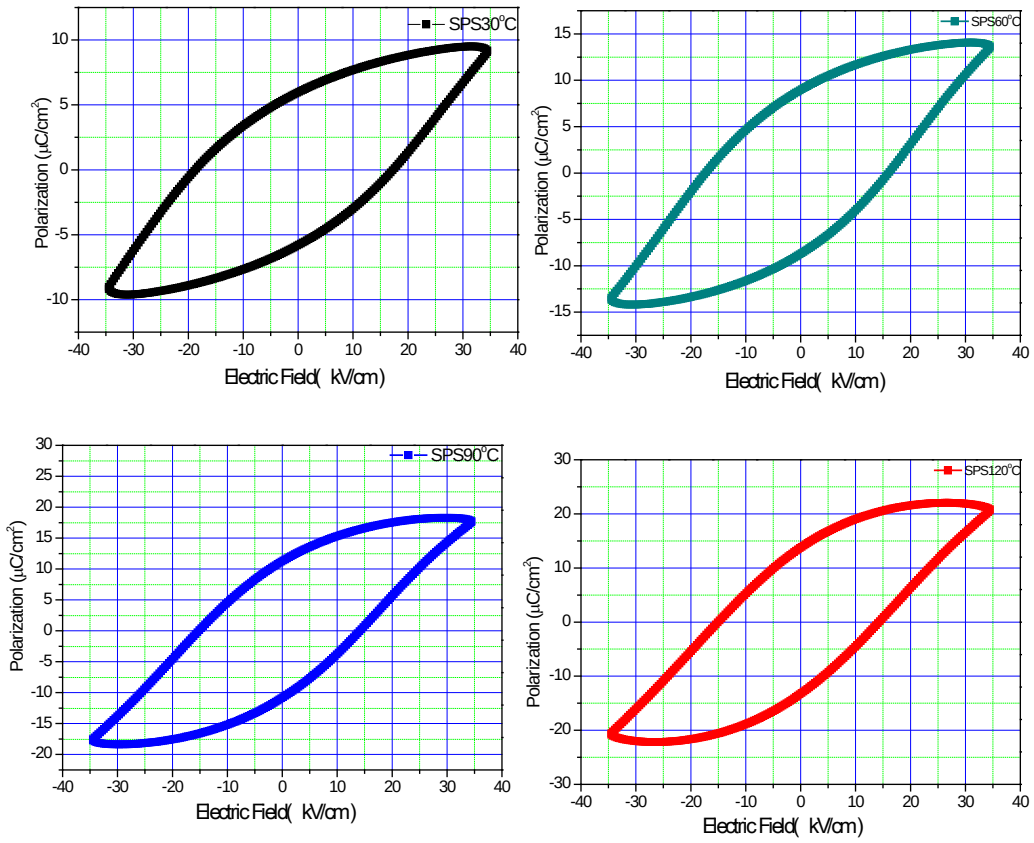

Figure 11.4. The temperature dependent hysteresis loop of 94NBT-6BT ceramics sintered with SPS method

In Figure 11.5, remanent polarization and coercive field values obtained from hysteresis loop of 94NBT-6BT materials sintered via CS and SPS method indicated above are given as depending on temperature. In Figure 11.5a, coercive field values of samples sintered via CS and SPS method depending on temperature. Coercive field of materials sintered via CS method is approximately 30 kV/cm at 30°C but decreases up to 20 kV/cm with increasing temperature. These values decreases from 17 kV/cm to 14 kV/cm for samples produced via SPS method. In Figure 11.5b, the remanent polarization values are given depending on the temperature. Polarization value of materials produced via CS method is about 5,5 μC/cm^2 initially but increases to 38 μC/cm^2 at 120°C. Similarly, for samples sintered via SPS method, remanent polarization value increase from 6 μC/cm^2 to 14 μC/cm^2 with increasing temperature.

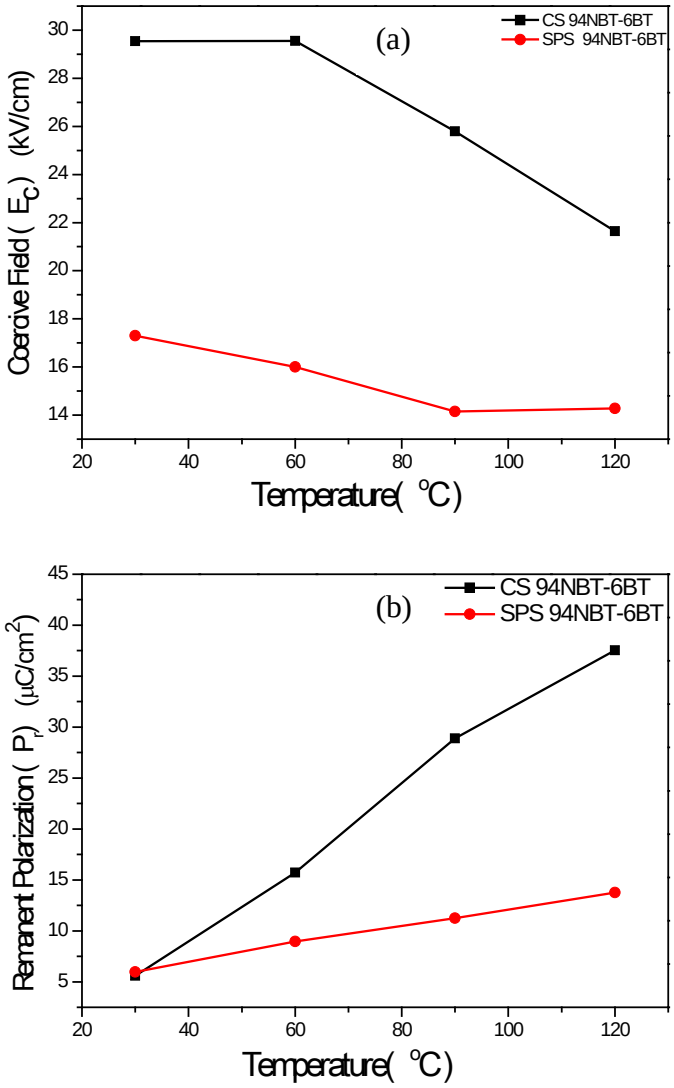

Fig. 11.5. Temperature dependent Ec (a) and Pr (b) changes for 94NBT-6BT ceramics sintered with CS and SPS

11.4. Determination of Temperature Dependent Leakage Current Densities of 94NBT-6BT Ceramic Produced by CS and SPS

As given in the previous sections, dielectric and piezoelectric properties of 94NBT-6BT ceramic sintered via SPS method is higher as compared to that of material sintered via CS method. Being high of this feature is associated with leakage current densities. Therefore, leakage current density of sintered materials produced via CS and SPS method are given in Figure 11.6. As seen in the figure, leakage current densities at different temperatures increase depending on the

electric field. In Figure 11.6, maximum leakage current densities for samples sintered via CS is varied between the values of $10*10^{-7}$ and $80*10^{-7}$ A/cm^2 with increasing temperature from 30^{o}C to 120^{o}C, respectively. In Figure 11.6b, the maximum leakage current densities of the samples sintered via SPS method varies in the range of $3*10^{-7}$ and $32*10^{-7}$ A/cm^2 at a given temperature range, respectively. It is obvious that maximum leakage current densities of ceramic produced via SPS method are nearly 3 times lower than that of materials produced via CS method.

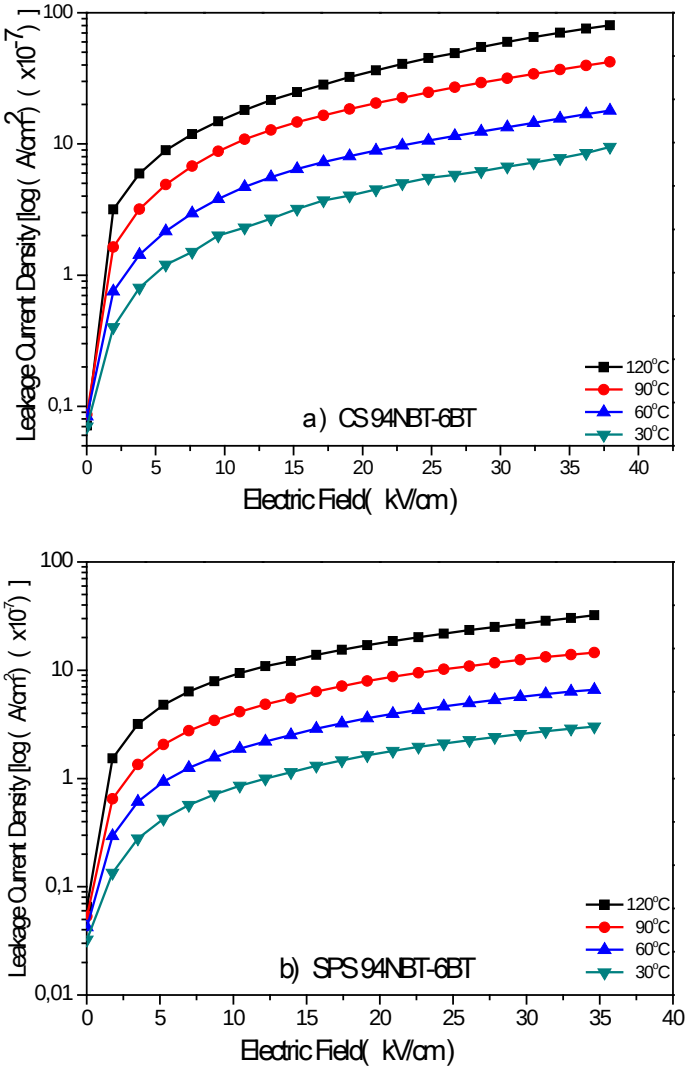

Figure 11.6. Temperature dependent leakage current density change of 94NBT-6BT ceramic sintered via CS (a) and SPS (b)

11.5. Temperature and Frequency Dependent Dielectric Properties of 94NBT-6BT Samples Produced by CS and SPS Method

Temperature and frequency dependent dielectric constant and dielectric loss values of NBT-BT samples sintered via CS and SPS method are given in Figure 11.7. In Figure 11.7a, dielectric constant of samples sintered via CS at 1-10-100 kHz are approximately 420, 410 and 380 at room temperature, whereas at 280^{o}C reached up to 2820, 2650 and 2500. In Figure 11.7b, dielectric losses are started with the value of approximately 0,04 at room temperature for 1-10-100 kHz but increase up to 0,2,0,09 and 0,08 with the increasing temperatures respectively.

.

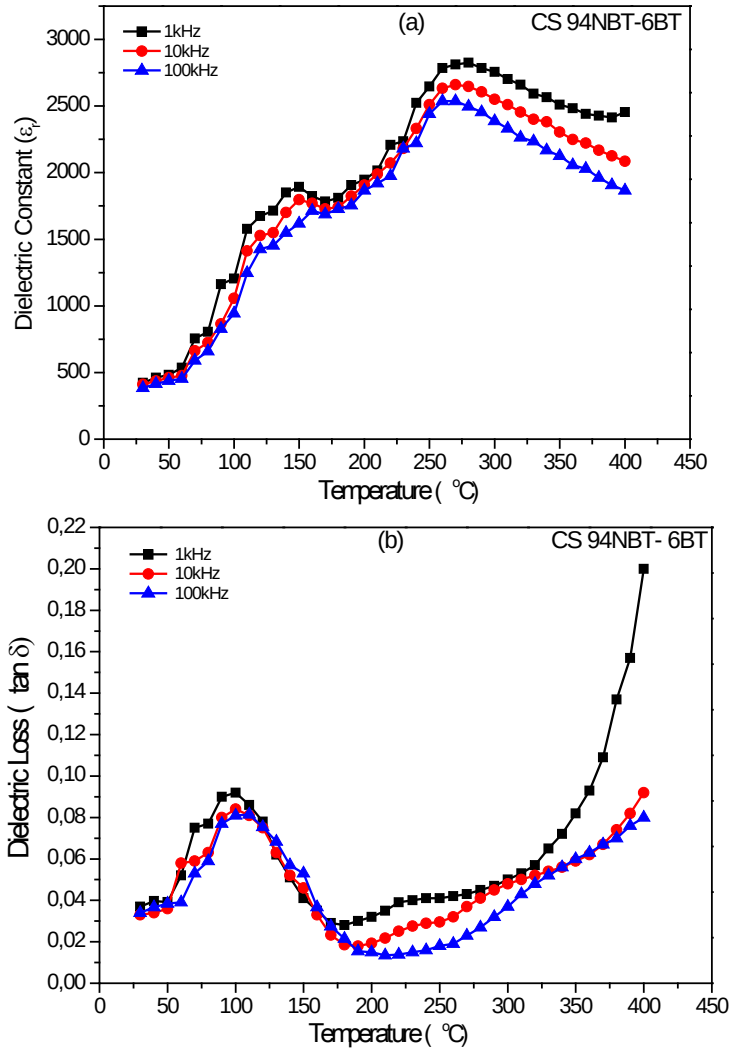

Figure 11.7. Temperature and frequency dependent dielectric constant (a) and dielectric loss (b) change for 94NBT-6BT ceramic sintered via CS method

In Figure 11.8, dielectric constant and dielectric loss values of 94NBT-6BT ceramics sintered via SPS method is given as depending on temperature and frequency. As can be seen in Figure 11.8a, from the values at 1-10-100 kHz, dielectric constants are approximately 740,715 and 690 at the beginning, whereas at 220^{o}C the values reached the maximum of 5070, 3180 and 2680 respectively. From the dielectric loss values given by Figure 11.8.b, they have the values starting from 0,03 at room temperature and at 1-10-100 kHz and increased with the increasing temperature to the values of 0,52, 0,18 and 0,12 respectively.

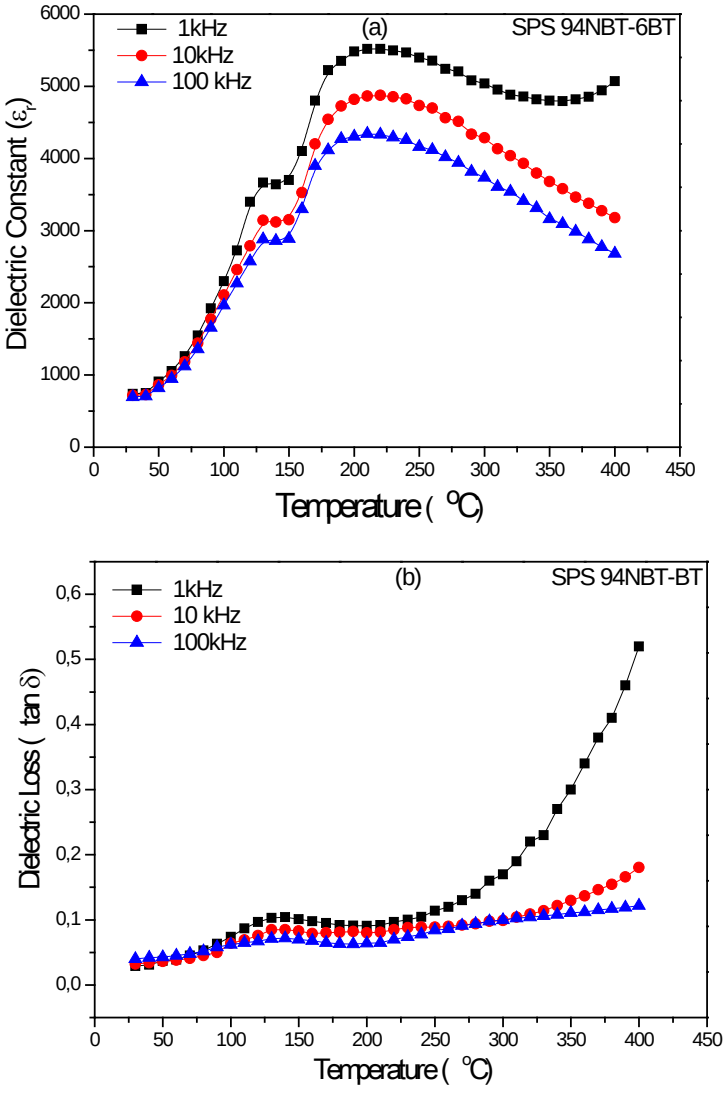

Figure. 11.8. Temperature and frequency dependent dielectric constant (a) and dielectric loss (b) change of 94NBT-6BT ceramics sintered via SPS method.

In Figure 11.9, dielectric constant and dielectric loss of samples sintered via CS and SPS method are given on the same graph. As can be seen in Figure 11.9a, it is clear that materials produced via SPS as given in the previous sections have higher dielectric feature.

.

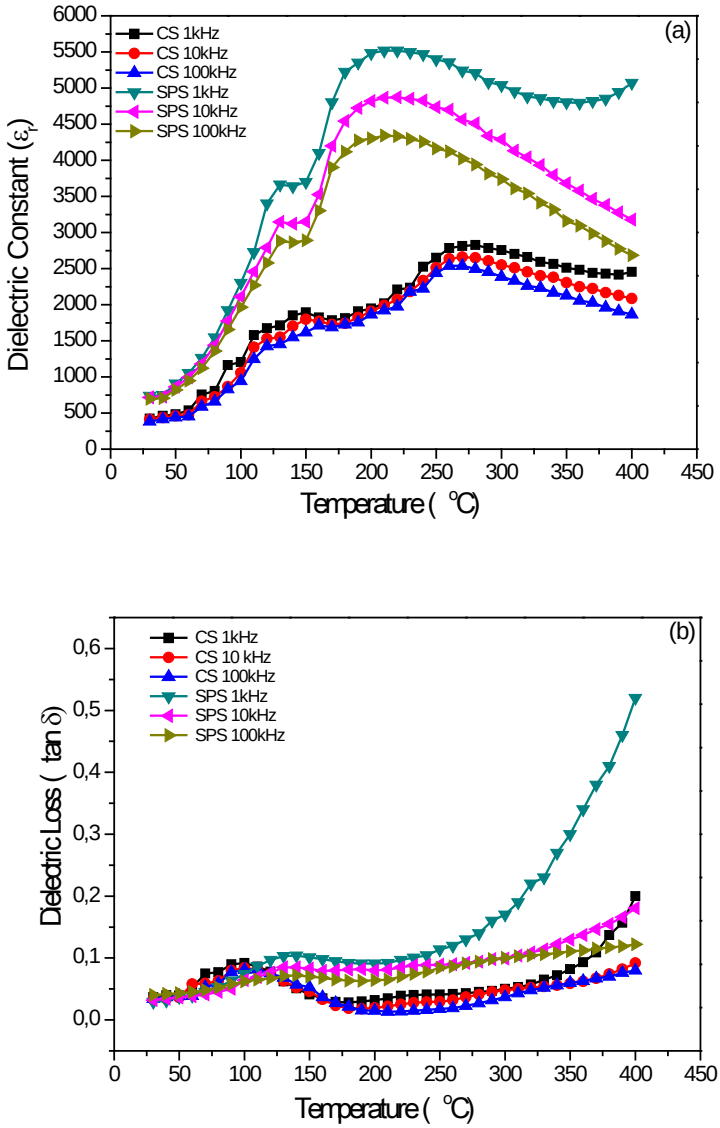

Figure 11.9. Comparison of temperature dependent change in dielectric constant (a) and dielectric loss (b) of 94NBT-6BT ceramics sintered via CS and SPS

As can be seen from the figures, there are peak deviation at two points for all frequency values depending on increasing temperature. The first peak deviation of the SPS is approximately at 130^{o}C and the second peak deviation is

approximately at 220^{o}C. The peak deviations of the samples sintered via CS method are about at 150 and 280^{o}C. Similarly, as can be seen from graph given in Figure 11.9b related with dielectric loss, there are peak deviations for the temperature of 130 and 150^{o}C. The reason of the peak deviation at the first point material is depolarized at this temperature. In other words, the material is transformed from ferroelectric phase to anti ferroelectric phase. This phase transition is very important, especially in practice. The second peak deviation is due to the transition from anti ferroelectric phase to paraelectric phase [94].

12. CONCLUSIONS

In this thesis $BaTiO_3$ and 94NBT-6BT single crystals were succesfully grown with flux growth technique. To briefly summarize the studies in this thesis

- Powder synthesis and characterization of $BaTiO_3$ with solid state synthesis method.
- Single crystal growth of $BaTiO_3$ with flux growth method using synthesized powder.
- Solid state synthesis of undoped and Li, Fe, Mn doped $94(Na0.5Bi0.5)TiO_3–6BaTiO_3$ (94NBT-6BT) powders and their characterisations.
- Flux growth of pure and Li, Fe, Mn doped $94(Na0.5Bi0.5)TiO_3–6BaTiO_3$ (94NBT-6BT) single crystals using synthesized powder and their characterisations.
- Conventional sintering (CS) and spark plasma sintering (SPS) assisted solid state single crystal production studies for 94NBT-6BT compositions.
- Electrical characterisation of 94NBT-6BT based single crystals from flux growth.
- Electrical characterization of sintered samples with CS/SPS sintering method for solid state single crystal growth studies.

As stated in the first part, $BaCO_3$ and TiO_2 were used as starting material for the production of $BaTiO_3$ polycrystal powder using solid state synthesis method. Due to the size of TiO_2 (25 nm), initially size of micron-sized rod like shaped $BaCO_3$ was decreased to increase the interaction between powders. Depending on grinding via planetary mill, size of rod like shaped structures was decreased to approximately 620 nm through grinding. It is determined that size distribution of powders dried via freeze dryer after grinding was the size of below 600 nm. As a result of the thermal analysis, decomposition of unground powder was begun at the temperature of 1000^oC, while the decomposition of $BaCO_3$ size

of which was reduced to below 600 nm was begun at the temperature of above 550^{o}C, so it started to be decomposed at quiet low temperature as compared to starting material. High degree particle size differences in solid state synthesis method causes formation of undesired intermediate phases at the end of the reaction and thus existence of unreacted materials in the structure. In addition, there were requirements emerged as high temperature and more time due to the variation in size for the completion of the reaction. Therefore, decreasing the size of $BaCO_3$ provided advantage for the synthesis of $BaTiO_3$ powder. There was only $BaTiO_3$ formation observed in the structure at the studies performed when Ti: Ba ratio is 1. It was determined from the XRD analysis of BTS coded powder having the ratio of Ti/Ba=1 that there was $BaTiO_3$ partial formation for the calcination time and temperature below 1050^{o}C and also identified that existence of unreacted $BaCO_3$ and Ba_2TiO_4 intermediate phases in the structure. It was also determined that there was only $BaTiO_3$ formation depending on the calcination temperature of 1050^{o}C and time in the case of temperature above 1050^{o}C. It is determined from the SEM analysis performed after synthesis that size of produced $BaTiO_3$ was smaller than the 200 nm. KF (fluxing agent) was added after the production of $BaTiO_3$ powder, and barium titanate ($BaTiO_3$) single crystalline was produced via the method of growth from melt after the application of heat treatment at 1200^{o}C for 15 hours. As a result of microscopic, crystallographic and chemical analysis of single crystalline materials it was determined that the structure of $BaTiO_3$ was polyhedron. Due to the very small dimensions of the crystals produced, electrical properties were not analysed.

After the production of barium titanate, undoped (pure) and Li, Fe, Mn doped polycrystal bismuth titanate-barium titanate based ceramic powders with the composition of 94($Na_{0.5}Bi_{0.5}$) TiO_3-6$BaTiO_3$ (94NBT-6BT) were produced via solid state synthesis method and analysed using XRD, SEM and EDX. It was determined from XRD analysis that, all pure and doped powder had the structure of perovskite 94($Na_{0.5}Bi_{0.5}$) TiO_3-6$BaTiO_3$ after heat treatment at 900^{o}C. SEM analysis showed that undoped powders were sharp-edged and Li-doped powders had the cubic structure with corners quite close to the rounded shape. Micro-structures of Fe and Mn doped 94NBT-6BT powders were determined as more

spherical. Considering pure and Li-doped 94NBT-6BT powders with the structure close to cubic morphology, it was realized that some particles reached the size of approximately 2 micron but in general smaller than that value. It was determined Mn doped 94NBT-6BT powder with spherical morphology were smaller than 500 nm.

Thermal analyses were performed for the determination of melting temperature of 94NBT-6BT based pure and Li, Fe and Mn doped powder. Melting temperature of 94NBT-6BT powder was determined as 1270^{o}C from DSC and heat microscopy analysis. To achieve complete melting, temperature for single-crystal growth from melt was designated as 1380^{o}C which was 100^{o}C higher than melting temperature. Produced powders were melted in a Pt cruciable at 1380^{o}C for 5-10 hours depending on the additives. After that, the crystals were gradually cooled to room temperature at very slow cooling rate. Size of pure and Li, Fe, Mn doped 94NBT-6BT produced crystals was ranged approximately from 3x3x1 and 5x5x1 mm as a result of polishing.

From the XRD analysis, diffraction was obtained from only a single plane for single crystals, whereas diffraction was obtained all planes for single crystals in powder form. It was determined that single crystalline material had completely perovskite 94($Na_{0.5}Bi_{0.5}$) TiO_3-6$BaTiO_3$ structure. In addition, it was observed that there was a peak separation of (003) and (021) from XRD (111) for 39-41^{o} and 45-48^{o}, and (200) from (002). It can be understood from these results that first peak separation was special for rhombohedral sodium bismuth titanate and second was for tetragonal barium titanate. In other words, both sodium bismuth titanate and barium titanate phase were existed together in the produced crystals, and thus this was confirmed that the structure had 94NBT-6BT composition. In addition, it was realized from SEM analysis that there were no grain boundaries for materials grown as single crystalline. Whether or not there were evaporation losses because of heat treatment for grown crystals was determined via EDX and XRF analyses. It was determined from the analysis expected values from composition and experimental results were quite similar especially for calcined powder. In addition, starting materials with 94NBT-6BT composition were used without calcination and grown as single crystalline. However, expected results from

elemental analysis could not be obtained because of high evaporation losses for single crystalline samples produced without calcination. However, a certain amount of $NaCO_3$ and Bi_2O_3 addition to synthesized powders were compensated for the evaporation losses arising from the system.

In addition to the studies for 94NBT-6BT-based single crystal growth from the melt, studies for solid-state single-crystal production method (SSCG) were also performed. Single crystals grown from the melt was used as seed material. In this method, especially strong seed-matrix interface bonding and the production of high density matrix structure were aimed. For studies performed using hot press reported in the literature, pores in the matrix material were swept away into crystal as a result of crystal growth. In addition, due to the structure of the porous matrix, the interaction of the seed matrix interface was very weak. In addition, there were evaporation losses due to high temperatures process. To avoid these problems, matrix materials were produced via spark plasma sintering method (SPS) and the interaction of the seed-matrix interface was investigated. In addition, studies were also performed using solid-state sintering method (CS) and the results were compared with the SPS method. Materials were sintered via CS method at the temperatures above 1100^{o}C for about 2 hours, whereas at temperatures of 950^{o}C for 5 minutes for SPS method. Theoretical density of 96-98% was achieved as a result of density measurement for materials produced via CS method, whereas for SPS method this value was nearly 100%. In other words, high density ceramics were produced at temperatures lower than 230^{o}C at shorter time as compared to CS method. It is determined from low- magnification SEM analysis that there was porosity in microstructures of materials sintered via CS method. On the other hand, materials sintered via SPS method had quite high density. Similarly, seed-matrix interactions of 94NBT-6BT based materials produced via both CS and SPS methods were investigated using SEM. Stronger seed-matrix interface interaction was achieved for materials sintered with SPS. According to the results, SPS assisted solid state single crystal production method can be used to produce 94NBT-6BT single crystals in the future.

In the last part of the thesis, characterization of electrical properties of 94NBT-6BT based single crystals and sintered 94NBT-6BT polycrystals with CS and SPS method were performed and compared. Dielectric properties of single crystals produced from calcined powder were higher than those of crystals produced directly from raw material and leakage current density of the crystals were lower. In the case of polarization behaviour of produced crystals, polarization of 94NBT-6BT was very difficult due to the alkaline within the structure. For the polarization studies, very few samples of about 120 pC/N piezoelectric constant have been achieved. Therefore, temperature dependent hysteresis loops were analysed and thus it was observed that these loops were expanding with increasing temperature. This was because the leakage current due to the conductive structure of material. Therefore, the effects of the additives on leakage current were analysed. According to the analysis, depending on the temperature and electric field, it was observed that leakage current densities were increased. Fe-containing 94NBFT-6BT single crystals had the highest leakage current density, whereas Mn-containing 94NBMT-6BT single crystals had the lowest. In addition, it was found out that, single-crystal materials produced using calcined powder had leakage current density lower than that of single crystals produced using not calcined powders. In addition, temperature and frequency dependent dielectric properties of 94NBT-6BT based single crystals was investigated before polarization process. It was clear from the analysis performed that single crystals produced via calcined powders had a higher dielectric strength. It was observed that the highest dielectric strength was for Mn doped 94NBMT-6BT single crystals having the lowest leakage current density.

Finally, electrical properties of 94NBT-6BT materials sintered via CS and SPS method were analysed and compared. Dielectric constant of materials produced using both SPS and CS showed a slight decrease after polarization as a function of frequency at room temperature. However, dielectric property of materials sintered via SPS was higher as compared to that of sintered via CS both before and after polarization. As to compare piezoelectric properties of these materials, the piezoelectric coefficient for both sintering method were very similar to each other. However, it was estimated that coupling factor and mechanical

quality factor of ceramics sintered via SPS was approximately two times and four times higher, respectively. In addition, the temperature-dependent hysteresis loops for ceramics produced via CS and SPS methods were attained. It was observed that loops were getting saturated with increasing temperature depending on the electric field. By using hysteresis loops of the samples sintered via CS and SPS method, coercive field values were determined. Coercive field value of samples sintered via CS method was 30kV/cm at 30^{o}C, but decreased to 20kV/cm with increasing temperature, however, for samples sintered via SPS method, this value was decreased from 17kV/cm to 14kV/cm at the same temperature. As to remanent polarization values, samples produced via CS method had the value of 5.5μC/cm^2 initially, 38μC/cm^2 after 120^{o}C heat treatment. Similarly, remanent polarization value of samples sintered via SPS was increased from 6μC/cm^2 to about 14μC/cm^2 with increasing temperature. As to compare leakage current density of materials produced via CS and SPS method, it was observed that leakage current densities of the samples produced via SPS method was approximately three times lower than that of material produced via CS method. It was determined that temperature dependent dielectric properties of crystals produced via SPS method was approximately two times higher than that of materials produced via CS method.

As a conclusion, especially 94NBT-6BT based single crystal ceramics has been produced successfully grown with flux growth method. In general, calcination of powders had positive effect (contribution) on the electrical properties. It was found that Mn-doped single crystals have a significant potential for usage due to the lowest leakage current density and the highest dielectric constant. Also, SPS assisted solid state single crystal production method (SSCG) can be used for fabrication of big sized 94NBT-6BT based single crystals.

REFERENCES

[1] Moulson, A.J., Herbert, J.M., *Electroceramics: Materials, Properties, Applications*, Second edition, John Wiley and Sons Ltd, England, 2003.

[2] Pi Ceramic Co., *Piezoelectric ceramic product*, http://www.piceramic.com/pdf/KATALOG_english.pdf

[3] Cass, R., Mohammadi, F., Leschin, S., *Innovative Products And Processes Based On Piezoelectric Ceramic Fıbers*, 2006 http://www.advancedcerametrics.com/files/File/ICC%20SYMPOSIUM%20MANUSCRIPT-July,%202006.pdf

[4] Murata Manufacturing Co., Ltd, *Piezoceramic sensors*, Katalog No:P19E6 http://www.symmetron.ru/suppliers/murata/sensors/p19e6.pdf

[5] Morgan Electroceramics Company, *Single crystal piezo*, http://www.morganelectroceramics.com/materials/piezoelectric/single-crystal-piezo/

[6] Zhengfa, L., Yongxiang, L., Jiwei, Z., "Grain growth and piezoelectric property of KNN-based lead-free ceramics," *Curr. Appl. Phys.*, **11**, S2-S13, 2011.

[7] Peng, C., Li, J.F., Gong, W., ''Preparation and properties of $(Bi_{1/2}Na_{1/2})TiO_3$–$Ba(Ti,Zr)O_3$ lead-free piezoelectric ceramics,'' *Materials Letters*., **59**, 1576– 1580, 2005.

[8] Damjanovic, D., *Recent devolepment in piezoelectric materials used for actuators and sensors applications*, http://www.fhkiel.de/fileadmin/data/maschinenwesen/Organisation_Personen/IMST/pdf/proceed/Damjanovic.pdf

[9] Phillips, J.R., *Piezoelectric Technology Primer*, http://www.ctscorp.com/components/pzt/downloads/Piezoelectric_Technology.pdf

[10] Lin, D. M., Xiao, D.Q., Zhu, J. G., Yu, P., Yan H.J., Li, L.Z., Zhang, W., ‘‘The relations of sintering conditions and microstructures of $[Bi_{0.5}(Na_{1-x-y}K_xLi_y)_{0.5}]TiO_3$ piezoelectric ceramics,’’ *Cryst. Res. Technol.*, **39**, No.1, 30 - 33, 2004.

[11] Heartling, G. H., ‘‘Ferroelectric Ceramics: History and Technology,’’ *J. Am. Ceram. Soc.*, **82** [4] 797–818, 1999

[12] http://www.americanpiezo.com/knowledge-center/piezo-theory/piezoelectricity.html

[13] Jaffe, B., Cook, W.R., *Piezoelectric ceramics*, Academic Press, London and New York, 1971

[14] Richerson, W. D., *Modern ceramic engineering: Properties, processing and use in design*, Marcell Deccer, Inc., New York, 1992.

[15] Zhu, X., *Piezoelectric ceramic materials, processing, properties, characterizations, and applications*, Materials Science and Technologies Series, New York, A.B.D., 2010.

[16] Buchanan, Z.C., *Ceramic Materials for Electronics: Processing, Properties and Applications, Second Edition*, Marcel Deccer Inc., ABD, 1991.

[17] Uzgur, E., *Zil tipi piezoelektrik kompozit transdüser tasarımı ve akustik uygulamaları*, Doktora Tezi, Anadolu Üniversitesi, Fen Bilimleri Enstitüsü Eskişehir, 2006.

[18] Randeraat, J. ve Setterington, R.E., *Piezoelectric Ceramics*, N. V. Philips Publishing, ABD, 1974.

[19] Uzun, M., *Katıhal reaksiyonu ile sentezlenen $Ba_xSr_{1-x}TiO_3$' ın elektriksel özellikleri*, Yüksek Lisans Tezi, Dumlupınar Üniversitesi, Fen Bilimleri Enstitüsü, Kütahya, 2005

[20] http://www.aurelienr.com/electronique/piezo/piezo.pdf

[21] http://www.honda-el.co.jp/ufile/file/249.pdf

[22] Pearson, S., *Characterization and Modeling of Piezoelectric Devices*, Master Thesis, Villanova University, The Department of Electrical and Computer Engineering, Villanova, 2006

[23] Efe, C., *Ferroelektrik seramiklerin elektrik ve mekanik özelliklerinin araştırılması*, Yüksek Lisans Tezi, Gebze Yüksek Teknoloji Enstitüsü, İstanbul, 2007

[24] Novacap, Co., *Technical brochure*, http://www.novacap.com/PdfFiles/tech_behavior.pdf

[25] Tıkız, S., *Çevre dostu kurşunsuz piezoelektrik seramiklerin üretimi ve kullanım güvenilirliğinin karakterizasyonu*, Yüksek Lisans Tezi, Afyon Kocatepe Üniversitesi, Fen Bilimleri Enstitüsü, Afyon, 2010

[26] Damjanovic, D., "Ferroelectric, dielectric and piezoelectric properties of ferroelectric thin films and ceramics," *Rep. Prog. Phys.*, **61**, 1267–1324, 1998.

[27] Gönülşen, T., *Synthesis, characterization and electrical properties of piezoelectric materials by sol-gel technique*, Master Thesis, Dokuz Eylul University, Graduate School of Natural and Applied Sciences, İzmir, 2006

[28] Jordan, T.L., Ounaies, Z., *Piezoelectric ceramics characterisation*. ICASE Report, No. 2001-28, 2001

[29] Muanghlua, R., Niemcharoen, S., C. Vittayakorn, W.C., Tungsitvisetkul, N., Chinwaro, P., Ruangphanit, A., Chaiyo, N., ve Vittayakorn, N., "Preparation and properties of lead free bismuthsodium titanate−bismuth zinc titanate ceramics," *Ferroelectrics*, **383**, 1–7, 2009

[30] Seifert, K., *Lead-free piezoelectric ceramics*, PhD Thesis,Technischen Universität Darmstadt, Darmstadt, 2010

[31] Binhayeeniyi, N., Sukvisut, P., Thanachayanont, C., Muensit, S., "Physical and electromechanical properties of barium zirconium titanate synthesized at low-sintering temperature," *Mater. Lett.*, **64**, 305–308, 2010

[32] Maeder, M.D., Damjanovic, D., ve Setter, N., "Lead free piezoelectric materials", *J. Electroceram*, **13**, 385–392, 2004

[33] Zhang, S., Xia, R., ve Shrout, T.R., "Lead-free piezoelectric ceramics vs. PZT?," *J. Electroceram*, **19**, 251–257, 2007

[34] Zhoua, C., Liu, X., Li, W., Changlai Yuan, C., "Dielectric and piezoelectric properties of $Bi_{0.5}Na_{0.5}TiO_3$–$Bi_{0.5}K_{0.5}TiO_3$–$BiCrO_3$ lead-free piezoelectric ceramics," *J.Alloy. Comp.*, **478**, 381–385, 2009

[35] Xu, Z., Chu, R., Hao, J., Li, G., Yin, Q., "Citrate-oxide method to prepare $SrBi_4Ti_4O_{15}$ powders and ceramics," J. Alloy. Comp., **479**, 500–504, 2009

[36] Hagh, N. M., Ashbahian, E., and A. Safari, *Lead-Free Piezoelectric Ceramic in the $K_{1/2}Na_{1/2}NbO_3$-Solid Solution System*, http://www.ultrasonics.org/Proceedings_2006_UIA/Hagh_2006_UIA.pdf

[37] Lam, K.H. Wang, X.X., Chan, H.L.W., "Lead-free piezoceramic cymbal actuator," *Sensor. Actuator. A*, **125**, 393–397, 2006

[38] Priya, S., Nahm, S., *Lead-free piezoelectrics*, Springer, New York, 2012

[39] Ringgaard, E., Wurlitzer, T., "Lead-free piezoceramics based on alkali nioba tes," *J. Eur. Ceram. Soc.*, **25**, 2701–2706, 2005

[40] Li, J., Sun, Q., "Characterization of $(Na_{0:47}K_{0:47}Li_{0:06})(SbxNb1\text{-}x)O_3$ ceramics prepared by molten salt synthesis method," *Solid. State. Commun.*, **149**, 581-584, 2009

[41] Kakimoto, K., Masuda, I., Ohsato, H., "Lead-free $KNbO_3$ piezoceramics synthesized by pressure-less sintering," *J. Eur. Ceram. Soc.*, **25**, 2719–2722, 2005

[42] Wua, D.W., Chen, R.M., Zhou, Q.F., Shung, K.K., Lin, D.M., Chan, H.L.W., "Lead-free KNLNT piezoelectric ceramics for high-frequency ultrasonic transducer application," *Ultrasonics*, **49**, 395–398, 2009

[43] Zuoa, R., Lv, Danya., Jian Fu, J., Liu, Y., Li, L., "Phase transition and electrical properties of lead free $(Na_{0.5}K_{0.5})NbO_3$–$BiAlO_3$ ceramics," *J.Alloy. Comp.*, **476**, 836–839, 2009

[44] Peng, C., Li, J.F., Gong, W.,"Preparation and properties of $(Bi_{1/2}Na_{1/2})TiO_3$–$Ba(Ti,Zr)O_3$ lead-free piezoelectric ceramics," *Mater. Lett.*, **59**, 1576– 1580, 2005

[45] Xiao,D.Q., Lin, D.M., Zhu, J.G., YU, Ping., Liao, Y.W.,Wu, L., Zhuang, Y., ve Wei, Q., "Recent progresses on researches of new BNT-based lead-free piezoelectric ceramics," *Ferroelectrics*, **358**, 93–97, 2007

[46] Saito, Y., Takao, H., Tani, T., Nonoyoma, T., Takatori, K., Homma, T., Nagaya, T., Nakamura, M., "High performance lead-free piezoelectric material," R&D Review of Toyota CRDL Vol.**41** No:2

[47] http://www.americanpiezo.com/knowledge-center/piezo-theory/new-materials.html

[48] http://www.ceracomp.com/sub/sub02_01_01.php

[49] Polla, L. D., Francis, L. F., "Processing and characterization of piezoelectric materials and ıntegration ınto microelectromechanical systems," Annu. Rev. Mater. Sci., **28**, 563-597, 1998

[50] http://www.polecer.rwth-aachen.de/News.2006/HYLee-Piezo2006.pdf

[51] Peng, J., Luo, H., He, T., Xu, H., Lin, D., "Elastic, dielectric, and piezoelectric characterization of $0.70Pb(Mg_{1/3}Nb_{2/3})O_3–0.30PbTiO_3$ single crystals," *Mater. Lett.*, **59**, 640– 643, 2005

[52] Luo, L., Li, W., Zhu, Y., Wang, J., "Growth and characteristics of Mn-doped PMN-PT single crystals," *Solid State Commun.*, **149**, 978-981, 2009

[53] Zhang, S., Xia, R., Lebrun, L., Anderson, D., Shrout, T.R., "Piezoelectric materials for high power, high temperature applications," *Mater. Lett.*, **59** 3471 – 3475, 2005

[54] Panda, P.K., "Review: environmental friendly lead free piezoelectric materials," *J. Mater. Sci.*, **44**, 5049-5062, 2009

[55] D-abkowski, A., D-abkowskaa, H.A., Greedan, J.E., Ren, W., Mukherjee, B.K., "Growth and properties of single crystals of relaxor PZN–PT materials obtained from high-temperature solution," *J. Cryst. Growth.*, **265**, 204–213, 2004

[56] Park, S.E., Hackenberger, W., "High performance single crystal piezoelectrics: applications and issues," *Curr. Opin. Solid. St. M.*, **6**, 11–18, 2002

[57] Lim, L.C., Shanthi, M., Rajan, K.K., Lim, C.Y.H., "Flux growth of high-homogeneity PMN–PT single crystals and their property characterization," *J. Cryst. Growth.*, **282,** 330–342, 2005

[58] Zhou, D., Chen, J., Luo, H., "Piezoelectric single crystals of $Pb(Mg_{1/3}Nb_{2/3})O_3$-$PbTiO_3$ and their applications in medical ultrasonic transducers," *International Conference on Biomedical Engineering and Informatics*, 2008

[59] Zhang, S., Lebrun, L., Rhee, S., Eitel, R.E., Randall, C.A., Thomas R. Shrout, T.R., "Crystal growth and characterization of new high curie temperature (1-x)$BiScO_3$–x$PbTiO_3$ single crystals," *J. Cryst. Growth.*, **236**, 210–216, 2002

[60] Yasuda, N., Ohwa, H., Kume, M., Hayashi, K., Hosono, Y., Yamashita, Y., "Crystal growth and electrical properties of lead indium niobate–lead titanate binary single crystal," *J. Cryst. Growth.*, **229**, 299–304, 2001

[61] Yia, X., Chen, H., Cao, W., Zhao, M., Yang, D., Ma, G., Yang, C., Han, J., "Flux growth and characterization of lead-free piezoelectric single crystal $[Bi_{0.5}(Na_{1-x}K_x)_{0.5}]TiO_3$," *J. Cryst. Growth.*, **281**, 364–369, 2005

[62] Zhang, Q., Zhao, X., Sun, R., ve Luo, H., "Crystal growth and electric properties of lead-free NBT-BT at compositions near the morphotropic phase boundary," *Phys. Status Solidi A* ., **208**, No. **5**, 1012–1020, 2011

[63] Dhanaraj, G., Byrappa, K., Prasad, V., Dudley, M., *Handbook of crystal growth*, Springer, New York, 2010

[64] Scheel, H. J., "The Development of crystal growth technology," *Crystal Growth Technology* (Ed: Scheel, H. J., ve Fukuda, T.), John Wiley & Sons, Ltd., Switzerland, 3-14, 2003

[65] Smith, W.F., (Çeviren:Kınıkoğlu, N.G.,), *Malzeme Bilimi ve Mühendisliği*, Literatür yayınları, İstanbul, 2001

[66] Chiang, Y.M., Birnie, III., D., Kingery, W.D., *Pysical ceramics: Principles for ceramic science and engineering*, MIT series in Materials Science&Engineering Series, John Wiley&Sons, Inc., 1997

[67] Sunagava, I., Crystals, Growth, Morphology and Perfection, Cambridge University Press, New York, A.B.D., 2005

[68] Shimamura, K., ve Fukuda, T., " Synthesis of Single Crystals" *Handbook of Advanced Ceramics* (Ed: Somiya S., *et al.*), Elsevier Inc., 535-591, 2003

[69] Yu, F.P., Yuan, D.R., Yin, X., Zhang, S.J., Pan, L.H., Guo, S.Y., Duan, X.L., Zhao, X., "Czochralski growth and characterization of the piezoelectric single crystal$La_3Ga_{5:5}Nb_{0:5}O_{14}$," *Solid. State. Commun.*, **149**, 1278-1281, 2009

[70] Cochet-Muchy, D., "Growth of piezoelectric crystals by Czochralski method," *J. Phys. IV France*, **04**, C2-33 C2-45, 1994

[71] Graham, R., *Crystal growth technique*, www.scribd.com/doc/95029672/Crystal-Growth-Techniques

[72] Zhou, J., Xu, J., Hua, W., Fan, S., "Bridgman growth of new piezoelectric single crystal $Sr_3Ga_2Ge_4O_{14}$," *Materials Science and Engineering B.*, **106,** 213–217, 2004

[73] Yi, Xi., Chen, H., Cao, W., Zhao, M., Yang, D., Ma, G., Yang, C., Han, J., "Flux growth and characterization of lead-free piezoelectric single crystal $[Bi_{0.5}(Na_{1-x}K_x)_{0.5}]TiO_3$," *J. Cryst. Growth.*, **281**, 364–369, 2005

[74] Burnett, T.L., Comyn, T.P., Bell, A.J., "Flux growth of BiFeO3–PbTiO3 single crystals," *J. Cryst. Growth.*, **285,** 156–161, 2005

[75] Uchino, K., *Advanced piezoelectric materials: science and technology*, Woodhead Publishing Limited, Oxford Cambridge Philadelphia New Delhi, 2010

[76] Lee, H.Y., Lee, J.B., Hur, T.M., Kim, D.H., *Methods for solid state single crystal growth*, A.B.D. Patent No: 0211515A1, 2009

[77] Moon, K.S., Rout , D., Lee, H.Y., Kang, S.J.L., "Solid state growth of $Na_{1/2}Bi_{1/2}TiO_3$–$BaTiO_3$ single crystals and their enhanced piezoelectric properties, " *J. Cryst. Growth.*, **317**, 28-31, 2011

[78] Fisher, J. G., Bencan, A., Holc, J., Kosec, M., Vernay, S., Rytz, D., "Growth of potassium sodium niobate single crystals by solid state crystal growth," *J. Cryst. Growth.*, **303**, 487–492, 2007

[79] Chen, W., Ye, Z.G., "Top seeded solution growth and characterization of piezo-/ferroelectric $(1-x)Pb(Zn_{1/3}Nb_{2/3})O_3$–$xPbTiO_3$ single crystals" *J. Cryst. Growth.*, **233**, 503–511, 2001

[80] Lin, C.T., Liang, B., Chen, H.C., "Top-seeded solution growth of Ca-doped YBCO single crystals," *J. Cryst. Growth.*, **237–239**, 778–782, 2002

[81] Aksel, E., ve Jones, J.L., "Advances in Lead-Free Piezoelectric Materials for Sensors andActuators," *Sensors*, **10**, 1935-1954, 2010

[82] Roleder, K., Franke, I., Glazer, A. M., Thomas, P.A., Miga, S., ve Suchanicz, J., "The piezoelectric effect in Na0.5Bi0.5TiO3 ceramics," *J. Phys.: Condens. Matter.*, **14**, 5399–5406, 2002

[83] Jarupoom, P., Pengpat, K., Pisitpipathsin, N., Eitssayeam, S., Intatha, U., Rujijanagul, G., Tunkasiri, T., "Development of electrical properties in lead-free bismuth sodium lanthanum titanate–barium titanate ceramic near themorphotropic phase boundary," *Curr. Appl. Phys.*, **8,** 253–257, 2008

[84] Jungho Ryu, Jong-Jin Choi, Byung-Dong Hahn, Dong-Soo Park, Woon-Ha Yoon, and Kun-Young Kim, "Sintering and piezoelectric properties of KNN ceramics doped with KZT," *IEEE T. Ultrason. Ferr.*, vol. **54**, no. 12, 2510-2515, 2007

[85] Lin, D., Li, Z., Zhang, S., Xu, Z., ve Yao, X., "Influence of MnO_2 doping on the dielectric and piezoelectric properties and the domain structure in $(K_{0.5}Na_{0.5})NbO_3$ single crystals" *J. Am. Ceram. Soc.*, **93 [4]**, 941–944, 2010

[86] Suzuki, M., Morishita, A., Kitana, Y., Noguchi, Y., Miyayama, M., "Polarization and piezoelektric properties of high performance bismuth sodium titanate single crystals grown by high-oxygen pressure flux method," *Jpn. J. App. Phys*, **49,** 09MD09, 2010

[87] Babu, J.B., Madeswaran, G., Chen, X.L., Dhanasekaran, R., "Effect of oxygen vacacies on ferroelectric behaviour of $Na_{1/2}Bi_{1/2}TiO_3$- $BaTiO_3$," *Mater. Sci. Eng. B.*, **156**, 36-41, 2009

[88] Babu, J.B., Madeswaran, G., He, M., Zang, D.F., Chen, X.L., Dhanasekaran, R., "Inhomogeneity issues in the growth of $Na_{1/2}Bi_{1/2}TiO_3$- $BaTiO_3$ single crystals," *J. Cryst. Growth.*, **310**, 467-472, 2008

[89] Zhang, Q., Zhang, Y., Wang, F., Lin, D., Li, X., Zhao, X., "Growth and electrical properties of $0.96Na_{0.5}Bi_{0.5}TiO_3$-$0.04BaTiO_3$ single crystal," *J. Cryst. Growth*., **312**, 457-460, 2010

[90] Chen, C., Jiang, X., Li, Y., Wang, F., Zhang, Q., ve Luo, H., "Growth and electrical properties of $Na_{1/2}Bi_{1/2}TiO_3$- $BaTiO_3$, lead free single crystal with morphotrophic phase boundary composition," *J. App. Phys.*, **108**, 124106, 2010

[91] Zhang, Q., Zhang, Y., Wang, F., Wang, Y., Lin, D., Zhao, X., Luo, H., Ge, W., ve Viehland, D., "Enhanced piezoelectric and ferroelectric properties in Mn-Doped $Na_{0.5}Bi_{0.5}TiO_3$-$BaTiO_3$ single crystals," *Appl. Phys. Lett.*, **95**, 102904, 2009

[92] Ge,W., Liu, H., Zhao, X., Li, X., Pan, X., Lin, D., Xu, H., Jiang, X., Luo, H., "Orientation dependence of electrical properties of $0.96Na_{0.5}Bi_{0.5}TiO_3$-$0.04BaTiO_3$ lead-free piezoelectric single crystal," *Appl. Phys. A.*, **95**, 761–767, 2009

[93] Ge, W., Liu, H., Zhao, X., Zhou, D., Pan, X., He, T., Lin, D., Xu, H., Luo, H., "Growth and characterization of $Na_{0.5}Bi_{0.5}$-$BaTiO_3$ lead free piezoelectric crystal by the TSSG method," *J. Alloy. Compd.*, **456**, 503-507, 2008

[94] Ge, W., Liu, H., Zhao, X., Fang, B., Li, X., Wang, F., Zhou, D., Yu, P., Pan, X., Lin, D., Luo, H., "Crystal growth and high piezoelectric performance of $0.95Na_{0.5}Bi_{0.5}$-$0.05BaTiO_3$ lead free ferroelectric materials," *J.Phys.D:Appl.Phys.*, **41,** 2008, 115403

[95] http://fnml.korea.ac.kr/lecture/cpec-02.pdf

[96] R.C. Ropp, *Solid state chemistry*, Elsevier Science B.V., Amsterdam, The Netherlands, 2003

[97] Zhang, Q., Zhao, X., Sun, R., Luo, H., "Crystal growth and electrical properties of lead-free NBT-BT at compositions near the morphotrophic phase boundary," *Physical Status Solidi A*, **208**, No 5, 1012-1020, 2011

[98] Fisher, J.G., Bencan, A., Kosec, M., "Growth of dense single crystal of potassium sodium niobate by a combination of solid-state crystal growth and hot pressing," *J. Am. Ceram. Soc.*, **91,** [**5**], 1503-1507, 2008

[99] Park, J.K., Chung, U.J., Kim, D.Y., "Application of spark plasma sintering for growing dense $Pb(Mg_{1/3}Nb_{2/3})O_3$-35mol%$PbTiO_3$ single crystal by solid state crystal growth", *J. Electroceram.*, **17**, 509-513, 2006

[100] Özüdoğru, R.E., *WC-Co Semente karbürlerin üretimi ve Karakterizasyonu*, Yüksek Lisans Tezi, İstanbul Teknik Üniversitesi, Fen Bilimleri Enstitüsü, İstanbul, 2008

[101] Dong, X., Lu, F., Yang, L., Zhang, Y., Wang, X., “Influence of spark plasma sintering temperature on electrochemical performance of $La_{0.80}Mg_{0.20}Ni_{3.75}$ alloy” *Mater. Chem. Phys.*, **112,** 596–602, 2008